SYNTHESIS, CHARACTERIZATION AND CATALYTIC ACTIVITY OF ORDERED MESOPOROUS METALLOSILICATE CATALYSTS

A THESIS

SUBMITTED TO THE

UNIVERSITY OF PUNE

FOR THE DEGREE OF

DOCTOR OF PHILOSOPHY

(**IN CHEMISTRY**)

BY

MISS. SUREKHA SHIVAJI KHAIRE

CATALYSIS DIVISION

NATIONAL CHEMICAL LABORATORY

PUNE 411008

INDIA

Dr. S. SIVASANKER

(RESEARCH GUIDE)

JULY 2006

CERTIFICATE

Certified that the work incorporated in the thesis **"Synthesis, Characterization and Catalytic Activity of Ordered Mesoporous Metallosilicate Catalysts",** submitted by **Miss. Surekha Shivaji Khaire,** for the degree of **Doctor of Philosophy,** was carried out by the candidate under our supervision in Catalysis Division, National Chemical Laboratory, Pune, India. Materials obtained from other sources have been duly acknowledged in the thesis.

Dr. S. Sivasanker — **Research Guide**

Dr. Rajiv Kumar — **Research Co-guide**

DECLARATION

I hereby declare that the thesis entitled **"Synthesis, Characterization and Catalytic Activity of Ordered Mesoporous Metallosilicate Catalysts",** submitted for the Degree of Doctor of Philosophy to the University of Pune, has been carried out by me at the National Chemical Laboratory, Pune under the supervision of Dr. S. Sivasanker (Research guide) and Dr. Rajiv Kumar (Research Co-guide). The work is original and has not been submitted in part or full by me for any other degree or diploma to this or any other University.

(**Surekha S. Khaire**)

DREAM MORE, THINK HIGH, ANALYZE TWICE,

CHOOSE THE BEST, PLAN PERFECT, BE CONFIDENT,

WORK HARD, EXECUTE WELL, THEN,

SUCCESS IS YOURS

DEDICATED

TO

MY BELOVED PARENTS

Acknowledgements

I take this opportunity to express my deep sense of gratitude to my research guide Dr. S. Sivasanker, Emeritus Scientist and former Head of Inorganic and Catalysis Division, NCL, for his stimulating and invaluable guidance throughout this work. His constant striving for excellence coupled with his quest for knowledge will always remain a source of inspiration for me. Had it not been due to his unending efforts to improve my skills and understanding the present work would not have taken the form in which it appears now.

I express my profound gratitude to my research co-guide, Dr. Rajiv Kumar, Head of Inorganic and Catalysis Division, NCL, for his encouragement, help and co-operation given to me in completing my research work successfully.

I owe my special thanks to Dr. S.S. Deshpande, Dr. S.A. Pardhy, Dr. S. Mayadevi, Dr. V.R. Chumbhale, Dr. S.P. Mirajkar, Dr. S. V. Awate, Ms. Agashe, Dr. D. Srinivas, Dr. A.P. Singh, Dr. Satyanarayana, Dr. S.B. Halligudi, Dr. V. Ramaswamy, Dr. A.J. Chandwadkar, Dr. M. K. Dongare, Dr. S.G. Hegde, Dr. S. Umbarkar, Dr. A. Belhekar, Dr. Kamble, Dr. Waghmare, Dr. Mamman, Dr. T. Raja, Ms. Violet, Mrs. Jacob, Mr. Jha, Dr. P. Manikandan, Dr. P.N. Joshi, Dr. Chaphekar, Dr. S. Ganapathy, Dr. Rajamohan, Dr. Ajitkumar, Dr. P. Ratnasamy, Dr. A. V. Ramaswamy, Dr. G. Pandey, Dr. M. Sastry, Mr. Vinod, Mrs. Renu, Mr. Gaikwad, Dr. Selvaraj, Mr. Tejas, Mr. Niphadkar, Mr. Purushottam, Mr. Kashinath, Mr. Madhu, Mr. Milind, Mr. Katti and my teachers, Dr. A.S. Kumbhar, Dr. A.K. Nikumbh, Dr. S.B. Padhye and all other scientific and technical staff for their help, inspiration and guidance.

I would like to thank my friends, Smita, Shalaka, Pallavi, Bennur, Pai, Vasu, Shanbhag, Suresh, Rohit, Rajendra, Sanker, Chidam, Shylesh, Devu, Ankur, Pranjal, Lakshi, Prashant, Reddy, Ankush, Vijayraj, Kala, Trissa, Dhanashri, Maitri, Suman, Nisha, Pooja, Nevin, Neelam, Vandana, Ganesh, Sachin, Surendran, Thiru, Kumbar, Shrikant, Santosh, Naresh, Biju, Amit, Sangamesh, Pradeep, Upendra, Shivram, Sriprashant, Meenakshi and many others for their co-operation, encouragement, invaluable help and moral support rendered by them.

The words are not enough to express all my love and thankfulness towards my parents for allowing me to pursue my research. It is because of their blessings that I could reach here. It gives me great pleasure to thank my brothers Santosh, Shekhar, sister Sonu, Suman vahini and my nephew Satyam for their love, encouragement and unfailing support shown during my research work.

I take this opportunity to thank Dr. S. Sivaram, Director, NCL, Pune, for allowing me to carry out research and providing all infrastructural facilities at NCL and to submit the work in the form of the thesis for the award of the Ph.D. degree. Finally, I would like to thank Council of Scientific and Industrial Research (CSIR), New Delhi for awarding me the research fellowship.

Surekha S. Khaire

ABBREVIATIONS

AA	Acetic anhydride
AAS	Atomic absorption spectroscopy
ACN	Acetonitrile
$AlPO_4$	Aluminophosphates
AN	anisole
As synt.	As synthesized
Av.	Avergae
BET	Braunauer-Emmett-Teller
BJH	Barrett-Joyner-Halenda
C.N.	Co-ordination number
Cal.	Calcined
ChBz	Chlorobenzene
CMC	Critical micellization concentration
Conc.	Concentrated
Conv.	conversion
CTACl	Cetyltrimethyl ammonium chloride
CTMA	Cetyltrimethylammonium
CTMABr	Cetyltrimethyl ammonium bromide
CVD	Chemical vapor deposition
DTA	Differential thermal analysis
DTG	Differential thermogravimetry
EB	Ethylbenzene
EDC	Ethylene dichloride
ESR	Electron spin resonance
Expt. No.	Experiment number
FSM-16	Folded sheet material
FTIR	Fourier transform infra-red
GC	Gas chromatography
HMS	Hexagonal mesoporous silica
HPA	Heteropolyacid
HRTEM	High resolution transmission electron microscopy
ICP-OES	Inductively coupled plasma-optical emission spectroscopy

IPA	Isopropyl alcohol or isopropanol
IUPAC	International Union for Pure and applied chemistry
LAT	Ligand assisted templating
LCT	Liquid crystal templating
MAS - NMR	Magic angle spinning - Nuclear magnetic resonance
MCM-41	Mobile composition of matter number 41
Mol. Wt.	Molecular weight
o-AP	*ortho*- allylphenol
Oct or Oh	Octahedral
o-Map	*ortho*- methoxyacetophenone
P123	Pluronic 123 triblock co-polymer
PAA	Phenyl acetic acid
PC	p-cresol
PEO-PPO-PEO	Polyethylene oxide-polypropylene oxide-polyethylene oxide
p-Map	*para*- methoxyacetophenone
Pore diam.	Pore diameter
Pore vol.	Pore volume
PW or PWA	Phosphotungstic acid
SANS	Small angle neutron scattering
SAXS	Small angle X-ray scattering
SBA-15	Santa Barbara amorphous number 15
Sel.	Selectivity
SEM	Scanning electron microscopy
Si/M	Si/Metal
SLC	Silcatropic liquid crysatls
Soln.	Solution
TBHP	*tert*-Butyl hydroperoxide
TCE	Tetrachloroethylene
TEM	Transmission electron microscopy
TEOS	Tetraethylorthosilicate
Tet or Td	Tetrahedral
TG	Thermogravimetry

TLC	Thin layer chromatography
TMAOH	Tetramethylammonium hydroxide
TOS	Time on stream
TPDA	Temperature programmed desorption of ammonia
TPR	Temperature programmed reduction
TS-1	Titanosilicate-1
Unit cell para.	Unit cell parameter
UV-Vis	Ultra violet – visible
VS-1	Vanadosilicate-1
Wall thick.	Wall thickness
WHSV	Weight hourly space velocity
Wt. %	Weight percentage
XRD	X-ray diffraction
XRF	X-ray fluorescence
ZSM-5	Zeolite Socony Mobile-5

CONTENTS

Chapter 1

INTRODUCTION

1.1 GENERAL BACKGROUND

Acid catalysts are used mainly in the areas of oil refining, petrochemicals and chemicals. They are responsible for producing more than 1 x 10^8 mt/year of products. The most commonly used acid catalysts are HF, H_2SO_4, $HClO_4$ and H_3PO_4. But these have many disadvantages such as difficulties associated with handling, plant corrosion, regeneration and environmentally safe disposal. In recent years, environmental and economic considerations have played a major role in redesigning commercially important processes so as to avoid the use of harmful substances and the generation of toxic waste. In this context, heterogeneous catalysis has played a key role in the development of environmentally benign processes for the petroleum industry and in the production of chemicals, for instance by the substitution of liquid acid catalysts by safe solids such as zeolites.

There are many types of solid acids such as zeolites, heteropolyacids, sulfated metal oxides and organic–inorganic composites that possess different acidities. Porous solids like zeolites have extensive applications as adsorbents, catalysts and catalyst supports due to their high surface area. According to the IUPAC definition, porous materials may be divided into three types based on their pore sizes, microporous: < 20 Å, mesoporous: 20-500 Å and macroporous: >500 Å [1]. Many kinds of porous materials such as, (pillared) clays, anodic alumina, carbon nanotubes and related porous carbons have been extensively described in the literature [2]. Well known microporous materials are zeolites and aluminophosphate molecular sieves, which are inorganic composites having a crystalline three-dimensional framework woven with tetrahedral atoms (T atom) like Al, Si, P etc. that are bridged by oxygen atoms. Modification of the framework and extra-framework composition makes these materials useful for catalyzing organic reactions. The most important application of zeolites is in reactions catalyzed by Brönsted and Lewis acids. Zeolites are attractive as heterogeneous catalysts due to properties such as well defined crystalline structure, high internal surface area, uniform pores of one or more discrete sizes, good thermal stability, ability to adsorb and concentrate hydrocarbons and highly acidic sites in the protonated form (Figure 1.1).

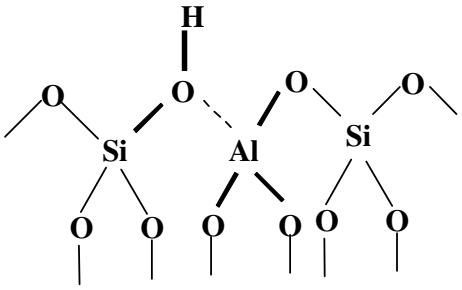

Figure 1.1 The bridging hydoxyl group and the oxo ligands of the Al-atom act as bifunctional Brönsted acid-Lewis base sites.

Eventhough zeolites have extremely interesting properties as acid catalysts and as molecular sieve catalysts, they are still limited in pore size, and can only deal with molecules smaller than about 8 Å. Indeed, while advances have been made in the synthesis of ultra-large pore zeolites and zeotypes [3, 4] the materials obtained still possess limited utility as catalysts due to their poor thermal stabilities. In this context, new siliceous mesoporous molecular sieves with periodically ordered pores have expanded the potential of zeolites [5, 6]. The ordered siliceous hexagonal mesoporous materials MCM-41 [7] and SBA-15 [8] have attracted much interest because of their high surface area, large pore volume and well-defined pore size. MCM-41 has a low hydrothermal stability because its inorganic oxide wall is disordered at the molecular level. SBA-15 has a higher hydrothermal stability than MCM-41 due to its larger wall thickness; it also possesses larger pores than MCM-41. MCM-41 can be made acidic by synthesizing it with tetrahedral Al-ions and its acidity is a compromise between amorphous silica-alumina and zeolites [9-11].

The first synthesis of an ordered mesoporous material was described in the patent literature in 1969. However, due to a lack of proper analysis, the remarkable features of this product were not recognized [12]. In 1992, a similar material was synthesized in Mobil Oil Corporation opening up a whole a new field of research [13]. MCM-41, which stands for Mobil Composition of Matter No.41, possesses a highly ordered hexagonal array of unidimensional pores with a very narrow pore size distribution [7, 14]. The walls, however, very much resemble amorphous silica. Other related phases such as MCM-48 and MCM-50, which possess cubic and lamellar mesostructures, respectively, were reported in these early publications as well. At approximately the same time, an alternative, but less versatile approach to

mesoporous materials was described by Yanagisawa et al. [15]. Kanemite, a layered silicate, served as the silica source; the pathway leading to the ordered mesoporous material is thought to proceed via surfactant intercalation into the silicate sheets, wrapping of the sheets and transformation to the hexagonally packed material [16, 17]. The obtained materials were designated as FSM-n, Folded Sheet Mesoporous Material-n, and here; n is the number of carbon atoms in the surfactant alkylchain used to synthesize the material.

The large regular pore structure of MCM-41 materials makes them suitable for liquid-phase acid catalysis by enabling rapid diffusion of reactants and products through the pores, thus minimizing consecutive reactions. Liquid-phase Friedel–Crafts alkylation and acylation reactions [18–22] have been reported using aluminosilicate MCM-41. Other reactions catalyzed by MCM-41 include the acetalysation of bulky aldehydes [23], glucosidation [24-a] and aldol condensations [24-b].

A variation of the MCM family of materials was reported by Pinnavaia et al. [25], who developed a neutral templating method using long-chain alkylamines to form hexagonal mesoporous molecular sieves (HMS materials). Organo-modified silicas are widely used in chromatographic and other analytical applications [26], and the techniques for their preparation are well documented. For example, silica functionalized with sulfonic acid groups is frequently used for binding metal ions [27]. The chemistry used to prepare these materials has recently been exploited to prepare a pure sulfonic acid-functionalized mesoporous silica [28, 29], which is a solid Brönsted acid. Sol gel preparation of thiol functionalized silica was performed by co-condensation of $Si(OEt)_4$ and 3-mercaptopropyltrimethoxysilane (MPTS) using either neutral or ionic templating methods, with subsequent oxidation producing HMS-SO_3H, and MCM-SO_3H, respectively [28]. These sulfonic acids exhibit high catalytic activity in the preparation of bisfurylalkanes from 2-methylfuran and acetone. Higher conversions of 2-methylfuran and high selectivities towards 2,2-bis(5-methylfuryl)propane are observed compared to reactions using zeolites H-β or H-US-Y which rapidly deactivate due to oligomerization of 2-methylfuran. Both sol gel and post-modified sulfonic acid silicas also exhibit considerable selectivity towards monoglyceride formation during the esterification of polyols with fatty acids [29].

The large and uniform pore structure of SBA-15 (Santa Barbara Amorphous) materials makes them suitable for catalyzing different organic reactions. Aluminosilica meso/macroporous SBA-15 monoliths (Si/Al=72) and mesoporous powders (Si/Al=70) have been investigated using a batch reactor in the Friedel- Crafts alkylation of aromatic compounds such as toluene, ethylbenzene, cumene and styrene with benzyl alcohol [30]. TiO_2 on SBA-15 and Ti-SBA-15 catalysts have been used in oxidation reactions with H_2O_2 and TBHP. The results have revealed that TiO_2 nanoparticles are active and selective in the epoxidaton of cyclohexene and in the oxidation of aniline [31]. Al-SBA-15 catalysts show high and durable activity in cumene cracking [32]. Ti-SBA-15 exhibits high catalytic activity for the epoxidation of styrene with a conversion of 38.2 % and an epoxidation selectivity of 49.7 % which is higher than over Ti-MCM-41 [33]. Vapor phase isopropylation of m-cresol has been studied over Al-SBA-15 catalysts; 73.5 % m-cresol conversion and 45.68 % thymol selectivity have been reported [34]. Isopropylation of naphthol over PW/SBA-15 catalysts exhibited higher conversion (84.3%) and selectivity to di-isopropylnaphthalenes (39.7%), β-isopropyl naphthalene and β, β-products (81.8 %) than pure acids [35]. The Beckmann rearrangement of cyclohexanone oxime to caprolactam was studied over an arenesulfonic acid functionalized SBA-15 (15 % SBA-15-Ar-SO_3H), 51.9 % oxime conversion and 81.3 % caprolactam selectivity were obtained [36]. Alkylation of benzene with 1-dodecene studied over PW/SBA-15 at atmospheric pressure in a batch reactor showed 90 % 1-dodecene conversion with 40 % 2-phenyldodecane and 100 % monoalkyl benzene selectivity [37].

1.2 SYNTHESIS AND FORMATION MECHANISM OF ORDERED MESOPOROUS MATERIALS

Based on the template used for synthesis and the interaction of the inorganic species and the organic template molecule, the mesoporous materials might be classified as listed in Table 1.1 [51].

Table 1.1 Possible pathways for the synthesis of mesoporous materials [51]

Template	Interaction		Synthesis conditions	Examples
Ionic surfactant	Direct interaction	I^-S^+ ^^^^^^^	Basic	MCM-41, MCM-48, MCM-50 [13,7,14], FSM-16 [16, 17]
	(Ionic)	I^+S^- ^^^^^^^	Neutral-Basic	(Al, Fe, Lead oxides, etc. [38 (b), (c)] AMS [41])
	Intermediate interaction	$I^+X^-S^+$ ^^^^^^^	Acidic	SBA-1, SBA-2, SBA-3 [42], HMS [25], TLCT [39]
	(Ionic)	$I^-X^+S^-$ ^^^^^^^	Basic	(Al, Zn oxides etc. [38 (b), (c)])
Non-ionic surfactant	(Non-ionic)	$I^\circ S^\circ$ ^^^^^^^		HMS [25,43]
Co-polymer		$I^\circ N^\circ$ ^^^^^^^	Acidic	MSU [44, 45], SBA-15 [8, 46], TLCT [39]
(Ligand assisted)	(Co-valent bonding)	I-S^^^^^^^		Nb-TMS [47, 48], Ta-TMS [49]
Nanocasting	-	-	-	CMK-n [40(a), 50]

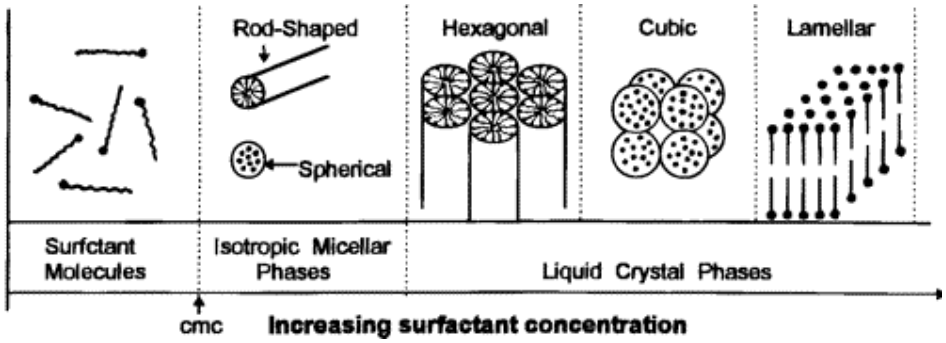

Figure 1.2 Phase sequence of surfactant-water binary system [52, 53].

1.2.1 Behaviour of surfactant molecules in an aqueous solution

In a simple binary system of water and a surfactant, the surfactant molecules possess different structures in accordance with increasing concentrations, as schematically shown in Figure 1.2. At low concentrations, they exist as monomolecules. With increasing concentration, surfactant molecules aggregate together to form micelles in order to decrease the system entropy. The initial concentration threshold at which monoatomic molecules aggregate to form isotropic micelles is called cmc (critical micellization concentration). As the concentration increases, hexagonal close packed arrays appear, producing the hexagonal phases [53]. The next step in the process is the coalescence of the adjacent, mutually parallel cylinders to produce the lamellar phase. In some cases, the cubic phase also appears prior to the lamellar phase. The cubic phase is generally believed to consist of complex, interwoven networks of rod-shaped aggregates [54]. The cmc decreases with increase in the chain length of a surfactant, the valency of the counterions, and the ionic strength in a solution. On the other hand, it increases with increasing counterion radius, pH, and temperature.

1.2.2 Synthesis and formation mechanism of MCM-41 molecular sieves

Mesoporous materials are synthesized in the presence of surfactant molecules. Most commonly used surfactants are quaternary ammonium salts (e.g. cetyltrimethylammonium halide). In the synthesis of mesoporous molecular sieves, the different types of mesophases formed depend on the surfactant to silica molar ratio as shown in Table 1.2 [14, 57(e)]. MCM-41 type molecular sieves are synthesized in alkaline [7, 14, 57] acidic [38 (b, c)] and neutral medium (HMS) [25].

A number of models have been proposed to explain the formation of mesoporous materials and to provide a rational basis to all the synthetic routes. A few of these mechanisms are discussed below.

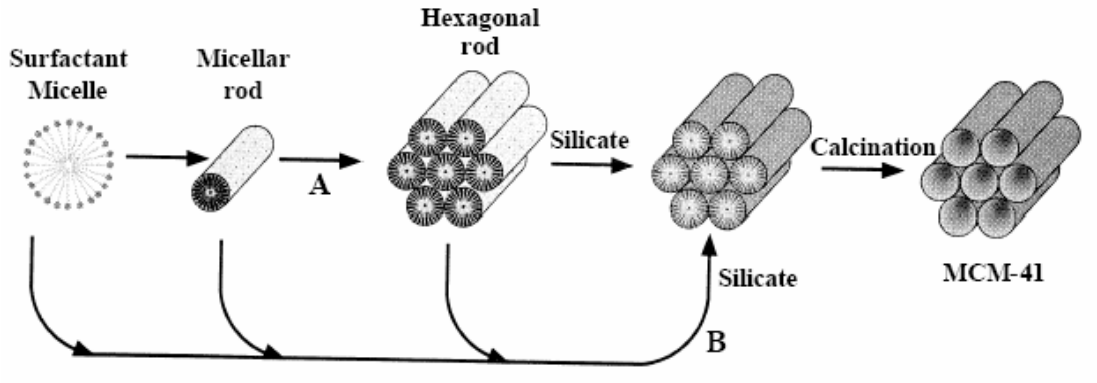

Figure 1.3 Possible mechanistic pathways for the formation of MCM-41: (A) liquid - crystal – phase initiated and (B) silicate – anion initiated [14].

Table 1.2 Dependance of mesophase structure on surfactant/silica (mole) ratio [14, 57(e)]

Name	Mesophase	Parameter (Surfactant/ Silica)
MCM-41	Hexagonal	< 1.0
MCM-48	Cubic	1.0 - 1.5
MCM-50	Lamellar	1.2 – 2.0
Cubic-octamer [(CTMA) $SiO_{2.5}]_8$	Cubic	2.0

(A) Liquid crystal templating (LCT) mechanism

A key feature of the LCT mechanism proposed by Beck et al. [14] is that the liquid crystalline mesophases or micelles act as templates rather than individual single molecules or ions. Accordingly, the final product is a silicate skeleton which contains voids that mimics these mesophases. The silicate condensation is not the dominant factor in the formation of the mesoporous structure. The whole process may be via two possible mechanistic pathways as schematically shown in Figure 1.3. In the first pathway (A), it is considered that first there is a formation of the surfactant hexagonal liquid-crystal phase around which the growth of the inorganic materials is directed. The $C_nH_{2n+1}(CH_3)_3N^+$ surfactant micelles aggregate to form hexagonal arrays of rods.

Silicate anions present in the reaction mixture interact with the surfactant cationic head groups. Condensation of the silicate species leads to the formation of an inorganic polymer. On calcination, the organic template is burnt off, leaving inorganic hollow cylinders in hexagonal arrangement. However, this pathway did not get much support in the literature. It has been observed that at lower concentrations only micelles exist in solution [58]. Moreover, in situ ^{14}N-NMR spectra revealed that the hexagonal liquid-crystalline phase of CTMA ions was not present at any time during MCM-41 formation [55, 56]. Thus the first synthesis scheme proposed by Beck et al. [14] was abandoned.

In the second pathway, it has been proposed that the randomly ordered rodlike micelles interact with silicate species by coulombic interactions in the reaction mixture to produce approximately two or three monolayers of silicate around the external surfaces of the micelles. These randomly ordered composite species spontaneously pack into a highly ordered mesoporous phase with an energetically favorable hexagonal arrangement, accompanied by silicate condensation. With increase in the heating time, the inorganic wall continues to condense (Figure 1.3; pathway B).

(B) Folded sheets mechanism

The "folded sheets" mechanism, proposed by Inagaki et al. [16] is based on the intercalation of the surfactant to the layered silicates (kanemite) and is described below (Figure 1.4). Initially, the surfactant cations intercalate into the bilayers of kanemite via an ion exchange process. As the ion exchange proceeds, interlayer cross-linking occurs by condensation of silanols. The silicate sheets of kanemite have the required flexibility to be folded due to its single sheet structure.

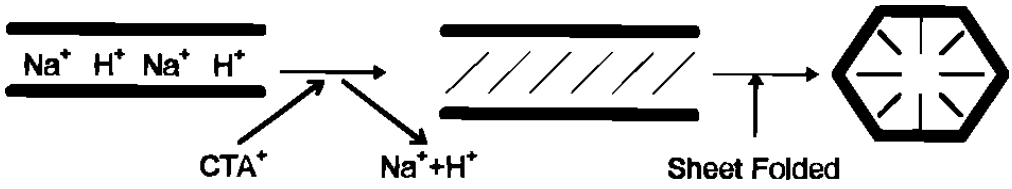

Figure 1.4 Model schematically representing "folded sheets" mechanism [16].

(C) Transformation mechanism from lamellar to hexagonal phase

Another formation mechanism proposed by Monnier et al. [38(a)] and Huo et al. [38(c)] is the transformation mechanism from lamellar to hexagonal phase. As polymerization of the silicate species in a lamellar arrangement of the surfactant and silicate ions proceeds, the average head group area (*A*) of surfactant assembly increases due to the decrease of the charge density of larger silicate polyanions. This leads to the corrugation of the silicate layers and ultimately results in the hexagonal mesophase precipitation. Figure 1.5 schematically shows the transformation mechanism from lamellar to hexagonal phase through charge matching.

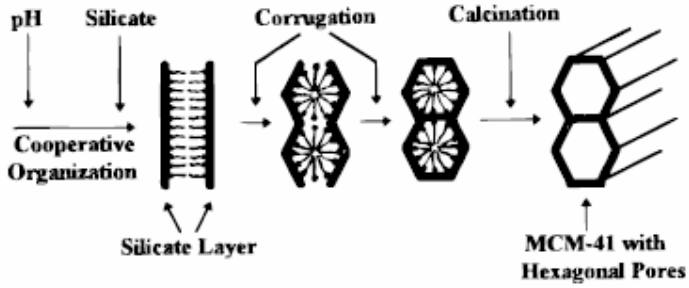

Figure 1.5 Mechanism for transformation from lamellar to hexagonal phase [38(a)].

1.2.3 Synthesis and formation mechanism of SBA-15 molecular sieves

Monnier et al. [38(c)] and Tanev and Pinnavaia [25, 60] showed that the assembly of mesoporous materials can also be driven by hydrogen bonds in the case of neutral templates such as nonionic poly (ethylene oxide) (PEO) surfactants and inorganic precursors. The assembly of the mesoporous silica organized by non-ionic alkyl-ethylene oxide surfactants or poly (alkene oxide) triblock copolymer species in acid media occurs through an (S^0H^+) (X^-I^+) path way [38 (c), 46]. First, alkoxysilane species are hydrolysed at a pH less than 2.

$$Si(OEt)_4 + n\,H_3O^+ \xrightarrow[p^H < 2]{\text{Hydrolysis}} Si(OEt)_{4-n}(OH_2^+)_n + n\,EtOH$$

This is followed by partial oligomerisation of the silica. The EO moieties of the surfactant in strong acid media associating with hydronium ions.

$$REO_m + yHX \xrightarrow{H_2O} REO_{m-y}[(EO).H_3O^+]_y.....yX^-$$

Where R = alkyl or poly (propylene oxide) and X^- = Cl^-, Br^-, I^-, NO_3^-, $H_ySO_4^{-2+y}$, $H_yPO_4^{-3+y}$

Zhao et al. [46] proposed that the formation of SBA-15 occurs through a scheme where the silica source is first hydrolyzed at low pH to form $Si(OMe)_{4-n}(OH_2^+)n$ species and the PEO moieties of the block copolymer associate with hydronium ions. Then, the charged PEO units and the cationic silica species are assembled together, via Cl^-, by a combination of electrostatic, hydrogen bonding and van der Waals interactions to form $REO_{m-y}[(EOH_3O^+]_y \ldots yX^- \ldots .I^+$, which can be designated as $(S^0H^+)(X^-I^+)$. Coordination sphere expansion around the silicon atom by anion (e.g. Cl^-) coordination of the form $X^-.Si\text{-}OH_2^+$ may play an important role [61]. Further condensation of the silica species and the organization of the surfactant and inorganic species result in the formation of the lowest energy silica-surfactant mesophase structure allowed by the solidifying inorganic network [59]. Furthermore, the time required for silica mesopore precipitation depends on the acid anion and is found to be the shortest in the presence of Cl^- anion when used in the form of hydrochloric acid.

The influence of block length of triblock copolymers [Pluronic surfactants (EO)x-(PO)y-(EO)x] on the formation of mesoporous silica was investigated by Flodstrom et al. [62]. They reported that for a hexagonal material (SBA-15) the wall thickness is largely dependent on the length of the EO-blocks while the PO-block length has a great effect on the pore diameter. It was shown that the EO-length determines which mesostructure is formed [63] as shown in Table 1.3. The length of the hydrophilic EO- block determines the silica mesostructure and influences the wall thickness of SBA-15. The hydrophobic PO-block affects the pore diameter and further, the PO-block length influences the templating ability as a longer PO-block results in more highly ordered domains and more well-defined particles.

Table 1.3 Influence of triblock copolymer on mesostructure formation [63]

Pluronic	EO units	Structure
L101	4	Lamellar
P103, P104, P105, P123	17-37	2D, hexagonal (p6mm- SBA-15)
F108	132	Body centered cubic (BCC –$Im\bar{3}m$-SBA-16)

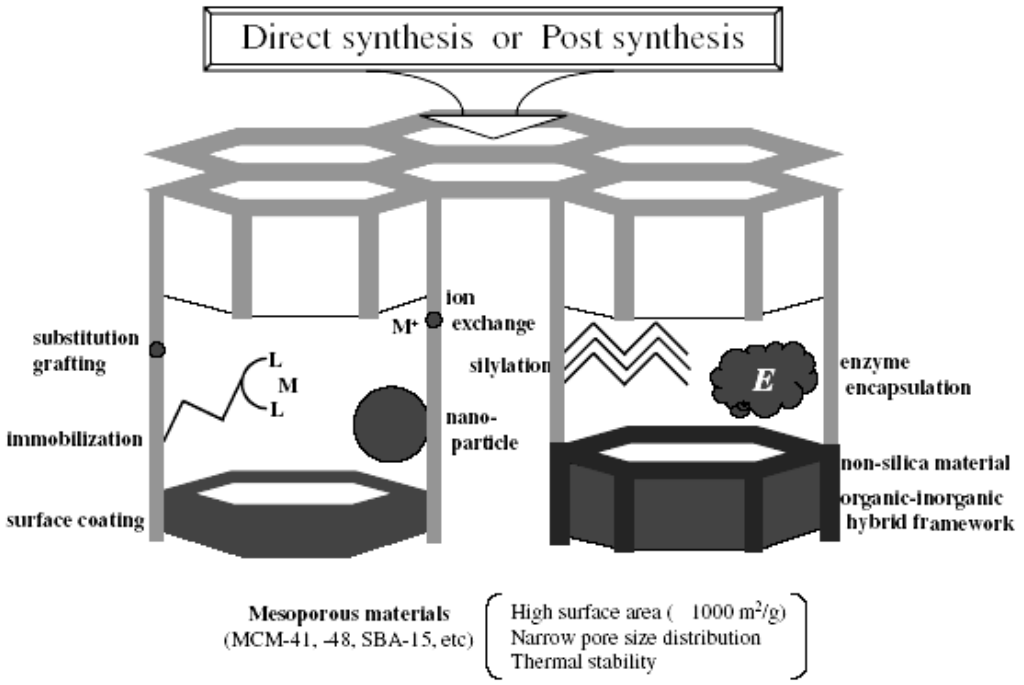

Figure 1.6 Schematic diagram of the various methods for the functionalization of mesoporous materials [51].

1.3 PREPARATION OF CATALYSTS – STRATEGIES AND PROPERTIES

Ordered mesoporous silicas are not often used as catalysts as such. More frequently, additional catalytic functions are introduced, by incorporation of active sites in the silica walls or by deposition of active species on the inner surface of the material. There are many possible pathways to modify mesoporous materials when one wants to give them a new catalytic function as schematically shown in Figure 1.6. Metal ions substituting silicon atoms in the framework as in zeolites, can act as acid or redox active sites and may be used for different classes of catalytic reactions. One should bear in mind, though, that the wall structure of ordered mesoporous silica rather resembles amorphous silica. Incorporation of other metal centers therefore does not lead to the formation of defined sites as in zeolites, but to a rather wide variety of different sites with different local environments. Therefore, the catalytic properties of such materials are closer to those of metal substituted amorphous silica than to those of framework substituted zeolites. Possibly more interesting is to exploit the exceedingly high surface area of these materials in support applications for metal or metal oxide particles or to deposit isolated species onto the wall surface. Interestingly,

these active sites can be constructed either directly or via post-synthesis procedures by a multitude of pathways, which means that the properties of these active sites are variable and controllable, depending on the synthetic procedure.

1.4 MODIFICATION OF MESOPOROUS MOLECULAR SIEVES

Much effort has been focused on the introduction of heteroatoms, such as B, Fe, Ga, Ti, V, Sn and particularly, aluminum, in the siliceous framework to modify the composition of the inorganic walls. This is especially important with respect to the catalytic applications, since substitution of silicon allows fine-tuning of the acidity or creation of redox properties, as observed in amorphous aluminosilicates or zeolites. Modification of the framework composition is possible by direct synthesis, i.e. from mixtures containing both silicon and the heteroelement to be incorporated, or by post-treatment of an initially prepared silica mesoporous material. The results of these two different methods are not necessarily identical. While the direct method typically will result in a relatively homogeneous incorporation of the heteroelement, post-synthesis treatment will primarily modify the wall surface and thus lead to an increased concentration of the heteroelement on the surface.

(A) Incorporation of heteroatoms by hydrothermal methods

When trivalent cations like Al^{3+}, B^{3+}, Ga^{3+} and Fe^{3+} [64-70] substitute for silicon in the walls of the mesoporous silica, the framework possesses negative charges that can be compensated by protons providing acid sites. The number of acid sites and strength depend on the amount and nature of the incorporated metal. These materials are useful in acidic reactions and have potential applications in various industrial processes [71-72]. When other cations like Ti^{4+}, V^{4+} etc. [73-76] are incorporated, the corresponding mesoporous materials are used in oxidation reactions. Ti and V containing MCM-41 molecular sieves have been used in a variety of oxidation reactions of bulky molecules using either H_2O_2 or TBHP as oxidant [74, 77-80]. A few reports describe the synthesis and characterization of mesoporous silica modified by metals like Cr [81-83], Mn [84] or Mo [82]. Cr-MCM-41[83] has been found to be catalytically active in the hydroxylation of phenol, 1 naphthol and the oxidation of aniline with aqueous H_2O_2.

(B) Grafting of heteroatoms

Mesoporous molecular sieves have a number of surface silanol groups, which can be functionalized by introducing organic functional groups. This is normally achieved through attachment of silane-coupling agents to the mesoporous walls of previously synthesized and calcined materials [85]. In one of the methods, functionality is directly introduced through the reaction of silanol groups [86-87]. In another method, a transition metal, metal oxide or a bimetal complex is grafted on the wall by reaction with the surface hydroxyl groups without the use of intermediate silane coupling agents. Ti grafted MCM-41 exhibits higher catalytic activity for the epoxidation of alkenes than other Ti containing catalysts [88]. Mesoporous materials anchored with $AlCl_3$, $SnCl_2$, $Zn(O_2CMe)_2$ or $Mn(O_2CMe)_2$ possess high stability and catalytic activity alongwith ion-exchange capacity [89].

(C) Impregnation of heteroatoms

Post-synthesis treatment will primarily modify the wall surface and thus lead to an increased concentration of the heteroelement on the surface. Certain reactions such as hydroisomerization and aromatization are carried out on bifunctional catalysts possessing acid functionality of the molecular sieves and hydrogenation-dehydrogenation property of the metal impregnated on the surface of the molecular sieves. Such catalysts are usually prepared by loading the metals (Ni, Co, Pt, Pd, W etc.) by impregnation methods. It has been reported that sulfided Co and Mo impregnated Al-MCM-41 show higher hydrogenation and hydrocracking activities than Co-Mo/Al_2O_3 catalysts [90]. Cu impregnated MCM-41 has been used in the liquid phase oxidation of benzene to phenol using O_2 as the oxidant. It has also been reported to be more active than Cu Supported ZSM-5, MgO, TiO_2, SiO_2, NaY and KL etc. [91]. Cs impregnated MCM-41 has been found to be a good basic catalyst for Michael addition of diethylmalonate to neopentyl glycol diacrylate and a high regioselectivity was obtained in contrast to bulk cesium oxide [92]. Impregnation of binary Cs-La oxide on MCM-41 has been found to produce a useful basic catalyst for the Knoevenagel addition of enolates to benzaldehyde and for the liquid phase Michael addition of ethyl cyanoacetate to ethyl acrylate [93]. Pt impregnated MCM-41 has been used for naphthalene hydrogenation [94].

Aluminum [95], Sn [96-97], Zn [97] or Zr [98] can be incorporated by post treatment and the resultant materials possess interesting catalytic activity. For

example, Zhu et al. [98] reported that zirconium 1-propoxide grafted SBA-15 has higher activities in the Meerwein–Ponndorf–Verley (MPV) reduction of 4-tert-butylcyclohexanone than SBA-15 grafted with aluminum 2-propoxide. Several publications report the formation of mesoporous materials with zeolitic fragments in the walls which were synthesized by impregnation [99]. The walls of mesoporous silica can also be coated with zeolitic fragments, as reported by Trong On and Kaliaguine [100–101]. The FT-IR spectrum after pyridine adsorption, using ZSM-5 coated SBA-15 as an example, shows the two intense absorption bands characteristic of Brönsted and Lewis acid sites, which are not observable in the parent mesoporous SBA-15 [100]. Titanium isopropoxide was grafted on SBA-15 with Si/Ti ratios between 80 and 5 with high dispersion [102]. The tetragonal ZrO_2 phase in the SBA-15 mesopores shows about three times higher capacity for sulfate adsorption than bulk ZrO_2 [103]. Iron oxide has been deposited on MCM-41 and MCM-48 by the incipient wetness technique [104]. MCM-41 supported γ-Fe_2O_3 prepared by vapor-phase deposition with $Fe(CO)_5$ as precursor exhibits a superparamagnetic behavior [105]. Ga_2O_3 or In_2O_3 supported on MCM-41 show catalytic activity in Michael addition of diethyl malonate to neopentyl glycol diacrylate [106] and Friedel–Crafts type benzene benzoylation and acylation [107] reactions. Highly dispersed rare earth oxides on SBA-15 were reported recently [108]. Polyoxometalates [109], for example, have been supported with high dispersion on mesoporous silica. Although polyoxometalates, like 12-tungstophosphoric acid ($H_3PW_{12}O_{40}$), possess strong acidity, polyoxometalates normally have a low surface area in the solid state and therefore, only a limited number of acid sites on the external surface are available for catalytic reactions [110].

(D) Immobilization of metals/metal complexes in mesoporous silicates

Immobilization of polynuclear molecular transition metal complexes in porous materials is also a promising method for the preparation of supported metal catalysts. Metal carbonyl complexes react with the surface silanol groups at elevated temperatures. Continuous adsorption of $Co_2(CO)_8$ on MCM-41 in a flow reactor resulted in maximum Co deposition of 20 wt%. The metal loading could be increased up to 41 wt% using the pulse deposition method [111,112]. Platinum carbonyl clusters like $[Pt_{15}(CO)_{30}](NR_4)_2$ or $[Pt_3(CO)_6]_5(NR_4)_2$ (R = methyl, ethyl, butyl, hexyl or

methylviologen) can be successfully prepared in FSM- 16 by the ‘‘Ship-in-the-Bottle’’ technique [113].

Good bimetallic hydrogenation catalysts based on MCM-41 supported Cu–Ru ($[Ru_{12}C_2Cu_4Cl_2(CO)_{32}][PPN]$) [114], Ru–Sn ($[PPN][Ru_6C(CO)_{16}SnCl_3]$) [115] and Pt–Ru ($[Ph_4P]_2$-$[Ru_5PtC(CO)_{15}]$, $[PPN]_2[Ru_{10}Pt_2C_2(CO)_{28}]$) [116], have been reported by the group of Thomas and Johnson in the hydrogenation of benzoic acid. Cu(II) acetate dimer was impregnated on MCM-48 from a copper acetate solution [117]. Tetrahedrally co-ordinated titanium is a good catalyst for alkene oxidation. Immobilization of the titanium silsesquioxane, $[\{(c\text{-}C_6H_{11})_7Si_7O_{12}\}$ Ti $(\eta^5\text{-}C_5H_5)]$, in MCM-41 has been reported [118].

The post-synthesis immobilization of metals and organometallic complexes on the surface of mesoporous silicates allows the preparation of multifunctional molecular sieves with desired catalytic properties. The processes for metal immobilization include wet impregnation [10], vapor deposition [119], treatment with $(NH_4)_2MF_6$ ($M = Si^{4+}$, Ti^{4+} etc.) [120] and metal alkoxides [121] and ion exchange with metal salts [122].

(E) Covalently anchored organo-functionalized mesoporous silicates

The advantages of inorganic-organic hybrid materials arise from the fact that inorganic components can provide mechanical, thermal or structural stability, while the organic features are more readily modified for specific applications in catalysis, separation or sensing [123]. The presence of large amount of silanol $[(\text{-O-})_3SiOH]$ groups in MCM-41 and HMS materials enables the anchoring of organic functional groups using the concept of organic functionalization in silica gel. The organic functional groups or ligands can then be used to attach different types of metal complexes with or without modification of the parent functional groups.

Organically functionalized mesoporous silicas have been prepared conveniently at room temperature [124] or at higher temperatures [125] by the co-condensation of tetraalkoxysilane ($Si(OR)_4$) and organosiloxanes (R^1-$Si(OR)_3$) in the presence of a surfactant (template) and auxiliary chemicals. Thus, it is possible to synthesize a variety of inorganic-organic hybrid materials, where the organic functional groups are attached covalently with the silica surface of MCM-41 through Si-C bonds with potential applications as catalysts. An acidic solvent extraction technique is generally used to remove the surfactant from the product to yield an

organofunctionalized ordered porous silica material [124-125]. Organo functional groups have also been introduced on the pore surface of mesoporous silica by post synthesis modification. The treatment of mesoporous silica with organosiloxane precursors produces hybrid inorganic-organic materials by hydrolysis and finally condensation of organosiloxane groups [126].

1.5 PHYSICOCHEMICAL CHARACTERIZATION

Porous materials need to be characterized to elucidate their structural features, pore architecture and catalytic behavior. A complete characterization of mesoporous molecular sieves requires information from a number of physical, chemical and spectroscopic techniques. These are XRD (X-ray diffraction), sorption, TEM (transmission electron microscopy), TG/DTG (thermogravimetry/ differential thermogravimetry), FTIR (Fourier Transform Infra Red spectroscopy), MAS NMR (Magic Angle Spinning Nuclear Magnetic Resonance Spectroscopy), TPD (temperature programmed desorption), TPR (temperature programmed reduction) and ESR (electron spin resonance spectroscopy).

(a) X-ray diffraction

Powder x-ray diffraction is used to identify the structure, phase purity, degree of crystallinity, unit cell parameters and crystallite size. It also helps in the study of the kinetics of crystallization of molecular sieves. As the powder pattern is the finger print of the molecular sieve structure, phase purity and percent crystallinity of the synthesized molecular sieve can be ascertained by comparing with the standard pattern for the molecular sieve under investigation. XRD patterns of mesoporous phases exhibit peaks in the low angle region, the most intense peak being the (100) reflection. Isomorphous substitution of a heteroatom in the framework of the molecular sieves results in changes in the unit cell parameters and unit cell volume. This is one of the ways to confirm isomorphous substitution.

(b) Adsorption measurements

Sorption capacities for probe molecules such as n-hexane, water, benzene, nitrogen etc. yield information about the hydrophilicity/hydrophobicity, pore dimensions and pore volume of the molecular sieves. The Braunauer-Emmett-Teller (BET) volumetric gas adsorption technique using N_2 or Ar is a standard method for

the determination of the surface area and pore size distribution of finely divided porous samples [127]. The relation between the amount adsorbed and the equilibrium pressure of the gas at constant temperature is defined as the adsorption isotherm. N_2-adsorption-desorption isotherms of MCM-41, MCM-48 and FSM-16 are of the type IV [128]. The steep increase in N_2 adsorption (in the p/p_0 range of 0.2 to 0.4) corresponds to capillary condensation within uniform pores. The sharpness and the height of this step reflect the uniformity of the pore size and the pore volume, respectively. The wall thickness of hexagonally packed silicates (MCM-41, HMS and SBA-15) is determined as the difference between the repeat distance (unit cell parameter) $a_0 = 2d_{100}/\sqrt{3}$ (from XRD) and the Horvath-Kawazoe [129] pore diameter using N_2 adsorption.

(c) Nuclear magnetic resonance (NMR)

High–resolution magic angle spinning nuclear magnetic resonance (NMR) spectroscopy in the solid state is a powerful complementary method to diffraction techniques for the investigation of zeolites and mesoporous molecular sieve structures [130]. The main fields of application are: (i) Evaluation of the environment of the silicon framework atoms, (ii) framework n_{Si}/n_{Al} ratio of the mesoporous molecular sieves, (iii) silicon and aluminium ordering, (iv) identification of framework and non-framework aluminium, (v) incorporation of metals into mesoporous molecular sieves, (vi) determination of acidity of hydroxyl groups.

(d) UV-Visible spectroscopy

Diffuse reflectance UV-Vis spectroscopy is known to be a very sensitive and useful technique for the identification and characterization of the metal ion coordination and its existence in the framework or extra-framework position of metal containing molecular sieves. It gives information about the d-orbital splitting through d-d transitions and the ligand-metal interaction through the ligand to metal charge-transfer transitions. The position of "ligand-to-metal charge transfer" (L→M) band depends on the ligand field symmetry surrounding the metal center and the electronic transitions from ligand-to-metal require higher energy for a tetra-coordinated metal ion than for a hexa-coordinated one.

(e) Fourier transform infrared (FTIR) spectroscopy

FTIR spectroscopy in the framework region (400-4000 cm^{-1}) provides additional information about the structural details of the zeolite and other molecular sieves. IR spectroscopy is the most convenient method for the characterization of heteropolyanions. Their characteristic bands can distinguish Keggin, Dawson and Lacunary heteropolyanions. [131]. Flanigen [132] has discussed the IR spectra of the hydroxyl groups of zeolites. The IR spectrum in the range 200-1300 cm^{-1} is used to characterize and to differentiate framework structures of different molecular sieves. Isomorphous substitution of metal ions such as B, Fe, Ga etc, for Al and Ti, Ge, V for Si also lead to shift in band positions. An additional band at 960 cm^{-1} may be observed for Ti or V substituted molecular sieves. The IR bands around 3600-3700 cm-1 confirm the presence of the silanol groups [133] or bridged hydroxyl groups in the molecular sieves and their Brönsted acidities can be compared. While only the Brönsted acid sites may be investigated with and without probe molecules, acidic Lewis sites, cations and basic sites can be identified and quantitatively determined only with the help of probes. Probe molecules frequently employed are typically pyridine, substituted pyridine, ammonia and amines for acidic centres and carbon dioxide or pyrrole for basic sites.

(f)Electron paramagnetic resonance (EPR) spectroscopy

Electron Spin Resonance (ESR) spectroscopy is the resonance absorption of electromagnetic (microwave) radiation by magnetically split states of unpaired electrons. In the case of some paramagnetic molecules, the formation of a charge-transfer complex can be determined by this technique. This technique provides valuable information on the redox site and the intermediate species formed in the catalytic reaction. With the help of this information, it is easier to focus on the status of framework and nonframework species formed in the transition metal incorporated molecular sieves.

Transition metal ions can be investigated by ESR spectroscopy. Some of the ions that have been well studied are: d^1 ions: Mo^{5+}, V^{4+}, Ti^{3+}, Cr^{5+}, W^{5+}, d^5 ions: Fe^{3+}, Mn^{2+}, and d^9 ions: Cu^{2+}, Ni^{+}, Ag^{+}. These ions may either be incorporated within a host lattice at interstitial or substitutional positions or deposited at the surface of a catalyst or at cationic positions of a zeolite. The location and unusual oxidation states of these metal ions in zeolites are revealed by ESR [134]. The formation mechanisms

of MCM-41, MCM-50 [135] and SBA-15 [136] have been studied by in situ EPR spectroscopy. ESR studies of Mn-containing MCM-41 have revealed the presence of Mn(II) species in both extraframework and framework sites [137]. The presence of different oxidation states of vanadium ions in as-synthesized and calcined MCM-41 has been characterized by ESR spectroscopy [76,138]. ESR spectroscopy has also been used to study isomorphous substitution of metal ions like Ni(I), Fe(III) and Cr(III) in MCM-41 [139]. ESR characterization of Ti(III) species obtained by reduction of Ti(IV) by γ-irradiation and thermal activation has been found to be useful in characterizing the different Ti-sites in the structure of Ti-MCM-41 [140].

(g) Temperature programmed techniques

(i) Temperature programmed desorption of ammonia (TPDA)

This technique can be used to characterize the acid sites present in solids such as zeolites and mesoporous materials. Probe molecules like ammonia or pyridine are commonly used for acidity determination. Ammonia is frequently used because of its size, stability and strong basic strength [141]. First the sample is contacted with the base to neutralize the acid sites present. Then the temperature is raised at a constant rate and the amount desorbed at different temperatures is recorded.

In a TPD spectrum, one or more peaks may be observed, the ones at low temperatures corresponding to NH_3 desorbing from the weaker acidic sites and the ones at higher temperatures corresponding to the stronger acidic sites. The areas under these peaks give information about the amount of acidic sites of different acidity, whereas the peak (–maximum–) temperatures give information about the relative acid strengths [142]. The TPD curves are deconvoluted into individual peaks and the areas under the peaks are converted into meq NH_3 per g catalyst based on injection of known volumes of NH_3 at similar conditions.

(ii) Temperature programmed reduction (TPR) by hydrogen

TPR determines the number of reducible species present in the catalyst and reveals the temperature at which the reduction occurs. In a TPR experiment, the catalyst material is placed in a fixed bed reactor in a flow of a reducing gas mixture (typically, argon or nitrogen containing a few volume percent of hydrogen) and subjected to a linear temperature ramp. The consumption of H_2 by adsorption/reaction

is continuously measured by monitoring the change in composition of the gas mixture after passing through the reactor. The degree of reduction can be calculated from the amount of H_2 consumed.

(h) Scanning electron microscopy (SEM)

This is an important tool for morphological characterization of microporous and mesoporous molecular sieve materials. Different types of morphology of the synthesized materials as well as the presence of any amorphous phase in the samples can be identified using this technique.

(i) Transmission electron microscopy (TEM)

TEM is used to elucidate the pore structure of mesoporous molecular sieves. It provides topographic information of materials at near atomic resolution. However, the exact analysis of pore sizes and thickness of the pore walls is difficult and not possible without additional simulations because of the 'focus' problem. HRTEM has been successfully used to examine the microstructural feature of mesoporous molecular sieves [143]. In addition to structural characterization, it can also be used to detect the location of metal clusters and heavy cations in the framework.

(j) Thermal analysis

Thermal analysis is widely used to study the structural stability of as-synthesized forms of molecular sieves. It provides information about the temperature required for the removal of adsorbed water, decomposition of the occluded organic cations in the pores and channels of molecular sieves and dehydroxylation at higher temperatures to produce Lewis acid sites. Data obtained from TG, DTA and DTG study are useful in evaluating the thermal properties of molecular sieves [144]. The temperature at which an exotherm appears in the DTA after the loss of water molecules, gives helpful information about the temperature required to remove the template molecules from the pores of the molecular sieves during calcination. Phase transformations are detected by differential thermal analysis (DTA) at higher temperatures.

1.6 CATALYTIC APPLICATIONS

The high surface area and large pore size of MCM-41 and SBA-15 favour high dispersion of the active species and provide easy accessibility to large feed stock molecules making them attractive supports and catalysts. Other potential applications for these novel materials are in sorption, separations, polymer chemistry etc. Mesoporous materials with narrow pore size distribution may in future replace zeolite catalysts in some commercial applications and in a few research applications they have already been reported to possess superior performance compared to conventional microporous zeolites or amorphous silica–alumina catalysts. To date, several mesoporous materials with significant catalytic properties have been synthesized. Some of the reactions studied on different silicate and metallosilicate molecular sieves are listed in Table 1.4.

Table 1.4 Catalytic applications of mesoporous molecular sieve catalysts

No.	Catalyst	Reaction [Reference]
1	Al-MCM-41	Alkylation of 2,4-di-ter-butyl phenol with cinnamyl alcohol [18]
2.	Al-MCM-41	Alkylation of unsubstituted phenol with methanol [145]
3.	Ti, V, Cr, Mn, Fe or Co- MCM-41	Liquid phase oxidation of cyclohexane [146]
4	MCM-41	Cracking of palm oil and asphalthene [147]
5.	Sulfated-ZrO_2-on MCM-41	Cumene and 1,3,5-triisopropylbenzene cracking [148]
6.	Sulfated-ZrO_2-on SBA-15	Condensation of tert-butanol and methanol to yield MTBE [103]
7.	Siliceous MCM-41	Acetalization of cyclohexanone with methanol [149]
8.	Heteropolyacids /MCM-41	Cracking of 1,3,5-triisopropylbenzene [109 (d)]
9.	$AlCl_3$-grafted MCM-41	Benzene alkylation with linear 1-olefins with a chain length of C_6 to C_{16} [150]
10.	Ga/MCM-41, Fe/MCM-41, Al-MCM-41, La-MCM-41	Friedel–Crafts alkylation of benzene with benzyl chloride in liquid phase [151]
11.	Siliceous/Al-substituted MCM-41	Acetalization of heptanal, 2-phenylpropanal or diphenylacetaldehyde with trimethyl orthoformate [152]
12.	Al-MCM-41	Acetalization of heptanal with methanol to produce jasminaldehyde [153]
13.	Al-substituted mesoporous silica / $Al(OPri)_3$ grafted	Diels–Alder reaction: cyclopentadiene + crotonaldehyde, cyclopentadiene and methylacrylate [154]

14.	Al-MCM-41	Beckmann rearrangement of cyclohexanone oxime to give ε-caprolactam [155]
15.	Sn-MCM-41	Prins condensation of β-pinene [156]
16.	Zr-1-propoxide grafted SBA-15	Meerwein–Ponndorf–Verley (MPV) reduction of a carbonyl substrate with a sec. alcohol. [157]
17.	Cs /Al-MCM-41	Transesterification of triolein with glycerol [158]
18.	Cs/MCM-41	Etherification of glycerol to di- or triglycerol [159]
19.	Ce/ MCM-41	Dehydration of cyclohexanol to cyclohexene [160]
20.	Ti -MCM-41	Selective oxidations [161]
21.	(Tert-butoxy)siloxy Ti-compds on MCM-41 and SBA-15.	Cyclohexene epoxidation to cyclohexene oxide [162]
22.	Fe/SBA-15	Oxidation of alkanes, alkenes and arenes [163]
23.	Mn /MCM-41	Epoxidation of stilbene and diphenylmethane [164]
24.	Fe, Cr, Co and Mo containing MCM-41	Oxidation of cyclohexane with H_2O_2 or TBHP [165]
25.	VOx/ MCM-41	Hydroxylation of benzene to phenol [166]
26.	Sn(IV)/ MCM-41	Bayer–Villiger oxidation of adamantanone [167]
27.	V-MCM-41	Dehydrogenation (ODH) of alkanes [168]
28.	V-MCM-41 and V-MCM-48	Partial oxidation of methane by air [169]
29.	V-MCM-41,V/SBA-15, Mo/ SBA-1	Formaldehyde from methanol [170]
30.	Nb-doped MCM-41	Methanol oxidation [171]
31.	Ga_2O_3 and In_2O_3, on MCM-41	Benzylation of benzene with benzyl chloride [172]
32.	MoS_2/MCM-41, Ni–WS_2/SBA-15	HDS of dibenzothiophene and hydrogenation of toluene [173]
33.	Fe_2O_3/ MCM-41	Oxidation of SO_2 [174]
34.	MCM-41 supported Ru-containing bimetallic catalysts	Hydrogenation of benzoic acid to cyclohexane carboxylic acid [175]
35.	Pd-grafted on mesoporous silica	Heck type carbon–carbon bond formation [176]
36.	Co/MCM-41	CO hydrogenation [177]
37.	Gold /MCM-41	Oxidation of CO and H_2 [178]
38.	Pt and Pd on CMK-1	Hydrogenation of nitrobenzene, 2-ethylanthraquinone [179]
39.	Fe/Al-MCM-41 Fe/Al-HMS	Reduction of NO with NH_3 [180]
40.	MCM-41, MCM-48 and SBA-15	Immobilization of trypsin [181]
41.	Mo-complex on MCM-41	Cyclooctene epoxidation [182]
42.	Ru, Rh and Pd supported mesoporous silica	Asymmetric hydrogenations catalyzed by diamine complexes [183]
43.	A chiral copper(II) bisoxazoline anchored to MCM-41	Asymmetric Diels–Alder or Friedel–Crafts reactions [184]

44.	Alkylammonium grafted MCM-41	Knoevenagel condensations, Michael addition and condensation [185]
45.	Immobilization of TEMPO(2,2,6,6 tetramethyl 1-piperidinyloxy) on the MCM-41	Selective oxidation of primary alcohols to either carboxylates or aldehydes [186]

1.7 SCOPE OF THE THESIS

Well ordered siliceous hexagonal mesoporous materials like MCM-41 [7] and SBA-15 [8] have attracted much interest because of their high surface area, large pore volume and well-defined pore size. These materials possess potential applications in catalytic reactions involving bulky molecules in the refining, fine chemical and pharmaceutical industries. MCM-41 has a low hydrothermal stability because its inorganic oxide wall is disordered at the molecular level. SBA-15 materials have higher hydrothermal stability than MCM-41 due to larger wall thickness; they also possess larger pores than MCM-41. Different metal loaded MCM-41 and SBA-15 catalysts have been reported to be useful in acid catalysis, base catalysis and redox catalysis. Though the incorporation of heteroatoms like Al, Ti and Sn during synthesis is rather easy in MCM-41, it is difficult in SBA-15 due to the highly acidic medium used for its synthesis. Hence post synthesis methods are generally used for metal incorporation in SBA-15 [187].

In recent years, environmental considerations have directed the need for safe solid catalysts and greener processes. In this context, a number of reactions such as molecular rearrangements, alkylation, acylation, condensation and selective oxidation reactions that are traditionally carried out using mineral acid catalysts and stoichiometric oxidants need to be practiced over safe solid catalysts. It is therefore proposed to investigate (in this work) the use of mesoporous catalysts based on MCM-41 and SBA-15 in a number of reactions of industrial importance.

1.8 OBJECTIVES OF THE PRESENT INVESTIGATION

The objectives of the present work are:

1. Preparation of ordered hexagonal mesoporous catalysts such as MCM-41, Al-MCM-41, Ga-MCM-41, Sn-MCM-41, Fe-MCM-41, V-MCM-41, SBA-15, Al-SBA-15 and PW/SBA-15 through hydrothermal or post synthesis procedures.

2. Characterization of the above mesoporous catalysts, by different physicochemical techniques such as XRD, IR, UV-Vis, NMR, TPD, TPR, ESR and adsorption studies.
3. Evaluating the catalytic activity of these materials in a number of typical acid catalyzed reactions such as Claisen rearrangement, Beckmann rearrangement, alkylation, acylation, Prins condensation and esterification.
4. To evaluate the activity of some of the metallosilicate mesoporous materials in a typical selective oxidation reaction.
5. To evaluate the influence of different reaction parameters and to optimize the reaction conditions for the above reactions.

A brief description of the specific reactions chosen in this study is given below:

(a) Claisen rearrangement: This involves the conversion of allyl phenyl ethers to the corresponding *o*-allylphenols by heating the ethers at an elevated temperature (> 473 K). In the present work, it is proposed to use solid acid catalysts (e.g. Al-MCM-41) at lower temperatures (< 383 K) to catalyze the rearrangement of allyl phenyl ether (APE). Also, the reaction over an acid catalyst is expected to lead to cyclization of the product (*o*-AP) into a benzofuran derivative. [188-189].

(b) Beckmann rearrangement: ε-caprolactam, used in the manufacture of Nylon-6 is normally prepared by the liquid phase Beckmann rearrangement of cyclohexanone oxime [190]. In the present work, the rearrangement will be carried out over benign solid acid catalysts (PW/SBA-15, Al-SBA-15 and Al-MCM-41) in the vapor phase.

(c) Friedel-Crafts acylation: This is a convenient route for the preparation of aromatic ketones [191(a)]. The use of a solid acid eliminates the problems associated with the classical Friedel-Crafts catalysts ($AlCl_3$, BF_3, HF etc.), namely, poor selectivity for the products, use of more than stiochiometric amount of catalysts and destruction of the catalyst during work-up. It is proposed to investigate the acylation of anisole with acetic anhydride over a number of acidic mesoporous catalysts.

(d) Alkylation of phenol: Many alkylphenols used in the manufacture of drugs, pharmaceuticals, dye stuffs, pesticides paints and plastics are prepared commercially by alkylation of phenol with alkylating agents. Among the several isopropylation products of methylphenols, the m-cresol derived thymol is most important because it is a precursor of menthol [191(b)], used in perfumery. In the present work, m-cresol

isopropylation is investigated over modified mesoporous MCM-41 and SBA-15 catalysts.

(e) Esterification: p-Cresylphenyl acetate has wide applications in the fragrance industry, beauty care and in the manufacture of floral soaps [192]. Esterification of p-cresol with phenylaceticacid is now studied over PW/SBA-15 catalysts.

(f) Prins condensation: Nopol is an optically active bicyclic primary alcohol, useful in the agrochemical industry for the synthesis of pesticides, soap fragrances and is prepared by the Prins condensation of β-pinene with paraformaldehyde [193]. In the present work, the use of solid acid catalysts such as Sn, Fe, V and Al modified MCM-41 and Al-SBA-15 catalysts will be investigated for the above Prins condensation reaction.

(g) Selective oxidation: Oxidation of ethylbenzene in the liquid phase will be studied over Sn, Fe and V modified MCM-41 catalysts using H_2O_2 and TBHP as the oxidants. Both H_2O_2 and TBHP are environmentally safe oxidants. Besides, the use of solid catalysts should enable the easy work up of the reaction products.

1.9 OUTLINE OF THE THESIS

The thesis is divided into seven chapters:

Chapter I: Introduction

Chapter 1 presents a general introduction to the importance of environmentally friendly solid acid catalysts, such as those based on MCM-41 and SBA-15. It also summarizes the available literature on mesoporous molecular sieves. It describes the synthesis strategies, the role of templating surfactants and the mechanisms proposed for their synthesis. The characterization techniques used to study mesoporous materials are described in brief. Some of the reported catalytic applications of ordered mesoporous materials are listed.

Chapter II: Synthesis

Chapter 2 presents a general introduction to the different synthetic methods used in the preparation of ordered mesoporous materials, such as MCM-41 and SBA-15, and their modification. It also presents a list of the chemicals and materials used in the synthesis of the different mesoporous catalysts. The chapter also describes the procedures used in the preparation of different metal incorporated MCM-41 samples

such as Al, Ga, Sn, Fe, and V-MCM-41 with different metal loadings by hydrothermal synthesis. The preparation of SBA-15 catalysts such as Al-SBA-15 and PWA/SBA-15 by post synthesis methods based on impregnation techniques is also described.

Chapter III: Characterization

Chapter 3 presents the results of the characterization studies on the mesoporous catalysts reported in chapter 2. AAS, ICP and XRF methods are used for the estimation of the different metals loaded on MCM-41 and SBA-15. TEM and SEM techniques are used to determine the morphology of the crystalline materials. N_2- sorption studies are used for the determination of surface area, pore diameter and pore volume. Powder X-ray diffraction technique is used to identify the structure and unit cell parameters. Temperature programmed desorption (TPD) of ammonia is used for acidity measurements of the samples. ESR studies are performed over Fe and V-MCM-41 catalysts. Solid state ^{29}Si MAS NMR spectra are recorded for MCM-41 and SBA-15 catalysts. ^{27}Al MAS NMR studies were performed over MCM-41 and SBA-15 catalysts to probe the nature of Al. ^{31}P NMR spectra are recorded for PW/SBA-15 catalysts. UV-Vis analysis is done for different MCM-41 type catalysts. The results of the above studies are discussed critically to arrive at the characteristics of the different catalysts.

Chapter IV: Claisen and Beckmann rearrangements

Chapter 4 is divided into two parts. Part 1 discusses the study of MCM-41 and SBA-15 catalysts in the Claisen rearrangement of allyl phenyl ether (APE). The effect of various reaction and catalyst parameters on conversion and product selectivity is reported in detail over Al-MCM-41 catalysts [189]. A kinetic analysis of the formation of the different products under various reaction conditions is also presented. The reaction kinetics is analyzed assuming a first order consecutive reaction. *o*-AP is produced initially, which then undergoes cyclization to form 2, 3-dihydro-2-methylbenzofuran [188]. Catalyst activity and product selectivity are examined for a series of Al-MCM-41 catalysts with different Al-contents. A comparative study of the activities of the Al-MCM-41, Ga-MCM-41, Al-SBA-15 and PW/SBA-15 catalysts in the Claisen rearrangement of APE is also reported.

Part 2 discusses the vapor phase Beckmann rearrangement of cyclohexanone oxime to ε-caprolactam [190] over modified MCM-41 and SBA-15 catalysts. The effects of various reaction parameters such as temperature, time on stream, use of different solvents, contact time and oxime concentration on transformation of oxime is studied in detail over Al-SBA-15 catalysts with different Si/Al ratios. A comparison of the activities of the Al-SBA-15, PW/SBA-15, Al-MCM-41, Ga-MCM-41, Sn-MCM-41, Fe-MCM-41 and V-MCM-41 catalysts is also made.

Chapter V: Acylation and alkylation

Chapter 5 is also divided into two parts. Part 1 describes the Friedel-Crafts acylation of anisole with acetic anhydride in the liquid phase over phosphotungstic acid (PW) supported on SBA-15 in the temperature range of 333-373 K**.** The major product of the reaction is p-methoxyacetophenone (*p*-MAP) with a small amount of o-methoxyacetophenone (*o*-MAP). The effect of catalyst acidity on the Friedel-Crafts acylation is investigated using PW/SBA-15 catalysts containing different amounts (10-40 wt. %) of phosphotungstic acid. The activity of Al-MCM-41 and Al-SBA-15 samples is compared.

Part 2 discusses the vapor phase isopropylation of m-cresol to yield thymol over MCM-41 and SBA-15 based catalysts. The influence of different reaction parameters such as temperature, reactant mole ratio and space velocity is investigated over these catalysts. The catalytic activity of Al-SBA-15 is compared with Al-MCM-41 and PW loaded SBA-15 catalysts.

Chapter VI: Other organic transformations

Chapter 6 contains 3 parts reporting the application of the mesoporous catalysts in the esterification of p-cresol, Prins condensation and the oxidation of ethylbenzene.

Part 1 presents the esterification [192] of p-cresol with phenyl acetic acid to p-cresylphenyl acetate over PW loaded SBA-15 catalysts. The influence of various reaction parameters such as temperature, reactant mole ratio, catalyst amount and different PW loading is studied for PW/SBA-15 catalysts in the esterification of p-cresol with phenyl acetic acid. The reaction is 100 % selective towards p-cresylphenyl acetate.

Part 2 is a study of Prins condensation [193] of β-pinene with paraformaldehyde over metal containing MCM-41 and Al-SBA-15 catalysts to yield Nopol (6, 6-dimethylbicyclo-(1, 1, 3)-hept-2-ene-2-ethanol). Sn-MCM-41 catalysts show higher conversion and selectivity for Nopol compared to the other mesoporous catalysts, Fe-MCM-41, V-MCM-41, Ga-MCM-41, Al-MCM-41 and Al-SBA-15.

Part 3 presents a brief study of the oxidation of ethylbenzene in the liquid phase over MCM-41 modified catalysts, such as V-MCM-41, Fe-MCM-41 and Sn-MCM-41. The influences of various reaction parameters such as temperature, oxidizing agent, reactant mole ratio and catalyst amount on conversion and product selectivity is reported. The major products of the reaction are acetophenone, 1-phenylethanol and benzaldehyde. A small amount of phenyl acetaldehyde is also produced.

Chapter VII: Summary and conclusions

Chapter 7 presents an overall summary of the work done and describes the major findings of the studies.

1.10 REFERENCES

1. K.S.W. Sing, D.H. Everett, R.A.W. Haul, L. Moscou, R. A. Pierotti, J. Rouquerol, T. Siemieniewska, Pure Appl. Chem. 57 (1985) 603.
2. F. Schuth, K. Sing, J. Weitkamp, "Handbook of Porous Solids", vol. I–V, Wiley-VCH, Weinheim. (2002).
3. S. I. Zones., M.E. Davis, Curr. Opin. Solid State Mater. Sci.1 (1996) 107.
4. C. C Freyhardt, M. Tsapatsis, R. F, Lobo K. J. Balkus, M.E. Davis, Nature 381 (1996) 295.
5. J.S. Beck, J.C. Vartuli, Curt. Opin. Solid State Mater. Sci.1 (1996) 76.
6. J. M. Garces, Adv. Mater. 8 (1996) 434.
7. C.T. Kresge, M. E. Leonowicz, W. J. Roth, J. C. Vartuli, J.S. Beck, Nature 359 (1992) 710.
8. D. Zhao, J. Feng, Q. Huo, N. Melosh, G. H. Fredrickson, B. F. Chmelka, G. D. Stucky, Science 279 (1998) 548.
9. A. Corma, M. S Grande., V. Gonzalez Alvaro, A. V. Orchilles, J. Catal. 159 (1996) 375.
10. A. Corma, A. Martinez, V. Martinez Sofia, J. B. Monton, J Catal. 53 (1995) 25.
11. A. Corma, V. Fornes, M. T. Navarro, J. Perez Pariente, J. Catal. 148 (1994) 569.
12. (a) V. Chiola, J.E. Ritsko, C.D. Vanderpool, US Patent No. 3 556725, 1971. (b)F. Di Renzo, H. Cambon, R. Dutartre, Micropor. Mater. 10 (1997) 283.
13. J.S. Beck, C.T.-W. Chu, I.D. Johnson, C.T. Kresge, M.E. Leonowicz, W.J. Roth, J.W. Vartuli, WO Patent 91/11390 (1991).
14. J.S. Beck, J.C. Vartuli, W.J. Roth, M.E. Leonowicz, C.T. Kresge, K.D. Schmitt, C.T.W. Chu, D.H. Olson, E.W. Sheppard, S.B. McCullen, J.B. Higgins, J.L. Schlenker, J. Am. Chem. Soc. 114 (1992) 10834.
15. T. Yanagisawa, T. Shimizu, K. Kuroda, C. Kato, Bull. Chem. Soc. Jpn. 63 (1990) 988.
16. S. Inagaki, Y. Fukushima, K. Kuroda, J. Chem. Soc. Chem. Commun. (1993) 680.
17. S. Inagaki, A. Koiwai, N. Suzuki, Y. Fukushima, K. Kuroda, Bull. Chem. Soc. Jpn. 69 (1996) 1449.
18. E. Armengol, M. L. Canto, H. Garcia, M. T. Navarro. J. Chem. Soc. Chem.

Commun. (1995) 519.

19. E. Armengol, A. Corma, H. Garcia, J. Primo. Appl. Catal. A: Gen. 126 (1995) 391.
20. E. Armengol, A. Corma, H. Garcia, J. Primo. Appl. Catal. A: Gen. 129 (1997) 411.
21. E. A. Gunnewegh, S. S. Gopie, H. Van Bekkum. J. Mol. Catal. A: Chem. 106 (1996) 151.
22. K. R. Kloestra and H. VanBekkum. J. Chem. Res. 1 (1995) 26.
23. M. J. Climent, A. Corma, S. Iborra, M. T. Navarro, J. Primo. J. Catal. 161 (1996) 783.
24. (a) M. J. Climent, A. Corma, S. Iborra, S. Miquel, J. Primo, F. Ray. J. Catal. 183 (1999) 76. (b) A. Corma. Chem. Rev. 95 (1995) 559.
25. P. T. Tanev and T. J. Pinnavaia, Science 267 (1995) 865.
26. J. P. Blitz and C. P. Little, "Fundamentals and Applied Aspects of Chemically Modified Surfaces", Royal Society of Chemistry, Cambridge (1999).
27. L. A. Ciolino and J. G. Dorsey. J. Chromato. A 675 (1994) 29.
28. W. M. VanRhijn, D. E. DeVos, B. F. Sels, W. D. Bossaert, P. A. Jacobs. Chem. Commun. (1998) 317.
29. W. D. Bossaert D. E. DeVos, W. M. VanRhijn, J. Bullen, P. J. Grobet, P. A. Jacobs. J. Catal. 182 (1999) 156.
30. J. J. Chiu, D. J. Pine, S. T. Bishop, B. F. Chmelka, J. Catal. 221 (2004) 400.
31. A. Tuel and L. G. Hubert-Pf alzgraf, J. Catal. 217 (2003) 343.
32. (a) Y. Yue, A. Gedeon, Jean-Luc Bonardet, N. Melosh, Jean Baptise D'Espinese, J. Fraissard, Chem. Commun. (1999) 1967; (b) A. Gedeon, A. Lassoued, J. L. Bonardet, J. Fraissard, Micropor. Mesopor. Mater. 44-45 (2001) 801.
33. Wen-Hua Zhang, J. Liu, Bo Han, M. Li, J. Xiu, P. Ying, Can Li, Chem. Mater. 14 (2002) 3413.
34. A. Vinu, G. Satishkumar, K. Ariga, V. Murugesan, J. Mol. Catal. A: Chem. 235 (2005) 57.
35. Qi-ying Liu, Wen-Liang Wu, J. Wang, Xiao-Qian Ren, Yan- Ru Wang, Micropor. Mesopor. Mater. 76 (2004) 51.
36. X. Wang, Chin-Chang Chen, Shih- Yuan Chen, Yun Mou, Soofin Chang, Appl.

Catal. A: General. 281 (2005) 47.

37. Jun Wang and Hai- Ou Zhu, Catal. Lett. 93, 3-4 (2004) 209.
38. (a) A. Monnier, F. Schuth, Q. Huo, D. Kumar, D. Margolese, R.S. Maxwell, G. Stucky, M. Krishnamurty, P. Petroff, A. Firouzi, M. Janicke, B. Chmelka, Science 261 (1993) 1299., (b) Q. Huo, D. Margolese, U. Ciesla, P. Feng, T. Gier, P. Sieger, R. Leon, P.M. Petroff, U. Ciesla, F. Schuth, G. Stucky, Nature 368 (1994) 317. (c) Q. Huo, D. Margolese, U. Ciesla, D. Demuth, P. Feng, T. Gier, P. Sieger, A. Firouzi, B. Chmelka, F. Schuth, G.D. Stucky, Chem. Mater. 6 (1994) 1176.
39. G.S. Attard, J.C. Glyde, C.G. Goltner, Nature 378 (1995) 366.
40. (a) R. Ryoo, S.H. Joo, S. Jun, J. Phys. Chem. B 103 (1999) 7743
41. (a) S. Che, A.E. Garcia-Bennett, T. Yokoi, K. Sakamoto, H. Kunieda, O. Terasaki, T. Tatsumi, Nature 2 (2003) 801. (b) A.E. Garcia-Bennett, O. Terasaki, S. Che, T. Tatsumi, Chem. Mater. 16 (2004) 813.
42. Q. Huo, R. Leon, P.M. Petroff, G.D. Stucky, Science 268 (1995) 1324.
43. P.T. Tanev, M. Chibwe, T.J. Pinnavaia, Nature 368 (1994) 321.
44. S.A. Bagshaw, E. Prouzet, T.J. Pinnavaia, Science 269 (1995) 1242.
45. E. Prouzet, T.J. Pinnavaia, Angew. Chem. Int. Ed. 36 (1997) 516.
46. D. Zhao, Q. Huo, J. Feng, B.F. Chmelka, G.D. Stucky, J. Am. Chem. Soc. 120 (1998) 6024.
47. D.M. Antonelli, J.Y. Ying, Angew. Chem. Int. Ed. 35 (1996) 426.
48. D.M. Antonelli, A. Nakahira, J.Y. Ying, Inorg. Chem. 35 (1996) 3126.
49. D.M. Antonelli, J.Y. Ying, Chem. Mater. 8 (1996) 874.
50. S.H. Joo, S.J. Choi, I. Oh, J. Kwak, Z. Liu, O. Terasaki, R. Ryoo, Nature 412 (2001) 169.
51. Akira Taguchi, Ferdi Schuth, Micropor. Mesopor. Mater. 77 (2005) 1.
52. D. Myers, “Surfactant Science and Technology”, VCH: New York, (1992).
53. M. J. Lawrence, Chem. Soc. Rev. (1994) 417.
54. P. Fromherz, Chem. Phys. Lett. 77 (1981) 460.
55. C.Y. Chen, H. Y. Li, M. E. Davis, Micropor. Mater. 2 (1993) 27.
56. A. Steel, S. W. Carr, M. W. Anderson, J. Chem. Soc. Chem. Commun. (1994) 1571.
57. (a) C.T. Kresge, M.E. Leonowicz, W.J. Roth, and J.C. Vartuli, U.S. Patent,

5,098,684 (1992). (b) J.S. Beck, , C.T. Chu, I.D. Johnson,., C.T. Kresge, M.E. Leonowicz, , W.J. Roth., J.C. Vartuli, U.S. Patent, 5, 108, 725 (1992). (c) J.S. Beck, D.C. Calabro, S.B. McCullen, B.P. Pelrine, K.D. Schmitt, J.C. Vartuli, U.S. Patent, 5, 145, 816 (1992). (d) J.S. Beck, C.T. Kresge, M.E. Leonowicz, W.J. Roth, J.C. Vartuli, U.S. Patent, 5, 264, 203 (1993). (e) J.C. Vartuli, C.T. Kresge, M.E. Leonowicz, A.S. Chu, S.B. McCullen, I.D. Johnson, E.W. Sheppard, Chem. Mater. 6 (1994) 2070.

58. C.F. Cheng, H. He, W. Zhou, J. Klinowski, Chem. Phys. Lett. 244 (1995) 117.
59. A. Firouzi, F. Atef, A.G. Oertli, G.D. Stucky, B.F. Chmelka, J. Am. Chem. Soc. 119 (1997) 3596.
60. S. A. Bagshaw, S.A. Prouzet, T. J. Pinnavaia, Science 269 (1995) 1242.
61. D.H. Olson, G.D. Stucky, J. C. Vartuli, U.S. Patent, 5, 364, 79 (1994).
62. K. Flodstrom, V. Alfredsson, Micropor. Mesopor. Mater. 59 (2003) 167.
63. P. Kipkemboi, A. Fogden, V. Alfredsson, K. Flodstrom, Langmuir 17 (2001) 5398**.**
64. A. Tuel, S. Gontier, Chem. Mater. 8 (1996) 114.
65. A. Sayari, I. Moudrakovaski, C. Danumah, C.I. Ratcliffe, J.A. Ripmeester, K.F. Preston, J. Phys. Chem. 99 (1995) 16373.
66. U. Oberhagemann, I. Topalovic, B. Marler, H. Gies, Stud. Surf. Sci. Catal. 98 (1995) 17.
67. S. Liu, H. He, Z. Luan, J. Klinowski, J. Chem. Soc. Faraday Trans.92 (1996) 2011.
68. C.F. Cheng, J. Klinowski, J. Chem. Soc. Faraday Trans. 92 (1996) 289.
69. C.F. Cheng, H.. He, W. Zhou, J. Klinowski, L.F. Sousa Goncalves, L.F. Gladden, J. Phys. Chem. 100 (1996) 390.
70. Z.Y. Yuan, S.H. Liu, T.H. Chen, J.Z Wang, H.X. Li, J. Chem. Soc. Chem. Commun. (1995) 973.
71. J.L. Casci, Stud. Surf. Sci. Catal. 85 (1994) 329.
72. A. Sayari, Chem. Mater. 8 (1996) 1840.
73. C.T. Kresge, M.E. Leonowicz, W.J. Roth, J.C. Vartuli, U.S. Patent, 5, 250, 282 (1993).
74. A. Corma, M.T. Navarro, J. Perez-Pariente, J. Chem. Soc. Chem. Commun. (1994) 147.

75. K.M. Reddy, I.L. Moudrakovski, A. Sayari, J. Chem. Soc. Chem. Commun. (1994) 1059.
76. Z. Luan, J. Xu, H. He, J. Klinowski, L. Kevan, J. Phys. Chem. 100 (1996) 19595.
77. A. Corma, M.T. Navarro, Perez-Pariente, F. Sanchez, Stud. Surf. Sci. Catal. 84 (1994) 69.
78. T.J. Pinnavaia, P.T. Tanev, J. Wang, W. Zhang, Mater. Res. Soc. Symp. Proc. 371 (1995) 53.
79. P.T. Tanev, M. Chibwe, T.J. Pinnavaia, Nature 368 (1994) 317.
80. J.S. Reddy, P. Liu, A. Sayari, Appl. Catal. A: Gen. 148 (1996) 7.
81. W. Zhang, T.J. Pinnavaia, Catal. Lett. 38 (1996) 261.
82. W. Zhang, J. Wang, P.T. Tanev, T.J. Pinnavaia, Chem. Commun. (1996) 979.
83. N. Ulagappan, C.N.R. Rao, J. Chem. Soc. Chem. Commun. (1996) 1047.
84. D. Zhao, D. Goldfarb, J. Chem. Soc. Chem. Commun. (1995) 875.
85. D.H. Olson, G.D. Stucky, J.C. Vartuli, U.S. Patent 5, 364, 797 (1994).
86. L. Mercier, T.J. Pinnavaia, Adv. Mater.9 (1997) 500.
87. A.Cauvel, G. Renard, D. Brunel, J. Org. Chem. 62 (1997) 749.
88. T. Maschmeyer, F.,Rey, G.,Sanker, J.M. Thomas, Nature 378 (1995) 159.
89. R. Ryoo, S. Jun, J.M. Kim, J. Chem. Soc. Chem. Commun. (1997) 2225.
90. S. Song, K.M. Reddy, Appl. Catal. A: Gen. 176 (1999) 1.
91. J. Okamura, S. Nishiyama, S. Tsuruya, M. Masai, J. Mol. Catal. A: Chem. 135(1998) 133.
92. K.L. Kloestra, H. van Bekkum, Stud. Surf. Sci. Catal. 105 A (1997) 431.
93. K.L. Kloestra, H. van Bekkum, J. Chem. Soc. Faraday Trans. 93 (1997) 1211.
94. Corma, A., Martinez, A., Martinez-Soria, V., J. Catal. 169 (1997) 480.
95. L.Y. Chen, Z. Ping, G.K. Chuah, S. Jaenicke, G. Simon, Micropor. Mesopor. Mater. 27 (1999) 231.
96. A. Corma, M.T. Navarro, M. Renz, J. Catal. 219 (2003) 242.
97. R. Ryoo, S. Jun, J.M. Kim, M.J. Kim, Chem. Commun. (1997) 2225.
98. Y. Zhu, S. Jaenicke, G.K. Chuah, J. Catal. 218 (2003) 396.
99. (a) Z. Zhang, Y. Han, L. Zhu, R. Wang, Y. Yu, S. Qiu, D. Zhao, F.-S. Xiao, Angew. Chem. Int. Ed. 40 (2001) 1258. (b) Y. Liu, W. Zhang, T.J. Pinnavaia, Angew. Chem. Int. Ed. 40 (2001) 1255. (c) W. Guo, L. Huang, P. Deng, Z.

Xue, Q. Li, Micropor. Mesopor. Mater. 44–45 (2001) 427. (d) X. Meng, D. Li, X. Yang, Y. Yu, S. Wu, Y. Han, Q. Yang, D. Jiang, F.-S. Xiao, J. Phys. Chem. B 107 (2003) 8972. (e) S.P.B. Kremer, C.E.A. Kirschhock, A. Aerts, K. Villani, J.A. Martens, O.I. Lebedev, G. Van Tendeloo, Adv. Mater. 15 (2003) 1705.

100. D. Trong On, S. Kaliaguine, Angew. Chem. Int. Ed. 41 (2002) 1036.
101. (a) D. Trong-On, A. Ungureanu, S. Kaliaguine, Phys. Chem. Chem. Phys. 5 (2003) 3534. (b) D. Trong On, S. Kaliaguine, in: S.-E. Park, R. Ryoo, W.-S. Ahn, C.W. Lee, J.-S. Chang, Stud. Surf. Sci. Catal. vol. 146 (2003) 561.
102. Z. Luan, E.M. Maes, P.A.W. van der Heide, D. Zhao, R.S. Czernuszewicz, L. Kevan, Chem. Mater. 11 (1999) 3680.
103. M.V. Landau, L. Titelman, L. Vradman, P. Wilson, Chem. Commun. (2003) 594.
104. (a) T. Abe, Y. Tachibana, T. Uematsu, M. Iwamoto, J. Chem. Soc. Chem. Commun. (1995) 1617. (b) M. Iwamoto, T. Abe, Y. Tachibana, J. Mol. Catal. A: Chem. 155 (2000) 143. (c) M. Froba, R. Kohn, G. Bouffaud, Chem. Mater. 11 (1999) 2858.
105. L. Zhang, G.C. Papaefthymiou, J.Y. Ying, J. Phys. Chem. B 105 (2001) 7414.
106. K.R. Kloetstra, H. van Bekkum, in: H. Chon, S.-K. Ihm, Y.S. Uh, Stud. Surf. Sci. Catal. Vol. 105 (1997) 431.
107. V.R. Choudhary, S.K. Jana, J. Mol. Catal. A: Chem. 184 (2002) 247.
108. J. Sauer, F. Marlow, B. Spliethoff, F. Schuth, Chem. Mater. 14 (2002) 217.
109. (a) I.V. Kozhevnikov, K.R. Kloetstra, A. Sinnema, H.W. Zandbergen, H. van Bekkum, J. Mol. Catal. A: Chem. 114 (1996) 287. (b) T. Blasco, A. Corma, A. Martinez, P. Martı´nez-Escolano, J. Catal. 177 (1998) 306. (c) M.J. Verhoef, P.J. Kooyman, J.A. Peters, H. van Bekkum, Micropor. Mesopor. Mater. 27 (1999) 365. (d) A. Ghanbari-Siahkali, A. Philippou, J. Dwyer, M.W. Anderson, Appl. Catal. A: Gen. 192 (2000) 57. (e) Q.-H. Xia, K. Kidajat, S. Kawi, J. Catal. 209 (2002) 433.
110. (a) T. Okuhara, N. Mizuno, M. Misono, Adv. Catal. 41 (1996) 113. [246] I.V. Kozhevnikov, Chem. Rev. 98 (1998) 171. (b) N. Mizuno, M. Misono, Chem. Rev. 98 (1998) 199.
111. S. Suvanto, T.A. Pakkanen, L. Backman, Appl. Catal. A: Gen. 177 (1999) 25.
112. S. Suvanto, J. Hukkamaki, T.T. Pakkanen, T.A. Pakkanen, Langmuir 16 (2000)

4109.

113. (a) T. Yamamoto, T. Shido, S. Inagaki, Y. Fukushima, M. Ichikawa, J. Am. Chem. Soc. 118 (1996) 5810. (b) T. Yamamoto, T. Shido, S. Inagaki, Y. Fukushima, M. Ichikawa, J. Phys. Chem. B 102 (1998) 3866.
114. D.S. Shephard, T. Maschmeyer, G. Sankar, J.M. Thomas, D. Ozkaya, B.F.G. Johnson, R. Raja, R.D. Oldroyd, R.G. Bell, Chem. Eur. J. 4 (1998) 1214.
115. S. Hermans, R. Raja, J.M. Thomas, B.F.G. Johnson, G. Sankar, D. Gleeson, Angew. Chem. Int. Ed. 40 (2001) 1211.
116. R. Raja, T. Khimyak, J.M. Thomas, S. Hermans, B.F.G. Johnson, Angew. Chem. Int. Ed. 40 (2001) 4638.
117. M. Eswaramoorthy, Neeraj, C.N.R. Rao, Chem. Commun. (1998) 615.
118. S. Krijnen, H.C.L. Abbenhuis, R.W.J.M. Hanssen, J.H.C. van Hooff, R.A. van Santen, Angew. Chem. Int. Ed. 37 (1998) 356.
119. Grubert, G., Rathousky, J., Schulz-Ekloff, G., Wark, M., and Zukal, A., Micropor. Mesopor. Mater. 22 (1998) 225.
120. Velarde, A. M., Bartl, P., Niessen, T. E. W., Hoelderich, W. F., J. Mol. Catal. A: Chem. 157 (2000) 225.
121. Ahn, W. S., Lee, D. H., Kim, T. J., Kim, J. H., Seo, G., and Ryoo, R., Appl. Catal. A: Gen. 181 (1999) 39.
122. (a) Ryoo, R., Kim, Mi J., Kim, J. M., and Jun, S., Chem. Commun. 2225 (1997); (b) Shen, S-C., and Kawi, S., Chem. Lett. 1293 (1999).
123. U. Schubert, New J. Chem. 18, 1049 (1994).
124. S. L. Burkett, S. D. Sims, S. Mann, Chem. Commun. 1367 (1996).
125. M. H. Lim, C. F. Blanford, A. Stein, J. Am. Chem. Soc. 119 (1997) 4090.
126. D. Brunel, Micropor. Mesopor. Mater. 27 (1999) 329.
127. S. Brunauer, P.H. Emmett, E. Teller, J. Am. Chem Soc. 60 (1938) 309.
128. S.J. Gregg, K.S. W. Suig, "Adsorption, Surface Area and Porosity", Academic Press, London, (1982) Ch. 4.
129. G. Horvath, K.J. Kawazoe, J. Chem. Eng. Jpn. 16 (1983) 470.
130. A. Bell and A. Pines, "NMR Techniques in Catalysis" Heinemann eds., Marcel Dekker, Inc. (1994).
131. (a) C. Rocchiccioli-Deltcheff, R. Thouvent, R. Franck, Spectrochim. Acta. 32 A (1976) 587. (b) D. H. Brown, Spectrochim. Acta. 19 (1963) 583. (c) T.

Okuhara, C. Hu, M. Hashimoto, M. Misono, Bull. Chem. Soc. Jpn. 67 (1994) 1186. (d) F. Boeschen, B. Brus, B. Krebs, Acta Crystallogr. B30 (1974) 48.

132. E.M. Flanigen, "Zeolite Chemistry and Catalysis" ACS monograph (J.A. Rabo, EDS.) 171 (1976) 118.

133. (a) N. Topsoe, R. Pedersen, E.G. Derouance, J. Catal. 70 (1984) 369.
(b) P.A. Jacobs and W.Y Martier, Zeolites 2 (1982) 226.

134. (a) J.C. Vedrine, "Characterization of Heterogeneous Catalysts" (F. Delannay) Marcel Dekker, Inc. (1984) 161; C. Defosse, "Characterization of Heterogeneous Catalysts" F. Delannay) Marcel Dekker, Inc. (1984) 225; F. Delannay and B. Delmon, "Characterization of Heterogeneous Catalysts" (F. Delannay) Marcel Dekker, Inc. (1984) 22. (b) B.D. Cullity, "Elements of X-Ray Diffraction", Addison-Wesley, Reading, Mass, (1956).

135. (a) J. Zhang, H. Zimmermann, Z. Luz, D. Goldfarb, Stud. Surf. Sci. Catal. 117 (1998) 535. (b) J. Zhang, Z. Luz, D. Goldfarb, J. Phys. Chem. B 101 (1997) 7087.

136. S. Ruthstein, V. Frydman, S. Kababya, M. Landau, and D. Goldfarb, J. Phys. Chem. B 107 (2003) 1739.

137. J. Xu, Z. Luan, T. Wasowicz, L. Kevan, Micropor. Mesopor. Mater. 22 (1998) 179.

138. (a) K.J. Chao, C.N. Wu, H. Chang, L.J. Lee, S.F. Hu, J. Phys. Chem. B 101 (1997) 6341. (b) V. Luca, D.J. MacLachlan, K. Morgan, Chem. Mater. 9 (1997) 2720.

139. (a) Z. Chang, Z. Zhu, L. J. Kevan, Phys. Chem. B 103 (1999) 9442; (b) M. Kosslick, G. Lischke, G. Walther, W. Storek, A. Martin, R. Fricke, Micropor. Mater. 9 (1997) 13; (c) Z.Y. Yuan, H.B. Zhang, T.H. Chen, J.Z. Wang, H.X., Li, J. Nat. Gas Chem. 6 (1997) 237.

140. A.M. Prakash, M. S. Hyung, L. Kevan, J. Phys. Chem. B 102 (1998) 857.

141. A. Satsuma, Y. Kamiya, Y. Westi, T. Hattori, Appl. Catal. A: Gen. 194 (2000) 253.

142. (a) H. Sato, Catal. Rev. Sci. Engg. 39 (1997) 395. (b) A. Alberti, Zeolites 19, (1997), 411. (b) G. Bagnasco, J. Catal. 159 (1996) 249. (c) L. Froni, F.P. Vatti, E. Ortoleva, Micropor. Mater. 3 (1995) 367.

143. (a) V. Alfredsson, M. Keung, A. Monnier, G.D. Stucky, K.K. Unger, F. Schüth,

J. Chem. Soc. Chem. Commun. (1994) 921. (b) A. Chenite, Y.L. Page, Sayari, Chem. Mater. 7 (1995) 1015.

144. R.M. Barrer and D.A. Langley, J. Chem. Soc. 3804, 3811 (1958).
145. M.V. Landau, E. Dafa, M.L. Kaliya, T. Sen, M. Herskowitz, Micropor. Mesopor. Mater. 49 (2001) 65.
146. W. A. Carvalho, P. B. Varaldo, Wallau, Martin, Schuchardt, Ulf, Zeolites 18 (1997) 408.
147. (a) F.A. Twaiq, A.R. Mohamed, S. Bhatia, Micropor. Mesopor. Mater. 64 (2003) 95. (b) E. Byambajav, Y. Ohtuska, Fuel 82 (2003) 1571.
148. Y. Sun, L. Zhu, H. Lu, R. Wang, S. Lin, D. Jiang, F.-S. Xiao, Appl. Catal. A: Gen. 237 (2002) 21.
149. M. Iwamoto, Y. Tanaka, N. Sawamura, S. Namba, J. Am. Chem. Soc. 125 (2003) 13032.
150. X. Hu, M.L. Foo, G.K. Chuah, S. Jaenicke, J. Catal. 195 (2000) 412.
151. (a) K. Okumura, K. Nishigaki, M. Niwa, Micropor. Mesopor. Mater. 44–45 (2001) 509. (b) N. He, S. Bao, Q. Xu, Appl. Catal. A: Gen. 169 (1998) 29.
152. M.J. Climent, A. Corma, S. Iborra, M.C. Navarro, J. Primo, J. Catal. 161 (1996) 783.
153. M.J. Climent, A. Corma, R. Guil-Lopez, S. Iborra, J. Primo, J. Catal. 175 (1998) 70.
154. (a) M. Onaka, N. Hashimoto, Y. Kitabata, R. Yamasaki, Appl. Catal. A: Gen. 241 (2003) 307. (b) T. Kugita, S.K. Jana, T. Owada, N. Hashimoto, M. Onaka, S. Namba, Appl. Catal. A: Gen. 245 (2003) 353. (c) M. Onaka, R. Yamazaki, Chem. Lett. (1998) 259.
155. L.-X. Dai, K. Koyama, T. Tatsumi, Catal. Lett. 53 (1998) 211.
156. A.L. Villade, P.E. Alarcon, C.M. de Correa, Chem. Commun. (2002) 2654.
157. Y. Zhu, S. Jaenicke, G.K. Chuah, J. Catal. 218 (2003) 396.
158. A. Corma, S. Iborra, S. Miquel, J. Primo, J. Catal. 173 (1998) 315
159. J.M. Clacens, Y. Pouilloux, J. Barrault, Appl. Catal. A: Gen. 227 (2002) 181.
160. (a) S.C. Laha, P. Mukherjee, S.R. Sainkar, R. Kumar, J. Catal. 207 (2002) 213. (b) O. Franke, J. Rathousky, G. Schulz-Ekloff, J. Starek, A. Zukal, Stud. Surf. Sci. Catal. Vol. 84 (1994) 77.
161. A. Corma, M.T. Navarro, J. Perez Pariente, J. Chem. Soc. Chem. Commun.

(1994) 147.

162. J. Jarupatrakorn, T.D. Tilley, J. Am. Chem. Soc. 124 (2002) 8380.

163. C. Nozaki, C.G. Langmuir, A.T. Bell, T.D. Tilley, J. Am. Chem. Soc. 124 (2002) 13194.

164. M. Yonemitsu, Y. Tanaka, M. Iwamoto, J. Catal. 178 (1998) 207. [200] V. Caps, S.C. Tshang, Catal. Today 61 (2000) 19.

165. (a) W.A. Carvalho, M. Wallau, U. Schuchardt, J. Mol. Catal. A: Chem. 144 (1999) 91. (b) A. Sakthivel, P. Selvam, J. Catal. 211 (2002) 134. (c) E. Armengol, A. Corma, V. Fornes, H. Garcıa, J. Primo, Appl. Catal. A: Gen. 181 (1999) 305. (d) R.K. Rana, B. Viswanathan, Catal. Lett. 52 (1998) 25

166. K. Lemke, H. Ehrick, U. Lohse, H. Berndt, K. Jahnisch, Appl. Catal. A: Gen. 243 (2003) 41.

167. (a) A. Corma, M.T. Navarro, M. Renz, J. Catal. 219 (2003) 242. (b) A. Corma, M.T. Navarro, L. Nemeth, M. Renz, Chem. Commun. (2001) 2190.

168. (a) Q. Zhang, Y. Wang, Y. Ohishi, T. Shishido, K. Takehira, J. Catal. 202 (2001) 308. (b) B. Solsona, T. Blasco, J.M. Lopez Nieto, M.L. Pena, F. Rey, A. Vidal-Moya, J. Catal. 203 (2001) 443.

169. H. Berndt, A. Martin, A. Bruckner, E. Schreier, D. Muller, H. Kosslick, G.U. Wolf, B. Lucke, J. Catal. 191 (2000) 384.

170. (a) B. Lin, X. Wang, Q. Guo, W. Yang, Q. Zhang, Y. Wang, Chem. Lett. 32 (2003) 860. (b) L.X. Dai, Y.H. Teng, K. Tabata, E. Suzuki, T. Tatsumi, Micropor. Mesopor. Mater. 44–45 (2001) 573.

171. X. Gao, I.E. Wachs, M.S. Wong, J.Y. Ying, J. Catal. 203 (2001) 18.

172. V.R. Choudhary, S.K. Jana, B.P. Kiran, J. Catal. 192 (2000) 257.

173. (a) E. Rivera-Munoz, D. Lardizabal, G. Alonso, A. Aguilar, M.H. Siadati, R.R. Chianelli, Catal. Lett. 85 (2003) 147. (b) L. Vradman, M.V. Landau, M. Herskowitz, V. Ezersky, M. Talianker, S. Nikitenko, Y. Koltypin, A. Gedanken, J. Catal. 213 (2003) 163.

174. A. Wingen, N. Anastasievic, A. Hollnagel, D. Werner, F. Schuth, J. Catal. 193 (2000) 248.

175. R. Raja, T. Khimyak, J.M. Thomas, S. Hermans, B.F.G. Johnson, Angew. Chem. Int. Ed. 40 (2001) 4638.

176. (a) C.P. Mehnert, J.Y. Ying, Chem. Commun. (1997) 2215. (b) C.P. Mehnert,

D.W. Weaver, J.Y. Ying, J. Am. Chem. Soc. 120 (1998) 12289.

177. A.Y. Khodakov, A. Griboval-Constant, R. Bechara, V.L. Zholobenko, J. Catal. 206 (2002) 230.

178. M. Okumura, S. Tsubota, M. Iwamoto, M. Haruta, Chem. Lett. (1998) 315.

179. S.H. Joo, S.J. Choi, I. Oh, J. Kwak, Z. Liu, O. Terasaki, R. Ryoo, Nature 412 (2001) 169.

180. R.T. Yang, T.J. Pinnavaia, W. Li, W. Zhang, J. Catal. 172 (1997) 488.

181. H.H.P. Yiu, P.A. Wright, N.P. Botting, Micropor. Mesopor. Mater. 44–45 (2001) 763.

182. M.J. Climent, A. Corma, S. Iborra, S. Miquel, J. Primo, F. Rey, J. Catal. 183 (1999) 76.

183. (a) C. Perez, S. Perez, G.A. Fuentes, A. Corma, J. Mol. Catal. A: Chem. 197 (2003) 275. (b) M.D. Jones, R. Raja, J.M. Thomas, B.F.G. Johnson, D.W. Lewis, J. Rouzaud, K.D.M. Harris, Angew. Chem. Int. Ed. 42 (2003) 4326.

184. (a) J.K. Park, S.-W. Kim, T. Hyeon, B.M. Kim, Tetrahedron: Asymmetry 12 (2001) 2931. (b) A. Corma, H. Garcıa, A. Moussaif, M.J. Sabater, R. Zniber, A. Redouane, Chem. Commun. (2002) 1058.

185. (a) I. Rodriguez, S. Iborra, A. Corma, F. Rey, J.L. Jorda, Chem. Commun. (1999) 593. (b) D.J. Macquarrie, D.B. Jackson, Chem. Commun. (1997) 1781.

186. D. Brunel, F. Fajula, J.B. Nagy, B. Deroide, M.J. Verhoef, L. Veum, J.A. Peters, H. van Bekkum, Appl. Catal. A: Gen. 213 (2001) 73.

187. Z. Luan, D. Zhao, M. Hartmann, L. Kevan, Chem. Mater.11 (1999) 1621.

188. K. Pitchumani, M. Warrier, V. Ramamurthy, J. Am. Chem. Soc.118 (1996) 9428.

189. N. T. Mathew, S. Khaire, S. Mayadevi, R. Jha, S. Sivasanker, J. Catal. 229 (2005) 105.

190. A. Thangraj, S. Sivasanker and P. Ratnasamy, J. Catal. 137 (1992) 252.

191. (a) P. Metivier, R. A. Sheldon, H. Van Bekkum (Eds), “Fine Chemicals through Heterogeneous catalysis”, Wiley-VCH. Weinheim, (2001) 161; (b) J. C. Leffingwell and R. E. Shackelford, “Cosmetics Perfumery”, 89 (6) (1974) 69.

192. G. D. Yadav, S. V. Lande, Org. Proc. Res. and Dev. 9 (3) (2005) 288.

193. J. P. Bain, J. Am. Chem. Soc. 68 (1946) 638.

Chapter 2

SYNTHESIS

2.1 INTRODUCTION

Several synthesis methods have been proposed and successfully used to synthesize mesoporous molecular sieves. These materials are normally synthesized by hydrothermal methods, under autogenous pressure; their structures being obtained from amorphous inorganic silica walls around the surfactant molecules. Hydrothermal synthesis involves the mixing of organic molecules (surfactants), silica, and/or silica alumina source to form a gel which is then crystallized at a temperature between 343-423 K for a selected period of time. The product obtained after crystallization is filtered, washed with deionised water and dried at ambient temperature. Surfactant molecules are removed by calcination leaving a porous silicate/aluminosilicate network. An alternative method for surfactant removal is based on the extraction of the organic template. Hydrothermal treatment increases both the polymerization of the silica precursor and the pore diameter of the mesoporous material. A higher degree of polymerization tends to impart improved thermal stability. The polymerization of inorganic species is normally achieved by adjusting the pH, and the reaction temperature.

An important feature of the preparation of mesoporous materials is the role of the templating agents. The templating molecules used are a self-assembled surfactant molecular array around which the main structure is built up. One of the most unique properties of mesoporous materials is the ability to tailor the pore diameter (15-100 Å). This can be achieved in three different ways. 1) By varying the chain length of the alkyl groups, 2) by adding auxiliary chemicals such as 1,3,5 tri-methylbenzene, which dissolve in the hydrophobic region of the micelles increasing their size and 3) by aging a sample prepared at a lower temperature in its mother liquor at a higher temperature for different periods of time. Besides, the pore diameter of mesoporous molecular sieves also depends on other factors such as temperature, pH, and crystallization time.

MCM-41 type ordered mesoporous materials can be prepared under alkaline [1-5], acidic [6, 10] and neutral [11] medium. Purely siliceous mesoporous molecular sieves having neutral framework have limited applications. In order to impart catalytic activity to the chemically inert mesoporous silicate framework, substitution of Si^{4+} ions by other heteroatoms like Al, Ti, V, Sn etc. can be made during hydrothermal synthesis or by impregnation of the heteroatom after the synthesis. SBA-15 reported by Zhao et al. [12] possesses well ordered hexagonal mesoporous structure and

possesses higher hydrothermal stability than MCM-41 due to a larger wall thickness. Different metal loaded SBA-15 catalysts have been reported to be useful in alkylation and oxidation reactions [13]. Incorporation of heteroatoms like Al, Ti, Sn etc. is difficult in SBA-15 due to the highly acidic synthesis medium. Therefore, the general route for metal incorporation in SBA-15 is the impregnation [14] method.

The present chapter describes the synthesis of MCM-41 and metal incorporated MCM-41. It reports the substitution of the heteroatoms Al, Ga, Sn, Fe and V by in-situ synthesis. It also describes the synthesis of SBA-15 and the preparation of Al and PW (phosphotugnstic acid) loaded SBA-15 catalysts by the impregnation method.

2.2 CHEMICALS AND REAGENTS USED

The chemical used in the synthesis of MCM-41 and SBA-15 catalysts are listed in Table 2.1.

2.3 EXPERIMENTAL

2.3.1 Synthesis of MCM-41 type ordered mesoporous metallosilicate catalysts

MCM-41 type molecular sieve catalysts were prepared under hydrothermal conditions in a Teflon lined autoclave under autogenous pressure in an alkaline medium. In this preparation procedure, cetyltrimethlammonium bromide (CTMABr) surfactant was used as the template. Tetramethylammonium hydroxide (TMAOH) was used as the structure directing agent and mineralizer. Tetraethylorthosilicate (TEOS) was used as the silica source.

In the present work, Si-MCM-41, Al-MCM-41, Ga-MCM-41, Sn-MCM-41, Fe-MCM-41 and V-MCM-41 with different Si/M (M=Al, Ga, Sn, Fe, V) ratios were prepared by direct synthesis.

Table 2.1 List of chemicals and reagents used

Chemical/ reagent	Source	Chemical formula	Purity (%)
Tetraethylorthosilicate (TEOS)	Aldrich	$Si(OC_2H_5)_4$	99
Cetyltrimethlyammonium bromide (CTMABr)	LOBA Chemie	$C_6H_{33}N(CH_3)_3Br$	99
Tetramethylammonium hydroxide (TMAOH) 25 wt.% soln. in water	Aldrich	$(CH_3)_4NOH$	99
Aluminium sulfate	s.d. Fine Chem.	$Al_2(SO_4)_3.18\ H_2O$	99
Stannic chloride	Aldrich	$SnCl_4.\ 5H_2O$	99
Gallium(III) nitrate hydrate	Aldrich	$Ga(NO_3)_3.xH_2O$	99.9
Vanadyl sulfate	LOBA Chemie	$VOSO_4.\ 5H_2O$	98
Ferric nitrate	LOBA Chemie	$Fe(NO_3)_3.9H_2O$	98
Pluronic (P123)-Triblock copolymer poly(ethylene oxide)-poly(propylene oxide)-poly(ethylene oxide) Mol. Wt. 5800	Aldrich	$EO_{20}PO_{70}EO_{20}$	99
Aluminium chloride	s. d. Fine Chem.	$AlCl_3$	99
Phosphotungstic acid	LOBA Chemie	$H_3PW_{12}O_{40}.xH_2O$	98
Conc. Hydrochloric acid	s. d. Fine Chem.	HCl	36-38
Methanol (Dry)	s. d. Fine Chem.	CH_3OH	99.5

(a) Synthesis of Si-MCM-41

A silica analog of MCM-41 was prepared hydrothermally in alkaline medium using a gel with molar composition, $1SiO_2$: 0.33 TMAOH: 0.55 CTMABr: 60 H_2O following a published method [15]. TEOS (20.83 g) was added drop-wise to an aqueous solution containing 20.043 g of CTMABr and 12.03 g of TMAOH (25 %) in water under stirring. After the addition, the mixture was stirred for 5 h and was transferred to a Teflon lined autoclave and heated at 383 K under autogenous pressure for 5 days. The resultant solid product was filtered, washed with distilled water and

then dried at ambient temperature. The as-synthesized material was calcined in air at 823 K for 8 h in a furnace whose temperature was raised slowly from ambient at the rate of 1 K/min. The yield of Si-MCM-41 (after calcination) was 5.85 g.

(b) Synthesis of Al-MCM-41

Samples of Al-MCM-41 with different Si/Al ratios were prepared, using the following molar gel composition, $1SiO_2$: 0.33 TMAOH: 0.55 CTMABr: 60 H_2O: x Al_2O_3, where x varied from 0.025 - 0.0005 moles. The preparation procedure was similar to that of Si-MCM-41 except that aluminum sulfate was added to the final gel and stirred well for 5 h. Four samples with different Si/Al ratios (gel) of 20, 30, 50 and 100 were prepared. The gel was autoclaved at 383 K for 5 days. The as-synthesized sample was calcined in air at 823 K for 8 h in a furnace whose temperature was raised slowly from ambient at the rate of 1 K/min. The yield of Al-MCM-41 (after calcination) was 6 g.

(c) Synthesis of M-MCM-41 (M= Ga, Sn, V and Fe)

M-MCM-41 samples with different Si/M ratios were prepared, using the following gel composition: $1SiO_2$: 0.33 TMAOH: 0.55 CTMABr: 60 H_2O: x M_2O_3 or MO_2 or M_2O_5 where x varied from 0.001 - 0.00035 moles. The preparation procedure was similar to that of Si-MCM-41 except that a salt of the heteroatom (M) was added to the final (SiO_2) gel and stirred well for 5 h and the gel was kept at 373 K for 3 days. The as-synthesized samples were calcined in air at 823 K for 8 h in a furnace whose temperature was raised slowly from ambient at the rate of 1 K/min. The metal salts used to incorporate the heteroatoms were gallium nitrate, tin chloride, vanadyl sulfate and ferric nitrate for Ga, Sn, V, and Fe-MCM-41 samples, respectively. The Si/M ratios (gel) used in the synthesis of the different metallosilicate samples were 20, 30 and 50. The yield of M-MCM-41 (after calcination) was 6 g.

2.3.2 Synthesis of SBA-15 type ordered mesoporous catalysts

SBA-15 type molecular sieve catalysts were synthesized under hydrothermal conditions in Teflon lined autoclave under autogenous pressure in an acidic medium (2 M HCl) following a published procedure [11]. In this, Pluronic (P123) triblock co-polymer (Mol. Wt. 5800) was used as the template. TEOS was used as the silica source. SBA-15 siliceous phase is synthesized in strongly acidic media (pH < 1).

Since the Al-ions remain in solution in acidic medium, incorporation of Al into the framework of SBA-15 by direct synthesis is difficult. This necessitates the use of alternate post-synthesis methods [14]. In the present work, Al and PW supported SBA-15 catalysts were prepared by impregnation.

(a) Synthesis of Si-SBA-15

Si-SBA-15 was synthesized by a hydrothermal method [12] using the gel composition: 4 g P123: 0.041 mol TEOS: 0.24 mol HCl: 6.67 mol H_2O. In a typical synthesis, 4 g of an amphiphilic triblock copolymer, Pluronic P123 (average mol.wt.-5800, Aldrich) was dispersed in 30 g of water and 120 g of 2 M HCl solution by stirring. TEOS (8.5 g, Aldrich) was added slowly to the mixture with continuous stirring. The gel mixture was stirred at 313 K for 24 h and finally crystallized in a Teflon lined autoclave at 373 K for 48 h. After crystallization, the solid white product was filtered, washed several times with deionized water and dried at ambient temperature. The material was calcined at 823 K for 6 h in air in a furnace whose temperature was raised from ambient at a rate of 1 K/min. The yield of Si-SBA-15 (after calcination) was 2.45 g.

(b) Synthesis of Al-SBA-15

Aluminium containing SBA-15 samples Al-SBA-15 with Si/Al ratios of 9, 20, 30, 46 and 71 were prepared by a post-synthesis method using $AlCl_3$ as the aluminium source. In a typical preparation, 1 g of freshly calcined SBA-15 was combined with 30 ml of dry methanol containing the required amount of $AlCl_3$ under continuous stirring. The mixture was refluxed for 24 h and the solvent was evaporated on a rotavapor. The material was then heated in a furnace at the rate of 1 K/min and calcined at 823 K for 6 h.

(c) Synthesis of phosphotungstic acid (PW) supported SBA-15 catalysts

$H_3PW_{12}O_{40}$/SBA-15 (PW/SBA-15) with different PW loadings of 10, 20, 30 and 40 wt % were prepared by a wet impregnation method. A weighed quantity of freshly calcined SBA-15 was added to a methanolic solution of PW and refluxed for 24 h. After evaporation of the solvent, it was dried at 373 K overnight.

2.4 REFERENCES

1. C.T. Kresge, M.E. Leonowicz, W.J. Roth, J.C. Vartuli, U.S.Patent 5,098,684 (1992).
2. C.T. Kresge, M.E. Leonowicz, W.J. Roth, J.C. Vartuli, J.S. Beck, Nature 359 (1992) 710.
3. J.S. Beck, C.T. Chu, I.D. Johnson, C.T. Kresge, M.E. Leonowicz, W.J. Roth, J.C. Vartuli, U.S.Patent 5,108,725, (1992).
4. J.S. Beck, D.C. Calabro S.B. McCullen, B.P. Pelrine, K.D. Schmitt, J.C. Vartuli, U.S. Patent 5, 145 (1992)
5. J.S. Beck, C.T. Kresge, M.E. Leonowicz, W.J. Roth, J.C. Vartuli, K.D. Schmidtt, C.T. Chu, D.H. Olson, E.W. Sheppard, S.B. McCullen, J.B. Higgins, J.L. Schlenker, J. Am. Chem. Soc. 114 (1992) 10834.
6. Q. Huo, D.I. Margolese, U. Ciesla, D.G. Demuth, P. T.E. Feng, Gier, P. Seiger, B.F. Chmelka, G.D. Stucky, Chem. Mater. 6 (1994) 1176.
7. D. Zaho, J. Feng, B.F. Chmelka, G.D. Stucky, J. Am. Chem. Soc.1120 (1998) 6024.
8. D.H. Olson, G.D. Stucky, J. C. Vartuli. U. S .Patent 5, 364, 79 (1994).
9. A. Firouzi, F. Atef, A.G. Oertli, G.D. Stucky, J. Am. Chem. Soc. 119 (1997) 3596.
10. Q. Huo Margolese, D. I. Ciesla, U. Feng, P. Geir, T.E. Seiger, P. Leon, R. P.M. Petroff, G.D. Stucky, Nature 368 (1994) 317.
11. P.T. Tanev, T.G. Pinnavaiva, Science 267 (1995) 865.
12. D. Zhao, J. Feng, Q. Huo, N. Melosh, G. H. Fredrickson, B.F. Chmelka, G. D. Stucky, Science 279 (1998) 548.
13. Trukhan, Romannikov, Kholdeeva, Micropor. Mesopor. Mater. 59 (2003) 73.
14. Z. Luan, D. Zhao, M. Hartmann, L. Kevan, Chem. mater.11 (1999) 1621.
15. N. T. Mathew, S. Khaire, S. Mayadevi, R. Jha, S. Sivasanker, J. Catal. 229 (2005) 105.

Chapter 3

CHARACTERIZATION

3.1 INTRODUCTION

In the present chapter, the characterization of the catalysts by different techniques is described. A brief description of the characterization techniques used and the results obtained are presented.

3.2 EXPERIMENTAL

(a) X-ray diffraction

Small angle X-ray diffraction patterns of as synthesized and calcined samples were obtained using a Rigaku Dmax 2500 diffractometer and Ni filtered Cu radiation at 40 Kv and 150 mA. Samples were scanned in the 2θ range of 0.5 to 5°. Wide angle X-ray diffraction patterns of as synthesized and calcined samples were recorded on Rigaku D/MINI- flex x-ray diffractometer (40 kV, 20 mA, Ni filtered Cu-Kα). The samples were scanned in the 2θ range of 5 to 60°. The samples were prepared as thin layers on glass or aluminium plates.

(b) Chemical analysis

Chemical compositions of the calcined mesoporous samples were determined by different techniques. A wavelength dispersive X-ray fluorescence spectrometer (XRF) (Rigaku 3070E with Rh target energized at 50 kV and 40 mA was used in the analysis of many elements). For XRF analysis, $K_{\propto}$ lines were selected. For the analysis of Si and Al, a pentaerythrital (PET) crystal was used whereas for the analysis of Sn, a lithium fluoride (LiF) crystal was used. Atomic absorption spectrometry (Hitachi, Model Z 8000, and Polarized Zeeman Spectrophotometer) was used to estimate Fe, V and W. For Ga estimation, inductively coupled plasma-optical emission spectroscopy (ICP-OES) was used.

(c) Adsorption measurements

Nitrogen adsorption-desorption isotherms were obtained at 77 K using a commercial instrument (Quanta chrome NOVA 1200 analyzer). The specific surface area, $A_{BET} = V_m.N.A_m$ where, Vm is the monolayer volume, N is the Avogadro number, and A_m is the cross-sectional area of the adsorbent, was determined from the linear part of the BET equation (p/p_0 = 0.05-0.3). The calculation of the pore size distribution (PSD) was performed using the desorption branches of the N_2 adsorption

isotherm and the Barrett-Joyner-Halenda (BJH) formula. The cumulative surface area, S_{BJH}, and the cumulative pore volume, V_{BJH}, were obtained from the PSD curves. The specific mesopore diameter, D_{BJH}, was calculated as $4V_{BJH}/S_{BJH}$.

(d)Transmission electron microscopy (TEM)

Transmission electron microscopic (TEM) pictures of the calcined samples were obtained by suspending them in isopropanol and placing on a polymer coated copper grid (JEOL 2000 FX). Images were recorded on conventional sheet films.

(e) Scanning electron microscopy (SEM)

The crystallite size and morphology of the SBA-15 samples were determined by a scanning electron microscope (SEM; Leica/ LEO, Stereoscan 440). The samples were sputtered with gold to prevent surface charging and to protect from thermal damage from the electron beam.

(f)Thermogravimetry

TG/DTG analysis of the as-synthesized samples was carried out using a computer controlled Mettler TG-50 type thermal analyzer. A linear rate of heating of 10 K min^{-1} from room temperature to 1000 K in airflow (30 ml min^{-1}) was employed to find out the temperature of decomposition of the organic additives, the thermal stability of the molecular sieves and weight loss.

(g) Fourier-transform infra-red (FTIR) spectroscopy

The FTIR spectra were recorded in the 400-4000 cm^{-1} range on a Shimadzu FTIR-8201 PC in DRS (diffuse reflectance spectrum) mode.

(h) Diffuse reflectance UV-Vis spectroscopy

The UV-Visible spectra were recorded in the range of 200-800 nm (Shimadzu; Model UV-2101 PC) using barium sulphate as the reference.

(i) Electron spin resonance (ESR) spectroscopy

The ESR spectra were recorded at room temperature (298 K) on a Bruker EMX spectrometer operating at X-band frequency and 100 KHz field modulation.

Microwave frequency was calibrated using a frequency counter fitted in the microwave bridge (Bruker ER 041XG-D) and the magnetic field was calibrated by a (ER 035M NMR) Gauss meter.

(j) Nuclear magnetic resonance (NMR) spectroscopy

The solid state magic angle spinning (MAS) NMR spectra were obtained on a Bruker MSL-300 FT NMR spectrometer. For ^{27}Al signal, aluminium nitrate was used as the reference compound, ^{29}Si MAS NMR spectra were recorded on Bruker MSL-300 FT NMR spectrometer; TEOS was used as reference for ^{29}Si.

^{31}P MAS NMR spectra were recorded on Bruker DSX-300 spectrometer at 121.5 MHz with a Bruker 4-mm probe head. The spinning rate was 10 KHz and the delay between two pulses was varied between 1 and 30 s to ensure complete relaxation of the ^{31}P nuclei. The chemical shifts are given relative to external 85 % H_3PO_4.

(k) Temperature programmed desorption (TPD) of ammonia

Acidity of the samples was characterized by the TPD of adsorbed NH_3 (Micromeritics, Autochem 2910). The standard procedure for TPD measurements involved the activation of the sample in flowing He at 873 K (3 h), cooling to 298 K adsorbing NH_3 from a stream of He-NH_3 (10 %), removing the physically adsorbed NH_3 by desorbing in He at 373 K for 1 h and finally carrying out the TPD experiment by raising the temperature of the catalyst in a programmed manner 10 K min^{-1}. The TPD curves were deconvoluted into two peaks and the areas under the peaks were converted into meq NH_3 per g catalyst based on injection of known volumes of the He-NH_3 mixture at similar conditions.

(l) Temperature programmed reduction (TPR)

Temperature programmed reduction was carried out on a Micromeritics Autochem 2910 catalyst characterization system equipped with a TCD detector. The reduction was carried out in 5 % H_2/Ar gas mixture flowing through the reactor at the rate of 20 ml/min. Approximately 0.1 g of the calcined sample was used for the analysis. The temperature was then increased to 1073 K at heating rate of 10 K min^{-1}.

3.3 RESULTS AND DISCUSSION

3.3.1 MCM-41 type mesoporous metallosilicate catalysts

This section of the chapter discusses the results of the characterization of Si-MCM-41, Al-MCM-41, Ga-MCM-41, Sn-MCM-41, Fe-MCM-41 and V-MCM-41. The procedure for the synthesis of these catalysts was described in chapter 2.

(a) Composition of the samples

The actual compositions (Si/M) of the calcined metallosilicates were estimated by XRF for Al-MCM-41, Sn-MCM-41 and V-MCM-41, by ICP for Ga-MCM-41, and by AAS for Fe-MCM-41. The Si/M ratios of the gels and the actual values obtained for the calcined samples are presented in Tables 3.1, 3.2 and 3.3 for the various metallosilicates. In all the tables, figures and texts in the thesis, the samples are identified by the measured Si/M ratio given in brackets and the name of the metallosilicate (Tables 3.1, 3.2 and 3.3).

It is noticed that the Si/M ratios of the calcined samples and the gels used for their synthesis are reasonably similar (difference being within 10 %) in the case of Al, Ga, Sn and Fe, while it is substantially different in the case of V, the values being nearly double for the calcined samples compared to the gels. The Si/M values of nearly all the calcined samples are larger than those of the input gels suggesting only partial incorporation of the metal atoms in the metallosilicates. The poor incorporation of V is due to the existence of V as V^{5+} ions in the alkaline medium used in the synthesis and the difficulty in incorporating pentavalent ions in a lattice of tetravalent ions. The V^{5+} ions present in the samples are presumably linked to three Si-ions (through V-O-Si linkages), the remaining valencies of V being satisfied by a V=O bond. Such a configuration for V^{5+} will be possible if the ions are present at the surface layer or inside the walls in defect sites.

(b) X-ray diffraction

The XRD-patterns of the as-synthesized and calcined samples, Si-MCM-41 and Al-MCM-41 are presented in Figure 3.1, those of Sn and Ga-MCM-41 are presented in Figure 3.2, and those of V and Fe-MCM-41 are presented in Figure 3.3. The XRD patterns are similar to those reported for MCM-41 [1] and consist of low angle (110) and (200) lines in all the samples characteristic of long-range order of crystallinity in the materials. Kresge et al. [1] indexed these lines for a hexagonal unit

cell whose parameter was calculated using the equation $a_o = d_{100}/\sqrt{3}$. The results of the XRD analysis are presented in Tables 3.1, 3.2 and 3.3 for Al-MCM-41, Sn and Ga-MCM-41, and V and Fe-MCM-41, respectively. The data of Si-MCM-41 is also presented in all the tables for comparison purposes. One uniform observation is that the d_{100} values of all the metallosilicates are shifted to higher values compared to Si-MCM-41. This is probably due to the substitution of Si^{4+} by the larger heteroatoms Al^{3+}, Sn^{4+}, Ga^{3+}, V^{4+} and Fe^{3+} (ionic radius values are shown in Table 3.0) in the walls ("framework") of MCM-41 and the consequent replacement of the shorter Si-O bonds by the longer M-O bonds causing an expansion of the unit cell (a_o) [2]. The change in the T-O-T bond angle on heteroatom substitution probably causes some long-range disorder in the system leading generally to slightly broader XRD lines for the metallosilicates compared to the parent Si-MCM-41 (Fig. 3.1, 3.2 and 3.3). On calcination, the d_{100} values of all the samples become smaller due to shrinkage of the unit cell as a result of the removal of the template and condensation of some Si–OH groups at the surface. The changes in d_{100} and a_o values on calcination in the case of Si- and Al-MCM-41 are presented in Table 3.1, for Sn-, Ga-MCM-41 in Table 3.2 and for V-, Fe-MCM-41 in Table 3.3.

Table 3.0 Ionic radii of metal ions

Metal ion	C.N.	Ionic radius (Å)	Metal ion	C.N.	Ionic radius (Å)
Si^{4+}	IV	0.26	V^{5+}	IV	0.35
Al^{3+}	IV	0.39		VI	0.54
Ga^{3+}	IV	0.47	V^{4+}	VI	0.38
	VI	0.62	Fe^{2+}	IV	0.63
Sn^{4+}	IV	0.55	Fe^{3+}	IV	0.49
	VI	0.69			

(C.N. = Co-ordination number)

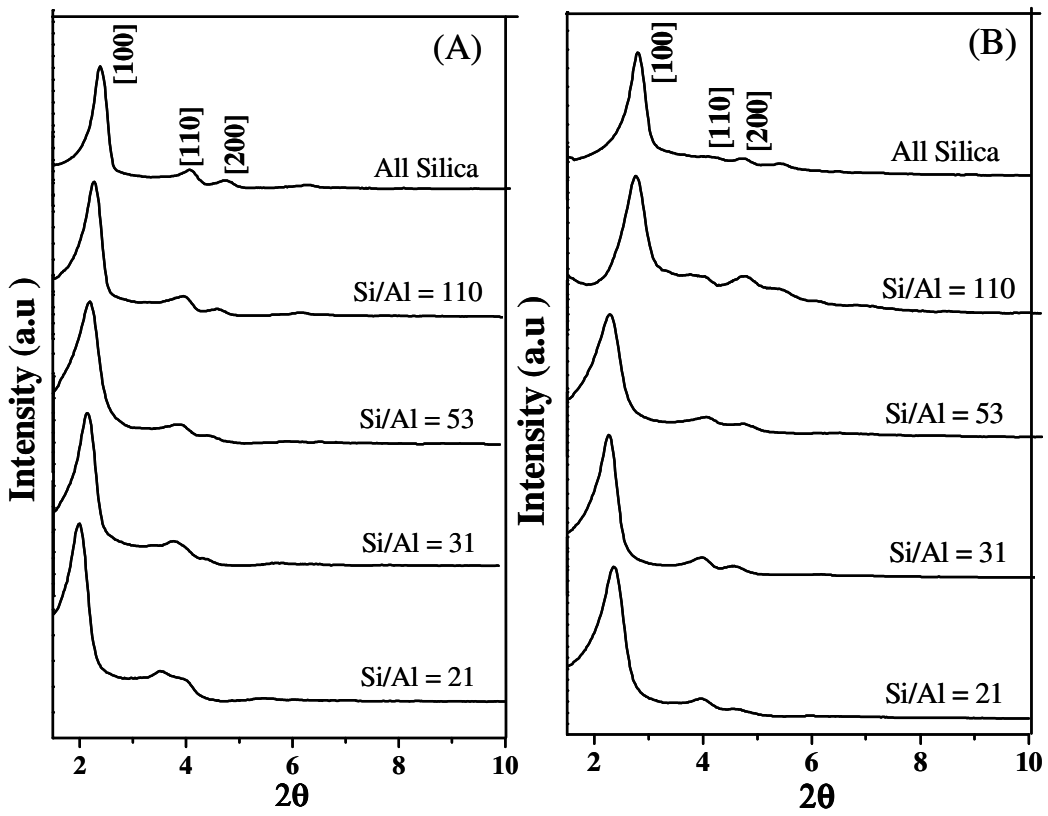

Figure 3.1 XRD patterns of (A) as synthesized and (B) calcined Si-MCM-41 and Al-MCM-41 with different Si/Al ratios.

Table 3.1 Composition and structural properties of Si- and Al-MCM-41 samples

Sample	Si/Al		d_{100} (Å)		Unit cell parameter [a] 'a_0' (Å)		Wall thick. (Å)
	Input gel	XRF Cal.	As synth.	Cal.	As synth.	Cal.	
Si-MCM-41	-	-	36.8	35.0	42.4	40.4	11.9
Al-MCM-41(110)	100	110	38.0	32.0	43.9	36.9	9.7
Al-MCM-41(53)	50	53.2	39.8	38.4	45.9	44.3	14.3
Al-MCM-41(31)	30	31.0	40.5	39.6	46.7	44.4	12.1
Al-MCM-41(21)	20	20.8	43.7	40.9	50.4	47.2	13.5

a- Unit cell parameter $a_0 = 2d_{100}/\sqrt{3}$: b- Wall thickness = a_0 - Pore diameter (from adsorption studies).

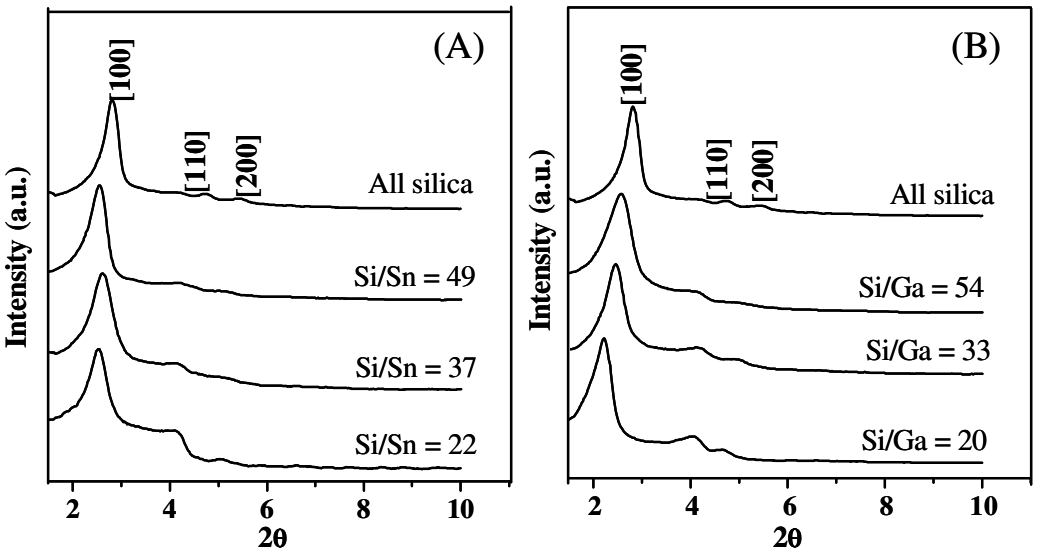

Figure 3.2 XRD patterns of calcined (A) Sn-MCM-41 and (B) Ga-MCM-41 with different Si/Sn and Si/Ga ratios respectively.

Table 3.2 Physicochemical properties of Si-, Sn- and Ga-MCM-41 (calcined)

Sample	Si/M			d_{100} (Å)	Unit cell para.[a] 'a_0' (Å)	S_{BET} (m^2/g)	Av. pore diam. D_{BJH} (Å)	Wall thick.[b] (Å)	Pore vol. V_{BJH} (cc/g)
	Input gel	By XRF	By ICP						
Si-MCM-41	-	-		35.0	40.4	975	30.0	10.4	1.06
Sn-MCM-41(49)	50	49.1	-	34.2	39.5	1064	25.5	14.0	0.71
Sn-MCM41 (37)	30	37.1	-	34.3	39.6	1063	26.8	12.8	0.68
Sn-MCM-41(22)	20	22.3	-	37.4	43.2	1024	27.8	15.4	0.71
Ga-MCM-41(54)	50	-	53.6	34.0	39.2	1085	28.2	11.0	0.76
Ga-MCM-41(33)	30	-	32.5	34.7	40.1	905	28.7	11.4	0.65
Ga-MCM-41(20)	20	-	20.3	39.1	45.1	1184	31.6	13.4	1.36

a- Calculated by the equation, $a_0 = 2d_{100}/\sqrt{3}$; b-Wall thickness = a_0- Pore diameter.

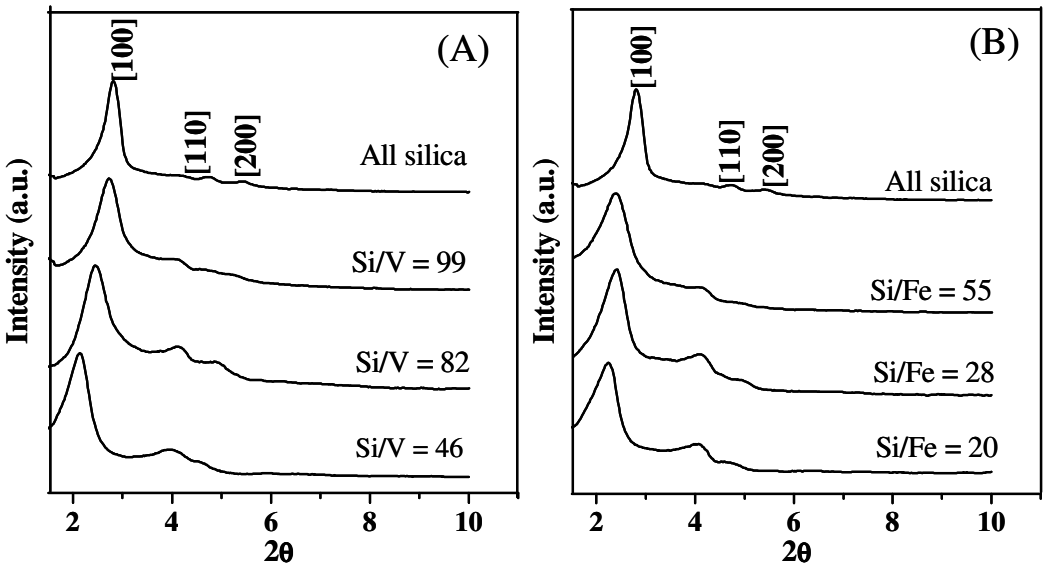

Figure 3.3 XRD patterns of calcined (A) V-MCM-41 and (B) Fe-MCM-41 with different Si/V and Si/Fe ratios respectively.

Table 3.3 Physicochemical properties of Si-, V- and Fe-MCM-41 (calcined)

Sample	Si/M			d_{100} (Å)	Unit cell para.[a] 'a_0' (Å)	S_{BET} (m^2/g)	Av. pore dia. D_{BJH} (Å)	Wall thick.[b] (Å)	Pore vol. V_{BJH} (cc/g)
	Input gel	XRF	AAS						
Si-MCM-41	-	-	-	35.0	40.4	975	30.0	10.4	1.06
V-MCM-41(99)	50	98.5	-	32.2	37.2	1131	27.8	9.4	0.78
V-MCM-41(82)	30	81.9	-	36.2	41.8	1109	30.7	11.1	0.85
V-MCM-41(46)	20	45.8	-	40.9	47.2	932	33.7	13.5	0.79
Fe-MCM-41(55)	50	-	54.5	36.8	42.5	1145	28.1	17.7	0.80
Fe-MCM-41(28)	30	-	28.0	37.4	43.2	1283	34.5	18.3	1.33
Fe-MCM-41(20)	20	-	20.2	38.7	44.7	1056	47.1	20.4	1.24

a- Calculated by the equation, $a_0 = 2d_{100}/\sqrt{3}$; b- Wall thickness = a_0- Pore diameter.

(c) Nitrogen sorption

The N_2 adsorption-desorption isotherms of Si-MCM-41 and all the metallosilicates are typically of the type IV with a hysterisis loop characteristic of mesoporous materials (Figure 3.4 for Si- and Al-MCM-41, 3.5 for Sn-, 3.6 for Ga-, 3.7 for V- and 3.8 for Fe-MCM-41). The isotherms exhibit three stages. The first stage is due to monolayer adsorption of nitrogen on the walls of the mesopores at low relative pressures ($p/p_0 < 0.2$). The second stage is characterized by a steep increase in adsorption ($p/p_0 > 0.2$). As the relative pressure increases, the isotherm exhibits a sharp inflection characteristic of capillary condensation within the uniform mesopores. The p/p_0 at the inflection is related to the diameter of the mesopore [3] and the steepness of this step indicates the uniformity of pore size distribution. The third stage in the adsorption isotherm is the gradual increase in volume with p/p_0 due to multilayer adsorption on the outer surface of the particles. The near coincidence of the two branches of the isotherm can be ascribed to the similar high degree of spontaneity (reversibility) of the adsorption and desorption process.

The surface area and average pore diameters of Si-MCM-41 and the metallosilicates with different Si/M ratios are given in Table 3.2 (Ga and Sn) 3.3 (V and Fe), and 3.4 (Al). It is generally found that with increasing M content, the pore diameter increases, while the surface area decreases with increasing M content. It is generally perceived that the BET equation may not be accurate to derive surface areas from materials with narrow pore diameters (such as MCM-41) due to the limited number of adsorbate layers possible on the surface. However, the BET areas are still useful to compare the characteristics of different mesoporous materials in a relative manner even though the values may not be accurate in an "absolute" sense. The pore size distributions of calcined Si-MCM-41 and the metallosilicates are also presented in the Figures 3.4 to 3.8. The figures show that all the materials possess pores of nearly uniform size with a narrow distribution. However, the distribution becomes broader, in general, with increase in the metal content due to the greater disorderliness arising from the insertion of the heteroatom inside the silicate walls.

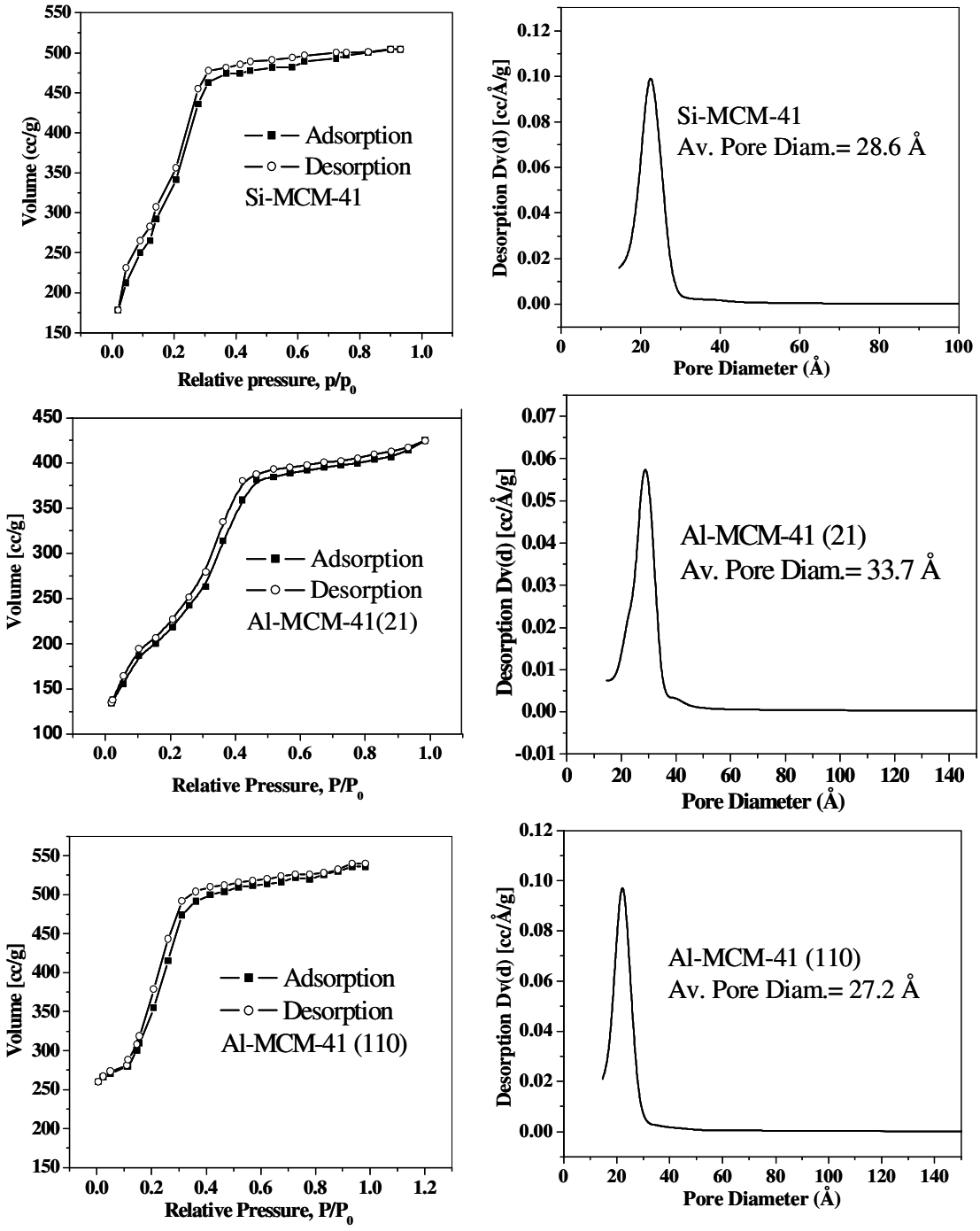

Figure 3.4 Nitrogen adsorption-desorption isotherms and corresponding pore size distributions of calcined Si-MCM-41 and Al-MCM-41 with Si/Al ratios of 21 and 110.

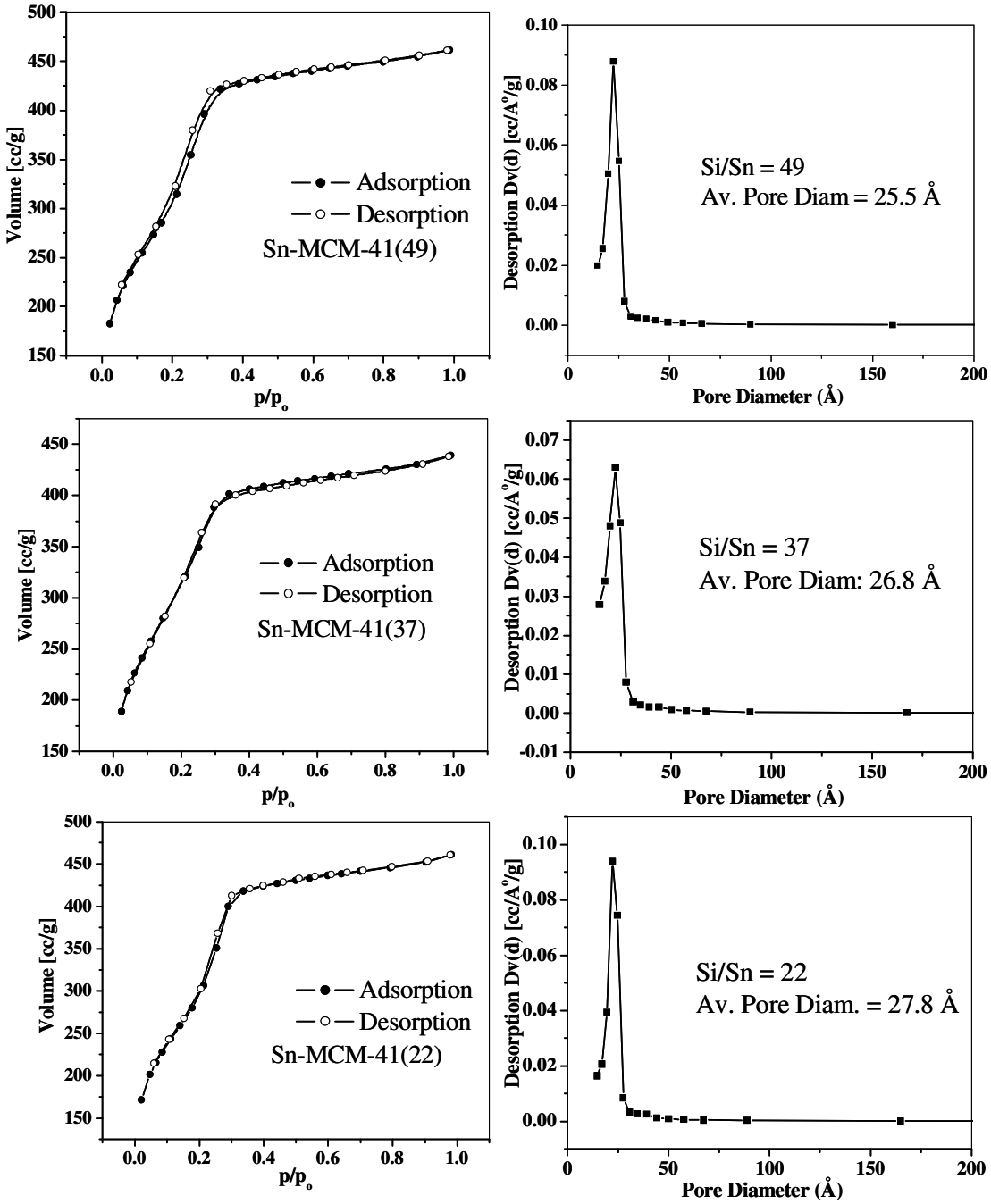

Figure 3.5 Nitrogen adsorption-desorption isotherms and corresponding pore size distribution of calcined Sn-MCM-41 with Si/Sn ratios of 49, 37 and 22.

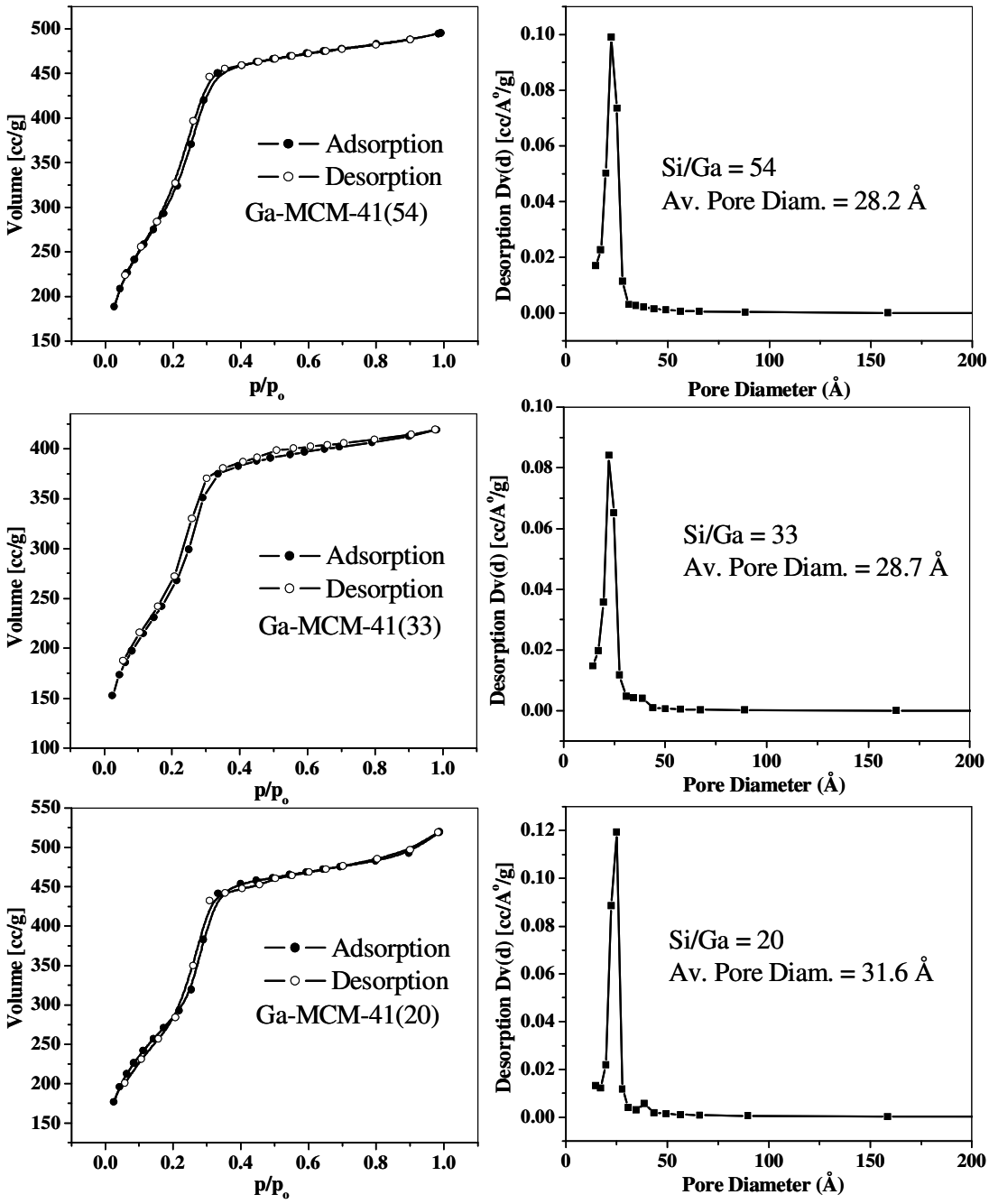

Figure 3.6 Nitrogen adsorption-desorption isotherms and corresponding pore size distribution of calcined Ga-MCM-41 with Si/Ga ratios of 54, 33 and 20.

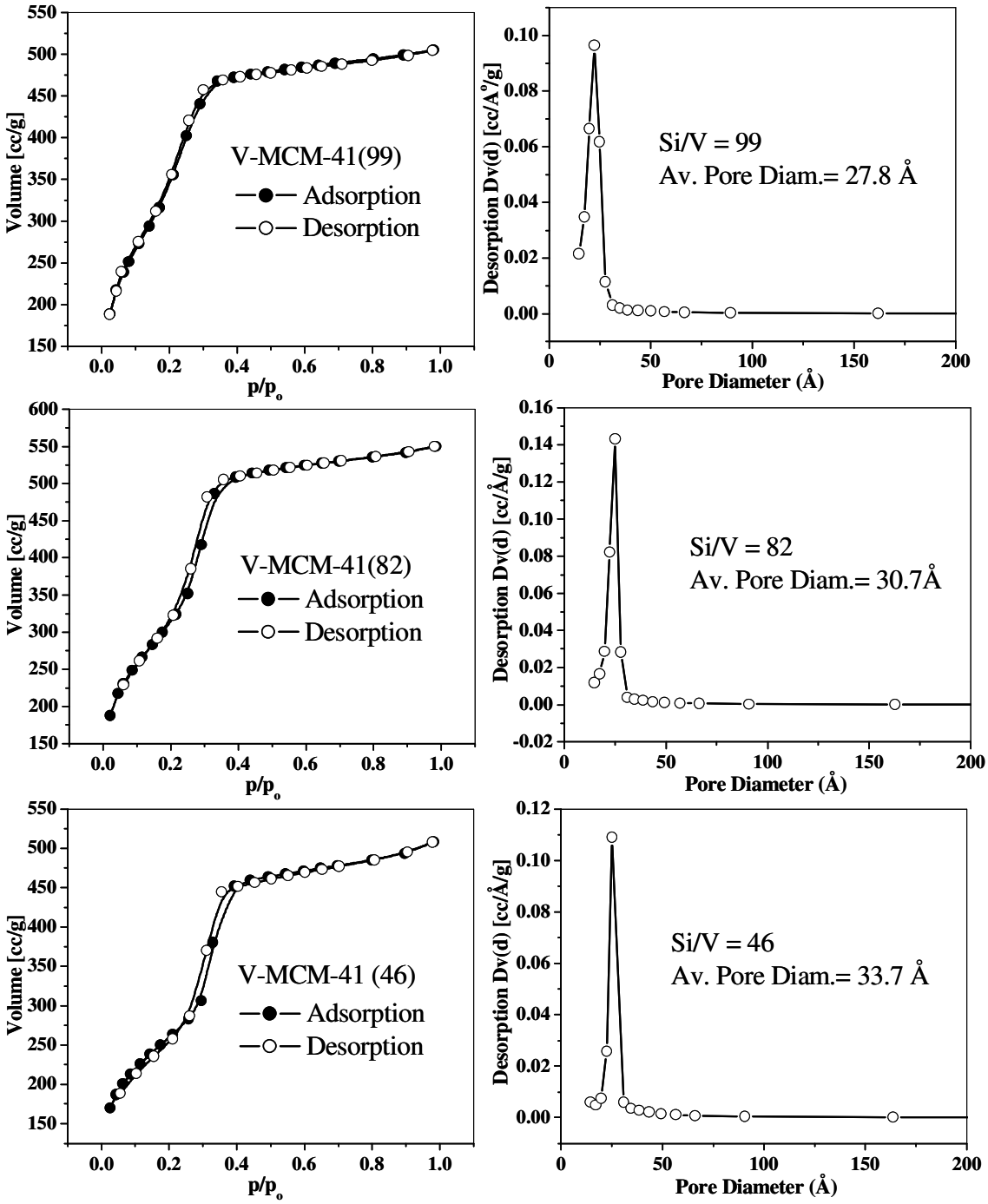

Figure 3.7 Nitrogen adsorption-desorption isotherms and corresponding pore size distribution of calcined V-MCM-41 with different Si/V ratios of 99, 82 and 46.

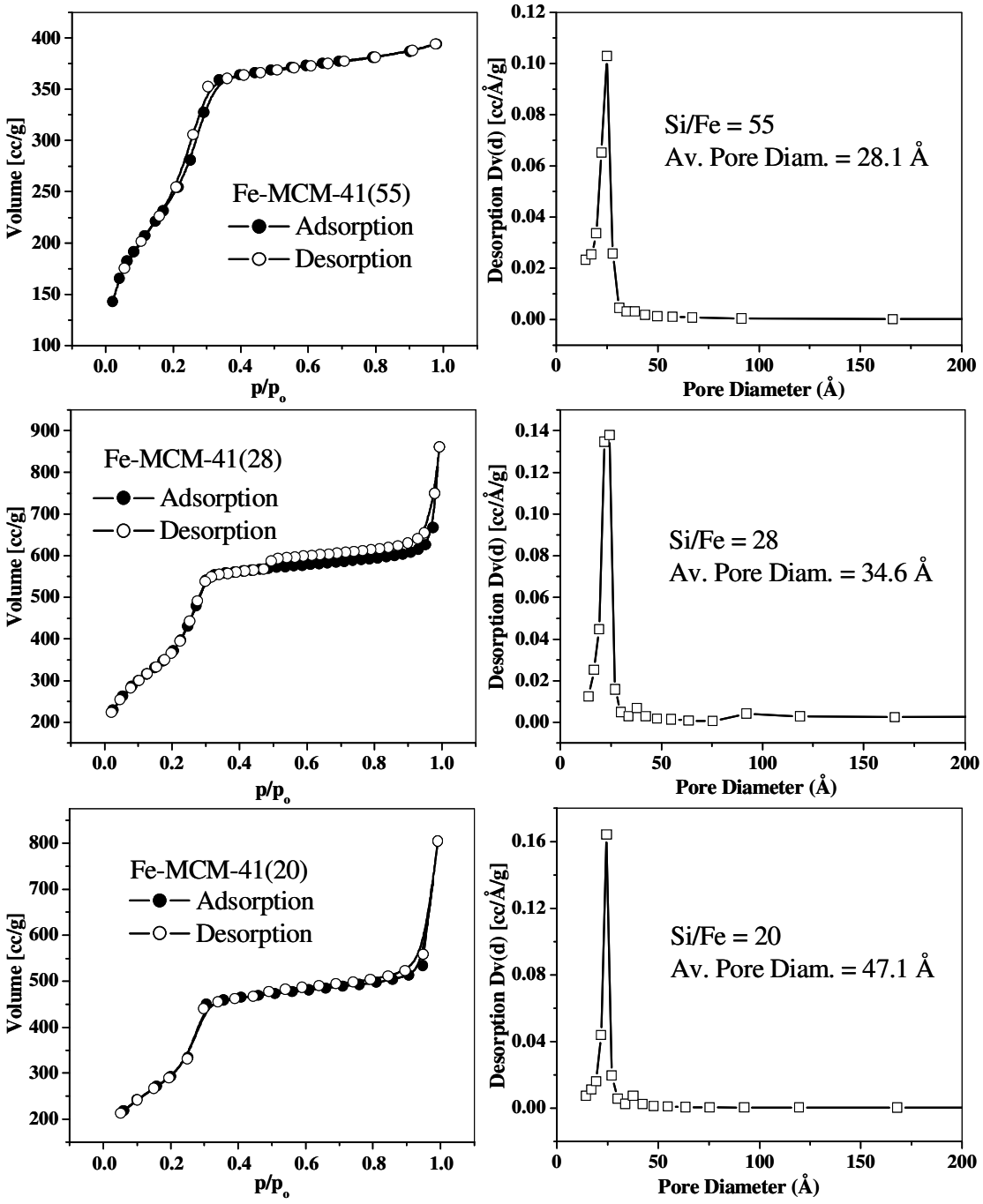

Figure 3.8 Nitrogen adsorption-desorption isotherms and corresponding pore size distribution of calcined Fe-MCM-41 with different Si/Fe ratios of 55, 28, and 20.

Table 3.4 Adsorption and acidity characteristics of Si- and Al-MCM-41 samples

Sample	S_{BET} (m^2/g)	Pore diam. D_{BJH} (Å)	Pore vol. V_{BJH} (cc/g)	Acidity by TPD of NH_3 (mmol/ g)			NH_3/Al^a (mmol/g)
				Weak acidity	Strong acidity	Total acidity	
Si-MCM-41	1094	28.6	0.78	-	-	0.0036	-
Al-MCM-41(110)	1219	27.2	0.83	0.042	0.058	0.100	0.39
Al-MCM-41(53)	996	30.0	0.89	0.064	0.093	0.157	0.30
Al-MCM-41(31)	873	31.4	0.69	0.091	0.134	0.225	0.26
Al-MCM-41(21)	785	33.7	0.66	0.098	0.152	0.250	0.20

[a] Moles of NH_3 desorbed from strong acid sites / mol of Al.

(d)Temperature programmed desorption of ammonia (TPDA)

The TPD profiles of Al-MCM-41 with different Si/Al ratios are presented in Figure 3.9 The amount of strong and weak acid sites in Al-MCM-41 with different Si/Al ratios, estimated from the deconvoluted TPD curves are given in Table 3.4. The table shows that the total number of acid sites including the strong and the weak acid sites increase with Al content [4]. The ratio of strong acid sites to weak acid sites also increases with increase in Al content. Strong acid sites or Brönsted acid sites are generated by tetrahedrally coordinated Al atoms forming Al-O(H)-Si bridges. The increase in the ratio of strong to weak acid sites with Al content implies that most of the added Al is tetrahedrally coordinated in the "framework" generating strong acid sites. Assuming that the strong acid sites are directly related to the Al ions in the samples, the ratio NH_3/Al (mole of NH_3 desorbed per mole Al) was calculated (Table 3.4). The results indicate an increase in the ratio with decreasing Al content, suggesting an increasing dispersion of Al at higher Si/Al ratios.

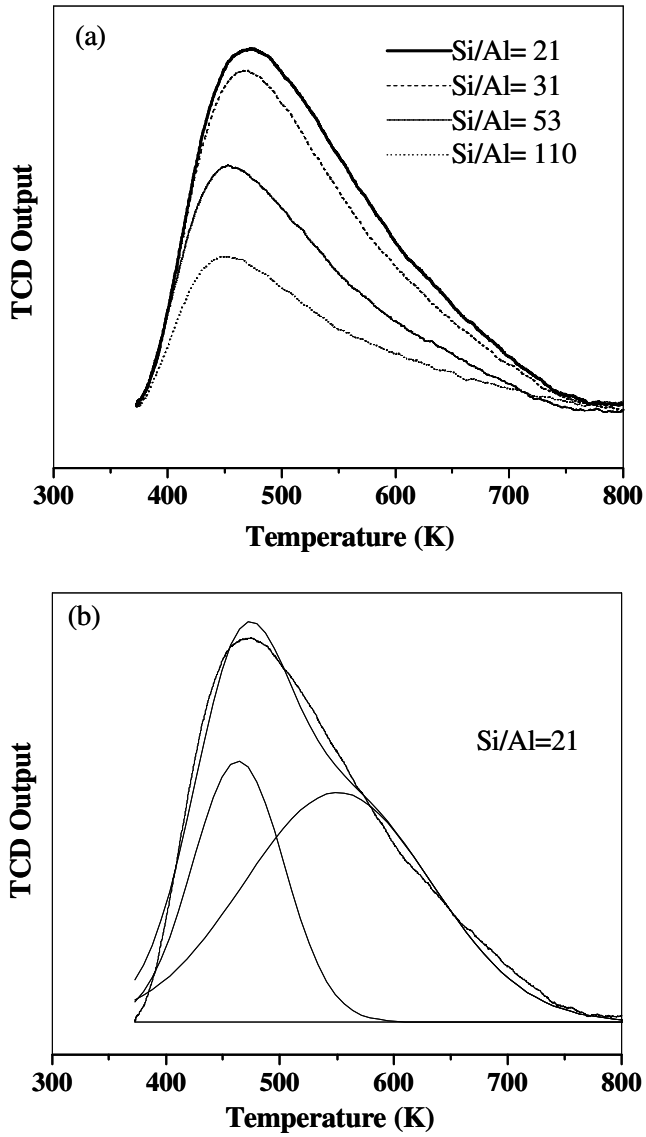

Figure 3.9 (a) Temperature programmed desorption of ammonia from Al-MCM-41 with different Si/Al ratios. (b) A typical deconvoluted plot for sample with Si/Al=21.

Table 3.5 Acidity of Sn-MCM-41 with different Sn contents by TPDA

Sample	Weak acidity (mmol/g)	Strong acidity (mmol/g)	Total acidity (mmol/g)
Sn-MCM-41(49)	0.058	0.061	0.12
Sn-MCM-41(37)	0.043	0.098	0.14
Sn-MCM-41(22)	0.059	0.13	0.19

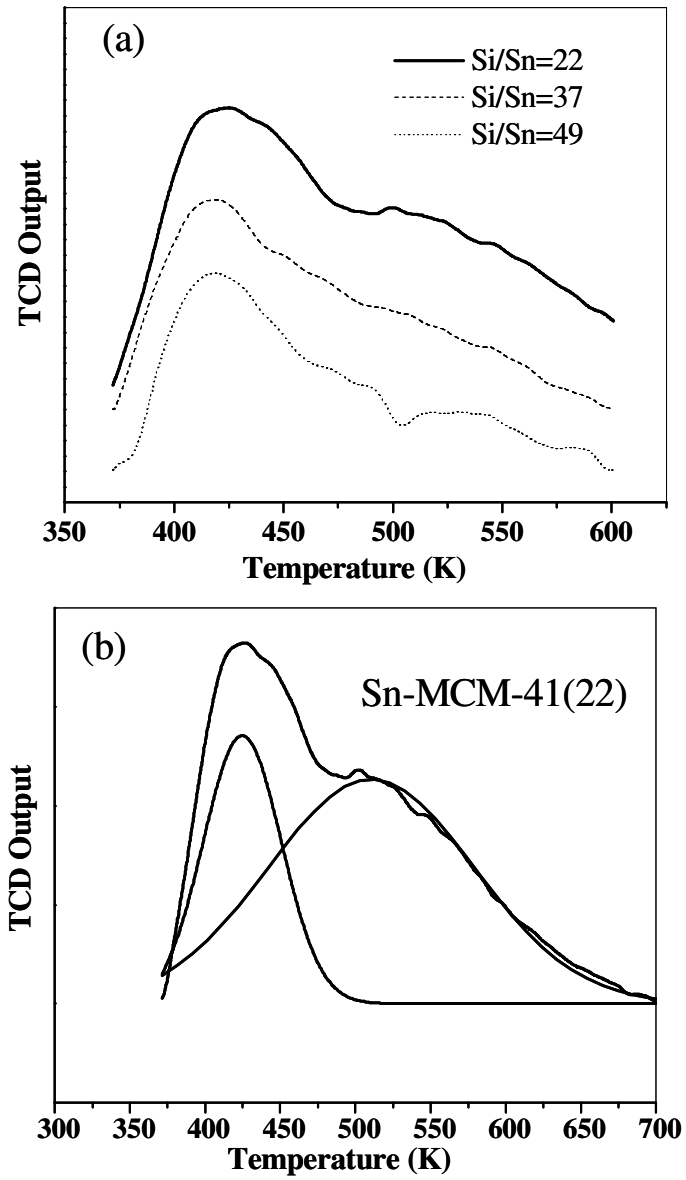

Figure 3.10 Temperature programmed desorption of ammonia from (a) Sn-MCM-41 with different Si/Sn ratios and (b) Typical deconvoluted plot for sample Si/Sn=22.

The TPD profiles of Sn-MCM-41 with different Si/Sn ratios and a typical deconvoluted plot for Si/Sn ratio of 22 are presented in Figure 3.10 (a) and (b), respectively. The amount of strong and weak acid sites in Sn-MCM-41 with different Si/Sn ratios, estimated from the deconvoluted TPD curves are given in Table 3.5. The table shows that the total number of acid sites including the strong and the weak acid

sites increase with metal content. The ratio of strong acid sites to weak acid sites also increases with increase in Sn content. One would expect that the substitution of a tetravalent ion (like Sn^{4+}) in the framework will not create any Brönsted acid sites (unlike in the case of Al^{3+}). Therefore, it is likely that the observed acidity is due to the Lewis acid character of Sn^{4+} and from defect Si–OH groups created due to Sn^{4+} incorporation. In any case, the origin of acidity in these samples is not clear.

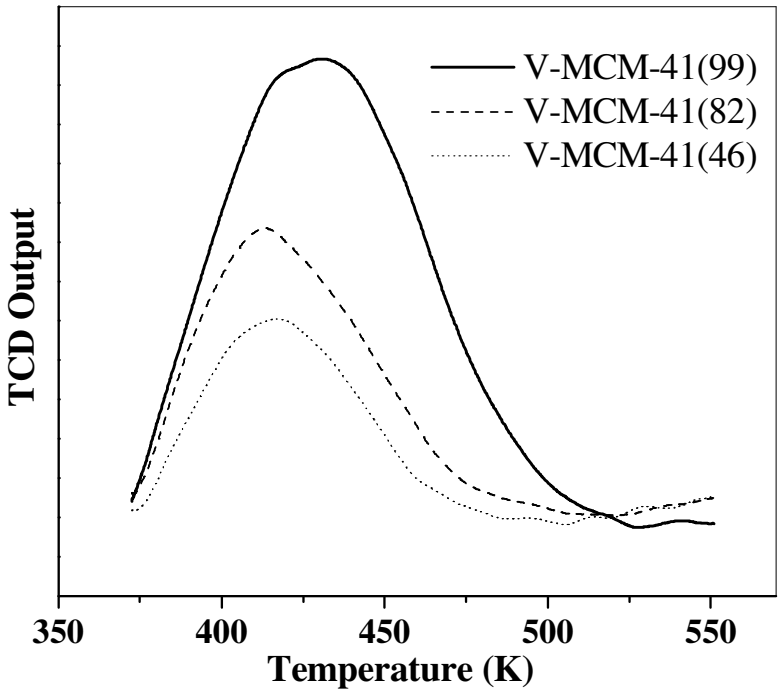

Figure 3.11 Temperature programmed desorption of ammonia from V-MCM-41 with different Si/V ratios.

Table 3.6 Acidity of V-MCM-41 with different V contents by TPDA

Sample	Metal content calcined sample (mmol/g)	Total acidity by TPD of NH_3 (mmol/g)
V-MCM-41 (99)	0.199	0.04
V-MCM-41 (82)	0.239	0.058
V-MCM-41 (46)	0.429	0.11

The TPD profile of V-MCM-41 with different Si/V ratios is presented in Figure 3.11. The number of acid sites increases slightly with the V content. The total acidity for V-MCM-41 is shown in Table 3.6. The origin and nature of the acid sites in V-MCM-41 are not clear. It is likely that the acid sites arise from V^{5+} Lewis acid centers and from –OH groups associated with V-ions.

(e) Nuclear Magnetic Resonance Spectroscopy

(i) ^{27}Al MAS NMR

^{27}Al MAS NMR spectrum of Al-MCM-41 with Si/Al ratio 21 reveals 2 peaks (Figure 3.12). The major peak with a chemical shift of 52.52 ppm is assigned to tetrahedrally coordinated Al presumably present in the Al-MCM-41 framework. The small peak at ~ 0 ppm is due to octahedrally co-ordinated (non-framework) Al present in the material [5]. The spectrum shows that most of the Al in Al-MCM-41 is tetrahedrally co-ordinated even at a high Al content (Si/Al = 21), and only a small amount of non-framework Al is present in the material.

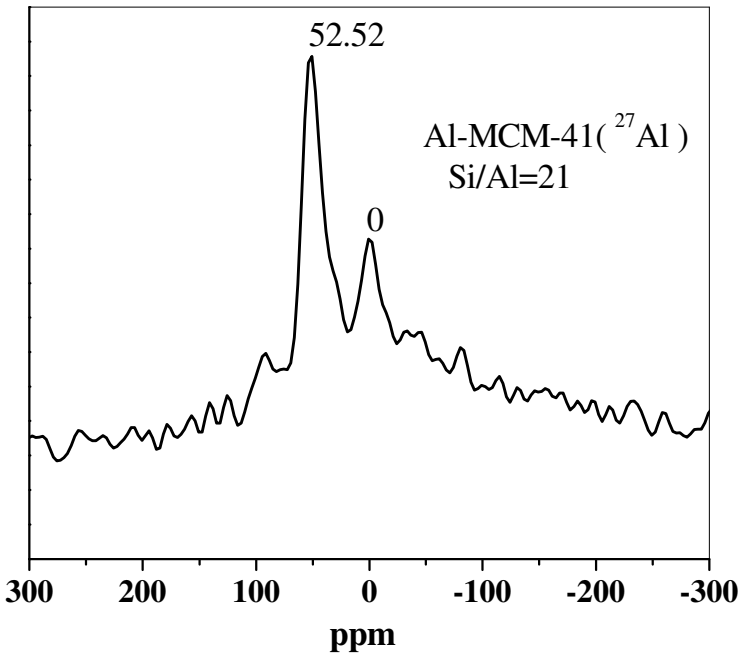

Figure 3.12 ^{27}Al-MAS NMR spectrum of calcined Al-MCM-41 with Si/Al=21.

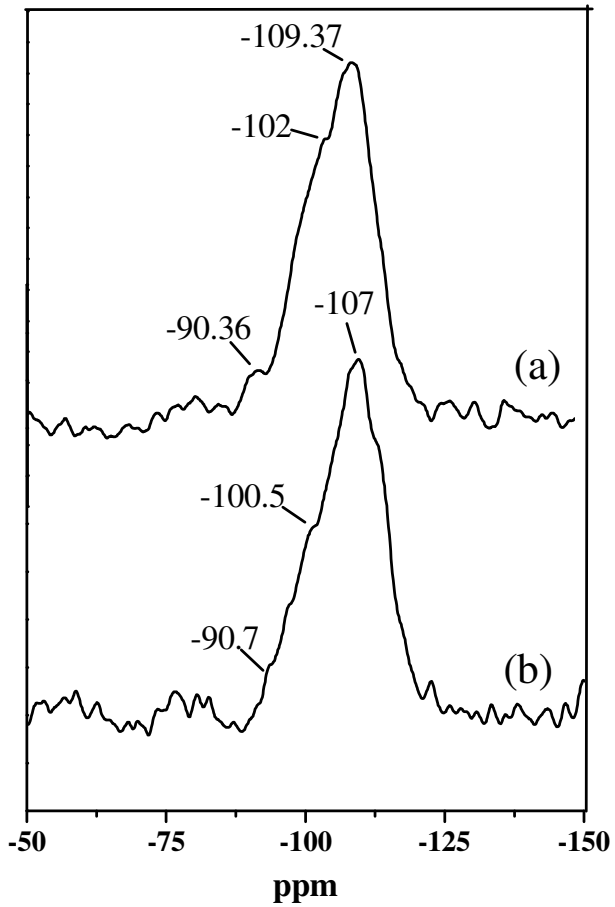

Figure 3.13 ^{29}Si MAS NMR spectra of (a) Si-MCM-41 and (b) Al-MCM-41 with Si/Al=21.

(ii) ^{29}Si MAS NMR

^{29}Si MAS NMR spectra of Si-MCM-41 and of Al-MCM-41(21) are shown in Figure 3.13. For purely siliceous MCM-41, we can observe the well resolved main peaks of Q^4 at -109.37 ppm corresponding to Si(4OSi), Q^3 at -102 ppm ,corresponding to Si(3OSi)OH) and a weak peak of Q^2 at –90.36 ppm corresponding to Si(2OSi)OH) units respectively. The incorporation of Al into the MCM-41 framework decreases the resolution of the ^{29}Si MAS NMR spectrum and a single peak at –107 ppm is observed with shoulders at –100.5 and –90.37 ppm, which correspond to Q^4, Q^3, and Q^2 respectively. These observations indicate the incorporation of Al into the MCM-41 "framework" [5].

(f) Diffuse reflectance UV-Visible spectroscopy

The UV-Vis spectra of calcined Sn-MCM-41 samples with different Si/Sn ratios and of SnO_2 are presented in Figure 3.14 (A). Sn-MCM-41 samples show a characteristic absorption band at around 208 ± 5 nm. The intensity of this absorption band increases with increasing Sn content. This band is reported to be due to the presence of Sn in tetrahedral coordination [6], which suggests that it is located in the walls ("framework") made up of Si^{4+} ions. The band at ~230 nm is attributed to the presence of small amounts of poorly dispersed (probably hexa- coordinated) Sn species at higher metal loadings. SnO_2 shows a broad absorption band at 280 ± 5 nm assigned to hexa- coordinated Sn-O-Sn type of polymeric species. These observations are similar to those made by Mal et al. for Sn-MFI molecular sieves [7].

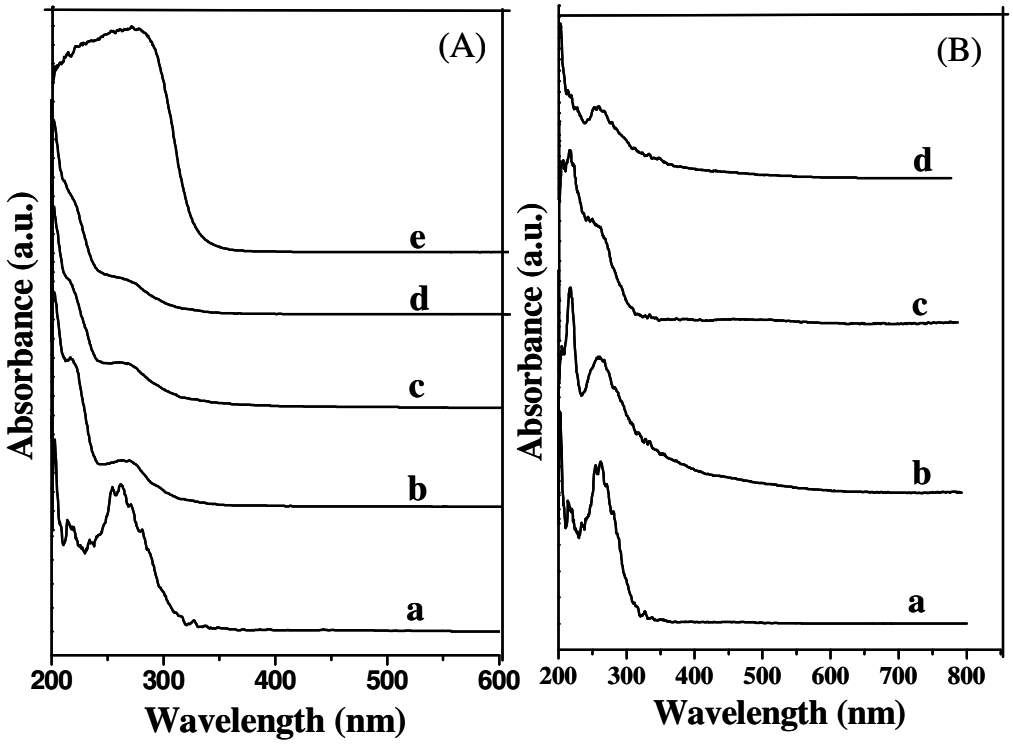

Figure 3.14 (A) UV-Visible spectra of calcined a) Si-MCM-41, b) Sn-MCM-41(49), c) Sn-MCM-41(37), d) Sn-MCM-41 (22) and e) SnO_2. (B) UV-Visible spectra of calcined a) Si-MCM-41, b) Ga-MCM-41(54), c) Ga-MCM-41(33), and d) Ga-MCM-41 (20).

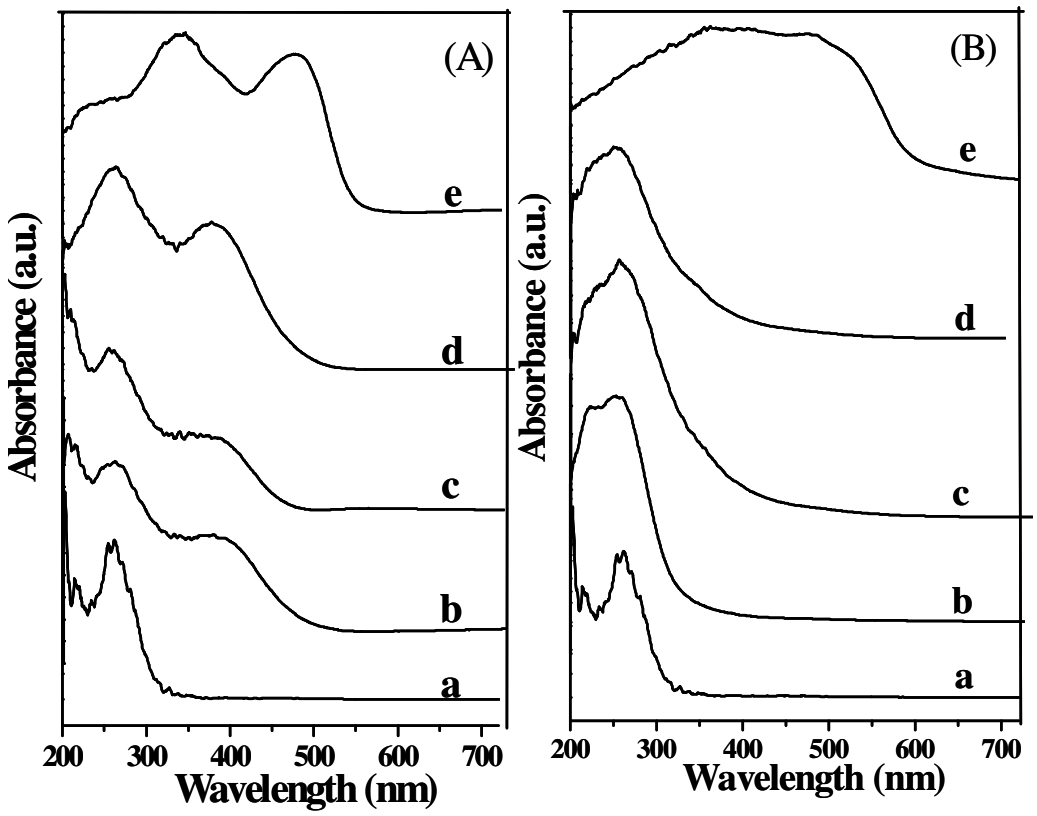

Figure 3.15 (A) UV-Visible spectra of calcined a) Si-MCM-41, b) V-MCM-41(99), c) V-MCM-41(82), d) V-MCM-41 (46) and e) V_2O_5. (B) UV-Visible spectra of calcined a) Si-MCM-41, b) Fe-MCM-41(55), c) Fe-MCM-41(28), d) Fe-MCM-41 (20) and e) Fe_2O_3.

The UV-Vis spectra of calcined Ga-MCM-41 samples with different Si/Ga ratios are presented in Figure 3.14 (B). Ga-MCM-41 samples show a characteristic absorption band at around 216 ± 2 nm. The intensity of this absorption band increases with increasing Ga content indicating that the Ga^{3+} ions are in tetrahedral co-ordination presumably in the "framework". Again, the presence of a band at 260 nm shows that small amounts of poorly dispersed, probably hexa- coordinated Ga species (Ga_2O_3) also exist at higher metal contents.

UV-Vis spectra of calcined V-MCM-41 samples with different Si/V ratios and of V_2O_5 are presented in Figure 3.15 (A). The reported assignments for different V-species are presented in Table 3.7. All the samples show two characteristic bands, one at about 250-260 nm corresponding to V^{5+} (Td) in the framework and another in

the 360-370 nm range indicating the presence of Td – V^{5+} species with V=O bonds [8,9]. Off-white as synthesized V-MCM-41 samples upon calcination changed to white. But after exposure to air a colour change was observed as shown in Table 3.8. This indicates additional co-ordination of water molecules to the V^{5+} ions. On the basis of these assignments, one may conclude that the charge transfer band observed at around 360-370 nm is due to V^{5+} ions with a short V=O double bond and three longer V-O bonds [8, 9]. These bands may be assigned to square pyramidal or octahedral V^{5+} species on the wall surfaces. It appears that upon exposure to air, the Td geometry of V first changes to square pyramidal and then to octahedral. Pure V_2O_5 exhibits 2 bands at around 340 and 470 nm that are attributed to V^{5+} (Td) in the surface and V^{5+} (O_h) respectively. As per the previous reports, the low energy charge transfer band (LCT, O→ V electron transfer) shows bands at around 330-500 nm which corresponds to V^{5+} in an O_h environment [9]. The LCT transition for V^{4+} shows an absorption band at 250-285 nm. [10]. Also, the bands at 295 and 340 nm have been assigned to O → V electron transfer $(\pi)t_2 \rightarrow (d)e$ and $(\pi)t_1 \rightarrow (d)e$, respectively, for V-silicalite samples [11].

The UV-Vis spectra of as-synthesized samples of Fe-MCM-41 reveal absorption bands at 220 and 245 nm. For the calcined samples (shown in Figure 3.15 (B)), a shift in the absorption band is observed at ~250-260 nm for Si/Fe = 55 and 28. This band is due to tetrahedrally co-ordinated Fe species and assigned to dπ-pπ charge transfer between Fe and O atoms in the framework of Fe-O-Si in the zeolite [12]. At higher Fe loading, one more extra band is observed at 350 nm for Si/Fe = 20, which is due to the presence of extra framework Fe or Fe oxide clusters.

Table 3.7 Assignment of UV-Vis adsorption bands of V-ions in V-MCM-41

Band position (nm)	Metal oxidation state (Ionic environment)	Type of transition	Reference
250-260	V^{5+} (Td) in the framework	C.T. O → V	[9, 10]
340	V^{5+} (Td) in the surface	C.T. O → V	[9,11]
450	V^{5+}(Distorted O_h)	-	[11]
330-500	V^{5+}(O_h)	C.T. O → V	[8,9]
605	V^{4+} (Td)	-	[9,11]

Table 3.8 Colors of V and Fe-MCM-41 samples

Sample Name	As synthesized	Calcined	Rehydrated
Si-MCM-41	White	White	White
V-MCM-41(99)	Off- white	White	Pale yellow
V-MCM-41(82)	Off- white	White	Pale green
V-MCM-41(46)	Off- white	White	Green
Fe-MCM-41(55)	White	White	White
Fe-MCM-41(28)	White	Off-white	Off-white
Fe-MCM-41(20)	White	Brown	Brown

Co-ordination environment of V and Fe: The V-MCM-41 samples with different Si/V ratios show (Table 3.8) different colors depending on their hydration state. As synthesized samples are of off-white. After calcination they turn white. But these samples change color again after exposure to ambient atmosphere. V species are easily affected by moisture in the air and change from distorted tetrahedral to probably square-pyramidal co-ordination by the co-ordination of H_2O or OH. The accessibility of the V-species to ambient moisture suggests that they are probably dispersed at or above the surface of the pore walls.

All as-synthesized Fe-MCM-41 samples are (Table 3.8) white suggesting that no bulk Fe oxide exists and all Fe cations are probably incorporated inside the "framework" after hydrothermal synthesis. The white colour was retained after calcination of the low Fe-content (Si/Fe = 55) sample. Fe-MCM-41 (Si/Fe = 28) was off-white suggesting the presence of some extra framework ions, while at a higher Fe content, Fe-MCM-41 (Si/Fe = 20) turns brown suggesting the presence of aggregated Fe-oxide clusters in the sample.

(g) TG/DTG

Figure 3.16 shows the TG/DTG curves of MCM-41 samples. It is found that there are three main weight losses for the MCM-41 materials. The first weight loss between 323 K and 423 K is due to adsorbed water, the second weight loss between 423 K and 573 K is due to the decomposition of the organic species and the small peak at 723 K may be due to the condensation of silanol groups or removal of coke during the calcination process. The weight loss due to the template increases with

aluminum content of the samples (Figure 3.16 (a)). Besides, the peak minimum of the differential thermogram (DTG- Figure 3.16 (b)) due to template removal is shifted to higher temperatures with increasing Al-content suggesting a stronger interaction of the template with the Al-species.

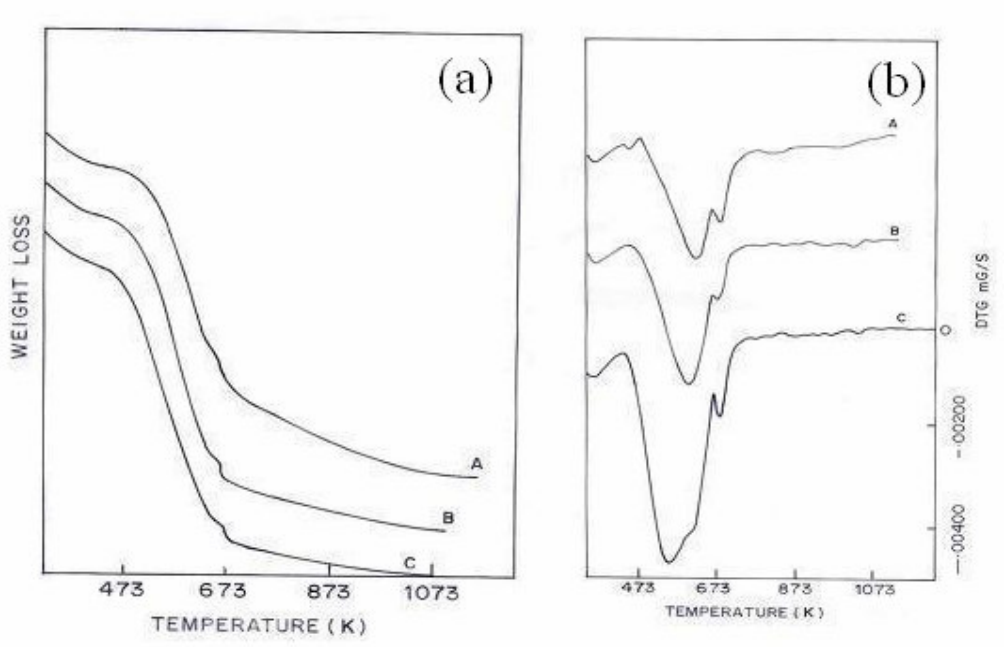

Figure 3.16 (a) TG plots of (A) Si/Al=21, (B) 53 and (C) Si-MCM-41; (b) DTG plots of (A) Si/Al=21, (B) 53 and (C) Si-MCM-41.

(h) Electron microscopy

Figure 3.17 shows the TEM images of Al-MCM-41 with Si/Al ratio of 53 and of pure Si-MCM-41. The samples reveal characteristic uniform pore sizes as reported by earlier workers [1].

SEM images of V-MCM-41(99) and Fe-MCM-41 (55) are shown in Figure 3.18. The V-MCM-41 sample exhibits rod like morphology with a relatively uniform size of ~ 1μm, which are randomly aggregated. Fe-MCM-41 is present as dispersed spherical particles of ~ 1μm. The particles are arranged uniformly to form a mesophase.

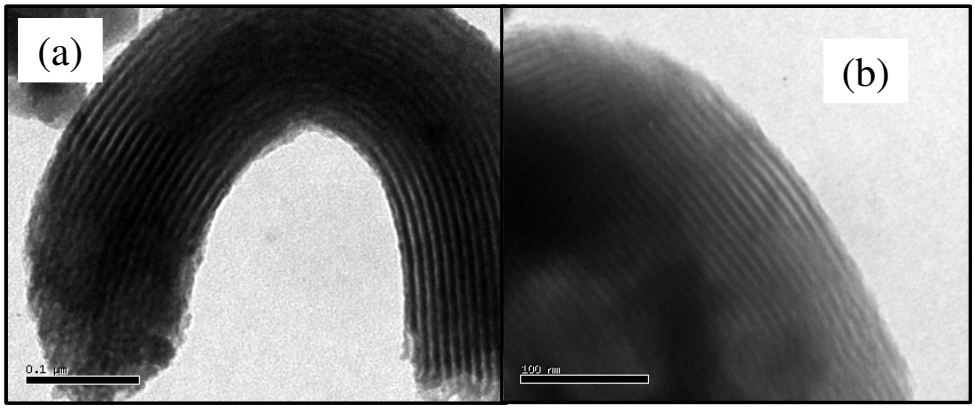

Figure 3.17 TEM images of (a) Al-MCM-41 (53) and (b) Si-MCM-41.

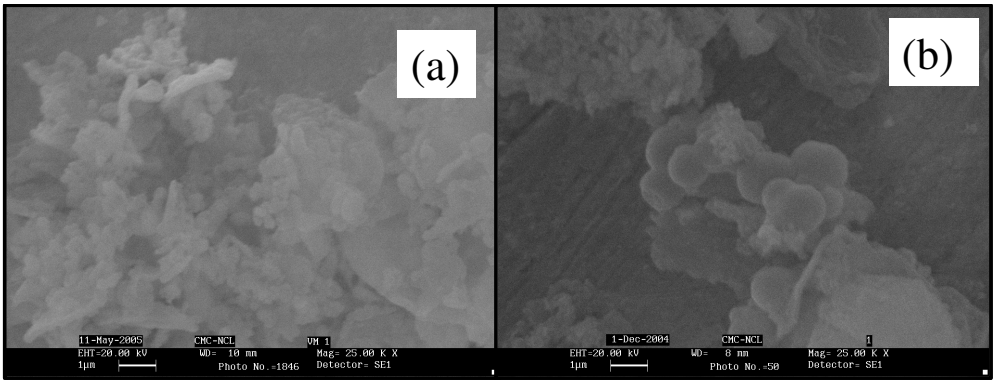

Figure 3.18 SEM images of calcined (a) V-MCM-41(99) and (b) Fe-MCM-41(55).

(i) Temperature programmed reduction (TPR)

The reducibility characteristics of the metal species are useful means for detecting interactions between the metal and the support. The reduction of Fe-MCM-41 samples was investigated by measuring the hydrogen uptake with increasing temperature (Figure 3.19). The hydrogen uptake values and other data are presented in Table 3.9. The uptake curves for Fe-MCM-41 samples with Si/Fe ratios of 55, 28 and 20 exhibit one broad maximum centered at 693, 701, and 703 K, respectively. Fe_2O_3 exhibits 2 peaks at 637 and 910 K. Only one electron transfer was reported to take place ($Fe^{3+} \rightarrow Fe^{2+}$) during the reduction of Fe-MCM-41 samples with lower Fe content, up to 923 K, which means that iron is stabilized in the mesoporous structure and probably linked to the framework via oxygen ions [13]. The total hydrogen consumption for Fe-MCM-41 samples increases with Fe content. At higher loadings, the consumed hydrogen slightly exceeds the amount needed for the reduction of iron

to the divalent state. Therefore, it appears that a small amount (less than 3 %) of the incorporated iron may be reduced to the zero valent state in samples with high Fe content.

Table 3.9 TPR measurements of V- and Fe-MCM-41 with different metal contents

Sample	Metal content [a] calcined sample (mmol/g)	H_2 uptake (mmol/g) up to 840 K calculated by TPR	T_{Max} by TPR (K)	e/Me by TPR	Average oxidation state by TPR
Si-MCM-41	-	-	-	-	-
V-MCM-41 (99)	0.199	0.1033	835	1.04	3.96
V-MCM-41 (82)	0.239	0.1628	827	1.36	3.64
V-MCM-41 (46)	0.429	0.2647	819	1.23	3.76
Fe-MCM-41(55)	0.328	0.1963	693	1.19	1.81
Fe-MCM-41(28)	0.639	0.2654	701	0.83	2.17
Fe-MCM-41(20)	0.886	0.4626	703	1.04	1.96

a- Fe estimated by AAS and V by XRF

The temperature programmed reduction profiles for V-MCM-41 with different Si/V ratios and for pure V_2O_5 is presented in Figure 3.20. The sample with Si/V = 99 shows 3 distinct peaks at 485, 715, 832 K. V-MCM-41 (82) shows 3 peaks at 482, 713 and 825 K, while at a higher loading (V-MCM-41 (46)); only one peak at 819 K is obtained. The results of the H_2 consumption for V incorporated MCM-41 catalysts are presented in Table 3.9. It is found that H_2 uptake increases with metal content. In principle, the hydrogen consumption observed could be due to an incomplete reduction of V^{5+} species to V^{3+} species (i.e. partial reduction to V^{4+}), the presence of small amounts of V^{4+} or V^{3+} species and/or the presence of non reducible V^{5+} species in the V-MCM-41 samples. An incomplete reduction of V^{5+} to V^{3+} species was reported by several authors for VOx/SiO_2 catalysts [14, 15, 16], while non-reducible V^{5+} and V^{4+} species were observed in V/MCM-41 samples by Grubert et al. [17] and by Luan et al. [9], respectively. The TPR profile for bulk V_2O_5 exhibits multiple

major reduction peaks at 898, 935 and 1005 K. Bosch et al. [18] reported a similar observation, and they attributed this to the reduction sequence $V_2O_5 \rightarrow V_6O_{13} \rightarrow V_2O_4 \rightarrow V_2O_3$.

The average oxidation state of V after H_2 reduction was found to be 3.96 to 3.60. The average vanadium valency state given in Table 3.9 was calculated assuming a complete reduction of the reducible V^{5+} species to V^{3+} species. This suggests that in the as-synthesized samples, a fraction of the V-ions are present as V^{4+} or V^{3+} species that are stabilized against oxidation to V^{5+} during calcination in air.

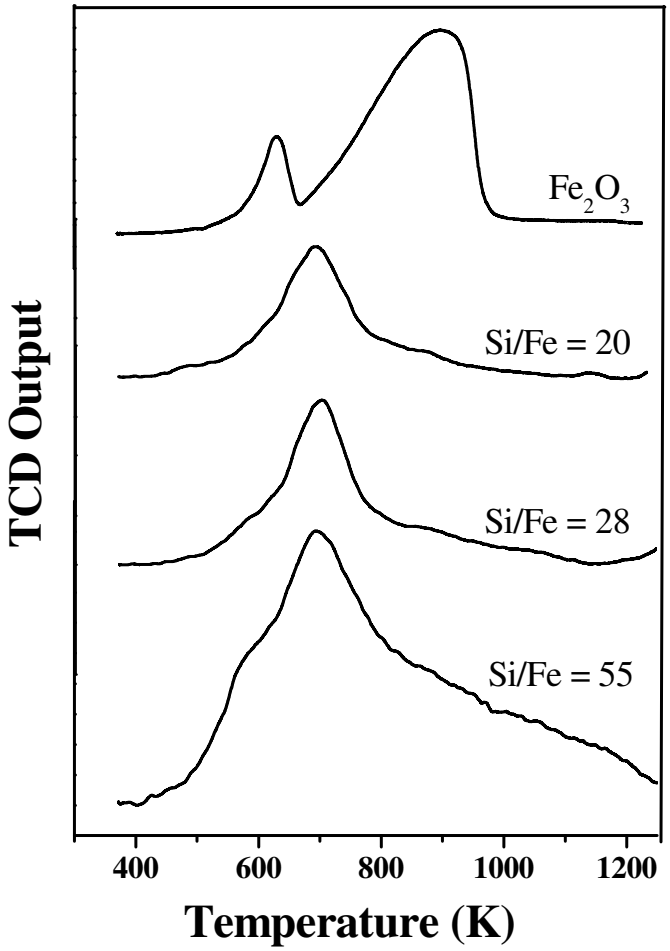

Figure 3.19 H_2-TPR reduction profiles of calcined Fe-MCM-41 with different Si/Fe ratios and of Fe_2O_3.

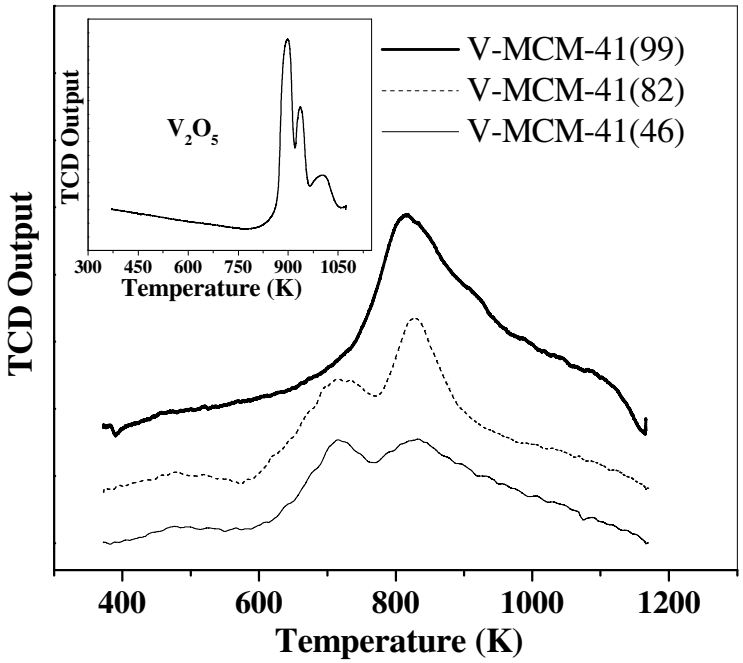

Figure 3.20 H_2-TPR reduction profiles of calcined V-MCM-41 with different Si/V ratios and of V_2O_5.

It is expected that at a lower temperature, a surface type (probably tetrahedral) species would be reduced, whereas at a higher temperature a more polymeric or bulk like vanadia would be reduced. It is also expected that vanadia species becomes more bulk like i.e. the particle size increases, with an increase in loading; the vanadia becomes more difficult to reduce due to bulk diffusion limitations resulting in a shift in the TPR peaks to higher temperatures. However, the low temperature peak does not shift significantly to higher temperatures with an increase in the vanadia loading. This suggests that this peak can be attributed to the reduction of a surface species.

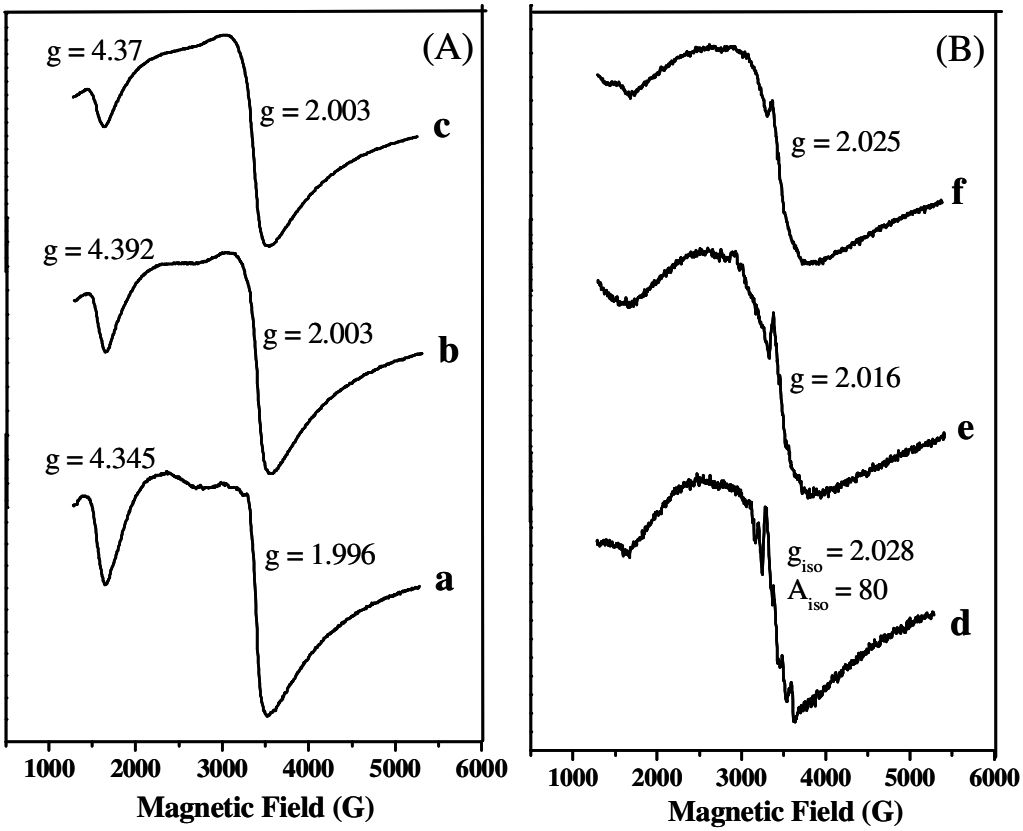

Figure 3.21 ESR spectra of (A) as synthesized Fe-MCM-41 samples with different Si/Fe ratios of (a) Si/Fe=55, (b) Si/Fe=28, and (c) Si/Fe=20; (B) calcined Fe-MCM-41 samples with different Si/Fe ratios (d) Si/Fe=55, (e) Si/Fe=28, and (f) Si/Fe=20.

(j) Electron spin resonance (ESR)

The structural arrangement of the iron species is easily detectable by ESR techniques [30, 31]. The ESR spectra of as-synthesized and calcined Fe-MCM-41 samples with different Si/Fe ratios are presented in Figure 3.21 (A) and (B), respectively. The as-synthesized and calcined samples exhibit 2 signals at g = 4.3 and g = 2.0, which can be attributed to Fe (III) in a tetrahedral co-ordination with strong rhombic distortion and Fe (III) in octahedral co-ordination, respectively [32, 33]. The intensity of the signal at g = 2.0 is large compared to the signal at g = 4.3. Hence, it appears that much of the iron is present as Oh species. These species could be hydrated Fe^{3+} ions close to the surface in the walls or attached to the surface of the pore walls. The Td species are probably present inside the walls. Besides the signal at g = 2.0, a very broad signal at g = 2.3 - 2.6 indicates the presence of couples of Fe^{3+} ions, e.g. $Fe^{3+} – O – Fe^{3+}$ clusters.

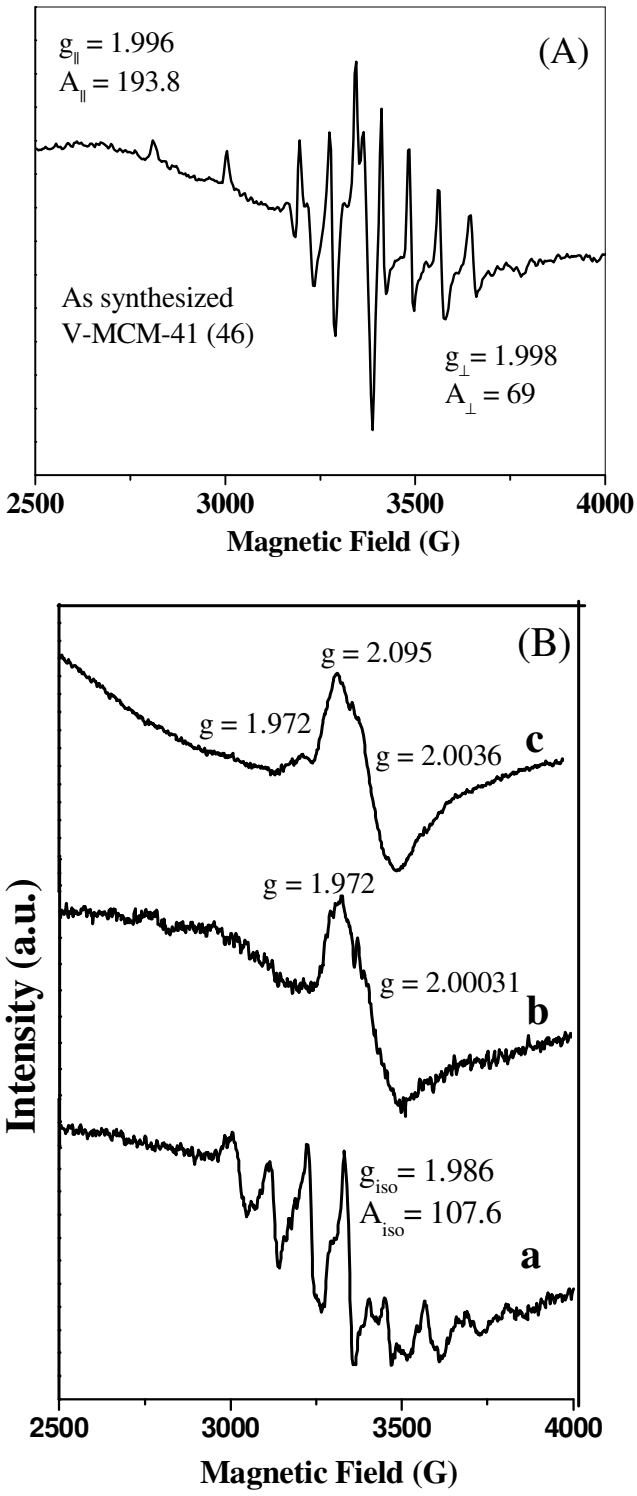

Figure 3.22 (A) ESR spectra of as synthesized V-MCM-41 (46) and (B) calcined V-MCM-41 with different Si/V ratios of (a) 99, (b) 82, and (c) 46, respectively.

All fresh as-synthesized V-MCM-41 samples exhibit ESR signals at room temperature as shown in Figure 3.22 (A); the eight line axially symmetric signals are from tetravalent vanadium originating from the interaction of the d^1 electron with the nuclear spin (I_n = 7/2 of ^{51}V; natural abundance 99.8 %). The ESR signal intensity of the as-synthesized material increases linearly with increasing vanadium content. The spin Hamiltonian parameters are, $g_{\parallel}$ = 1.996, $A_{\parallel}$ = 193.8 G, $g_{\perp}$ = 1.998, and $A_{\perp}$ = 69 G where **A** is the hyperfine coupling constant. Since no superimposed broad singlet is observed, the VO^{2+} species appear to be isolated and well dispersed. These g values and hyperfine coupling constants are typical of vanadyl VO^{2+} complexes with square pyramidal co-ordination [19] that have been observed in several molecular sieves [20, 21].

On calcination, the typical eight line spectra of V^{4+} nearly disappears and a broad single line spectrum is noticed for V-MCM-41 samples (Si/V = 82 and Si/V = 46) suggesting the oxidation of V^{4+}.to V^{5+}. A low intensity eight line spectrum is also superimposed on the broad signal. The overall intensity of the broad signal of the calcined sample is much lower than that observed for the as-synthesized sample. In the case of the sample with a low V content (V-MCM-41 (99), the eight line spectrum does not disappear completely upon calcination and still shows the presence of a vanadyl species (Figure 3.22 (B)). Also, the low intensity of the axially symmetric ESR signal of the vanadyl species indicates that most of the VO^{2+} ions are oxidized to V^{5+}. These observations suggest that in V-MCM-41, two types of species are present, one of it being less accessible and strongly bound to the "framework" preventing its oxidation. The other more easily oxidized species is present to a larger amount in samples containing larger amount of V. These observations are in agreement with the UV-Vis results that suggest 2 kinds of tetrahedrally coordinated V^{5+} species located inside and on the internal surface of the hexagonal tubular walls [9].

3.3.2 SBA-15 type ordered mesoporous metallosilicate catalysts

This section of the chapter discusses the characterization of SBA-15 type ordered mesoporous metallosilicate catalysts, namely Si-SBA-15, Al-SBA-15 with different Si/Al ratios and PW loaded SBA-15 catalysts.

Table 3.10 Physicochemical properties of calcined SBA-15 and Al-SBA-15 with different Si/Al ratios

Sample	Si/Al In put	Si/Al XRF	d_{100} (Å)	Unit cell para.[a] 'a_0'(Å)	S_{BET} (m^2/g)	Pore dia. D_{BJH} (Å)	Wall thick.[b] (Å)	Pore vol. V_{BJH} (cc/g)
Si-SBA-15		-	103.8	119.9	822	67.7	52.2	1.11
Al-SBA-15 (71)	70	70.7	102.6	118.5	769	67.4	51.1	1.02
Al-SBA-15 (46)	50	45.7	102.6	118.5	734	67.5	51.0	0.99
Al-SBA-15 (30)	30	30.4	102.6	118.5	787	67.4	51.1	1.09
Al-SBA-15 (19)	20	18.7	102.6	118.5	667	67.4	51.1	0.92
Al-SBA-15 (9)	10	8.6	102.6	118.5	485	67.4	51.1	0.67

a- Unit cell parameter $a_0 = 2d_{100}/\sqrt{3}$; b- Wall thickness = a_0- pore diameter

(a) Chemical analysis

The chemical analyses of Al-SBA-15 samples obtained by XRF methods are presented in Table 3.10. The calcined samples have Si/Al ratios close to the input values as the samples were prepared by a post synthetic route by impregnation (chapter 2). All the samples (Al-SBA-15 and PW-SBA-15) are identified by their Si/Al ratios (values inside brackets) or wt. % of PW present in them.

(b) X-ray diffraction

The XRD patterns of the calcined SBA-15 and Al-SBA-15 with different Si/Al ratios are shown in Figure 3.23. The patterns reveal a prominent peak at 0.8^o and two weak peaks at 1.6 and 1.7^o. 2θ that match well with the typical pattern reported for SBA-15 [22, 23]. The XRD peaks indexed as the [100], [110], and [200] diffraction planes are characteristic of a hexagonal arrangement of the pores in SBA-15. XRD-patterns do not reveal significant changes in the hexagonal mesoporous structure after Al incorporation. The d_{100} spacing of Al-SBA-15, 102.6 Å is close to that of SBA-15 (103.8 Å; Table 3.10). Similarly, much change in a_0 value is also not noticed.

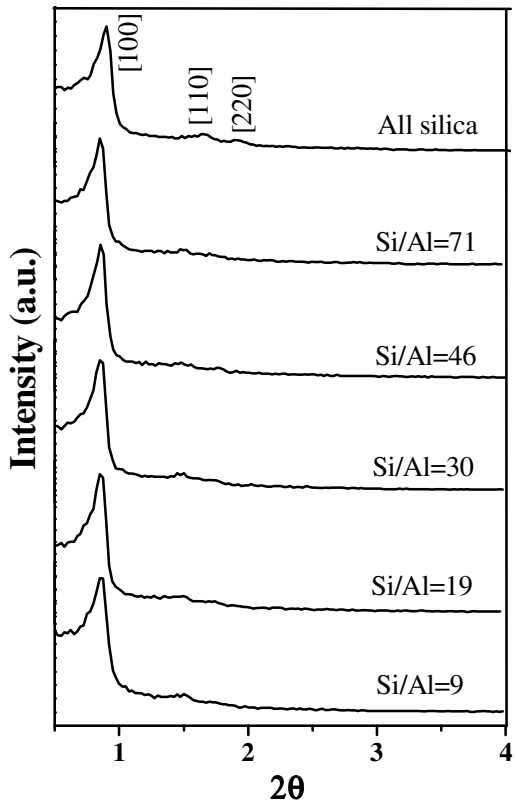

Figure 3.23 Low angle XRD patterns of calcined Si-SBA-15 and Al-SBA-15 with different Si/Al ratios.

Table 3.11 Physicochemical properties of calcined SBA-15 and PW/SBA-15

Sample	d_{100} cal. (Å)	Unit cell para.[a] 'a_0' (Å)	S_{BET} (m^2/g)	Av. pore diam. D_{BJH} (Å)	Wall thick.[b] (Å)	Pore vol. V_{BJH} (cc/g)
Si-SBA-15	103.8	119.9	822	67.7	52.2	1.11
10 wt. % PW/ SBA-15	102.6	118.5	594	65.7	51.1	0.95
20 wt.% PW/ SBA-15	102.6	118.5	572	60.5	51.0	0.87
30 Wt.% PW/ SBA-15	102.6	118.5	552	61.0	51.1	0.84
40 Wt.% PW/ SBA-15	102.6	118.5	496	66.4	51.1	0.81

a- Unit cell parameter $a_0 = 2d_{100}/\sqrt{3}$; b- Wall thickness = a_0- Pore diameter.

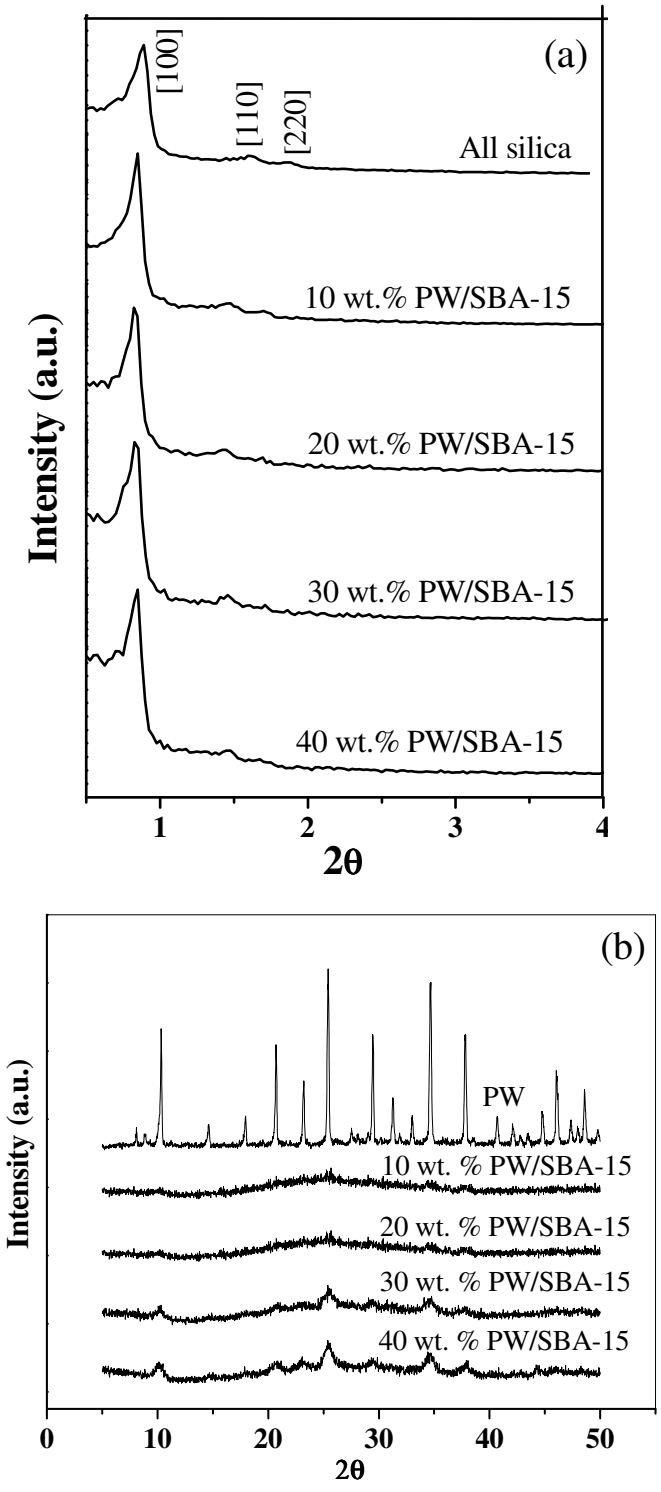

Figure 3.24 XRD patterns of PW/SBA-15 with various PW loadings (a) low angle and (b) wide angle.

The low angle XRD patterns of PW supported on SBA-15 [24] are similar to the all silica SBA-15 [23] [Figure 3.24 (a)]. It is clear that even after PW loading, the structure of SBA-15 is retained. The d_{100} distances, unit cell parameter (a_0) values and the wall thickness calculated from d_{100} and pore diameters are presented in Table 3.11. It is found that these values are not significantly influenced by PW loading suggesting that the structural integrity of SBA-15 is maintained to a large extent in the samples.

The wide-angle XRD spectrum [2θ, 5-50^o Figure 3.24 (b)] shows that as the percentage of PW loading increases, the reflections resemble the PW pattern more closely. Even so the lines are broad suggesting substantial dispersion of the PW. It appears that much of the PW is well dispersed in the samples with only a small amount of bulk PW (crystallite size >30 (Å) that contributes to the XRD pattern) being present.

(c) N_2 sorption

Figure 3.25 (a) presents the N_2 adsorption-desorption isotherms and corresponding pore size distribution for siliceous SBA-15. A typical type IV adsorption isotherm with a H1 hysteresis loop is observed. The isotherm exhibits a sharp inflection in the p/p_0 range of 0.65 to 0.80 characteristic of capillary condensation within fairly uniform pores. The nitrogen adsorption–desorption isotherms for the different Al containing samples presented in Figure 3.25 (b) are almost similar to that of Si-SBA-15 except for a decrease in the amount of adsorption with increasing Al- loadings.

The loss in adsorption is especially significant for Al-SBA-15 (9). The BET surface areas, pore volumes and average pore diameters of the samples are presented in Table 3.10. As the Al content increases, the surface area decreases slightly. Alumination by reacting SBA-15 with $AlCl_3$ in dry methanol does not affect the average pore diameter of the samples. The wall thickness for the Al-SBA-15 samples also remains the same as that of SBA-15.

An interesting aspect of the data of Table 3.10 is the nearly similar values of surface areas (~ 780 ± 40 m^2/g; ± 5 %) and pore volumes (1.05 ± 0.06 cc/g; ± 6 %) for all the samples except Al-SBA-15 (9) whose values of S_{BET} and pore volume are 485 m^2/g and 0.67 cc/g, being ~ 37 % less than the average values for other samples. The

large loss in area and volume cannot be accounted for by the ~11 % wt gain due to alumina loading. As the average pore diameter of Al-SBA-15 (9) is still the same as those of the others (~ 67 Å), it appears that a portion of the pores in the sample is fully blocked by the Al_2O_3 formed and not accessible to N_2. Apparently, the other samples with lower Al-loading possess a near uniform distribution of Al inside the pores. The calculation of the pore size distribution (PSD) was performed using the desorption branches of the N_2 adsorption isotherms using the Barrett-Joyner-Halenda (BJH) formula.

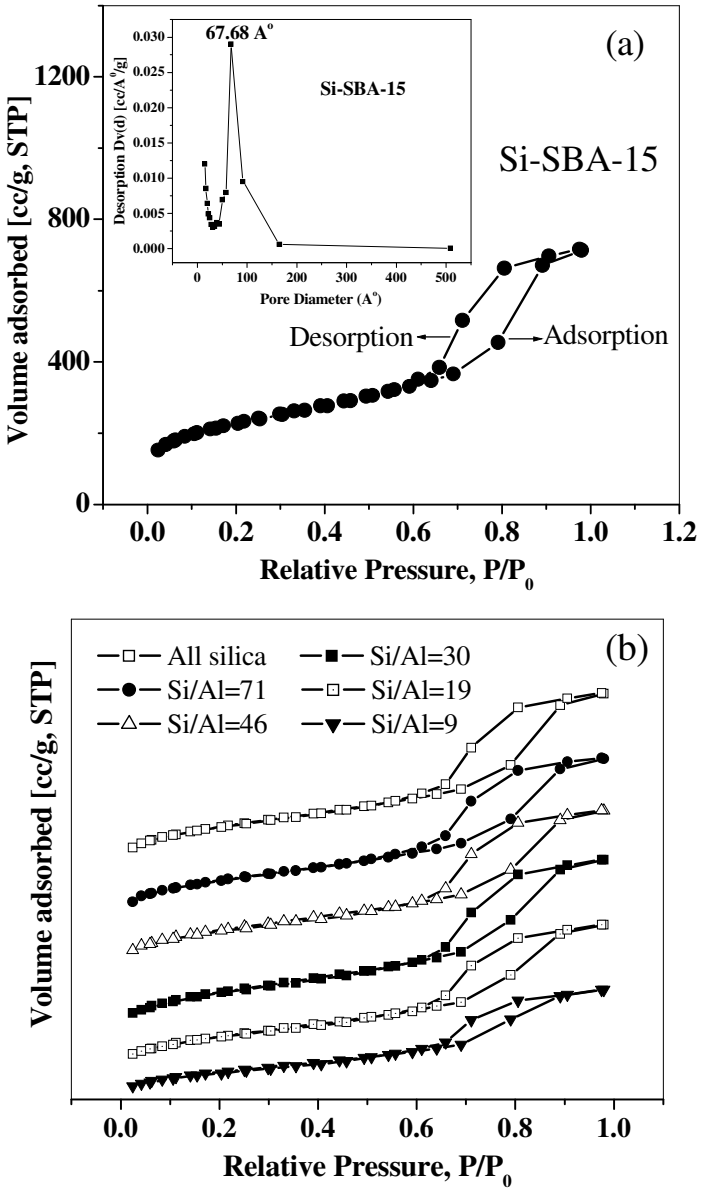

Figure 3.25 (a) N_2 adsorption-desorption isotherms and corresponding pore size distribution of calcined Si-SBA-15 and (b) Al-SBA-15 with different Si/Al ratios.

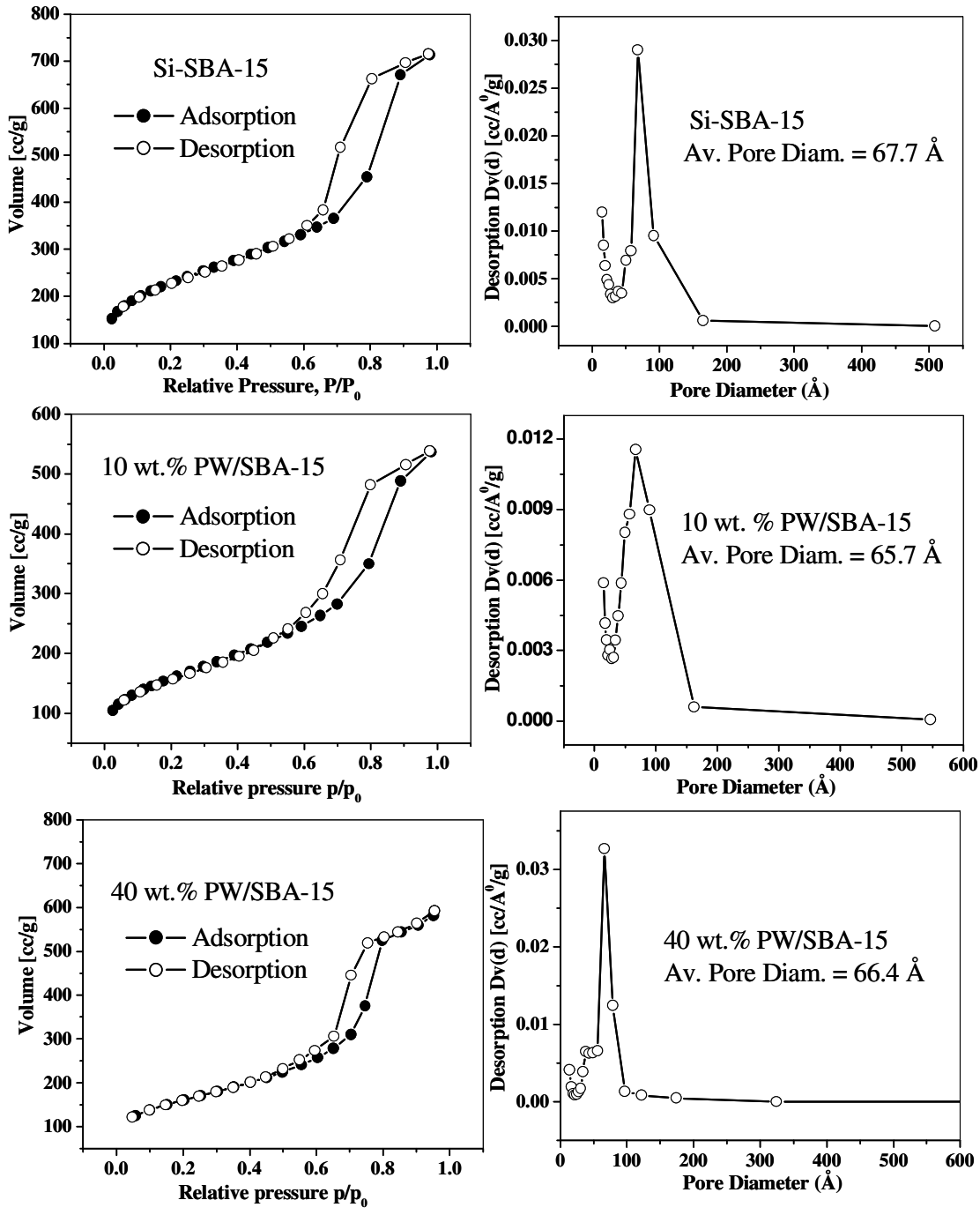

Figure 3.26 N_2 adsorption isotherms and corresponding pore size distribution of Si-SBA-15, 10 wt. % PW/SBA-15 and 40 wt. % PW/SBA-15.

The surface area of bulk PW is ~ 5 m^2/g [25] which is very low, while Si-SBA-15 has a high surface area of 822 m^2/g and a pore volume of 1.11 cc/g. The nitrogen adsorption-desorption isotherms and corresponding pore size distributions of Si-SBA-15 and 40 wt. % PW/SBA-15 are shown in Figure 3.26. The isotherms are typically of the type IV and are very similar for the three samples. The surface area values of all the samples are presented in Table 3.11. It is found that surface area and pore volume decrease with PW loading. This is a typical observation noticed during impregnation in many catalyst systems involving mesoporous oxides. The decrease is attributable to many reasons, such as the loaded material (low area heteropoly acid) contributes to the total weight of the sample, blockage of some pores and coverage of surface and some destruction of the mesopore structure during impregnation and calcination.

(d)Temperature programmed desorption of ammonia

The TPD profiles of Al-SBA-15 with different Si/Al ratios are presented in Figure 3.27. The amounts of strong and weak acid sites in the Al-SBA-15 samples estimated from the deconvoluted TPD profiles are given in Table 3.12. It is noticed, as expected [23], that the total number of acid sites increases with Al content. Strong acid sites (Brönsted) are generated by tetrahedrally coordinated Al atoms forming Al-O(H)-Si bridges. The increase in the ratio of strong to weak acid sites with Al content implies that most of the added Al is tetrahedrally co-ordinated in the framework. Assuming that the strong acid sites are directly related to the Al ions in the samples, the ratio NH_3/Al (mole NH_3 desorbed per mole Al) was calculated (Table 3.12). The results indicate a decrease in the ratio with increasing Al content, suggesting a decrease in dispersion of Al at higher Al loading.

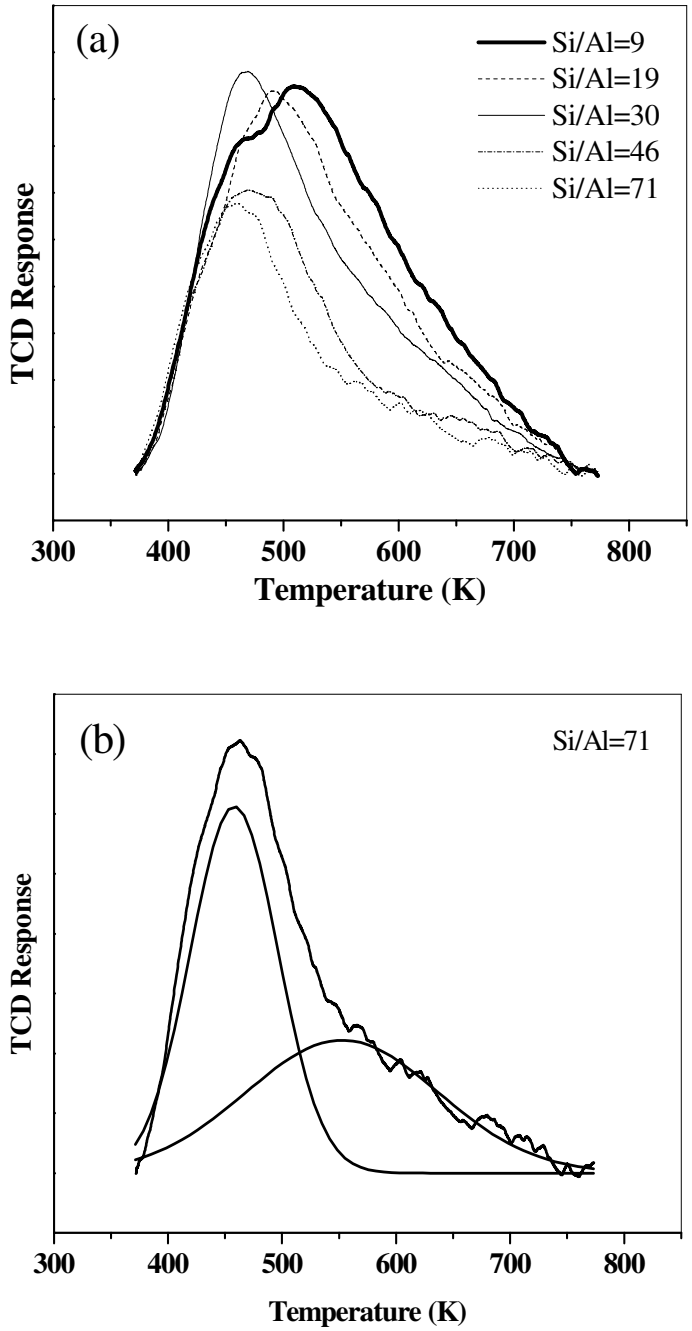

Figure 3.27 (a) Temperature programmed desorption of ammonia from Al- SBA-15 with different Si/Al ratios. (b) Typical deconvoluted plots for sample with Si/Al=71.

Table 3.12 Acidity of Si- and Al-SBA-15 with different Si/Al ratios by TPDA

Sample	Acidity by TPDA (mmol/g)			NH_3/Al^a
	Weak	Strong	Total	(mmol/g)
Si-SBA-15	--	---	0.004	---
(Al)SBA-15 (71)	0.09	0.12	0.21	0.52
(Al)SBA-15 (46)	0.08	0.17	0.25	0.48
(Al)SBA-15 (30)	0.16	0.18	0.34	0.34
(Al)SBA-15 (19)	0.18	0.19	0.37	0.23
(Al)SBA-15 (9)	0.19	0.23	0.42	0.13

[a] Moles of NH_3 desorbed /mol of Al; based on strong acid sites

The TPD profiles of PW/SBA-15 with different PW loadings (Figure 3.28 (a)) reveal that the number of acid sites increases with the PW content. The TPD profiles were deconvoluted (as shown in Figure 3.28 (b)) for all the samples into two peaks and the amount of weak and strong acidity was estimated (Table 3.13). The amount of strong acidity is roughly proportional to the amount of PW present in the samples. As the samples were preheated at 873 K during the TPD studies, it is likely that at least part of the PW molecules (Keggin units) decomposed into the oxides as shown: $H_3PW_{12}O_{40} = 1/2\ P_2O_5 + 12\ WO_3 + 3/2\ H_2O$. Earlier workers have reported a decrease of average acid strength owing to interaction with the support for PW supported on silica [26] and MCM-41 [27]. However, the TPD methodology used in our studies is not expected to reveal minor changes in the acid strengths of the samples.

Table 3.13 Acidity of PW/ SBA-15 with different PW loadings by TPDA

Sample	Acidity by TPDA (mmol/g)		
	Weak	Strong	Total
Si-SBA-15	--	---	0.004
10 wt.% PW/ SBA-15	0.086	0.094	0.18
20 wt.% PW/ SBA-15	0.154	0.166	0.32
30 wt.% PW/ SBA-15	0.20	0.26	0.46
40 wt.% PW/ SBA-15	0.22	0.42	0.64

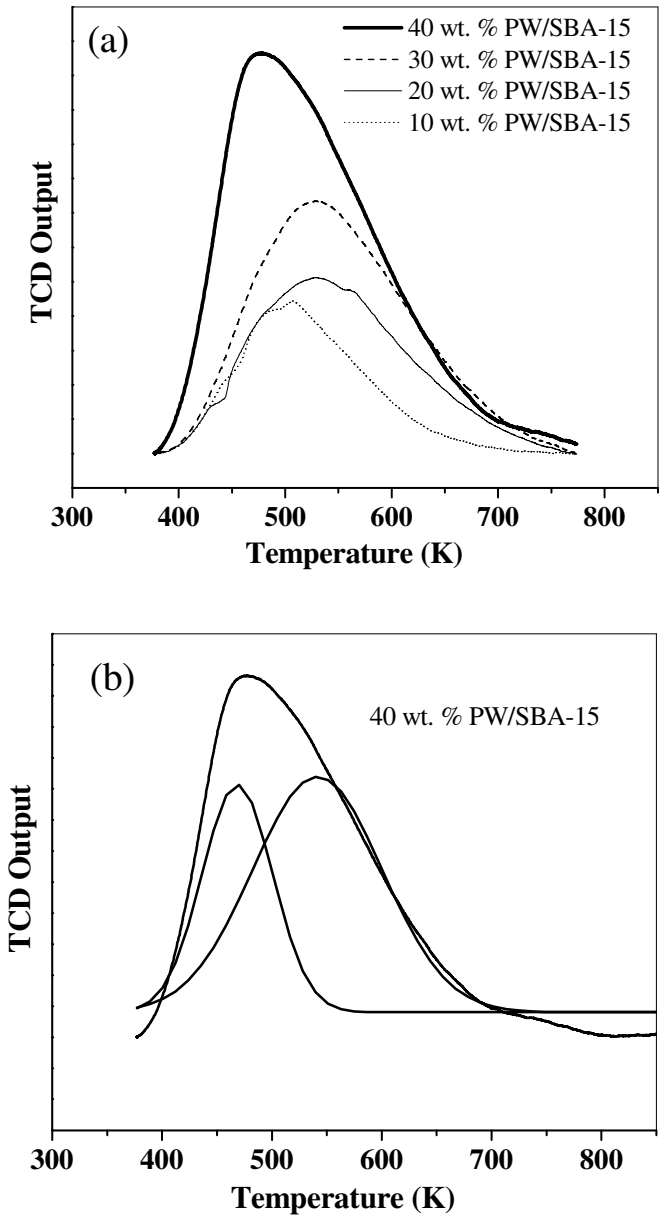

Figure 3.28 (a) Profiles of TPD of ammonia of PW/SBA-15 with different amount of PW loading. Typical deconvoluted plots of (b) 40 wt. % PW/SBA-15 catalyst.

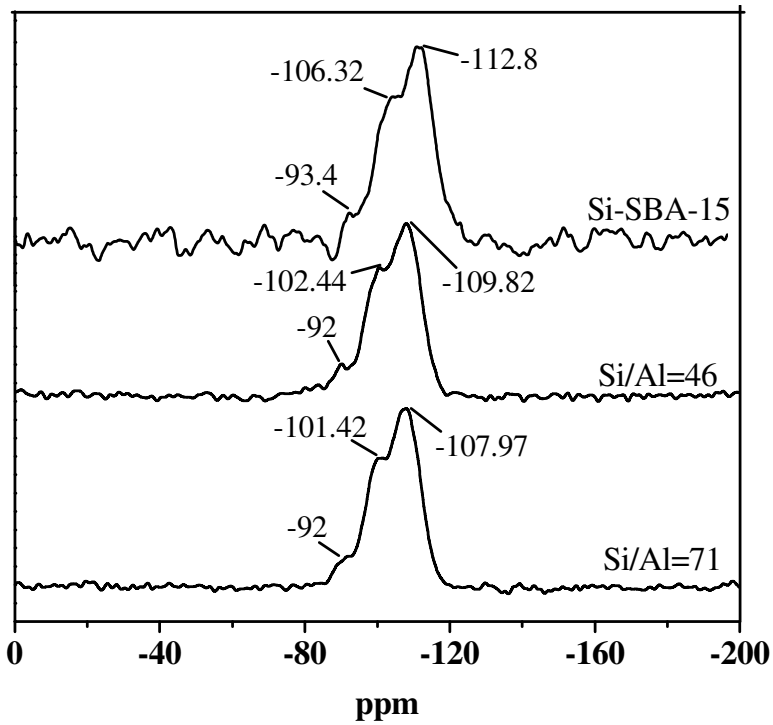

Figure 3.29 ^{29}Si MAS NMR spectrum of purely siliceous SBA-15 and Al-SBA-15 (Si/Al=46 and Si/Al=71) prepared using TEOS as the source of silicon.

(e) MAS NMR

(i) ^{29}Si MAS NMR

Figure 3.29 presents the ^{29}Si MAS NMR spectra of calcined SBA-15, and Al-SBA-15 samples, respectively. Purely siliceous calcined SBA-15 shows 3 peaks at -93.4, -106.3 and -112.8 ppm corresponding to Q_2 (Si(2OSi)OH), Q_3 (Si(3OSi)OH) and Q_4 (Si(4OSi), respectively. Similarly, calcined Al-SBA-15 with Si/Al=46 and Si/Al =71 exhibits 3 peaks of Q_2, Q_3 and Q_4 as shown in Figure 3.31. The broadness of the signals is attributed to a larger distribution of T-O-T angles.

Figure 3.30 shows the ^{29}Si MAS NMR spectra of PW loaded SBA-15 catalysts. All the catalysts with PW loadings of 10, 20, 30 and 40 % show peaks at -92, -102 and -110 ppm, which are assigned to Q_2, Q_3, and Q_4 species respectively. Purely siliceous SBA-15 sample exhibits Q_2, Q_3, and Q_4 peaks at, respectively, -93.4, -106.32 and -112.8. The shifting of the peaks of PW loaded SBA-15 catalysts suggest that the heteropolyacids interact strongly with the "framework".

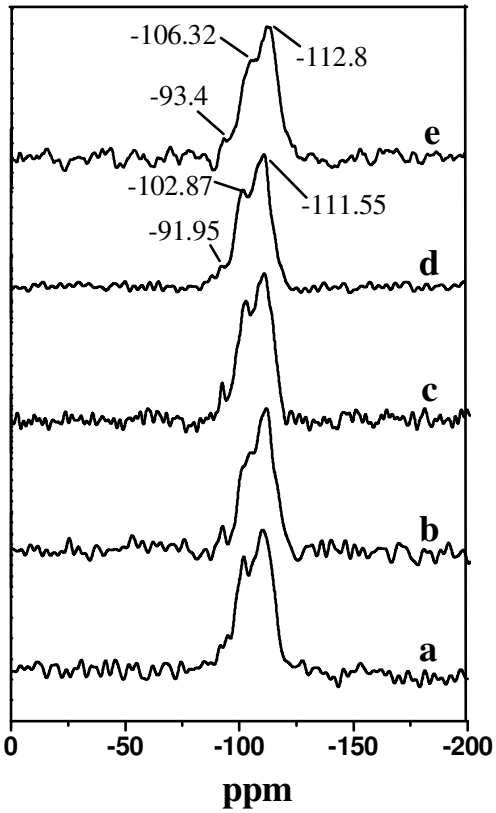

Figure 3.30 ^{29}Si MAS NMR spectra of PW/SBA-15 catalysts with (a) 10, (b) 20, (c) 30, (d) 40 wt. % loading of PW and of (e) Si-SBA-15.

(ii) ^{27}Al MAS NMR

^{27}Al MAS NMR spectrum of calcined Al-SBA-15 with Si/Al ratio of 30, 46 and 71 is presented in Figure 3.31. The peak in the range of 52-54 ppm is assigned to Al in a tetrahedral environment (AlO_4 structural unit, Al (tet)), in which Al is covalently bound to four Si atoms via oxygen bridges. The peak at 0 ppm is assigned to octahedral Al (AlO_6 structural unit, Al (oct)) [4]. NMR spectrum of gamma alumina shows both Td and Oh Al-species [31]. It is therefore likely that some of the Td and Oh Al-ions seen in the Al-SBA-15 samples arises from bulk alumina like species formed at the surface, especially at higher Al-loadings. As XRD of the samples did not detect any alumina phase on the surface these species must be XRD invisible micro-domains (< 30 Å). It appears, therefore, that the Al-ions in SBA-15 exist in different configurations; as Al-associated with Si-ions in the pore walls (both Td and Oh species) and on the surface as well as dispersed alumina like domains

containing Td and Oh-types of Al-ions. The general broadness of the peaks is a result of small variations in the symmetry of the aluminium sites in the calcined sample.

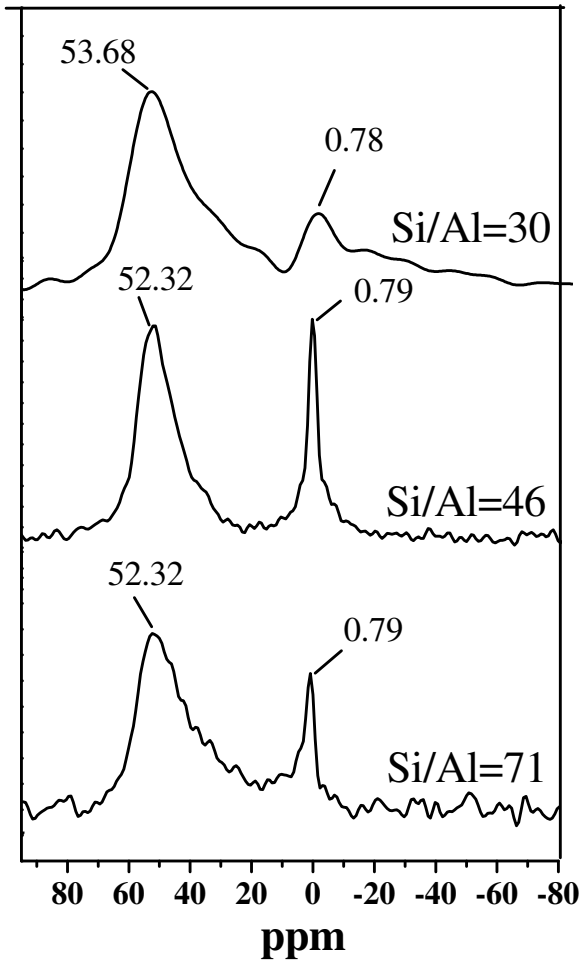

Figure 3.31 ^{27}Al MAS NMR spectrum of Al-SBA-15 samples with different Si/Al ratios of 30, 46 and 71 prepared using aluminium chloride.

(iii) ^{31}P MAS NMR

The ^{31}P MAS NMR of PW/SBA-15 catalysts with 10, 20, 30 and 40 wt. % loading of PW are presented in Figure 3.32. ^{31}P MAS NMR shows a peak at -15.26 ppm, which is attributable to an intact Keggin structure as has already been reported for PW supported on MCM-41 and SiO_2 [27].

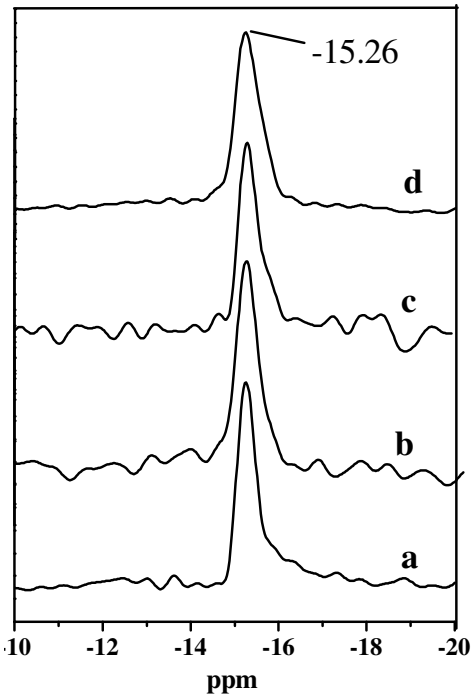

Figure 3.32 ^{31}P MAS NMR spectra of PW/SBA-15 catalysts with (a) 10, (b) 20, (c) 30 and (d) 40 wt. % loading of PW.

(f) Electron microscopy

(i) SEM

SEM images of as-synthesized Si-SBA-15 (Figure 3.33 (a)) reveal many rope-like domains with a relatively uniform size of ~ 1μm, which are aggregated into wheat-like microstructures. After calcinations in air at 823 K, the calcined Si-SBA-15 sample (Figure 3.33 (b)) reveals needle and rod like morphologies, arising from the shrinkage of the crystallites.

SEM image of 40 wt. % PW/SBA-15 [Figure 3.33 I] reveals needle and rod like morphologies.

(ii)TEM

TEM images of calcined Si-SBA-15 [Figure 3.34 (a) and (b)], Al-SBA-15 (Si/Al=30) [Figure 3.34 (c) and (d)] and 40 wt.% PW/SBA-15 [Figure (e) and (f)] reveal characteristic regular hexagonal arrays of uniform channels for both Al-SBA-15 and Si-SBA-15 samples.

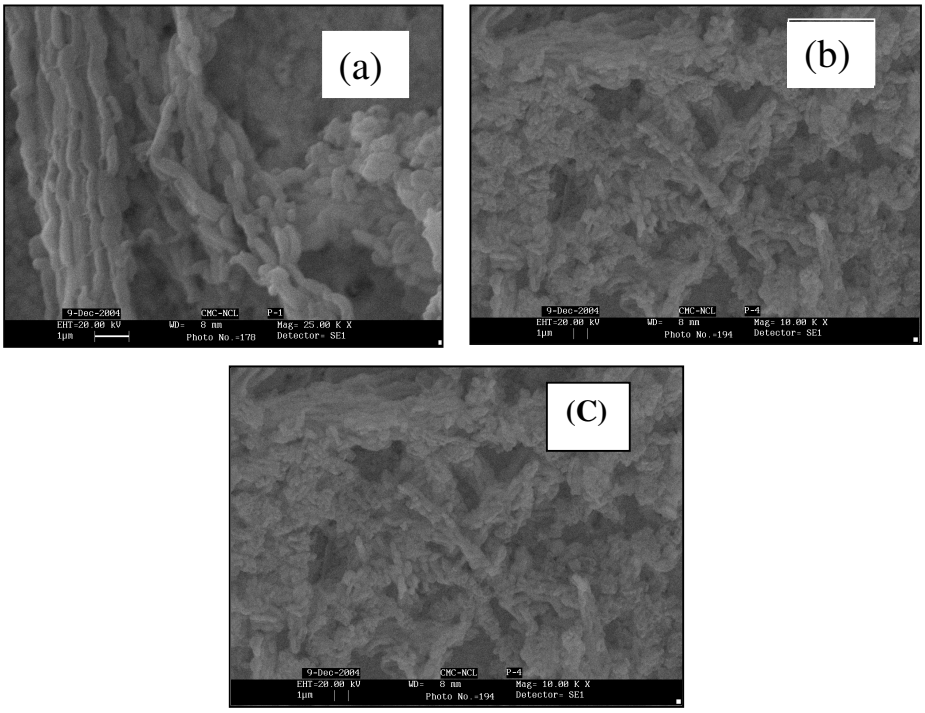

Figure 3.33 SEM images of (a) as synthesized Si-SBA-15, (b) calcined Si-SBA-15 and (c) 40 wt. % PW/SBA-15.

(g) FT-IR

FT-IR spectra of PW/SBA-15 are shown in Figure 3.35. The IR frequencies of bulk PW are in good agreement with the reported values [28]; 1081 (P-O in the central tetrahedron), 982 (terminal W=O), 897 and 800 cm^{-1} (W-O-W) asymmetric stretching vibrations associated to the typical Keggin anions [29]. All the samples (10-40 wt. % PW/SBA-15) exhibit vibration bands at approximately 982, 897 and 800 cm^{-1}. These bands become more intense on increasing the PW loading from 10 to 40 wt. %. However, these bands associated with PW are less intense in the supported samples. It appears that the Keggin structure of the PW is retained in the PW/SBA-15 samples (even at 10 wt. % PW loading).

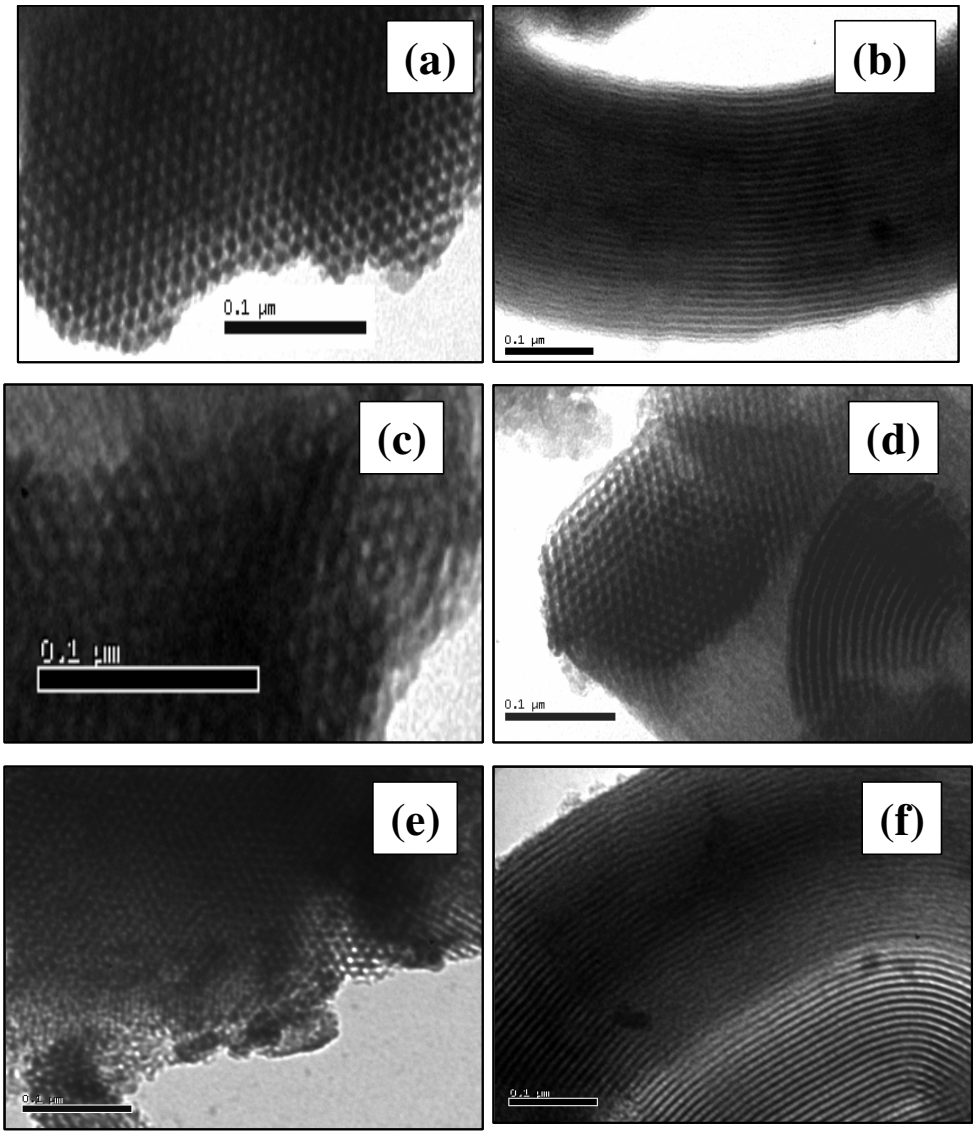

Figure 3.34 TEM images of calcined Si-SBA-15 [(a), (b)], Al-SBA-15 (Si/Al=30) [(c), (d)], and of 40 wt. % PW/SBA-15 [(e), (f)]. Viewed in the direction {(a), (c), (e)} [100] of the pore axis and {(b), (d), (f)} [110] in the direction perpendicular to the pore axis.

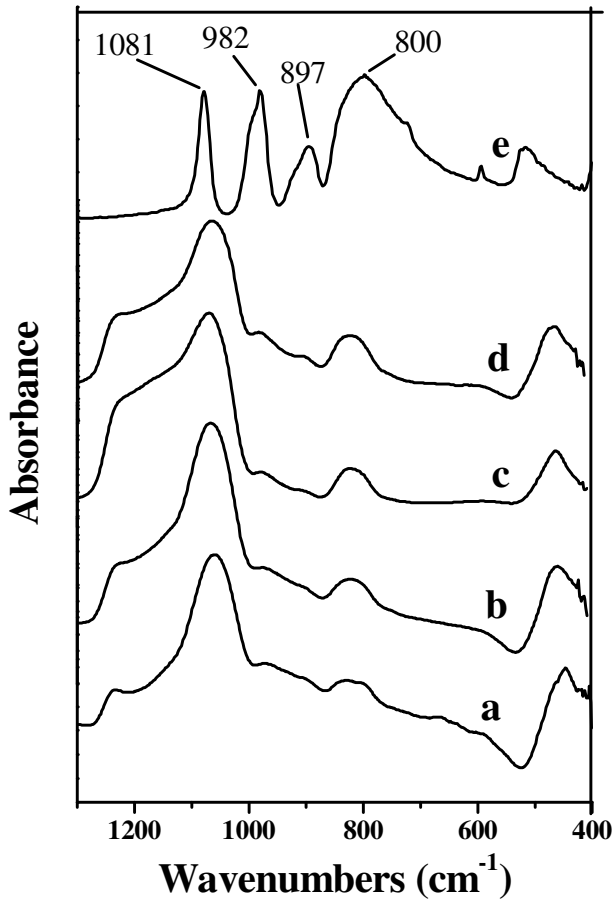

Figure 3.35 FT-IR spectra of a) 10 wt. % PW/SBA-15, b) 20 wt. % PW/SBA-15, c) 30 wt. % PW/SBA-15, d) 40 wt. % PW/SBA-15 and of e) PW.

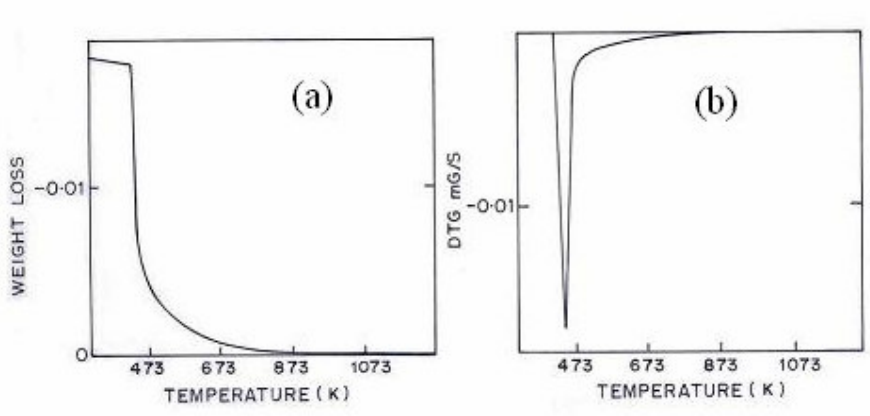

Figure 3.36 (a) TG and (b) DTG plots of as-synthesized SBA-15.

(h) Thermogravimetry

The TG analysis of an as-synthesized SBA-15 sample reveals a single main step occurring at relatively low temperature as shown in Figure.3.36. Removal of physisorbed water, below 423 K, and the decomposition of the organic template take place in step [30] between 423 K and 553 K with a weight loss of 52 %.

.

3.4 REFERENCES

6. C.T. Kresge, M.E. Leonowicz, W.J. Roth, J.C. Vartuli, J.S. Beck, Nature 359 (1992) 710.
7. R.B. Borade and A. Clearfield, Catal. Lett. 31 (1995) 267.
8. S.J. Gregg, K.S. W. Sing, "Adsorption, Surface Area and Porosity", Academic Press, London, (1982) Ch.4.
9. H. Kosslick, G. Lischke, B. Parlitz, W. Storek, R. Fricke, Appl. Catal. A: Gen. 184 (1999) 49.
10. X. Chen, L. Huang, G. Ding, Q. Li. Catal. Lett. 44 (1997) 123.
6. (a) K. Chaudhari, T. K. Das, P. R. Rajmohanan, K. Lazar, S. Sivasanker, A.J. Chandwadkar, J. Catal 183 (1999) 281; (b) M. Chatterjee, T. Iwasaki, Y. Onodera, T. Nagase, H. Hayashi, T. Ebina, Chem. Mater. 1 (2000) 1654.
7. N. K. Mal, A.V. Ramaswamy; J. Mol. Catal. A: Chem. 105 (1996) 149.
8. K.M. Reddy, C. Song, Cata. Lett. 36 (1996) 103.
9. Z.H. Luan, J. Xu, H. He, J. Klinowski, L. Kevan , J. Phys. Chem. 100 (1996) 19595.
10. T. Sen, V. Ramaswamy, S. Ganapathy, P.R. Rajamohanan, S. Sivasanker, J. Phys. Chem., 100 (1996) 3809.
11. J. Kornatowski, B. Wichterlova, J. Jirkovsky, E. Loffler, W. Pilz, J. Chem. Soc. Farady Trans. 92 (1996) 1067.
12. B. Echchahed, A. Moen, D. Nicholson, L. Bonneviot, Chem. Mater. 9 (1997) 1716.
13. A. Szegedi, Z. Konya, D. Mehn, E. Solymar, G. Pal-Borbely, Z. Horvath, L. Biro, I. Kiricsi, Appl. Catal. A: Gen. 272 (2004) 257.
14. M. Koranne, J.G. Goodwin, G. Marcelin, J. Catal. 148 (1994) 388.
15. F. Arena, N. Giordeno, A. Paramaliana, J. Catal. 167 (1997) 66.
16. K. N. Nag and F. E. Marsota, J. Catal. 124 (1990) 127.
17. G. Grubert, J. Rathousky, G. Schulz-Ekloff, M. Wark, A. Zukal, Micropor. Mesopor. Mater. 22 (1998) 225.
18. H. Bosch, B. J. Kip, J.G. van Ommen, and P. J. Gellings, J. Chem. Soc. Faraday Trans. 180 (1984) 2479.
19. (a) J. Kornatowski, B. Wichterlova, M. Rozwadowski, W. H. Baur, "In Zeolite

and Related Microporous Materials: State of Art,"1994. (b) J. Weitkamp, H.G. Karge, H. Pfeifer, W. Holderich, Eds: Stud. Surf. Sci Catal, Vol. 84; Elsevier: Amsterdam, (1994)117.

20. P. R. Hari Prasad Rao, R. Kumar, A. V. Ramaswamy, P. Ratnasamy, Zeolites 13 (1993) 663.
21. C. Montes, M.E. Davis, B. Murray, M. Narayana, J. Phys. Chem. 94 (1990) 6425.
22. Luan, Z.; He, H; Cheng C.F.; Zhou, W.; Klinowski, J., J. Phys. Chem. B 9 (1995) 1018.
23. D. Zhao, J. Feng, Q. Huo, N. Melosh, G. H. Fredrickson, B. F. Chmelka, G. D. Stucky, Science 279 (1998) 548.
24. J. Wang, H. Zhu, Catal. Lett. 93 (2004) 209.
25. Qi-Ying Liu, Wen-Liang Wu, Jun Wang, Xiao-Qian Ren, Yan-Ru Wang, Micropor. Mesopor. Mater. 76 (2004) 51.
26. F. Lefebvre, J. Chem. Soc. Chem. Comm. (1992) 756.
27. I.V. Kozhenikov, K. R. Kloestra, A. Sinnema, H.W. Zandbergen, H. Van Bekkum, J. Mol. Catal. A: Chem. 114 (1996) 287.
28. Cardoso, Walter, Gonzaga, E. Aguiar, Andrade, J. Mol. Catal. A: Chem. 209 (2004) 189.
29. P. Staiti, S. Freni, S. Hocevar, J. Power Sources 79 (1999) 250.
30. F. Kleitz, W. Schmidt, F. Schuth, Micropor. Mesopor. Mater. 65 (2003) 1.
31. C. S. John, N.C.M. Alma, G. R. Hays, Appl. Catal. 6 (1983) 341.

Chapter 4

CLAISEN AND BECKMANN REARRANGEMENTS

The use of modified MCM-41 and SBA-15 based catalysts in molecular rearrangements is presented in this chapter. Part 1 describes the study of Claisen rearrangement of allyl phenyl ether (APE) to o-allylphenol (*o*-AP), while part 2 describes the Beckmann rearrangement of cyclohexanone oxime to ε-caprolactam.

4.1 PART 1 CLAISEN REARRANGEMENT OF ALLYL PHENYL ETHER

4.1.1 INTRODUCTION

The Claisen rearrangement involves the conversion of allyl phenyl ethers to the corresponding *o*-allylphenols and is generally performed by heating the ethers at an elevated temperature (> 473 K), but has been also reported to be susceptible to catalysis by Lewis and Brönsted acids [1, 2]. In the presence of acids, *o*-AP undergoes cyclization to produce a dihydrobenzofuran derivative. Thus, the reaction presents an attractive route to the synthesis of benzofuran derivatives from substituted allyl aryl ethers [3]. When the rearrangement is carried out with amino- and thio-derivatives, the corresponding heterocylic compounds are obtained.

Reports of the use of solid acids in the above rearrangement are rather scarce. Pitchumani et al. have observed shape selectivity in ZSM-5 and ZSM-11 during their study of photo-assisted Claisen rearrangement [4]. Diastereoselective asymmetric induction in the thio-Claisen rearrangement over zeolites was reported by Sreekumar et al. [4a]. Sheldon et al. have investigated the use of H-FAU and H-MOR in the rearrangement of allyl phenyl ether in benzene medium [5, 6]. Other solid catalysts that have been investigated are mesoporous silica [7] and bentonite [8]. Greyghton et al. have reported the multifunctional probe, allyl 3, 5-di-tert-butylphenyl ether, for testing the outer surface acidity of zeolites [9]. The Brönsted acid catalyzed Claisen rearrangement of the probe molecule, followed by the cyclization of the primary product to 4,6-di-tert-butyl-2-methyldihydrobenzofuran illustrates the use of the probe to provide information regarding the outer surface acidity of H-MOR and H-BEA. This reaction proved to be useful for the investigation of the effects of various modifications of H-MOR on outer surface acidity [9]. The use of large pore zeolites for the rearrangement has also been reported by Wagholikar et al. [10]. They have suggested that even over large-pore zeolites, the rearrangement occurs primarily at the external surface or at the pore mouth [10].

The mesoporous molecular sieve MCM-41 has received much attention because of its large surface area, uniform size and shape of the pores over micrometer length scales [11, 12]. High thermal and hydrothermal stability and the advantage of tuning the pore size make these materials interesting for use as supports and catalysts for various heterogeneous catalyzed reactions.

In the present study, the use of MCM-41 and SBA-15 based catalysts in the Claisen rearrangement of APE is explored. A comparative study of the activities of Al-MCM-41, Ga-MCM-41, Al-SBA-15 and PW/SBA-15 catalysts in the Claisen rearrangement of allyl phenyl ether is presented. The effect of various reaction and catalyst parameters on conversion and product selectivity over MCM-41 catalysts is reported. A kinetic analysis of the formation of the different products under various reaction conditions is also presented.

4.1.2 EXPERIMENTAL

(a) Preparation of allyl phenyl ether

APE (purity 99%) was synthesized by the reaction of allyl bromide and phenol, and purified by standard methods [13]. APE was prepared in a round-bottomed flask (250ml) equipped with a magnetic stirrer and a reflux (cold water) condenser. The flask was charged with phenol (5 g) and allyl bromide (6 g) (1:1.5 mole ratios). Acetone was used as the solvent (30 ml). Freshly dried K_2CO_3 (9.5 g) was added and the mixture was stirred for 6 h at reflux temperature. The progress of the reaction was monitored by TLC. The acetone in the reaction mixture was distilled off using a rotary evaporator and the contents of the flask were dissolved in ethyl acetate. The potassium carbonate was removed by taking the reaction mixture in a separating funnel and washing with water. The unreacted phenol was removed by washing the organic layer with 10 % sodium hydroxide (100 ml). The reaction mixture was further washed with water and brine solution, and the organic layer was dried over anhydrous sodium sulphate. Further, it was concentrated by evaporating the solvent using a rotary evaporator and purified by column chromatography. The purity and chemical structure were ascertained by GC, GC-MS and GC-IR.

(b) Reaction procedure

The reactions were carried out in a batch mode in a two-necked round-bottomed flask (capacity 25 ml) in a nitrogen atmosphere, using 0.67 g of APE in 10 g

of the solvent (tetrachloroethylene TCE) and 0.075 g of freshly calcined catalyst. Aliquots of the reaction mixture were collected at different time intervals and analyzed by GC (Varian Model No: Star 3400 Cx- Gas Chromatograph; column: CP Sil 5CB, 30 m; i.d. 0.05mm; FID detector). Identification of the products was done by GC- MS and GC- IR.

4.1.3 RESULTS AND DISCUSSION

(A) Claisen rearrangement of APE over Al-MCM-41

The reaction scheme for Claisen rearrangement is shown in Figure 4.1. It is reported that the ether first undergoes rearrangement to produce allyl hexadienone followed by enolization to give o-ally phenol (*o*-AP) which cyclizes to give 2, 3-dihydro-2-methyl benzofuran (benzofuran) [14]. However, the intermediate allyl hexadienone could not be identified in any of the products in this study.

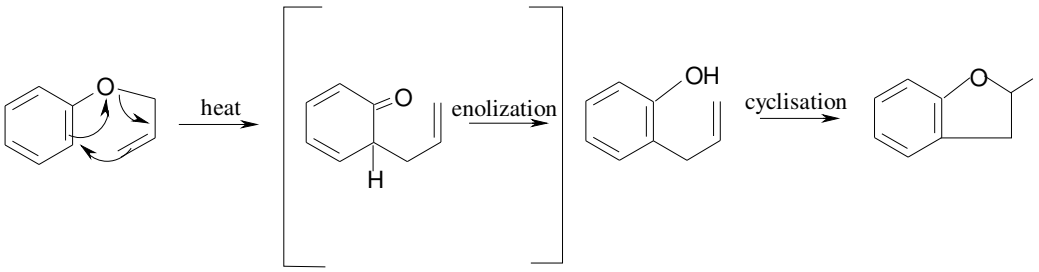

Figure 4.1 Reaction scheme for the Claisen rearrangement of allyl phenyl ether.

The catalytic activity of the calcined MCM-41 samples with different Si/Al ratios was compared for the Claisen rearrangement of APE. The influence of duration of run and reaction temperature on conversion and product yields was examined over the catalysts. Besides a kinetic analysis of the data was also carried out.

(i) Influence of duration of run

The effect of run duration (up to 12 h) on conversion, and *o*-AP and benzofuran selectivities over the catalysts (with different Si/Al ratios) at 393 K is shown in Figure 4.2. In general, both conversion and benzofuran formation increase with duration of run while *o*-AP decreases. The activity increases with increase in the Al content, the sample with the largest Si/Al ratio (~110) being the least active.

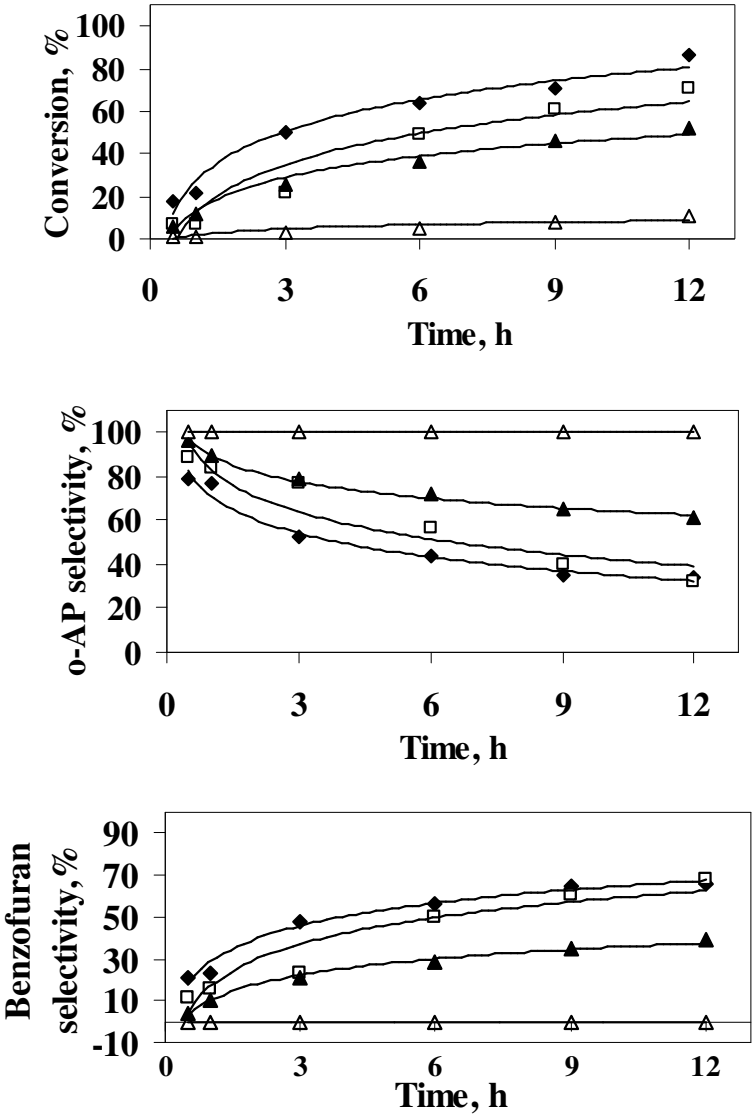

Figure 4.2 Influence of Si/Al ratio on conversion and selectivity (Reaction temperature: 393 K Symbols: ◆ : Si/Al = 21, □ : Si/Al = 31, ▲ : Si/Al = 53, △ : Si/Al = 110).

(ii) Influence of temperature

The influence of temperature on APE conversion, and o-AP and benzofuran selectivities for the samples with different Si/Al ratios are presented in Figure 4.3. Conversion and ring formation increase with temperature at all Si/Al ratios, though the effect is less noticed for the most siliceous sample (Si/Al ~ 110). *o*-AP selectivity

increases with increase in Si/Al ratio and decrease in temperature, the influence of temperature being less at higher Si/Al ratios.

(iii) Influence of Si/Al ratio

Both conversion and selectivity in Claisen rearrangement are found to be dependent on the Si/Al ratio of MCM-41. Purely siliceous (Al-free) MCM-41 exhibited negligible conversion. Figure 4.4 shows the influence of the Si/Al ratio on the reaction at different temperatures. APE conversion decreases with decrease in the aluminum content (increase in the Si/Al ratio) of the catalyst. The figure shows that a maximum conversion of up to 86.7 % can be obtained with Al-MCM-41 (21) at 393 K at the end of a 12 h reaction. The selectivity for *o*-AP increases and that for benzofuran decreases with increase in the Si/Al ratio of Al-MCM-41. As the reaction is catalyzed by the acid sites of Al-MCM-41, the observed behavior must be due to the decrease in the acidity of Al-MCM-41 with increase in Si/Al ratio.

A plot of APE conversion and acidity (strong and weak) vs Al content is shown in Figure 4.5 (a). It is found that both acidity and conversion increase with Al content. The close relationship between acidity and conversion suggests that the reaction occurs inside the pores of MCM-41. In the case of zeolites, however, the reaction was suggested to occur mainly on the external surface or at the pore-mouth as an inverse relation between acidity (or Al content) and conversion was noticed [10].

The turnover frequency (TOF, mol of APE converted or product formed per hour per mol of Al present in the sample) is found to decrease with increasing Al content (for the samples with Si/Al ~ 21, 31 and 53) [Figure 4.5 (b)]. The data of the sample with Si/Al ~ 110 does not fall in the above trend due to an unexpectedly small TOF suggesting the non-accessibility of the acid sites to the reactant molecules at low Al contents.

On the other hand, an increase in the TOF is noticed with increasing Al content for benzofuran formation. When the TOF (conversion of APE or formation of *o*-AP) is calculated based on the total number of acid sites (mol NH_3 desorbed) in the three samples (Si/Al ~ 21, 31 and 53), a nearly constant value (TOF = 8 ± 1 mol/mol NH_3.h) is obtained revealing a direct relationship between acidity and activity in these samples.

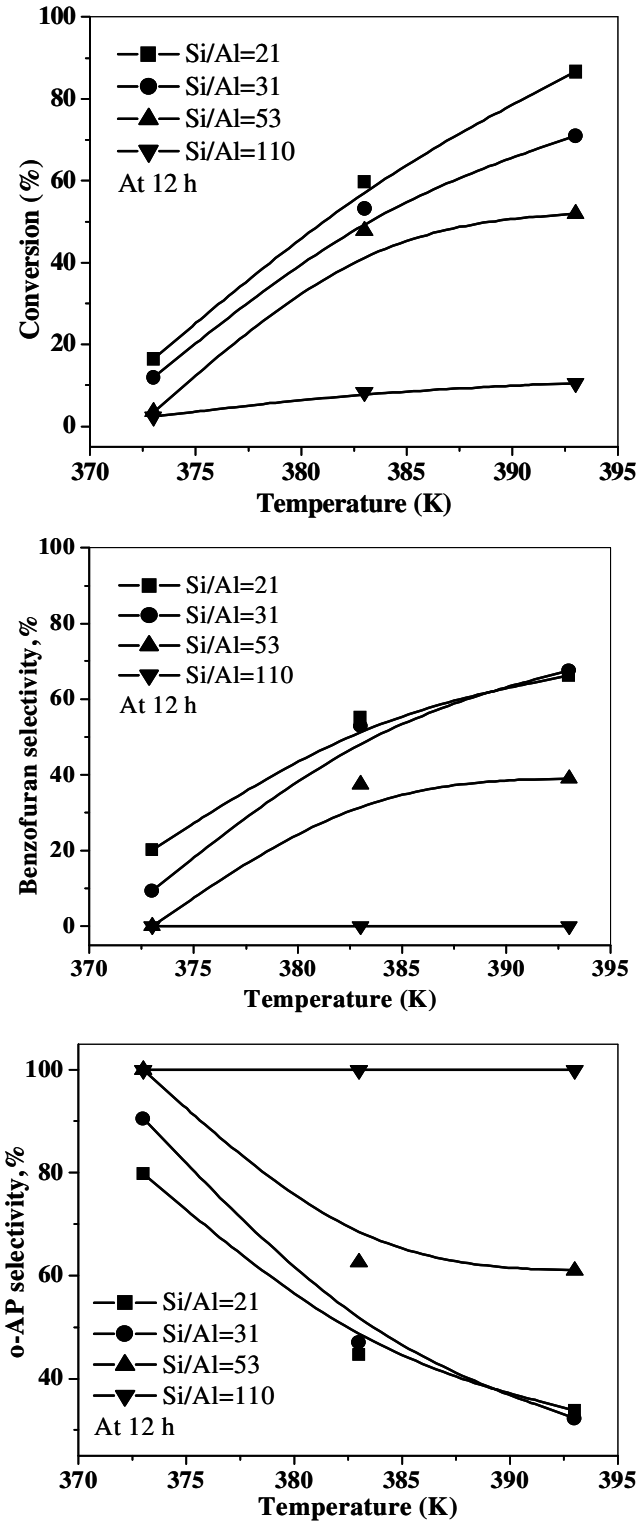

Figure 4.3 Influence of temperature on conversion and selectivity over Al-MCM-41 with different Si/Al ratios.

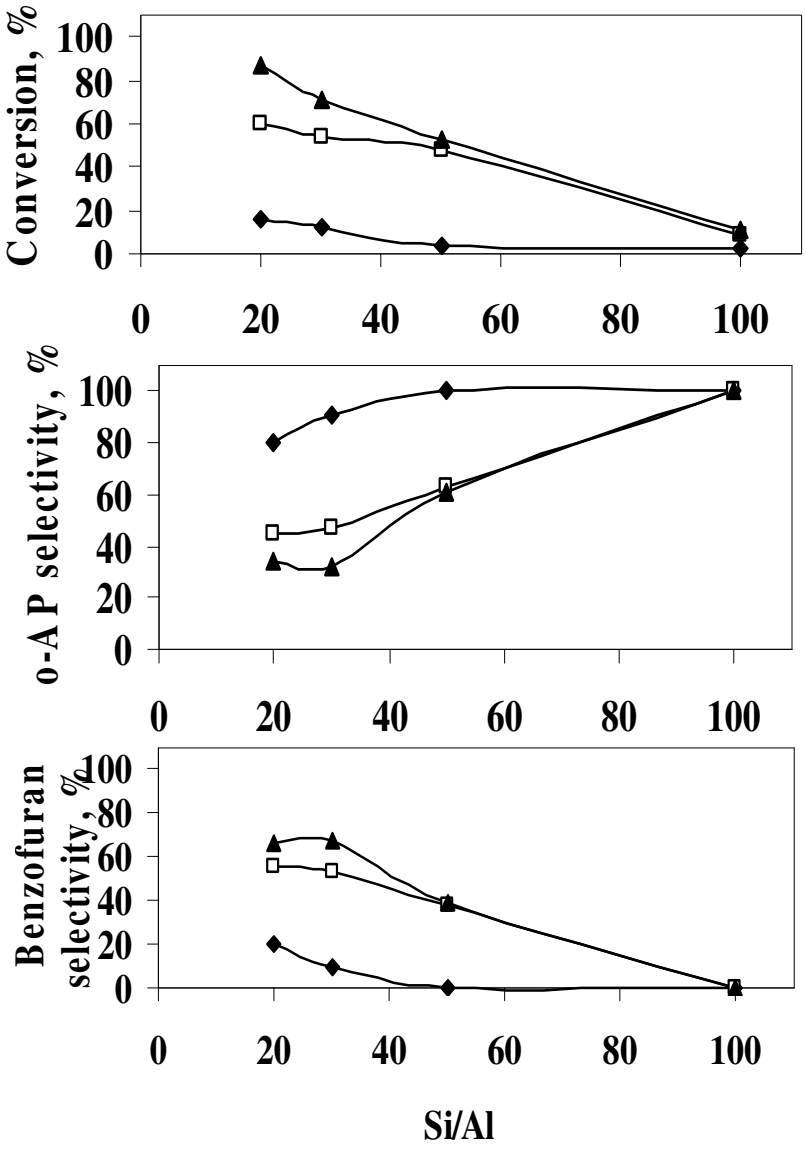

Figure 4.4 Influence of Si/Al ratios on conversion and selectivity at different temperatures (Reaction time: 12 h; ◆: 373 K, □: 383 K, ▲: 393 K).

(iv) Mechanism of the reactions

A plausible mechanism for the Claisen rearrangement to produce the allylphenol and its subsequent conversion to the ring compound is presented in Figure 4.6 (a) and (b). The steps are catalyzed by acid centers. First the acid site protonates the 'O' of the ether. This is followed by intramolecular rearrangement of the protonated (adsorbed) species into the *o*-AP as shown in Figure 4.6 (a). The

allylphenol is next protonated at the allylic double bond to produce the secondary carbenium ion that reacts again intramolecularly with the phenolic 'O' to produce the benzofuran [Figure 4.6 (b)].

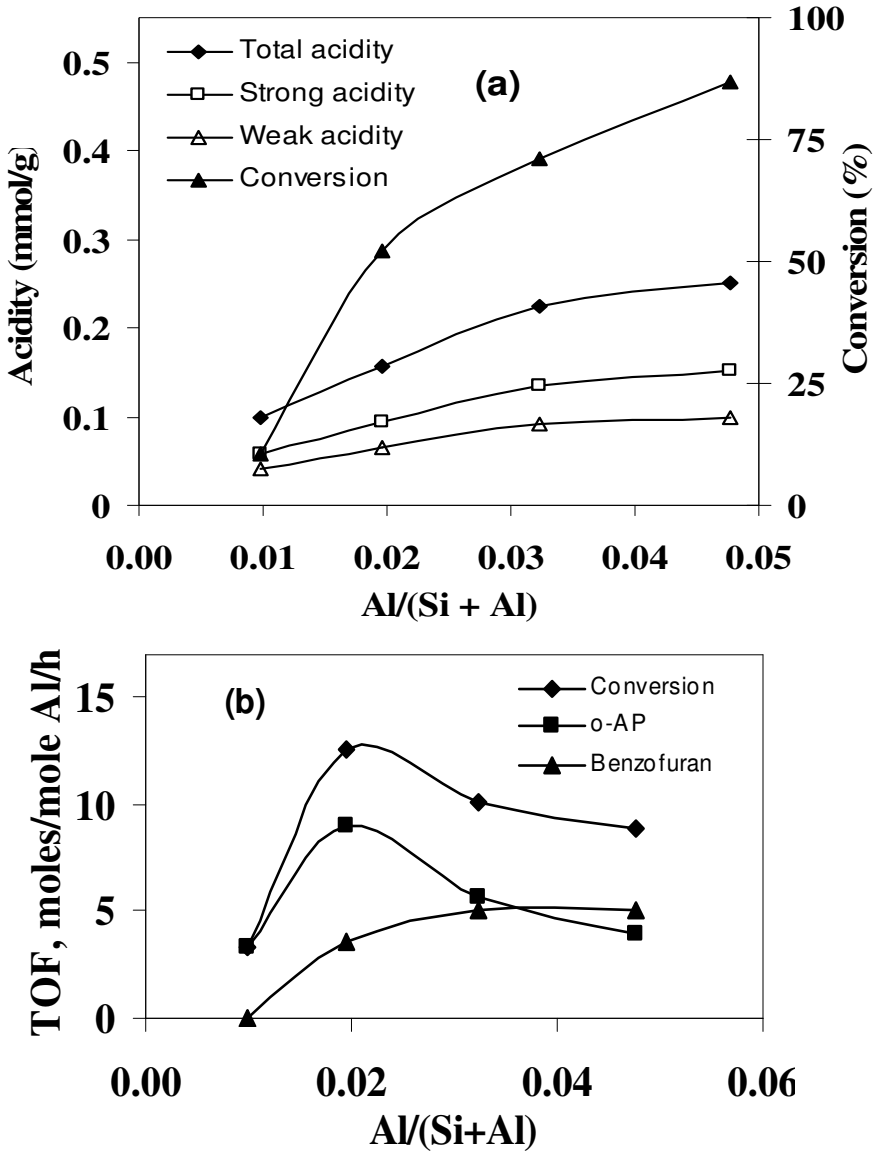

Figure 4.5 (a) Influence of Al-content on APE conversion and catalyst acidity; (b) Influence of Al-content on TOF (Reaction temperature: 393 K, time: 12 h).

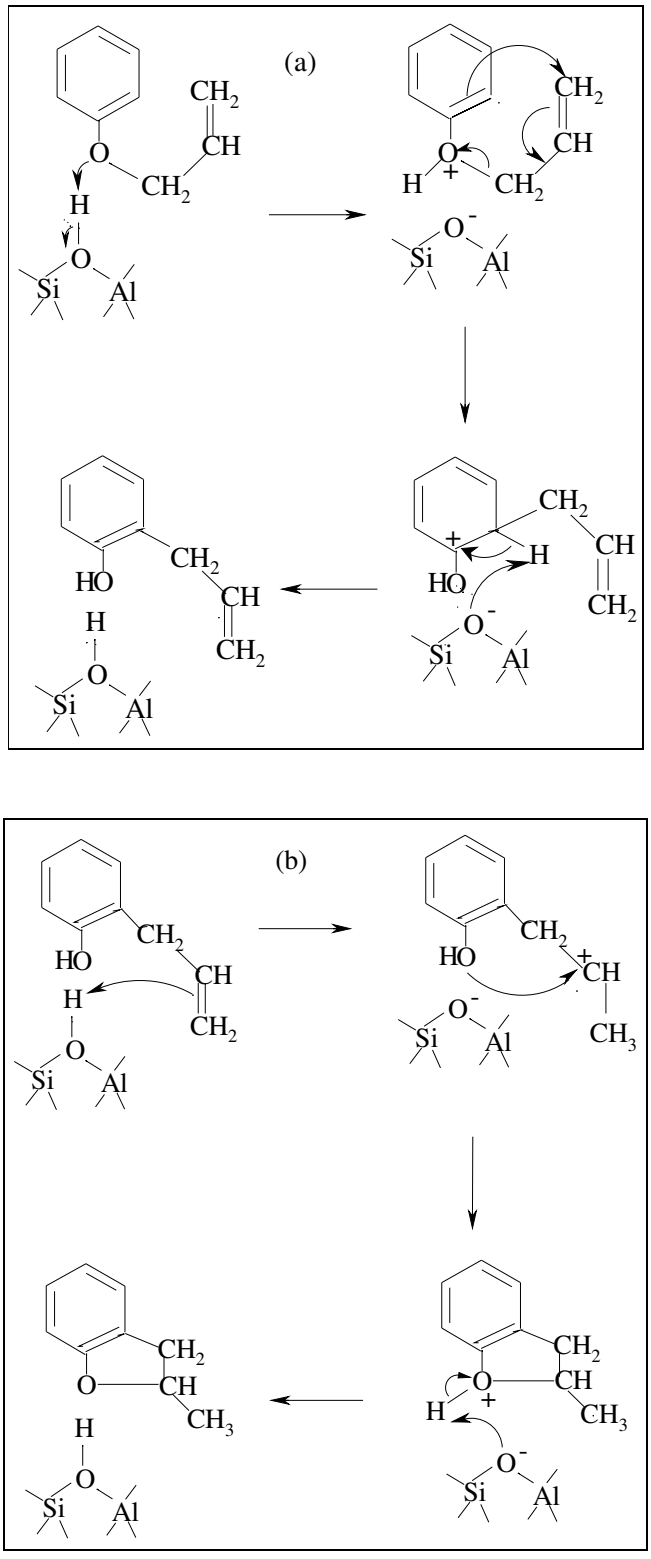

Figure 4.6 Plausible mechanism of Claisen rearrangement of APE over solid acids (Al-MCM-41) (a) for the formation of o-AP and (b) for the formation of ring product

(v)Kinetic Analysis

The scheme presented in Figure 4.1 shows that the reaction involves two consecutive steps for the formation of benzofuran. Hence this was treated as a first order series reaction with *o*-AP and benzofuran as the intermediate and final products, and the standard equations for a first order series reaction were used for the determination of rate constants. These are:

$$C_A/C_{A0} = e^{-k_1 t} \quad (1)$$

and

$$C_R/C_{A0} = k_1 (e^{-k_1 t} - e^{-k_2 t}) / (k_2 - k_1) \quad (2)$$

In the above equations, C_{A0} and C_A are the concentrations of APE at initial time, and at time t, respectively, C_R is the concentration of the intermediate product *o*-AP at time t, k_1 and k_2 are the rate constants for the first and second step respectively.

The concentration profiles of APE, *o*-AP and benzofuran for two temperatures (383 and 393 K) and Si/Al ratios (Si/Al = 21 and 31) in the Claisen rearrangement of APE are presented in Figure 4.7. The lines represent the theoretical profiles. The profiles are those expected for typical first order consecutive reactions. The nature of the profile, especially that for *o*-AP depends on the relative values of k_1 and k_2. The rate equations and the time t_{max}, at which the intermediate o-AP concentration is maximum, are presented in Table 4.1. It can be seen from the table that t_{max} varies with both the reaction temperature and the Si/Al ratio of MCM-41. For a given catalyst, t_{max} decreases with reaction temperature and Al content.

The influence of temperature and Si/Al ratio (21 and 31) on the reaction rate constants, k_1 and k_2 are presented in Figure 4.8. The figure shows that both k_1 and k_2 increase with increase in temperature. It is found that k_2 is not much affected by variation in the Si/Al ratio whereas k_1 is sensitive. The reasons for this are not clear.

The activation energy for the two steps was calculated using the Arrhenius expression. The activation energy for the reaction of APE on Al-MCM-41 with Si/Al ratio 21 is estimated to be 8.9 kcal/mol. The activation energy for the formation of benzofuran from *o*-AP is estimated to be 10.3 kcal/mol. The activation energies of the reactions were not found to be significantly affected by a change in the Si/Al ratio.

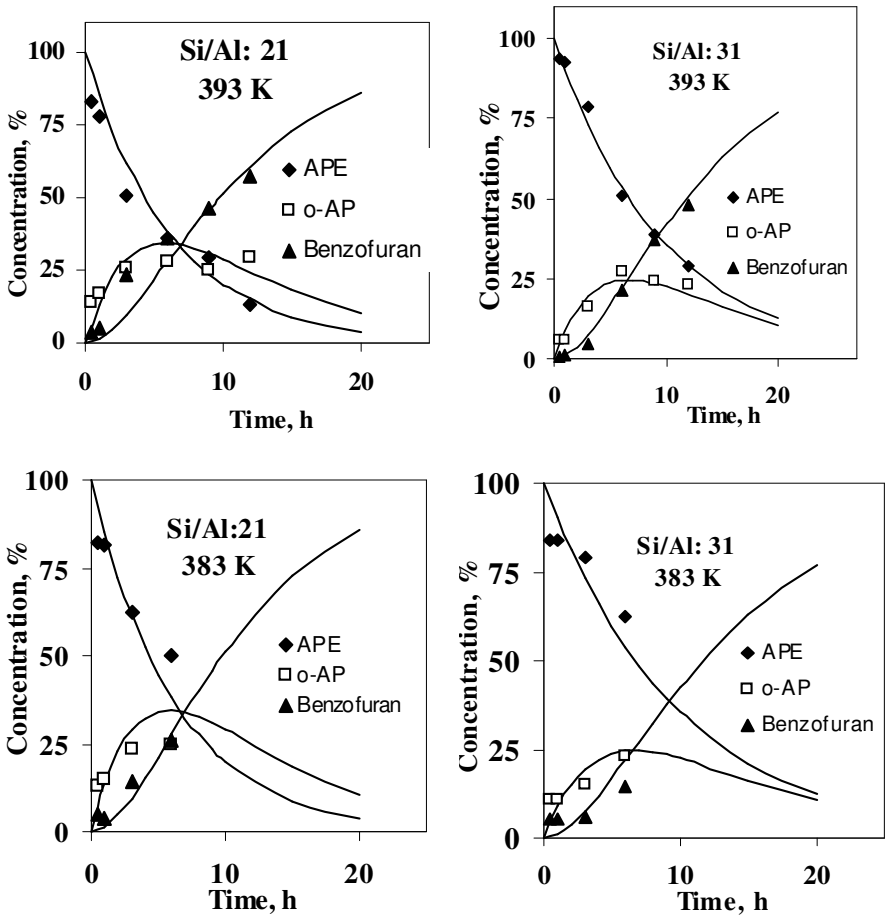

Figure 4.7 Plots of experimental and fitted model data for the Claisen rearrangement of allyl phenyl ether at two different Si/Al ratios and temperatures; experimental values are presented by symbols.

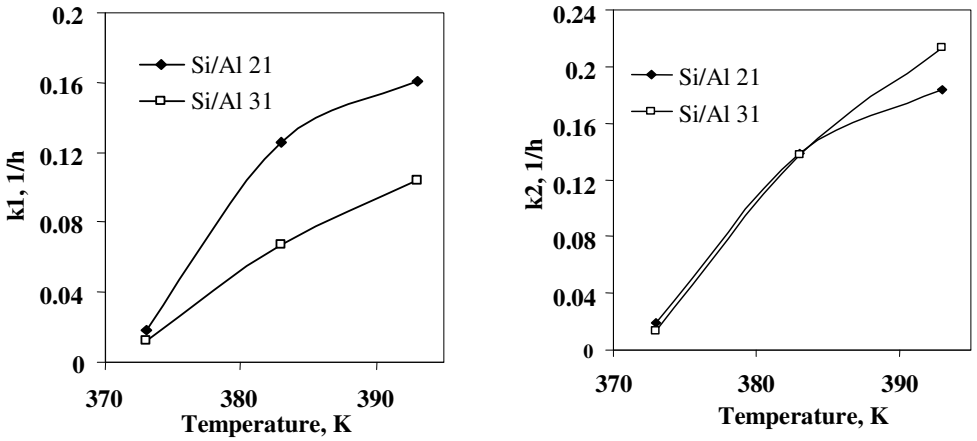

Figure 4.8 Influence of temperature and Si/Al ratio on the reaction rate constants.

Table 4.1 Results of kinetic analysis for Al-MCM-41 catalysts with Si/Al = 21 and 31

Si/Al	T[a]	Rate constants		Rate Expressions		t_{max}[c]
	(K)	k_1 (1/h)	k_2 (1/h)	Eqn. (1)[b]	Eqn. (2)[b]	(h)
21	383	0.13	0.14	$C_A/C_{A0} = e^{-0.13\,t}$	$C_R/C_{A0} = 0.13\,(e^{-0.13\,t} - e^{-0.14\,t}) / 0.01$	7.55
	393	0.16	0.18	$C_A/C_{A0} = e^{-0.16\,t}$	$C_R/C_{A0} = 0.16\,(e^{-0.16\,t} - e^{-0.18t}) / 0.02$	5.80
31	383	0.07	0.14	$C_A/C_{A0} = e^{-0.07\,t}$	$C_R/C_{A0} = 0.07\,(e^{-0.07\,t} - e^{-0.14\,t}) / 0.07$	10.18
	393	0.10	0.21	$C_A/C_{A0} = e^{-0.10\,t}$	$C_R/C_{A0} = 0.10\,(e^{-0.10\,t} - e^{-0.21\,t}) / 0.11$	6.58

[a] Reaction temperature

[b] See text, kinetic analysis

[c] The time at which the concentration of *o*-AP reaches a maximum value

(B) Claisen rearrangement of APE over Ga-MCM-41, Al-SBA-15 and phosphotungstic acid supported SBA-15 catalysts

Claisen rearrangement of APE over the above catalysts was compared with Al-MCM-41 data under similar reaction conditions (Section 4.1.2 (b)) at 393 K.

(i) Ga-MCM-41

The effect of run duration (up to 12 h) on conversion, *o*-AP and benzofuran selectivities over the catalysts with different Si/Ga ratios at 393 K is shown in Figure 4.9 (a). In general, both conversion and benzofuran formation increase with duration of run while *o*-AP decreases.

Both conversion and selectivity in the Claisen rearrangement are found to be dependent on the Si/Ga ratio of MCM-41. The APE conversion decreases with decrease in the Ga content (increase in the Si/Ga ratio) of the catalyst. The figure shows that a maximum conversion of up to 81.1 % can be obtained with Ga-MCM-41 with Si/Ga ratio of 20 at 393 K at the end of a 12 h reaction. The selectivity for *o*-AP increases and that for benzofuran decreases with increase in the Si/Ga ratio of Ga-MCM-41. As the reaction is catalyzed by the acid sites of Ga-MCM-41, the observed behavior must be due to the decrease in the acidity of Ga-MCM-41 with increase in Si/Ga ratio.

Figure 4.9 (b) shows the influence of Ga content on APE conversion and selectivity for benzofuran and *o*-AP at 393 K for 12 h. The figure shows that APE conversion and benzofuran selectivity increase with Ga content, while allylphenol selectivity decreases.

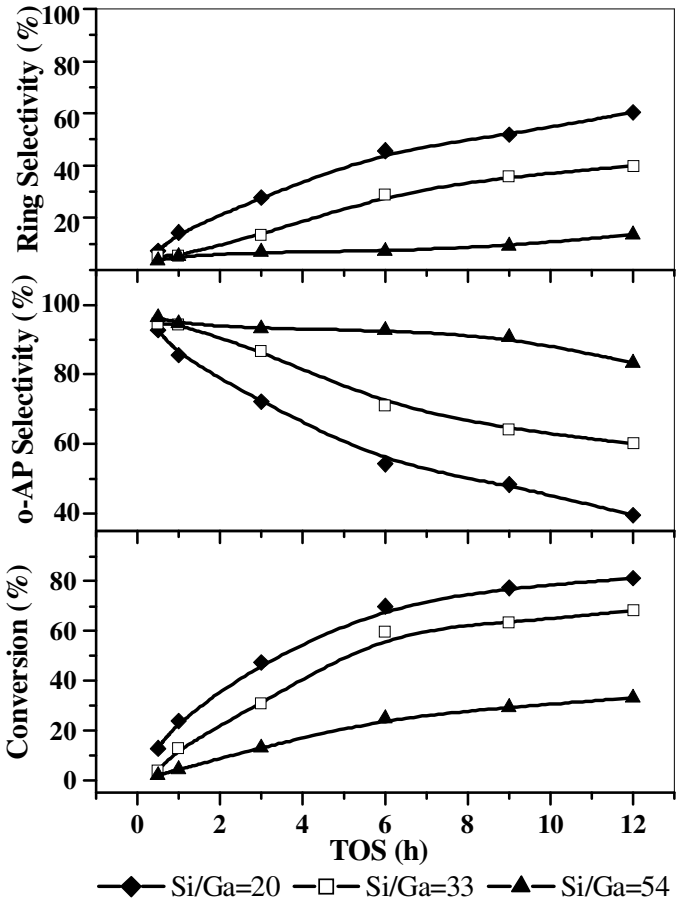

Figure 4.9 (a) Influence of Si/Ga ratio on the conversion and selectivity.

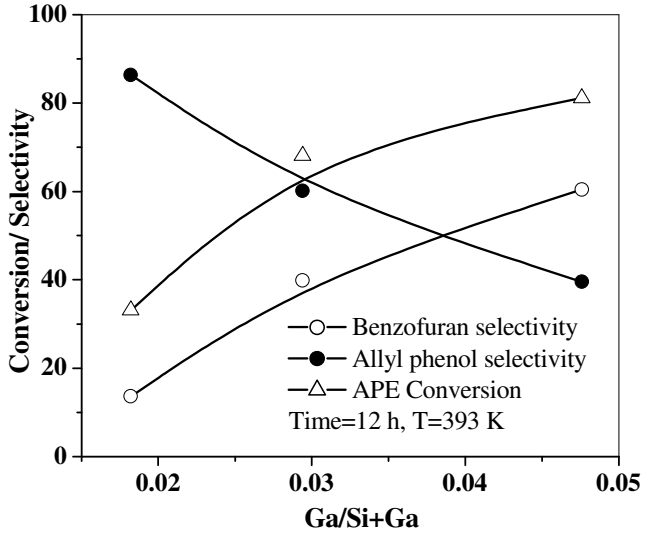

Figure 4.9 (b) Influence of Ga content on APE conversion and selectivity for benzofuran and allylphenol.

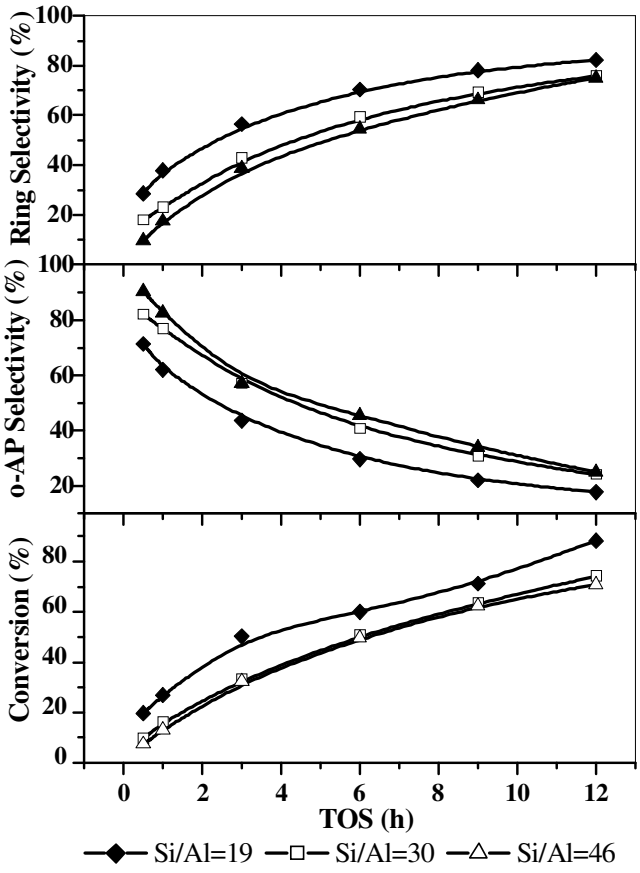

Figure 4.10 (a) Influence of Si/Al ratio on APE conversion and selectivity (Al-SBA-15).

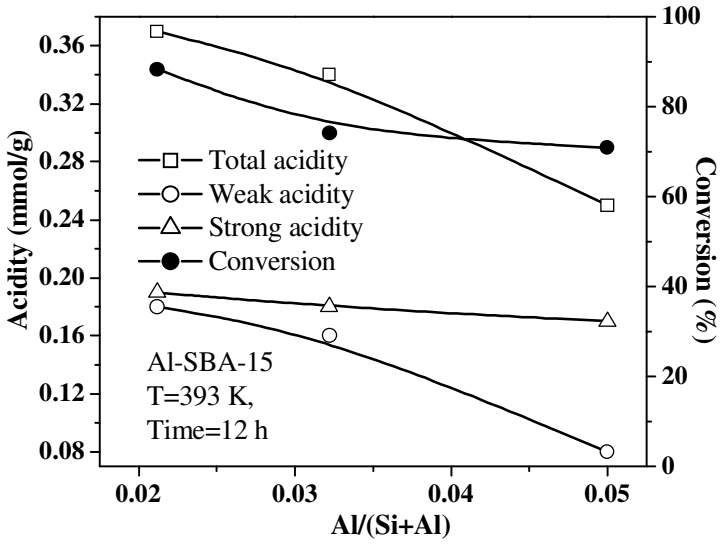

Figure 4.10 (b) Influence of Al content on APE conversion and catalyst acidity (Al-SBA-15).

(ii) Al-SBA-15

The effect of run duration (up to 12 h) on conversion, and *o*-AP and benzofuran selectivities over the catalysts with different Si/Al ratios at 393 K is shown in Figure 4.10 (a). In general, the conversion and benzofuran formation increase with duration of run while *o*-AP decreases. The activity increases with increase in the Al content.

Both conversion and selectivity in the Claisen rearrangement are found to be dependent on the Si/Al ratio of SBA-15. Purely siliceous SBA-15 exhibited negligible conversion. The APE conversion decreases with decrease in the Al content (increase in the Si/Al ratio) of the catalyst. The figure shows that a maximum conversion of up to 88.3 % can be obtained with Al-SBA-15 with Si/Al ratio 19 at 393 K at the end of a 12 h reaction.

The selectivity for *o*-AP increases and that for benzofuran decreases with increase in the Si/Al ratio of Al-SBA-15. As the reaction is catalyzed by the acid sites of Al-SBA-15, the observed behavior must be due to the decrease in the acidity of Al-SBA-15 with increase in Si/Al ratio.

Influence of Al content on APE conversion and catalyst acidity over Al-SBA-15 catalysts (12 h at 393 K) is shown in Figure 4.10. (b). Conversion increases from 70.9 % to 88.3 % as the Al content increases (decrease in Si/Al ratio, acidity increase). Therefore the conversion is dependent on the acidity of the catalyst. As acidity increases, the conversion also increases.

(iii) PW/SBA-15

The effect of run duration (up to 12 h) on conversion, and o-AP and benzofuran selectivities over SBA-15 catalysts with different PW loadings at 393 K is shown in Figure 4.11(a). In general, both conversion and benzofuran formation increase with duration of run while *o*-AP decreases.

The activity increases with increase in the PW content. The conversion of APE increases up to 30 wt. % PW loading, however at 40 wt. % PW loading, the conversion decreases. The figure shows that a maximum conversion of up to 23.3 % can be obtained with PW/SBA-15 with 30 wt. % PW loading at 393 K at the end of a 12 h reaction.

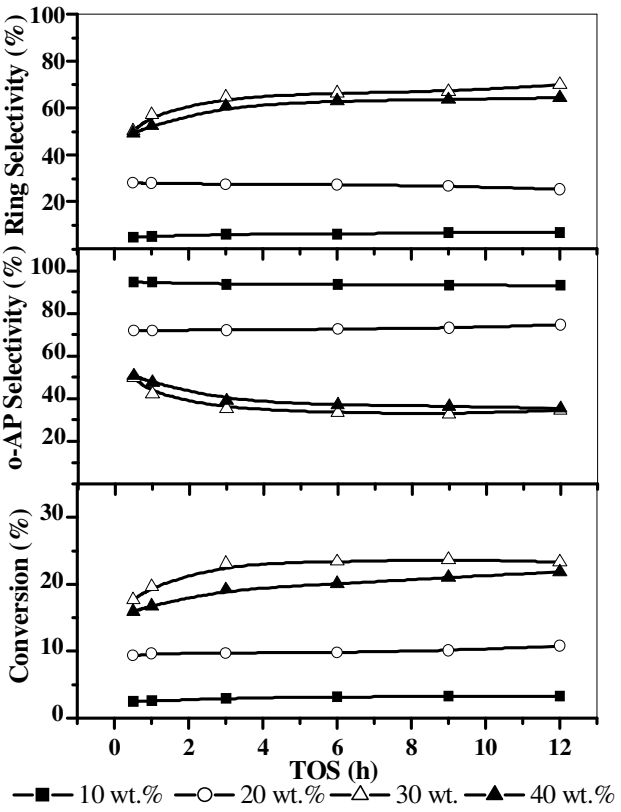

Figure 4.11 (a) Influence of PW content on APE conversion and selectivity over PW/SBA-15.

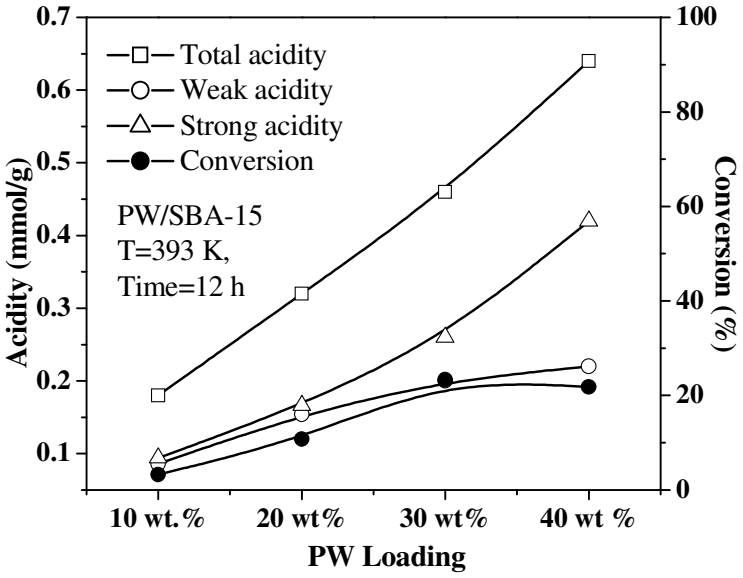

Figure 4.11 (b) Influence of PW content on APE conversion and catalyst acidity for PW/SBA-15 catalysts with different PW loading.

The selectivity for *o*-AP increases and that for benzofuran decreases with increase in the PW content of PW/SBA-15. As the reaction is catalyzed by the acid sites of PW/SBA-15, the observed behavior is due to the increase in the acidity of PW/SBA-15 with increase in PW content (Figure 4.11 (b)). As both conversion and selectivity over 40 wt. % PW/SBA-15 are less compared to the 30 wt. % catalyst, it appears that at high loadings the dispersion of PW is less on the catalyst. Besides, some pore blockage and decrease of accessible surface occurs at high PW loadings. It was already noted (chapter 3, Table 3.11) that at high PW loadings surface area decreases presumably due to blockage of pores. A comparison of activities of all the catalysts is presented in Table 4.2. Both conversion and selectivity are highest for Al-SBA-15 with Si/Al ratio of 19. It may be due to the ready accessibility of the active sites as the Al-SBA-15 catalyst was prepared by an impregnation method. The activity for Claisen rearrangement for the different catalyst varies as Al-SBA-15 > Al-MCM-41 > Ga-MCM-41 > PW/SBA-15.

Table 4.2 Comparison of catalytic activity for Claisen rearrangement

Catalyst (Si/Metal calcined sample)	APE Conversion (%)	*o*-AP Selectivity (%)	Benzofuran Selectivity (%)
Al-MCM-41 (21)	86.7	33.8	66.2
Al-MCM-41 (31)	68.0	33.6	66.3
Al-MCM-41 (53)	52.0	61.0	39.0
Ga-MCM-41 (20)	81.1	39.5	60.4
Ga-MCM-41 (33)	68.1	60.1	39.8
Ga-MCM-41 (54)	33.1	83.4	16.6
Al-SBA-15 (19)	88.3	17.7	82.3
Al-SBA-15 (30)	74.1	24.0	76.0
Al-SBA-15 (46)	70.9	25.0	75.0
10 wt.% PW/SBA-15	3.2	93.0	7.0
20 wt.% PW/SBA-15	10.7	74.6	25.3
30 wt.% PW/SBA-15	23.3	34.5	65.5
40 wt.% PW/SBA-15	21.8	35.4	64.6

Reaction conditions: APE=0.67 g, TCE= 10 g, catalyst amount= 0.075 g, T= 393 K, TOS=12 h.

4.1.4 CONCLUSIONS

The Claisen rearrangement of APE over Al-MCM-41 proceeds with ease in TCE. o-Allyl phenol is produced initially, which then undergoes cyclization to form 2, 3-dihydro-2-methylbenzofuran. The reaction takes place on the acid sites of the catalyst. Both catalyst acidity and substrate conversion increase with Al content in MCM-41. There is a close relationship between acidity and conversion, which suggests that the reaction occurs inside the pores of MCM-41.Both conversion and benzofuran formation increase with run duration while *o*-AP decreases as is expected for a consecutive reaction. The temperature effects on conversion and selectivity are more pronounced at low Si/Al ratios than at high Si/Al ratios. *o*-AP selectivity increases with increase in Si/Al ratio and decrease in temperature.

The reaction kinetics was analyzed assuming it to be a first order consecutive reaction. On Al-MCM-41, both k_1 (APE conversion) and k_2 (benzofuran formation) increase with increase in temperature. k_2 is not much affected by variation in the Si/Al ratio whereas k_1 is sensitive. The time, at which the intermediate *o*-AP concentration is maximum, (t_{max}) varies with both the reaction temperature and the Si/Al ratio of MCM-41. For a given catalyst, t_{max} decreases with reaction temperature and Al content.

The Claisen reaction was also studied (at 393 K for 12 h) over Ga-MCM-41, Al-SBA-15 and PW/SBA-15. The conversion and selectivity were higher for Al-SBA-15 with a Si/Al ratio of 19 compared to the other catalysts. The order of activities of the catalysts for Claisen rearrangement is: Al-SBA-15 > Al-MCM-41 > Ga-MCM-41 > PW/SBA-15.

4.2 PART 2 BECKMANN REARRANGEMENT OF CYCLOHEXANONE OXIME

4.2.1 INTRODUCTION

ε-caprolactam, an intermediate in the manufacture of Nylon-6 is normally manufactured by the liquid phase Beckmann rearrangement of cyclohexanone oxime using sulphuric acid as the catalyst. To overcome the problems associated with the use of H_2SO_4, attempts have been made to use solid catalysts such as silica-alumina [15] zeolite Y- [16] titanium silicalites [17], B-MFI [18, 19], silicalite-1 [20], SAPO-11 [21]. hydrotalcite like compounds [22] and B_2O_3/TiO_2-ZrO_2 [23, 24]. Recently, a process using a high silica MFI zeolite catalyst combined with a novel fluid bed reaction system has been put into commercial practice by Sumitomo [25]. Aucejo et al. reported that [26] the strong Brönsted acidity of zeolite catalysts is responsible for the formation of ε-caprolactam. However, the majority of the researchers [27, 28, 29] have suggested that weak or intermediate strength acid sites or even neutral silanol groups present on the external surface of the zeolites [30] and silanol nests are effective for this rearrangement, and strong acid sites accelerate the formation of by-products [31] [32]. Mesoporous materials like MCM-41 possess well-ordered hexagonal pores having a large number of surface SiOH groups with weak acidity [33]. Studies on MCM-41 [34] and Al-MCM-41 [35, 36] suggest that the weak acid sites and/or surface silanol groups are effective for the vapor phase Beckmann rearrangement of cyclohexanone oxime.

The vapor phase Beckmann rearrangement of cyclohexanone oxime to ε-caprolactam over SBA-15 and Al-SBA-15 catalysts with different Si/Al ratios prepared by a post-synthesis procedure has been investigated [37]. The effects of various reaction parameters such as temperature, time on stream, use of different solvents, contact time and feed oxime concentration on conversion and caprolactam selectivity are presented. Also, a comparative study of the activities of a number of acidic mesoporous catalysts, namely, Al-SBA-15, PW/SBA-15, Al-MCM-41, Ga-MCM-41, Sn-MCM-41, Fe-MCM-41 and V-MCM-41 in above reaction is also reported.

4.2.2 EXPERIMENTAL

(a) Preparation of catalysts

The synthesis procedure for the preparation of Al-SBA-15 samples with different Si/Al ratios, Ga-MCM-41, Al-MCM-41, Sn-MCM-41, Fe-MCM-41, V-MCM-41 and PW/SBA-15 has been described in chapter 2. Additionally, an NH_4-exchanged SBA-15 was prepared by heating SBA-15 (with stirring) in a solution of 1M NH_4NO_3 at 353 K for 6 h, filtering, washing with water and drying at 573 K. This treatment is expected to create more surface -OH groups.

(b) Reaction procedure

The catalytic experiments were carried out in a vertical down flow glass reactor (i.d. = 15 mm and 35 cm length) at atmospheric pressure using 2 g of the catalyst. The catalyst was pelletized and then sieved to 16-20 mesh size prior to use. The reactor was placed inside a temperature controlled vertical furnace. The thermocouple tip was centered at the middle of the catalyst bed. A solution of cyclohexanone oxime in a solvent (methanol, benzene, acetonitrile) was fed using a syringe pump (SAGE instrument). The WHSV values were calculated based on the oxime solution injected. Nitrogen (60 ml/min) was co-fed using a mass flow controller. The catalyst was calcined at 823 K for 6 h before start of run. The reaction products were analyzed using a HP 5890 gas chromatograph fitted with a mega bore column (SE-52, cross linked 5% PhMe silicone, 30 m in length, 0.53 mm id, 0.3 μm film thickness) and a FID. The product identification was done by GCIR and GCMS.

4.2.3 RESULTS AND DISCUSSION

(A) Vapor phase Beckmann rearrangement of cyclohexanone oxime over Al-SBA-15 catalysts

The major product observed over SBA-15 catalysts was the rearrangement product, caprolactam. The other products that were identified were cyanopentane, cyanopentene, cyclohexanone and cyclohexenone. The formation of these products is believed to be as shown below [35].

1. Cyclohexanone oxime $\rightarrow$ caprolactam $\rightarrow$ 5-cyano-pent-1-ene
2. Cyclohexanone oxime $\rightarrow$ 5-cyano-pent-1-ene
3. Cyclohexanone oxime + water $\rightarrow$ cyclohexanone + hydroxylamine

The probable sequence of the different reactions [35] is shown in Figure 4.12. The rearrangement to caprolactam is likely to be catalyzed by the acid sites in Al-SBA-15 while Si-OH groups may be responsible for the hydrolysis of the oxime.

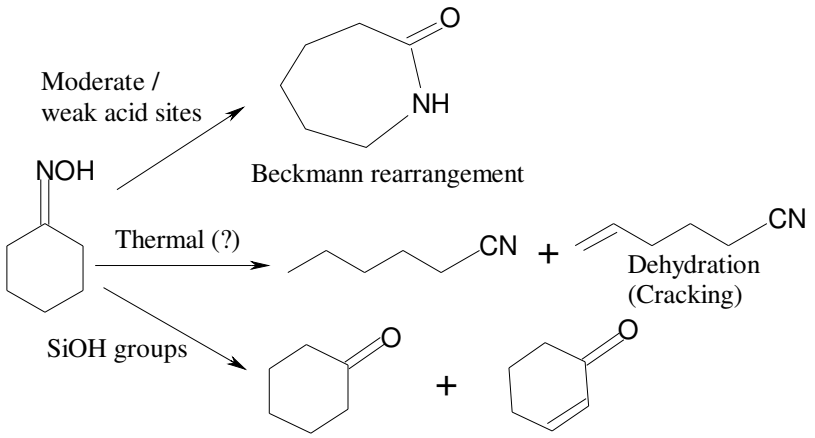

Figure 4.12 Different reactions of cyclohexanone oxime occurring on solid acid catalysts [35].

(i) Effect of time on stream

The oxime conversion and selectivity (at 623 K) for caprolactam as a function of time (TOS) are shown in Figure 4.13. The conversion of cyclohexanone oxime remains nearly constant (± 5 %) with TOS over all the catalysts. However, the selectivity for caprolactam gradually increases with TOS and reaches a plateau at around 4-6 h. The initial increase in selectivity is probably due to deactivation of the strong acid sites. During the reaction side products such as cyanopentane, cyanopentene, cyclohexanone and cyclohexenone are also formed. The selectivity for cyanopentane and cyanopentene decrease with TOS for all the catalysts. The selectivity for cyclohexanone and cyclohexenone slightly decrease first and then remain constant after a TOS of about 4 h for all the catalysts.

(ii) Influence of space velocity

The influence of contact time in the WHSV range of 1.5 - 9.6 h^{-1}on conversion and caprolactam selectivity was studied at 623 K over Al-SBA-15 (9) and the results are presented in Figure 4.14. It is observed that, with increase of feed rate the oxime

conversion decreases from 91 to 77 %, while the yield of caprolactam reaches a plateau at a WHSV of 3.02 h^{-1}. The yields of the other products, cyanopentane and cyclohexanone decrease with decreasing contact time.

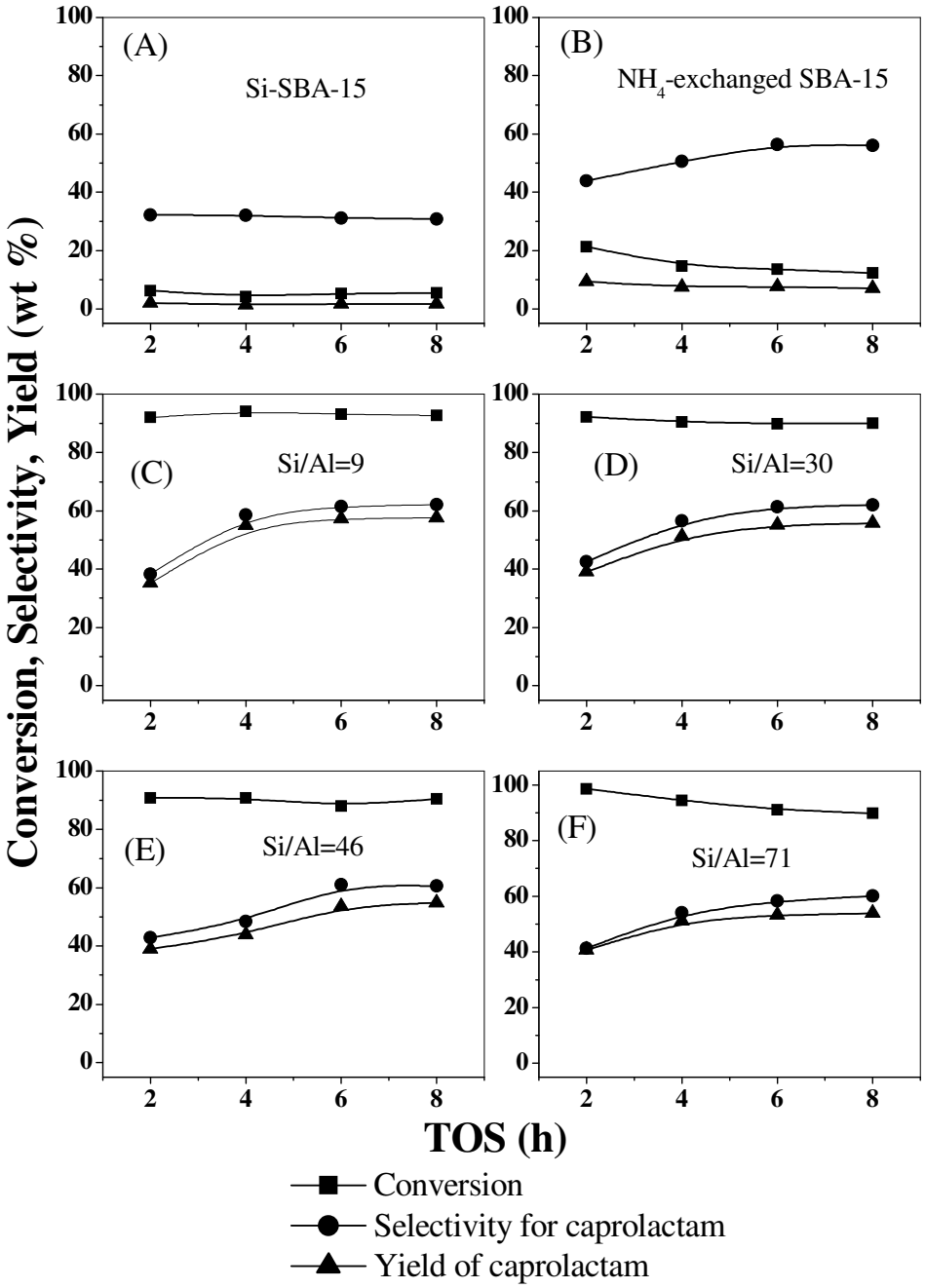

Figure 4.13 Effect of time on stream on cyclohexanone oxime transformation over Si-SBA-15 and Al-SBA-15 with different Si/Al ratios. Catalyst wt. = 2 g; Feed = 1/8 (oxime /methanol) wt. ratio, WHSV = 3.02 h^{-1}; N_2 = 60 ml/min; T= 623 K.

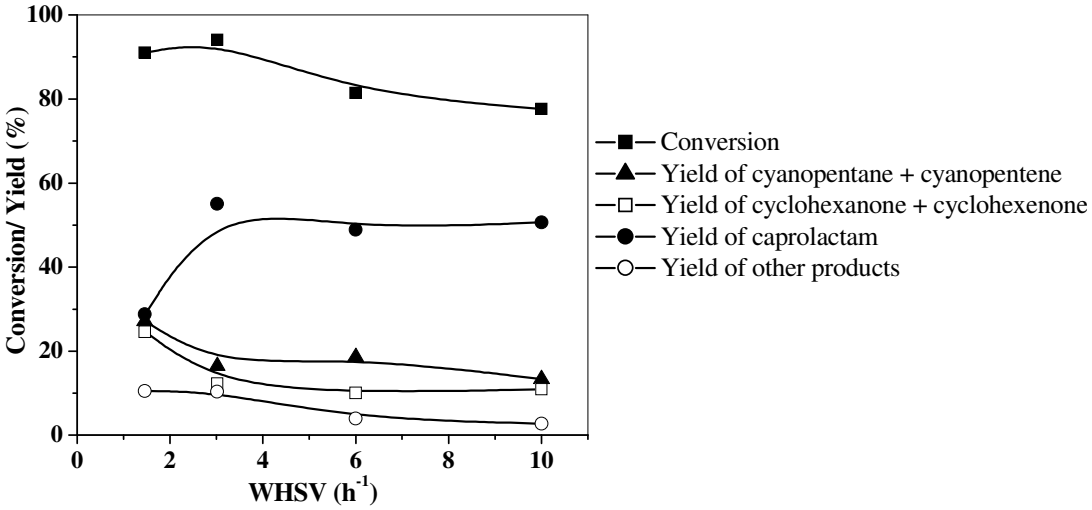

Figure 4.14 Effect of WHSV (h^{-1}) on cyclohexanone oxime transformation over Al-SBA-15 (Si/Al=9).Catalyst weight = 2 g; Feed = 1/8 (oxime / methanol) wt. ratio, TOS = 2 h, N_2 = 60 ml/min, T= 623 K.

(iii) Influence of temperature

The transformation of cyclohexanone oxime to caprolactam was studied in the temperature range of 573-723 K on calcined SBA-15, ammonium exchanged SBA-15 and Al-SBA-15 catalysts. The influence of temperature on conversion and product selectivity are presented in Figure 4.15. For SBA-15 and ammonium exchanged SBA-15 catalysts (Figure 4.15 (A) and 4.15 (B) respectively) conversion is found to be rather low at 573 K. However it increases steadily and reaches a near constant value above 30 % at 673 K. Selectivity for caprolactam steadily decreases with increase in temperature for SBA-15 (from 40 % at 573 K to 25 % at 723 K) but goes through a maximum (about 58 % at 673 K) for SBA-15 treated with NH_4^+. For the Al-SBA-15 catalysts cyclohexanone oxime conversion increases from around 71 % at 573 K and reaches nearly 95% at about 623 K over all the catalysts. Selectivity for caprolactam is nearly constant (± 5%) for the catalysts, though a small initial increase of selectivity with temperature is noticed for Al-SBA-15 (9). The best catalyst is Al-SBA-15 with a Si/Al ratio of 9 which shows a conversion of around 95 % and a selectivity of around 59 % at 623 K. The small decrease in selectivity generally noticed at higher temperatures is probably due to the decomposition of caprolactam on the catalyst surface and an increase in the side reactions. At higher temperatures, the formation of cyclohexanone decreases whereas cyanopentene formation increases. The selectivity

for other compounds (mostly dimers) increases with temperature. The selectivity for by products is relatively large over these catalysts as these are products formed by the hydrolysis of both caprolactam and cyclohexanone over the surface Si-OH groups.

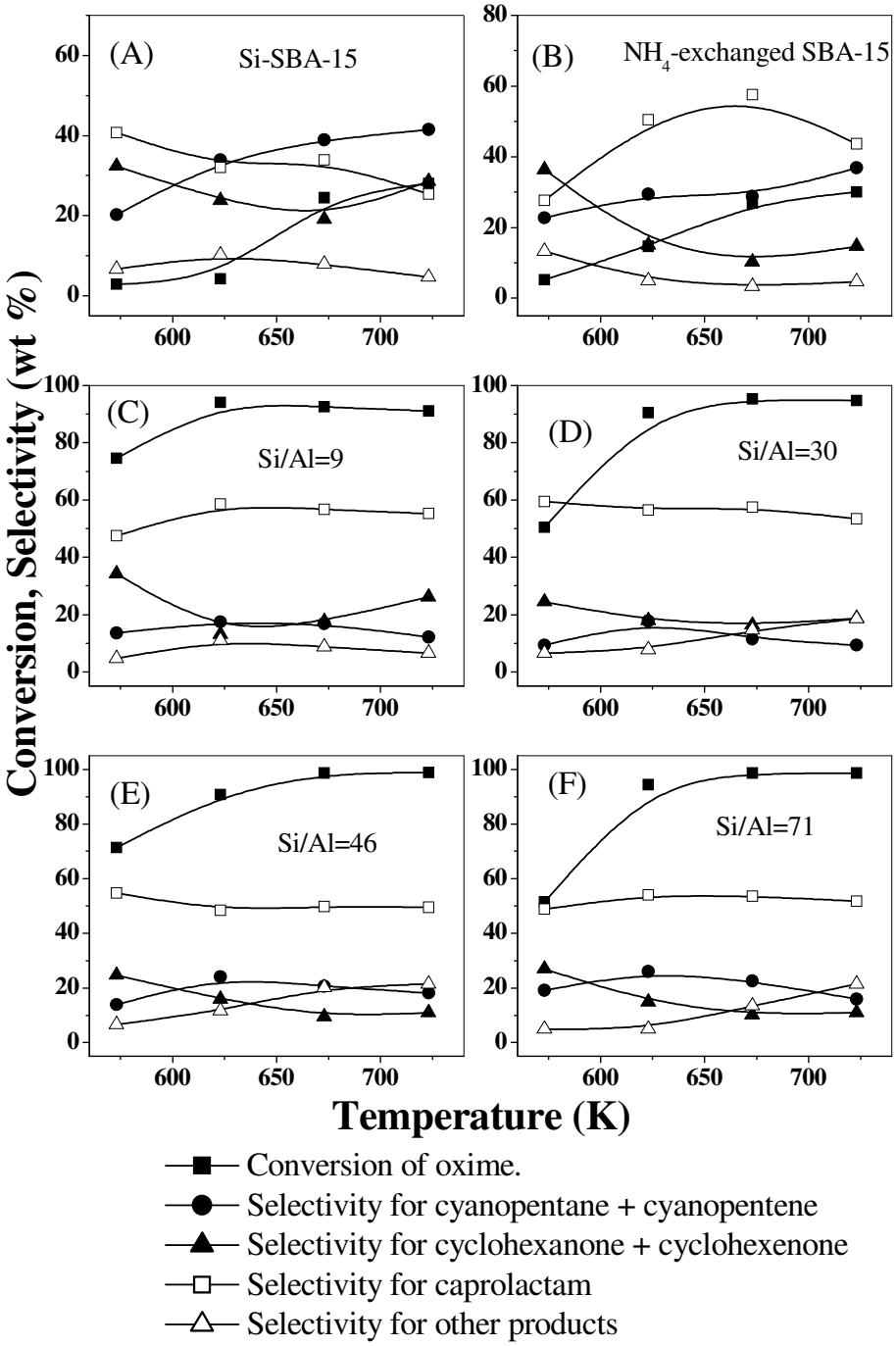

Figure 4.15 Effect of reaction temperature on cyclohexanone oxime transformation over Si-SBA-15 and Al-SBA-15 with different Si/Al ratios. Catalyst wt. = 2 g; Feed = 1/8 wt. ratio, (oxime /methanol); WHSV = 3.02 h^{-1}; N_2 = 60 ml/min; TOS = 4 h.

(iv) Influence of concentration of oxime

At a low oxime to methanol weight ratio (1:8), the selectivity for caprolactam is high (Figure 4.16) and at higher ratios, the formation of the by products cyanopentene, cyanopentane, cyclohexanone, cyclohexenone is high. At higher concentrations of oxime, deactivation of the catalyst is faster.

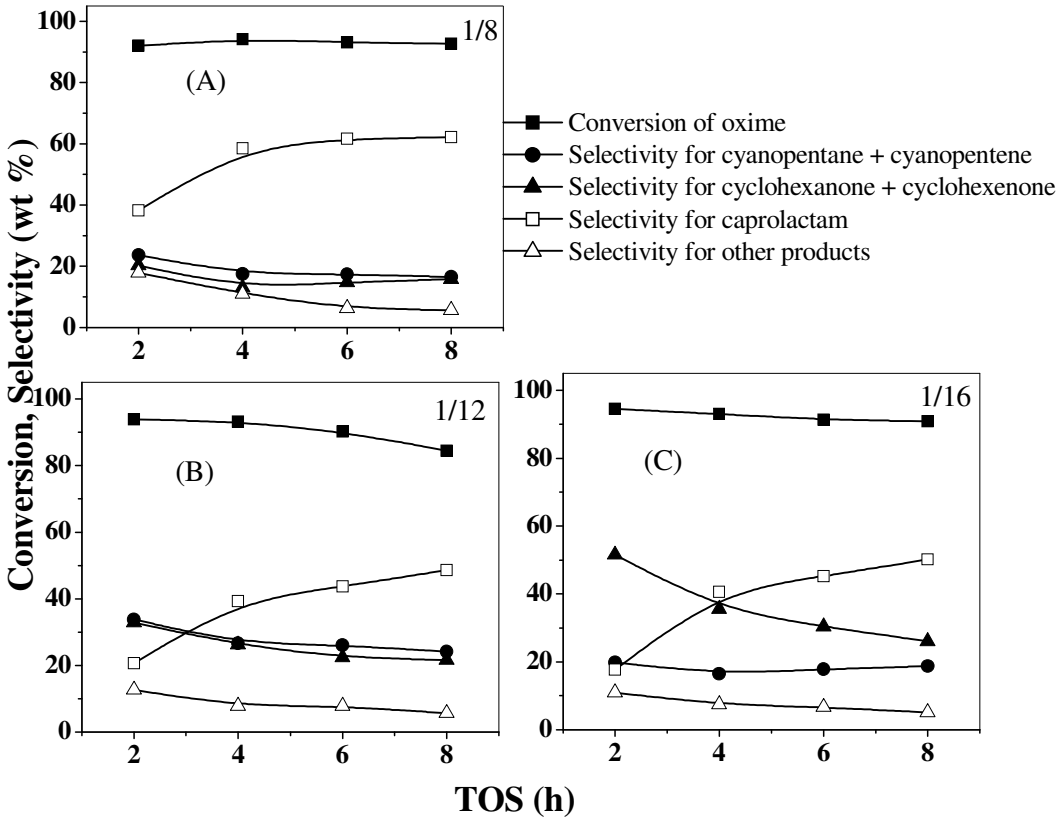

Figure 4.16 Effect of time on stream on cyclohexanone oxime transformation over Al-SBA-15 with Si/Al = 9 at different oxime /methanol weight ratios: (A) 1/8, (B) 1/12 and (C) 1/16. Catalyst wt. = 2 g, WHSV=3.02 h^{-1}, N_2 = 60 ml/min, T = 623 K.

(v) Influence of solvent

The influence of solvents on the reaction was studied over Al-SBA-15 (9) catalyst and the results are presented in Figure 4.17. The solvents used were benzene (dielectric constant = 2.3), methanol (dielectric constant = 33.6) and acetonitrile (dielectric constant = 37.5). The selectivity for caprolactam is more in the medium polar solvent methanol. T. Komatsu et al. [20] reported that medium polarity solvents such as alcohols gave specific improvements in the selectivity for caprolactam probably due to the effect of OH groups and the desorption of caprolactam induced by

the attack of the alcohol molecules, which was confirmed by IR measurements. The selectivity is higher in methanol probably also due to the attenuation of strong acidity by the water formed during the dehydration of the solvent, methanol. Conversion of the oxime in the case of benzene and acetonitrile is almost 100 % but selectivity for caprolactam is less than in methanol (50-55 % compared to 60 % in methanol). In the case of benzene and acetonitrile, selectivity for the by-products cyanopentane, cyanopentene, cyclohexanone and cyclohexenone is high.

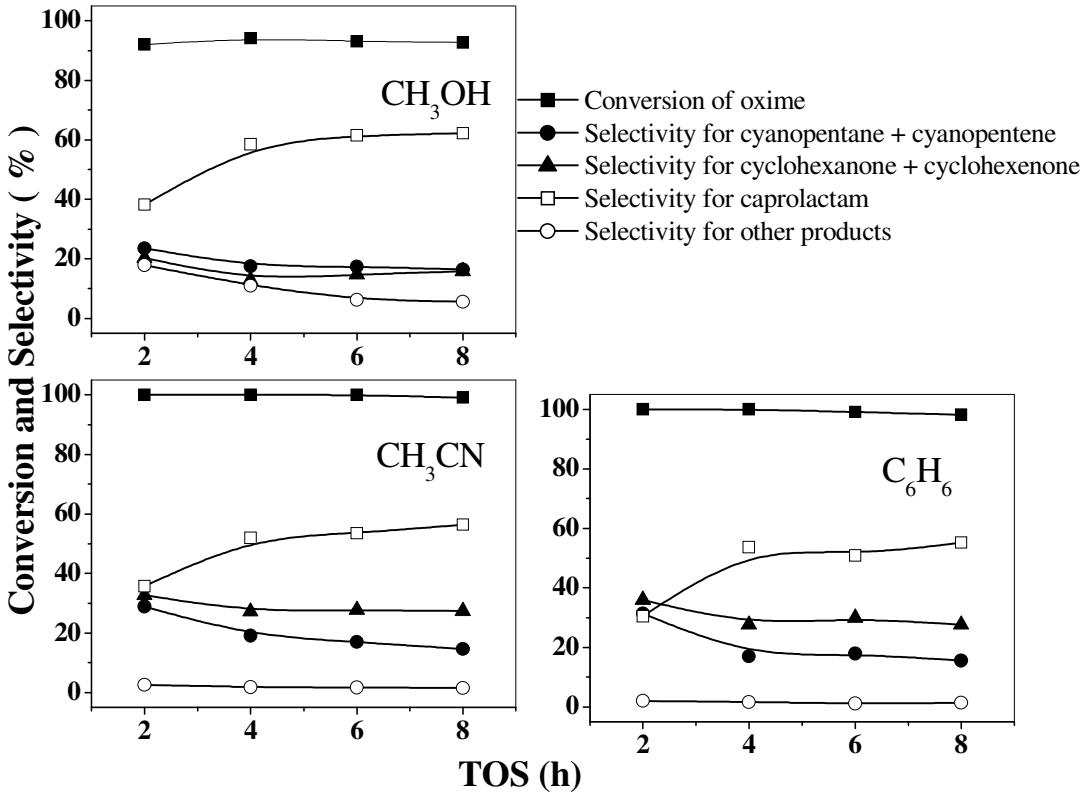

Figure 4.17 (a) Effect of time on stream on cyclohexanone oxime transformation over solvents methanol, acetonitrile and benzene over Al-SBA-15 (Si/Al = 9), catalyst wt. = 2 g, Feed = 1/8 wt ratio, WHSV = 3.02 h^{-1}; N_2 = 60 ml/min; T = 623 K.

(vi) Influence of addition of water

The influence of addition of water in the feed is shown in Figure 4.18. It is found that both conversion and oxime selectivities increase with amount of water and reach a maximum at about 1.5:1 (water: oxime) mole ratio (Figure 4.18). When water is added, it forms steam which cleans the catalyst surface of strongly adsorbed products and increases catalyst acidity.

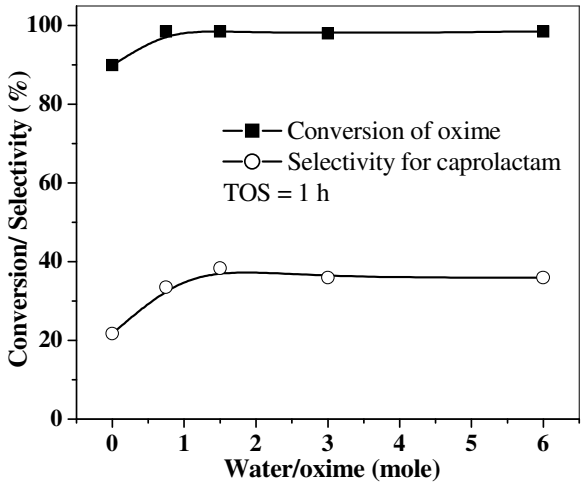

Figure 4.18 Effect of water addition on cyclohexanone oxime transformation over Al-SBA-15 (Si/Al = 9). Feed: 1/8 wt ratio of oxime/ methanol. Catalyst weight = 2 g, WHSV = 3.02 h^{-1}, N_2 Carrier = 60 ml/min, TOS = 1 h, T= 623 K.

(vii) Influence of Si/Al ratio

The effect of Al content in the Al-SBA-15 samples on the reaction was investigated over catalysts with different Si/Al ratios of 9, 30, 46, 71. The results obtained at a TOS of 8 h are presented in Figure 4.19 (A). Data obtained over the catalysts at different temperatures was presented in (Figure 4.15). The selectivity for caprolactam is more over Al-SBA-15 samples than over SBA-15. It increases with increase in Al content. The highest yield of caprolactam is over the sample with Si/Al = 9. It is noticed that the side products decrease with increasing Al content in the catalyst. The silanol groups present on Si-SBA-15 and ammonium exchanged SBA-15 is not sufficiently acidic to catalyze the rearrangement though they are able to catalyze the formation of the by-products (Figure 4.15). The above studies reveal that the formation of caprolactam is mainly favored over the moderate acid centers of Al-SBA-15. The large yields of the deaminated product cyclohexanone over Si-SBA-15 and ammonium exchanged SBA-15 suggest that it is formed more over the neutral surface silanol groups. The C-C bond cleavage products, cyanopentane, and cyanopentene are formed over SBA-15, ammonium exchanged SBA-15 and Al-SBA-15. Apparently, these are produced from dehydration and cracking reactions both catalyzed and non-catalyzed.

Influence of Al content on oxime conversion and catalyst acidity over Al-SBA-15 catalysts at a TOS of 8 h at 623 K is shown in Figure 4.19 (A). Conversion

increases from 89.9 % to 92.6 % with increase in Al content apparently due to an increase in the number of acid sites (Figure 4.19 (B)).

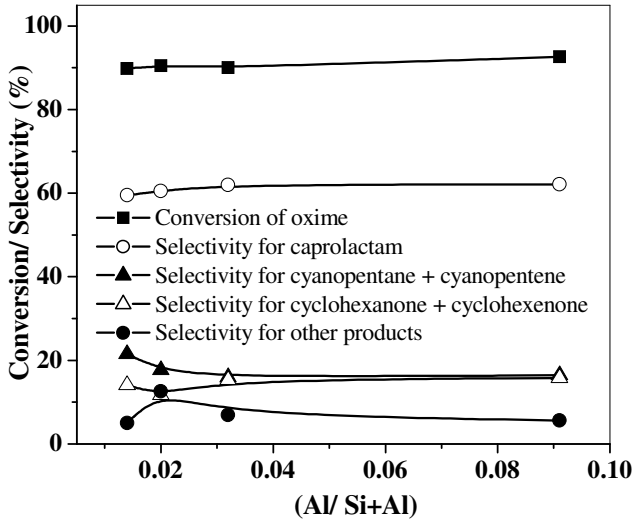

Figure 4.19 (A) Effect of Al content on cyclohexanone oxime transformation. Feed: 1/8 wt ratio of oxime/ methanol. Catalyst weight = 2 g; WHSV = 3.02 h^{-1}; N_2 = 60 ml/min; TOS = 8 h; T = 623 K.

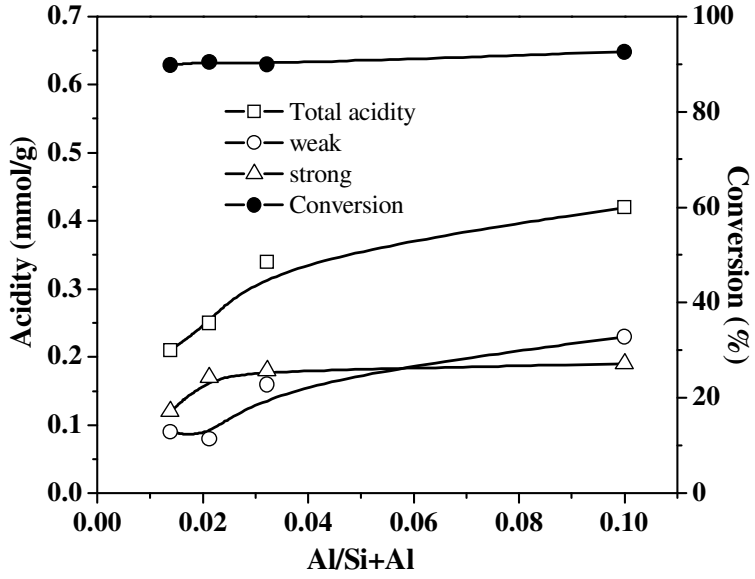

Figure 4.19 (B) Influence of Al content on oxime conversion and catalyst acidity over Al-SBA-15 catalysts with different Si/Al ratios. Reaction conditions: TOS = 8 h, T=623 K, WHSV=3.02 h^{-1}, oxime: methanol = 1:8 wt. ratio, catalyst wt. = 2.0 g.

(B) Vapor phase Beckmann Rearrangement over MCM-41 type catalysts

The reaction procedure used was the same as for the SBA-15 catalysts (section 4.2.2 (ii)). All the catalysts were studied and compared at 623 K using an oxime: methanol wt. ratio of 1:8 at a WHSV of 3.02 h^{-1}.

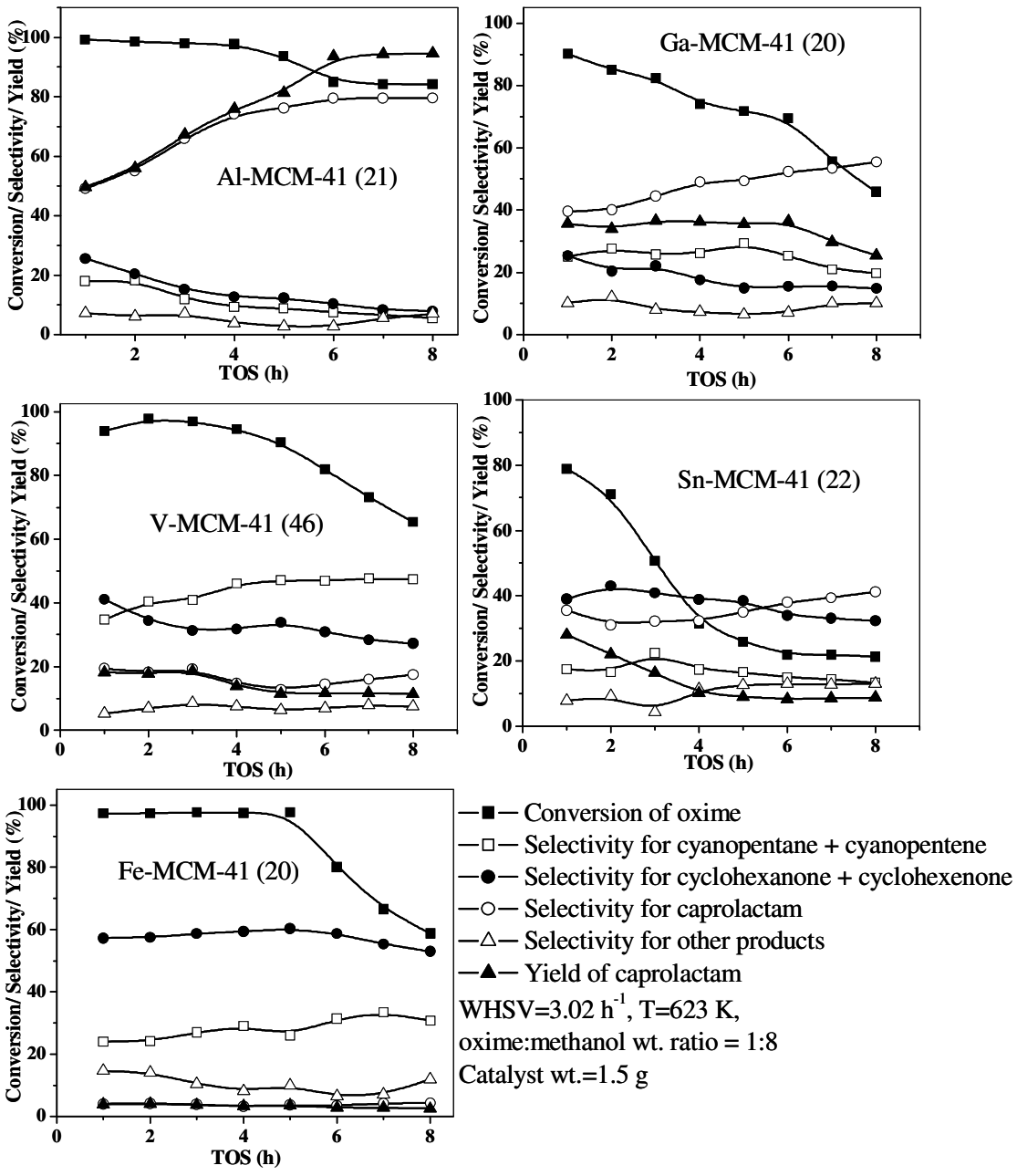

Figure 4.20 Effect of TOS on oxime transformation over MCM-41 type catalysts.

(i) Effect of time on stream

Oxime conversion, yield and selectivity to caprolactam with time are presented in Figure 4.20. The conversion of cyclohexanone oxime is high initially and decreases at higher TOS over all the catalysts. However, the selectivity for caprolactam gradually increases with TOS and reaches a maximum at around 4 h. The initial increase in selectivity is probably due to the deactivation of the strong acid sites. The selectivity for caprolactam increases in the order Al-MCM-41 > Ga-MCM-41 > Sn-MCM-41 > V-MCM-41 > Fe-MCM-41. A bar chart comparing the different catalysts is shown in Figure 4.21. Oxime conversion is very high over V and Fe-MCM-41. Selectivity for caprolactam is however much lower over these catalysts than over the others (Figure 4.21). V-MCM-41 shows a high selectivity for cyanopentane and cyanopentene while Fe-MCM-41 shows a high selectivity for cyclohexanone and cyclohexenone.

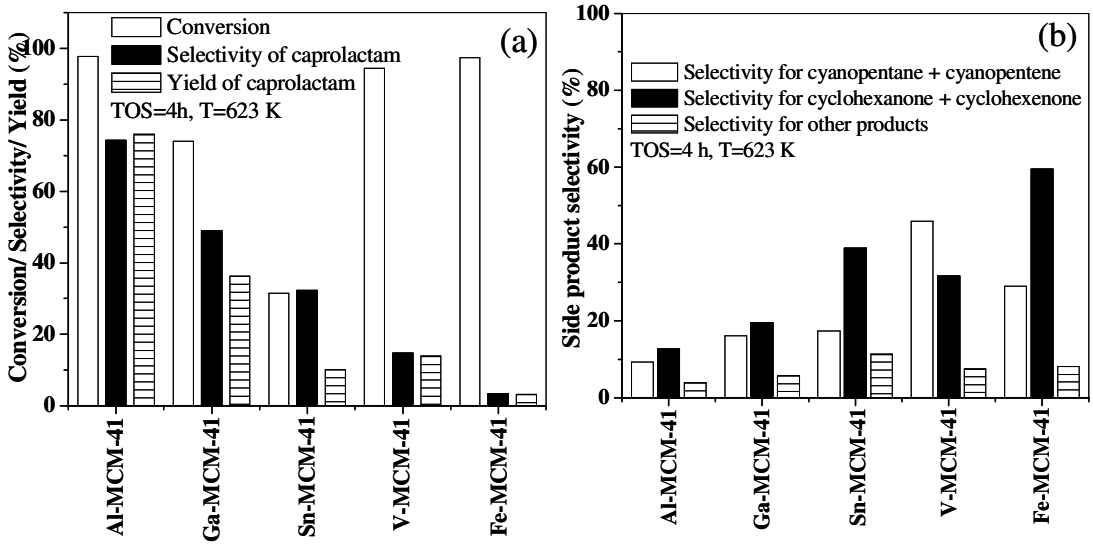

Figure 4.21 (a) Conversion, selectivity and yield of caprolactam, (b) side product selectivity at TOS = 4 h, catalyst wt. = 1.5 g; Feed = 1/8 wt. ratio (oxime /methanol); WHSV = 3.02 h^{-1}; N_2 = 60 ml/min; T = 623 K.

(C) Vapor phase Beckmann Rearrangement over PW/SBA-15 type catalysts

Investigations of the Beckmann rearrangement over PW loaded SBA-15 catalysts with 10, 20, 30 and 40 wt. % PW loading (at 623 K using an oxime: methanol wt. ratio of 1:8 and a WHSV of 3.02 h^{-1}) are presented below.

(i) Effect of time on stream

Oxime conversion and selectivity for caprolactam with time on stream are shown in Figure 4.22. The conversion of cyclohexanone oxime remains nearly constant (>95%) with TOS over all the catalysts. However, the selectivity gradually increases with TOS and remains constant after 4 h**,** reaching 80% for all the catalysts. Selectivity for other products such as cyanopentane + cyanopentene and cyclohexanone + cyclohexenone is nearly constant with TOS, though small deviations are noticed for the different catalysts and products.

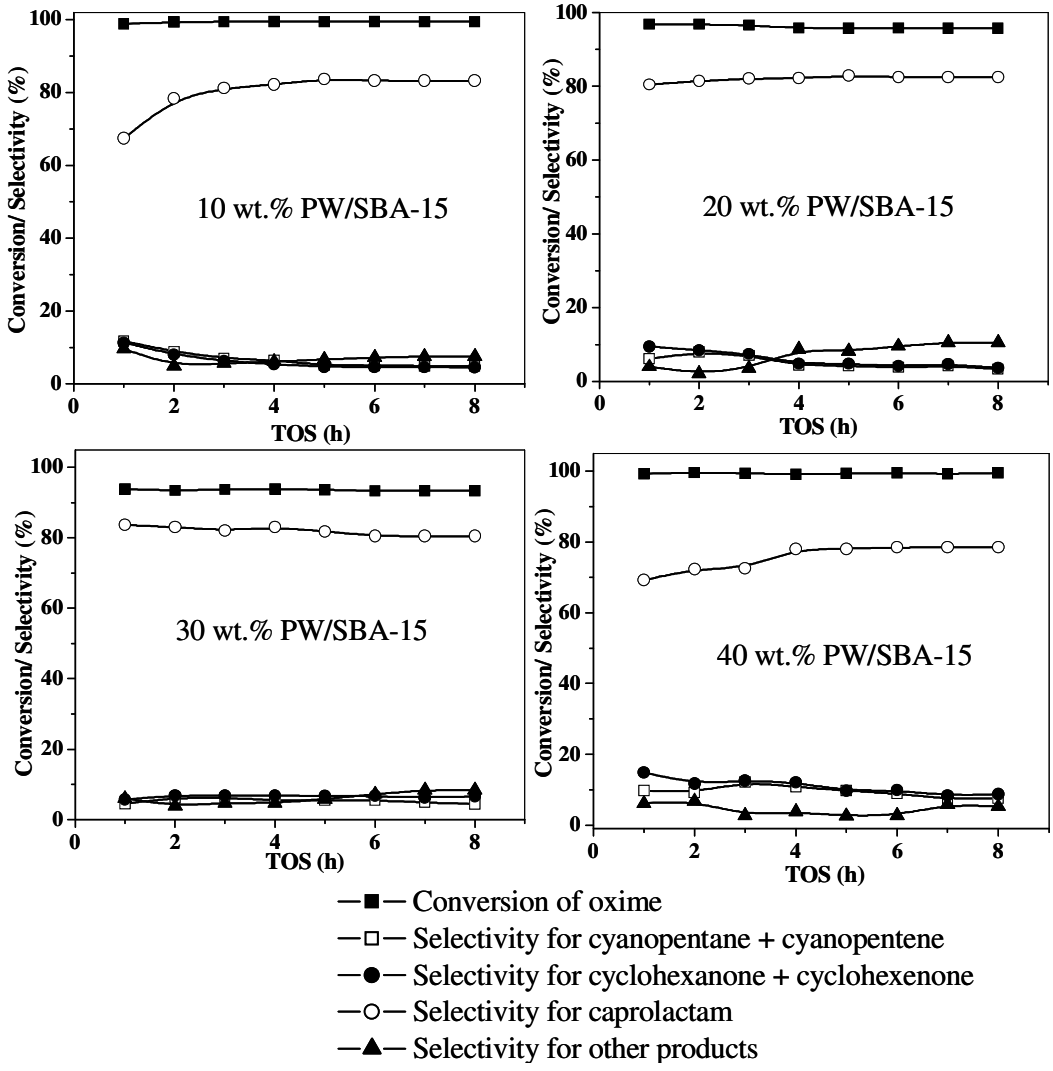

Figure 4.22 Conversion and selectivity for the products over PW/SBA-15 catalysts. Catalyst wt. = 1.5 g, oxime /methanol wt. ratio =1/8, WHSV = 3.02 h^{-1}, N_2 = 60 ml/min, T = 623 K.

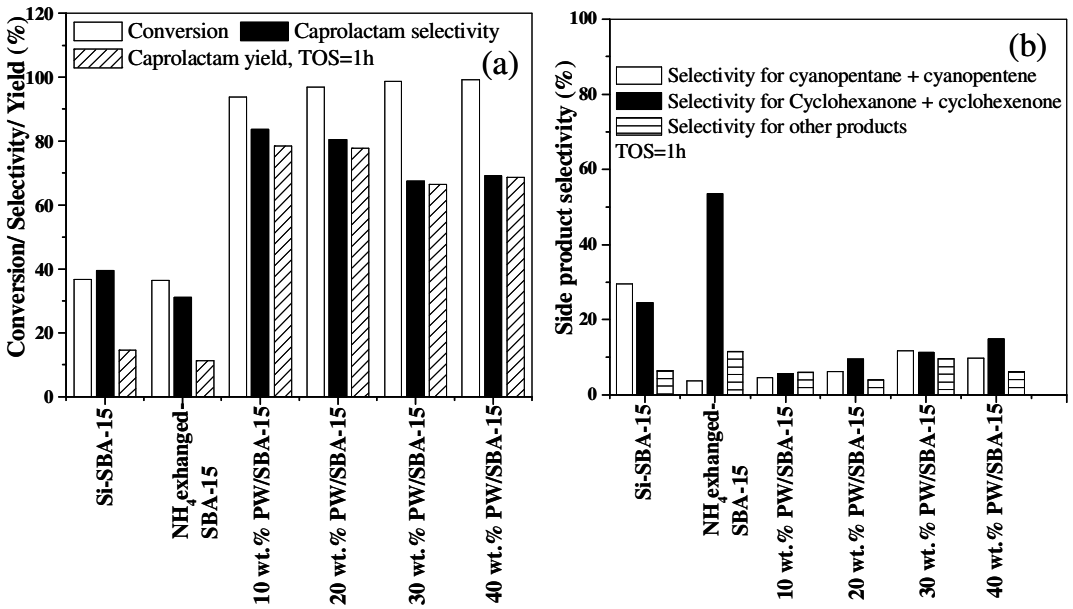

Figure 4.23 (a) Conversion, selectivity and yield of caprolactam and (b) Side product selectivity for Si-SBA-15, NH_4-exchanged SBA-15 and PW/SBA-15 catalysts. Catalyst wt. = 1.5 g, oxime /methanol = 1/8 wt. ratio, WHSV = 3.02 h^{-1}, T = 623 K. N_2 = 60 ml/min, TOS=1 h.

(ii) Effect of PW loading

Oxime conversion and caprolactam selectivity on Si-SBA-15 and PW/SBA-15 at 623 K at a TOS of 1 h are presented in Figure 4.23 (a). The effects of run duration on conversion and product selectivity over PW/SBA-15 have already been presented in Figure 4.22. Si-SBA-15 and NH_4-exchanged SBA-15 catalysts exhibit a low conversion of 36.8 and 36.4 %, respectively at a TOS = 1 h. It is observed that there is not much change in the conversion of oxime with the PW loading being between 95-98 % over all the PW catalysts. Selectivity at a TOS of 1 h decreases with PW loading, though after a TOS of about 4 h, the selectivity is nearly constant (about 80 %) over all the catalysts (Figure 4.22).

Influence of PW content on oxime conversion (and catalyst acidity) over PW/SBA-15 catalysts at TOS 8 h at 623 K is shown in Figure 4.24 (A). Conversion is more than 95 % for all the catalysts. Acidity increases with phosphotungstic acid loading, but its effect is not noticed over these catalysts due to the very high conversions achieved.

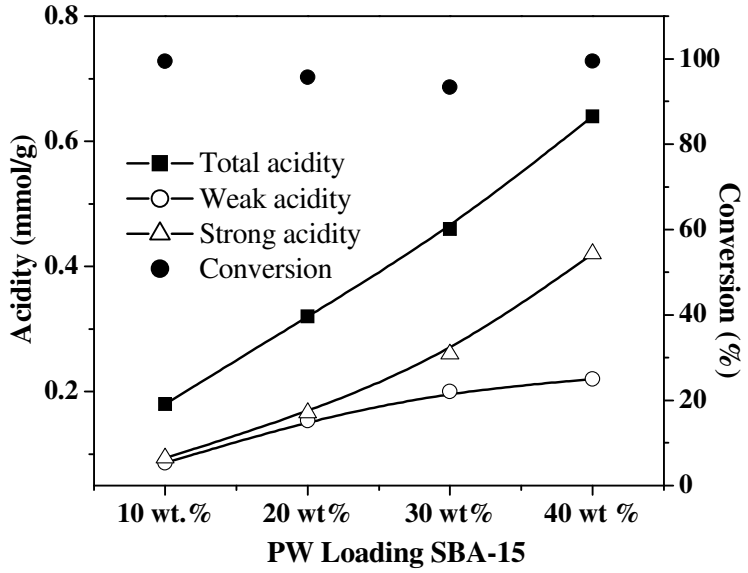

Figure 4.24 (A) Influence of PW content on oxime conversion (and catalyst acidity) over PW/SBA-15 catalysts with different phosphotungstic acid loading. Reaction conditions: TOS = 8 h, T = 623 K, WHSV =3.02 h^{-1}, oxime: methanol = 1:8 wt. ratio, catalyst wt. = 1.5 g.

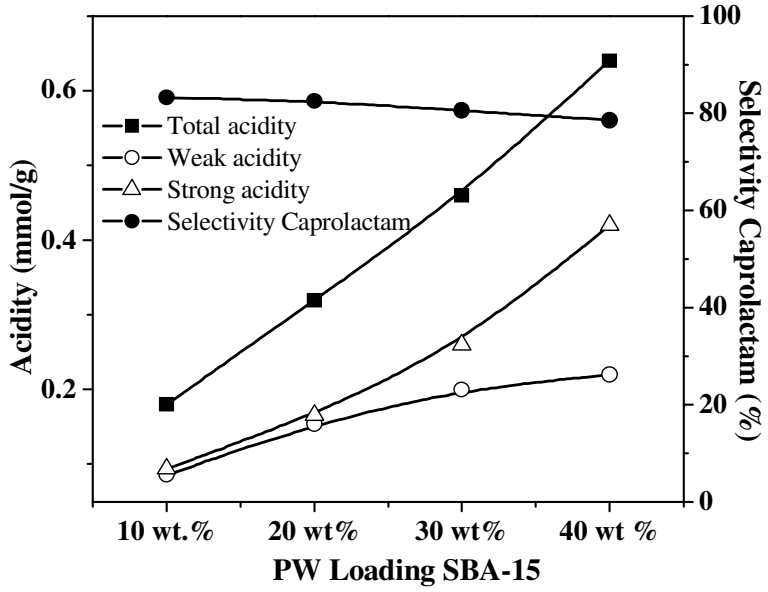

Figure 4.24 (B) Influence of PW content on caprolactam selectivity (and catalyst acidity) over PW/SBA-15 catalysts with different phosphotungstic acid loading. Reaction conditions: TOS = 8 h, T = 623 K, WHSV =3.02 h^{-1}, oxime: methanol-1:8 wt. ratio, catalyst wt =1.5 g.

The influence of PW content on caprolactam selectivity (and catalyst acidity) over PW/SBA-15 catalysts at a TOS of 8 h at 623 K is shown in Figure 4.24 (B). There is a marginal decrease in the selectivity from 83.2% for 10 wt. % PW catalyst to 78.5 % for 40 wt. % catalyst.

Table 4.3 Comparison data for all catalysts at TOS= 4 h

Catalyst (Si/ metal ratio)	Conv.	Selectivity (%)				Yield of
	oxime	A	B	C	Others	C (%)
Si-SBA-15 [a]	4.2	34.0	23.8	32.0	10.2	1.3
NH_4-exchanged SBA-15 [a]	14.7	29.4	15.0	50.5	4.9	7.4
Al-SBA-15 (9) [a]	94.1	17.5	13.0	58.5	11.0	55.0
Al-MCM-41 (19)	97.8	9.2	12.7	74.2	3.9	72.6
Al-MCM-41 (30)	73.6	16.1	19.5	65.5	5.8	48.3
Ga-MCM-41 (20)	74.0	26.1	17.6	49.0	7.3	36.3
Sn-MCM-41 (22)	31.5	17.4	38.9	32.3	11.3	10.2
V -MCM-41 (46)	94.5	46.0	31.7	14.7	7.5	13.9
Fe –MCM-41 (20)	97.4	29.0	59.4	3.3	8.2	3.2
10 wt. % PW/SBA-15	99.4	6.4	5.3	82.1	6.1	81.7
20 wt. % PW/SBA-15	95.8	4.3	4.8	82.2	8.7	78.7
30 wt. % PW/SBA-15	93.8	5.4	6.8	83.0	4.7	77.8
40 wt. % PW/SBA-15	99.2	10.8	12.0	72.5	4.6	72.0

Reaction conditions: T = 623 K, TOS = 4 h., N_2 = 60 ml/min, WHSV = 3.02 h^{-1}, oxime: methanol- 1:8 wt ratio, catalyst wt. =1.5 g, (**a -** catalyst wt. = 2 g)**.** A- cyclohexanone + cyclohexenone, B-cyanopentane + cyanopentene, C- caprolactam, others- dimers.

(iii) Comparison of activity of different catalysts

A comparison of activity of different catalysts (at 623 K and TOS 4 h) is presented in Table 4.3. The activity of the catalysts for oxime conversion as well as selectivity for caprolactam is in the order, Si-SBA-15 < NH_4-exchanged SBA-15 < Fe –MCM-41 < V -MCM-41 < Sn-MCM-41 < Ga-MCM-41 < Al-SBA-15 < Al-MCM-41 < PW/SBA-15.

4.2.4 CONCLUSIONS

A study of the transformation of cyclohexanone oxime to ε-caprolactam was carried out on SBA-15, ammonium exchanged SBA-15 and Al-SBA-15 samples with different Si/Al ratios. The vapor phase Beckmann rearrangement was studied at different reaction conditions of temperature, space velocity and time on stream. The effect of polarity of solvents was also investigated over the catalysts. Conversion of oxime remains nearly constant with TOS up to 8 h over all the catalysts at the temperatures studied in the range (573-723 K). Selectivity for caprolactam increases with TOS. Caprolactam yield is highest for Al-SBA-15 with Si/Al ratio of 9 at 623 K and WHSV of 3.02 h^{-1}. While acidic sites appear to catalyze the rearrangement, Si-OH groups catalyze the formation of by-products. The moderate polar solvent methanol exhibits the best performance for caprolactam selectivity.

The Beckmann rearrangement was also studied over as Fe–MCM-41, V-MCM-41, Sn-MCM-41, Ga-MCM-41, Al-MCM-41, and PW/SBA-15. The activity of these catalysts was compared at 623 K. The results show that oxime conversion as well as selectivity for caprolactam for these catalysts varied in the order, Si-SBA-15 < NH_4-exchanged SBA-15 < Fe –MCM-41 < V -MCM-41 < Sn-MCM-41 < Ga-MCM-41 < Al-SBA-15 < Al-MCM-41 < PW/SBA-15.

4.3 REFERENCES

1. J. March, "Advanced Organic Chemistry", 4th Eds., Wiley, New York, (1992).
2. (a) R. P. Lutz, Chem. Rev. 84 (1984) 205; (b) D. S. Tarbell, Org. React. 2 (1944) 1.
3. K. Pitchumani, M. Warrier, V. Ramamurthy, Res. Chem. Intermed. 25 (1999) 623.
4. (a) K. Pitchumani, M. Warrier, V. Ramamurthy, J. Am. Chem. Soc. 118 (1996) 9428; (b) R. Sreekumar, R. Padmakumar, Tet. Lett. 38 (1997) 2413.
5. J.A. Elings, R.S. Downing, R.A. Sheldon, Stud. Surf. Sci. Catal. 94 (1995) 87.
6. R.A. Sheldon, J.A. Elings, S.K. Lee, H.E.B. Lempers, R.S. Downing, J. Mol. Catal. A: Chem. 134 (1998) 129.
7. Sucholeiki, I., Pavia, M.R., Kresge, C.T., Mc Cullen, S.B., Malek, A., Schram, S., Mol. Diversity 3 (1998), 151-171; CA: 129: 202736 (1999).
8. Cruz-Almanza, R., Perez-Flores, F., Brena, L., Tapia, E., Ojeda, R., Fuentes, A., J. Heterocycl. Chem. 32 (1995) 219.
9. E. J. Creyghton, J. A. Elings, R.S. Downing, R.A. Sheldon, H. van Bekkum, Micropo. Mater. 5 (1996) 299.
10. S. G. Wagholikar, S. Mayadevi, S. P. Mirajkar, S. Sivasanker, in: E. Van Steen, L. Callanan, M. Claeys, C.T. O'Connor (Eds), Proceedings of 14th International Zeolite Conference, Cape Town (2004) 2731.
11. C. T. Kresge, M.E. Leonowicz, W. J. Roth, J. C. Vartuli, J. S. Beck, Nature 359 (1992) 710.
12. J. S. Beck, J. C. Vartuli, W. J. Roth, M.E. Leonowicz, C.T. Kresge, K. D. Schmitt, C. T. W. Chu, D. H. Olson, E, W. Scheppard, S. B. MacCullen, H. B. Higgins, J. L. Schlenker, J. Am. Chem. Soc.114 (1994) 10834.
13. Vogel's Textbook of Qualitative organic analysis (1977).
14. V.G.S. Box, P.C. Meleties, Heterocycles 48 (1998) 2173.
15. P. B. Venuto, P. S. Landis, Adv. Catal. 18 (1968) 259.
16. P. S. Landis, P.B. Venuto, J. Catal. 6 (1966) 245.
17. A. Thangraj, S. Sivasanker and P. Ratnasamy, J. Catal. 137 (1992) 252.
18. J. Roseler, G. Heitmann, W. F. Holderich, Appl. Catal. A: Gen. 144 (1996) 319.
19. G. P. Heitmann G. Dahlhoff, W. F. Holderich, J. Catal. 194 (2000) 122.

20. T. Komatsu, T. Maeda, T. Yashima, Micropor. Mesopor. Mater. 35-36 (2000) 173.
21. P. S. Singh, R. Bandyyopadhyay, S. G. Hegde, B.S. Rao, Appl. Catal. A: Gen. 136 (1996) 249.
22. R. Bechara, A. D'Huysser, M. Fournier, L. Forni, G. Fornasari, F. Trifiro, A. Vaccari, Catal. Lett. 82 (2002) 59.
23. D. Mao, G. Lu, Q. Chen, Z. Xie, Y. Zhang, Catal. Lett. 77, 1-3 (2001) 119.
24. D. Mao, Q. Chen, G. Lu, Appl. Catal. A: Gen. 244 (2003) 273.
25. Sumitomo Chemicals; "Focus on catalysts", Vol.2004, 10, 2004, 6 (European chemical news (2004) 81, 2111, 17.
26. A. Aucejo, M. Burget A. Corma, V. Fornes, Appl. Catal. 22 (1986) 187.
27. T. Yashima, K. Miura and T. Komatsu, Stud. Surf. Sci. Catal. 84 (1994) 1897.
28. T. Curtin, J. P. McMonagle and B.K. Hodnett, Appl. Catal. A: Gen. 93 (1992) 75.
29. T. Curtin, J. P. McMonagle and B.K. Hodnett, Appl. Catal. A: Gen. 93 (1992) 91.
30. H. Sato, K. Hirose, M. Kitamura and Y. Nakamura, Stud. Surf. Sci. Catal. 49 (1989) 1213.
31. T. Ushikubo, and K. Wada, J. Catal. 148 (1994) 138.
32. M. A. Camblor, A. Corma, H. Garcua, V. Semmere- Herledan and S. Valencia- J. Catal. 177 (1998) 267.
33. J. S. Beck, J. C. Vartuli, W. J. Roth, C. R. Kresge, J. B. Higgins, and J. L. Schlenker, J. Am. Chem. Soc. 114 (1992) 10834.
34. Lian- Xin Dai, K. Koyama, T. Tatsumi, Catal. Lett. 53 (1998) 211.
35. K. Chaudhari, R. Bal, A. J. Chandwadkar, S. Sivasanker, J. Mol. Catal. A: Chem. 177 (2002) 247.
36. An-Nan Ko, C. Hung, C. Chen, K. Ouyang, Catal. Lett. 71, 3-4 (2001) 219.
37. Z. Luan, M. Hartmann, D. Zhao, W. Zhou, L Kevan, Chem. Mater. 11 (1999) 1621.

Chapter 5

ACYLATION AND ALKYLATION

The present chapter contains 2 sections. Part 1 discusses the study of acylation of anisole over modified SBA-15 and MCM-41 catalysts, while part 2 discusses the vapor phase isopropylation of m-cresol over modified MCM-41 and SBA-15 catalysts.

5.1 PART 1 FRIEDEL-CRAFTS ACYLATION OF ANISOLE

5.1.1 INTRODUCTION

Aromatic ketones used as intermediates in manufacturing fine and speciality chemicals, and pharmaceuticals are generally synthesized by two routes, namely, Friedel-Crafts aromatic acylation and the related Fries rearrangement [1]. The Friedel-Crafts reaction occurs by interaction of the aromatic compound with a carboxylic acid derivative (e.g. acid anhydride, acyl chloride or the acid itself) in the presence of an acid catalyst and involves acylium ion intermediates that are generated from the acylating agent by interaction with the acid catalyst. The present industrial practice involves the use of stoichiometric amounts of metal halides (soluble Lewis acids e.g. $AlCl_3$, $FeCl_3$) or strong mineral acids (HF, H_2SO_4) as catalysts and acyl chlorides as the acylation agents, which results in the formation of substantial amounts of by-products. Therefore, in view of increasingly strict environmental legislation, the use of heterogeneous catalysts becomes very attractive especially due to ease of separation of the catalyst, its reusability and environmental benefits. The acylation of anisole with acetic anhydride, reportedly using a zeolite catalyst, has been commercialized by Rhodia [2]. Friedel-Crafts chemistry using solid-acid catalysts such as zeolites, clays, Nafion-H, and heteropolyacids (HPA) has been investigated by many authors [3-6]. Heteropolyacids are promising solid-acid catalysts for Friedel-Crafts reactions [7-10]. These acids are stronger than many conventional solid acids such as mixed–oxides and zeolites. The Keggin-type HPAs are typically represented by the formula H_{8-x} $[XM_{12}O_{40}]$, where X is the heteroatom (most frequently P^{5+} or Si^{4+}), x is its oxidation state and M is the addenda atom (usually W^{6+} or Mo^{6+}). The strong Brönsted sites on HPA are able to generate acylium ions, which are the active intermediates in the acylation of aromatic substrates through an electrophilic attack at the π-electron system of the substrate. A Wheland type transition state has been suggested as the intermediate in the formation of aromatic ketones [11, 12].

Incorporation of heteropolyacids (HPA) into porous materials to obtain shape-selective catalysts has long been a challenge. However, conventional zeolites are not suitable for this because their pores are too small to adsorb the large (12 Å) HPA molecules. $H_3[PW_{12}O_{40}]$ (PW) encapsulated into a mesoporous pure silica molecular sieve (MCM-41) [13] has been studied in various catalytic reactions [14, 15]. Similarly, PW/SBA-15 catalysts have been reported to possess larger selectivity and stability in the alkylation of benzene with 1-dodecene compared to HY zeolite [16].

The acylation of anisole with acetic anhydride over PW/SBA-15 catalysts with different PW loadings is reported in the present work. The influence of reaction parameters such as temperature (333-373 K), molar ratio of the reactants, catalyst amount and different PW loadings are investigated. A comparison of the activities of Al-MCM-41, Al-SBA-15 and PW/SBA-15 catalysts for the acylation of anisole (at 373 K) is made.

5.1.2 EXPERIMENTAL

(a) Reaction procedure

The acylation reaction was carried out in the liquid phase in a 50 ml glass reactor equipped with a condenser and a magnetic stirrer. The reactions were carried out in the temperature range of 333-373 K and anisole to acetic anhydride molar ratio of 10. The amount of anisole used in the reactions was 0.1 mole. No solvent was used. The pre-activated catalyst was added to the reactor in an appropriate amount. In order to monitor the reaction, 0.1 ml of the reaction mixture was taken out periodically, diluted to 1 ml with 1,2-dichloromethane and analyzed by GC (Varian Star 3400 CX Gas Chromatograph; column- CP Sil 5 CB, 30 m, id = 0.5 mm). The product identification was done by GC-IR and GC-MS.

5.1.3 RESULTS AND DISCUSSION

(A) Acylation of anisole over PW/SBA-15 catalysts

The performance of PW/SBA-15 catalysts with different PW loadings was investigated in the temperature range of 333-373 K and anisole to acetic anhydride molar ratios (AN/AA) of 10. *para*- Methoxyacetophenone (*p*-MAP) was the dominant product while *ortho*- methoxyacetophenone (*o*-MAP) was formed in smaller amounts. The selectivity for mono-acylation was almost 100 % over all the catalysts, no other aromatic products being detected in the product. Conversion is expressed as the

percentage of acetic anhydride (the limiting reagent) converted into the product. Reaction scheme is as shown in Figure 5.1.

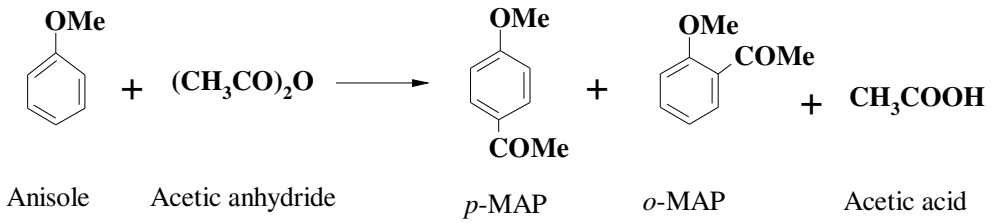

Figure 5.1 Reaction Scheme: Acylation of anisole with acetic anhydride.

(i) Influence of temperature

The influence of temperature on the conversion of acetic anhydride, and *o*-MAP and *p*-MAP yields studied in the temperature range of 333 to 373 K for 2 h over 10, 20, 30 and 40 wt. % PW/SBA-15 catalysts is presented in Figure 5.2. It is found that as the temperature increases from 333 to 373 K, the conversion and the yield of *p*-MAP increase with increase in PW content, while the yield for *o*-MAP decreases. Over 10 wt. % PW/SBA-15 the conversion was 76 % at 333 K, which increased to 94 % at 373 K. At higher loadings of 20, 30 and 40 wt. % PW, the conversion is very high and is 80 % to 100 % in the temperature range of 333 to 373 K as shown in Figure 5.2. *p*-MAP yield increases with PW content of the catalyst.

(ii) Effect of catalyst amount

The effect of catalyst amount (0.05 g, 0.1 g and 0.15 g) was investigated at an anisole to acetic anhydride mole ratio of 10:1 at a temperature 333 K over a 10 wt. % PW/SBA-15 catalyst (Table 5.1). As expected, conversion increases with catalyst amount (Table 5.1). Conversion was less than 67 % for 0.05 g catalyst charge while it is more than 80 % for 0.1 and 0.15 g catalyst amount at a TOS of 2 h. Selectivity is almost more than 95 % under all the conditions.

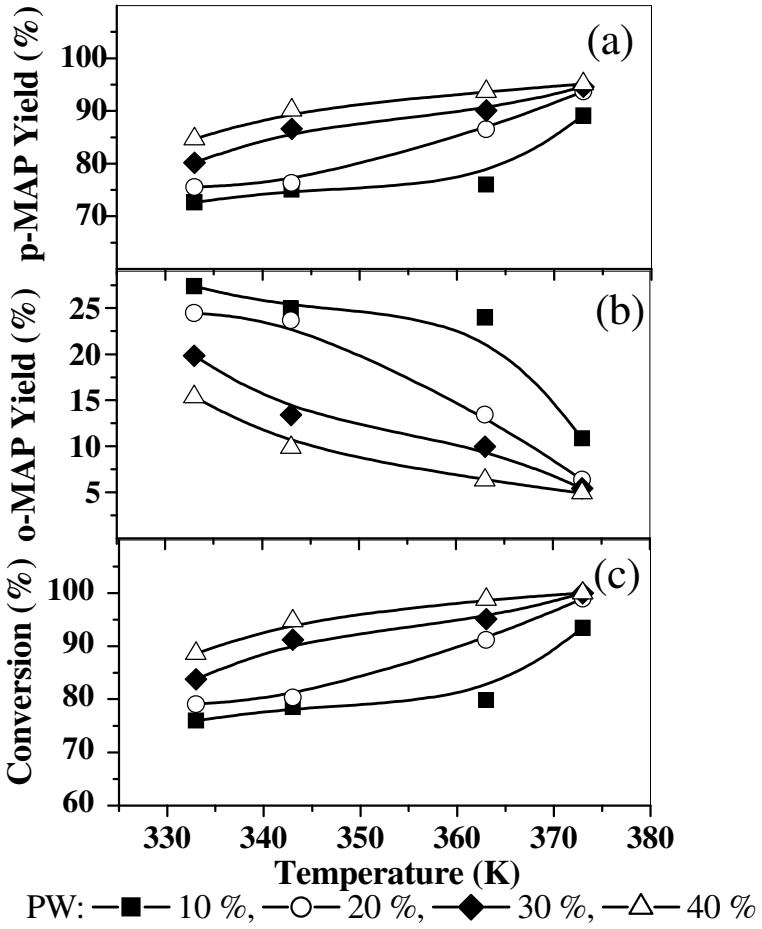

Figure 5.2 Influence of temperature on (a) conversion and yield of (b) *o*-MAP and (c) *p*-MAP at different PW loadings. Reaction conditions: AN/AA=10:1 mole ratio, catalyst = 0. 1 g, TOS=2 h.

Table 5.1 Effect of mole ratio and catalyst amount on conversion and selectivity

Catalyst	AN:AA Mole ratio	Catalyst wt. (g)	Conversion (%)	*p*-MAP selectivity (%)
10 wt. % PW/SBA-15	5:1	0.1	67.3	95.5
	10:1	0.1	83.0	95.6
	20:1	0.1	88.2	95.5
	30:1	0.1	92.1	95.4
10 wt. % PW/SBA-15	10:1	0.05	59.8	96.8
	10:1	0.1	83.0	95.6
	10:1	0.15	93.2	95.6

Reaction conditions: T = 333 K, TOS = 2 h

(iii) Effect of mole ratio

The effect of mole ratio was studied at anisole to acetic anhydride ratio of 5:1, 10:1, 20:1 and 30:1 at a temperature of 333 K over 10 wt. % PW/SBA-15 catalyst and the results are presented in Table 5.1. Both conversion and yield of p-MAP are found to increase with increase in molar ratio. Selectivity is almost 95 % at all molar ratios; it is initially even higher and then reaches a constant value after 1 h. Both the initial reaction rate and *p*-MAP yield at quasi-stationary state increase, in this case, for higher values of the AN/AA molar ratio. It is likely that acetic anhydride is more strongly adsorbed than anisole and that *p*-MAP is more strongly adsorbed than acetic anhydride. Therefore, a more favorable ratio of the reactants is achieved when the anisole to acetic anhydride molar ratio is increased and thus also a higher initial reaction rate. Excess anisole acts as solvent for *p*-MAP, which is more strongly adsorbed than acetic anhydride, product inhibition is reduced, and the product yield is therefore higher [17].

(iv) Influence of duration of run

The effect of run duration (up to 3 h) on conversion and on *o*-MAP and *p*-MAP yields over catalysts with different PW loadings at 373 K is shown in Figure 5.3. In general, the conversion and *p*-MAP formation increase with run duration while the *o*-MAP decreases. The activity increases with increasing PW content; the sample with 40 wt.% PW loading shows a high conversion of almost 100 % and a *p*-MAP yield of about 95 %. The slowing down of the reaction after 1 h is due to the kinetic effect of a pseudo first order reaction due to depletion of the reactant.

The acylation of anisole over the PW/SBA-15 catalysts appears to be a truly heterogeneously catalyzed reaction as the reaction stops when the catalyst (10 wt. % PW/SBA-15) is filtered off under hot conditions at the reaction temperature at 333 K after 30 min of reaction (Figure 5.4).

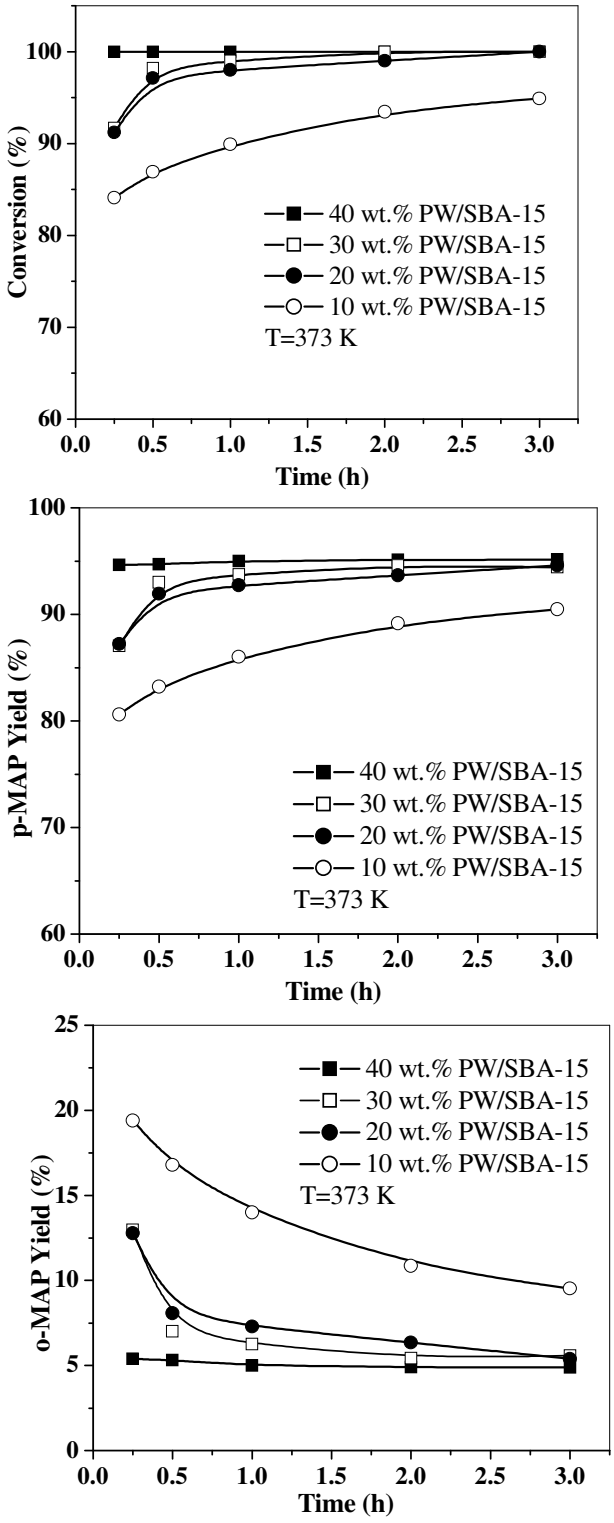

Figure 5.3 Effect of run duration on conversion, yield of *p*-MAP and *o*-MAP on different PW loaded SBA-15 catalysts at 373 K.

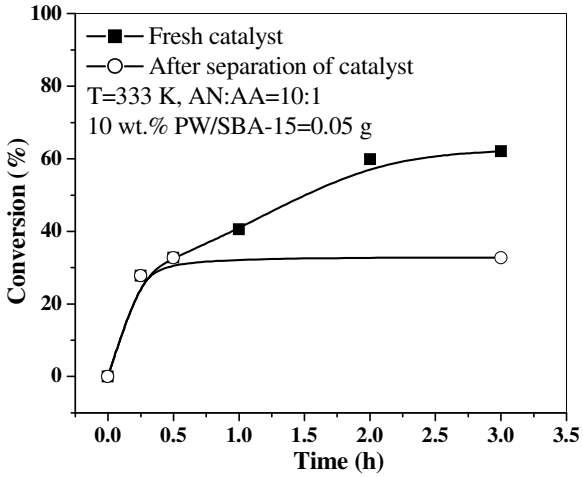

Figure 5.4 Test for heterogeneity of reaction (catalyst: 10 wt. % PW/SBA-15).

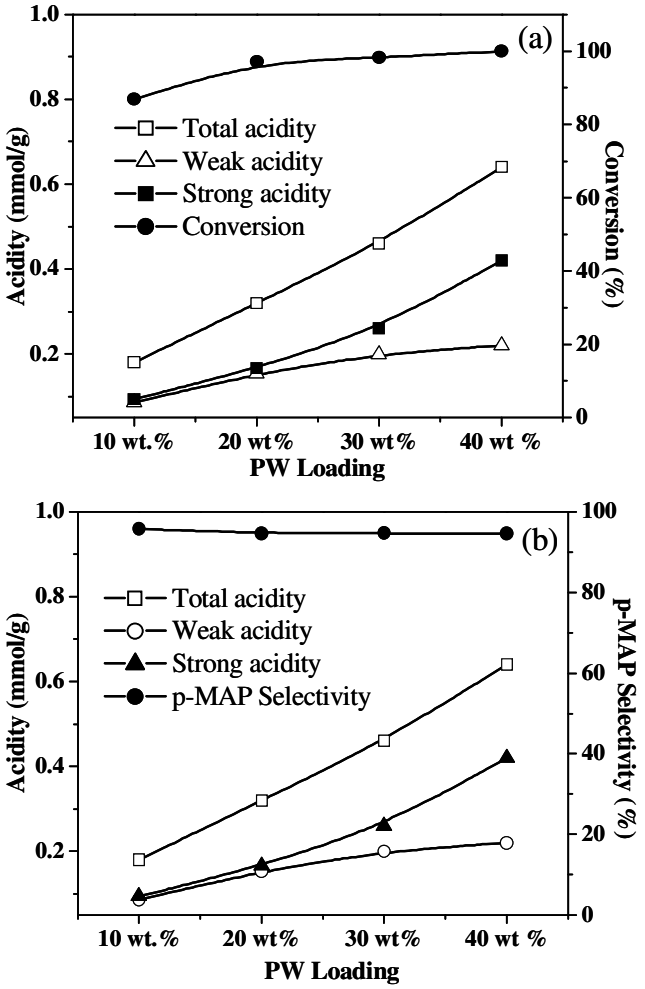

Figure 5.5 Influence of PW content and catalyst acidity on (a) conversion, (b) selectivity of *p*-methoxyacetophenone (*p*-MAP). Reaction conditions: T=373 K, AN: AA=10:1 mole ratio, Time = 0.5 h (30 min), catalyst amount = 0.1 g.

(v) Effect of PW loading

Influence of PW content and acidity on conversion and *p*-MAP selectivity is presented in Figure 5.5. Conversion increase with increase in acidity, an increase in PW content increases the total acid sites. Maximum conversion of 100 % is obtained over 40 wt. % PW/SBA-15 catalyst. The selectivity of *p*-MAP is more than 95 % over all catalysts.

(B) Acylation of anisole over Al-MCM-41 and Al-SBA-15 catalysts

The acylation of anisole with acetic anhydride was also investigated over the above catalysts. The results are being compared with data obtained over PW/SBA-15 catalysts at 373 K.

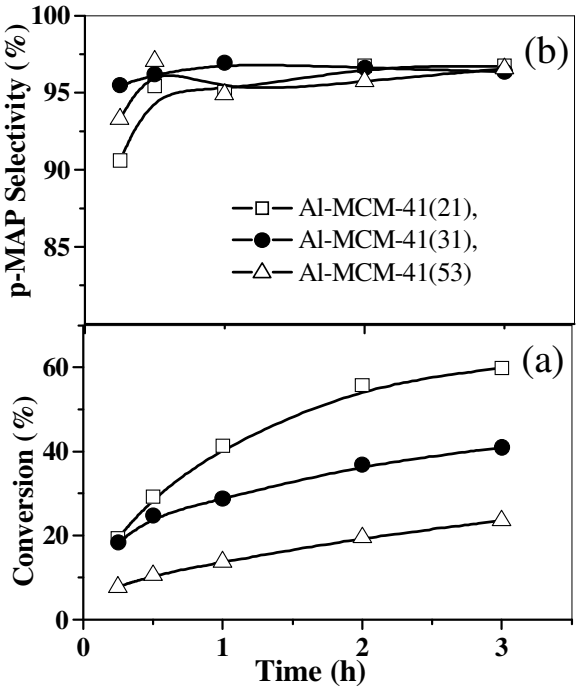

Figure 5.6 Influence of run duration on (a) conversion and (b) *p*-MAP selectivity over MCM-41 catalysts with different Si/Al ratios. Reaction conditions: T=373 K, AN: AA=10:1 mole ratio, catalyst amount: 0.1 g.

(i) Al-MCM-41

The effect of run duration (up to 3 h) on conversion and selectivity for *p*-MAP over Al-MCM-41 with different Si/Al ratios at 373 K is shown in Figure 5.6. As already noted, in general, conversion and *p*-MAP formation increase with run duration, while *o*-MAP decreases. The conversion for the sample with the Si/Al ratio

21 increases from 19.4 % to 59.9 % while for Si/Al ratio 31 and 53, the conversion increases from 18.3 to 40.9 % and 7.8 to 23.6 %, respectively between 15 min to 3 h reaction time at a temperature of 373 K. Selectivity for *p*-MAP is more than 96 % over all the catalysts with Si/Al ratios of 21, 31 and 53. Influence of Al content and catalyst acidity on conversion and selectivity for *p*-MAP is presented in Figure 5.7. It shows that conversion increases with acidity; an increase in Al content increases the total acid sites. The *p*-MAP selectivity is more than 96.5 % for all Si/Al ratios.

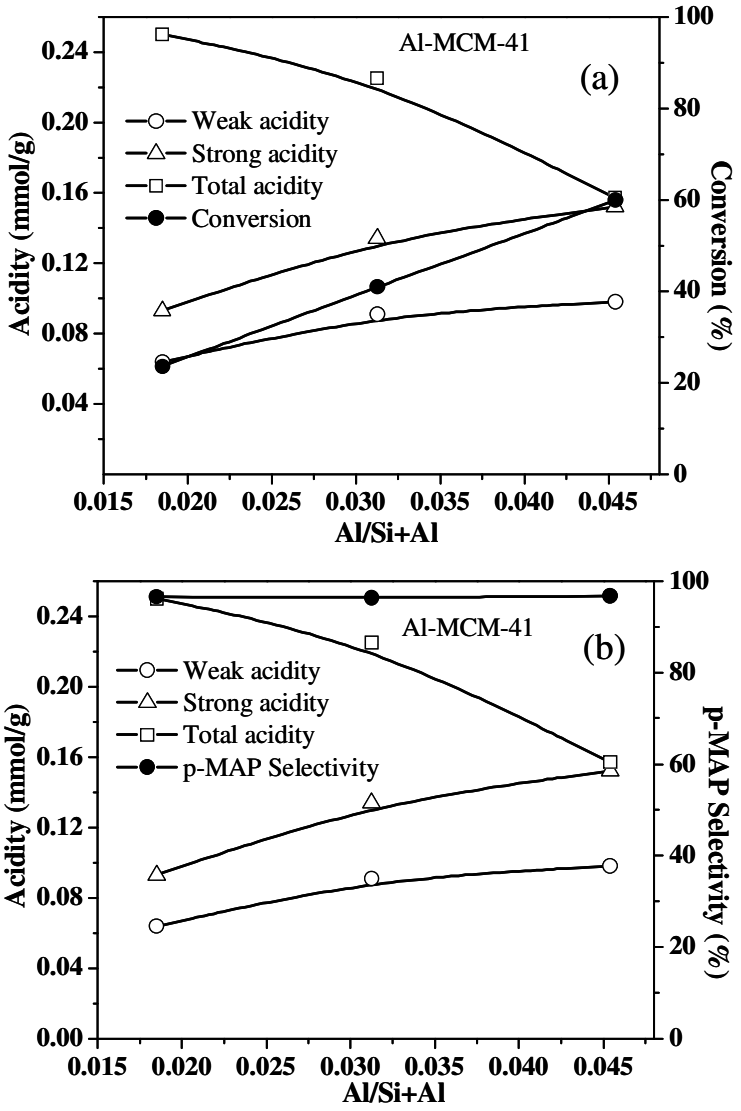

Figure 5.7 Influence of Al content and catalyst acidity on (a) conversion and (b) selectivity of p-MAP. Reaction conditions: T=373 K, AN: AA=10:1 mole ratio, catalyst amount: 0.1 g, Time =3 h.

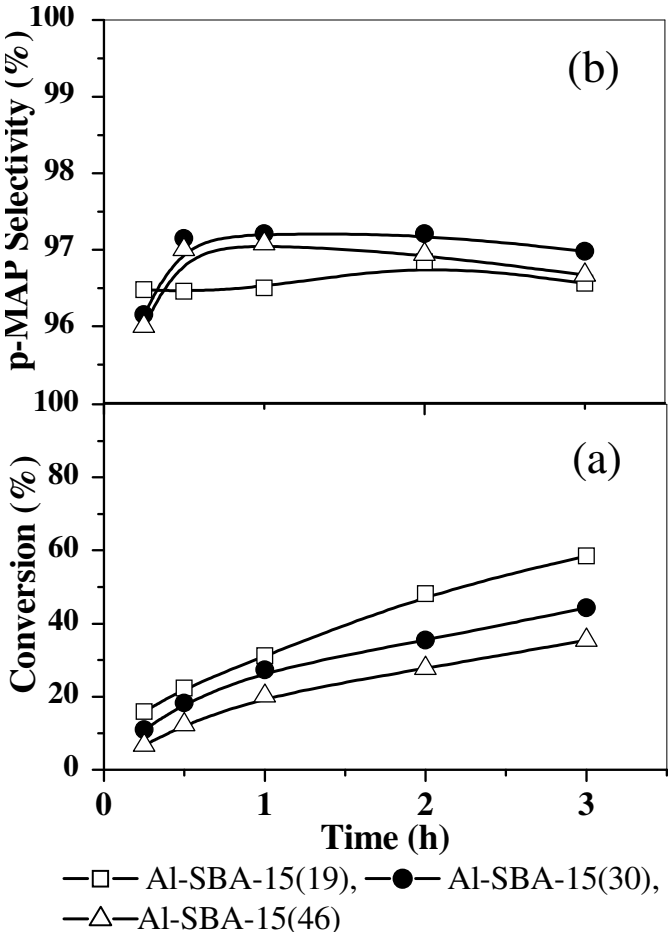

Figure 5.8 Influence of run duration on (a) conversion and (b) *p*-MAP selectivity over SBA-15 catalysts with different Si/Al ratios. Reaction conditions: T=373 K, AN: AA=10:1 mole ratio, catalyst amount: 0.1 g.

(ii) Al-SBA-15

The effect of run duration (up to 3 h) on conversion and selectivity for *p*-MAP over the catalysts with different Si/Al ratios at 373 K is shown in Figure 5.8. In general, the conversion and *p*-MAP formation increase with run duration, while *o*-MAP decreases. The conversion for the sample with the Si/Al ratio 19 increases from 16 % to 59 % while for Si/Al ratio 30 and 46 conversions increase from 11 to 44 % and 7 to 35 %, respectively, at 3h reaction time at 373 K. Selectivity for *p*-MAP is more than 96 % over all the catalysts with Si/Al ratios of 19, 30 and 46.

Influence of Al content and catalyst acidity on conversion and selectivity for *p*-MAP is presented in Figure 5.9. It shows that conversion increases as the acidity increases.

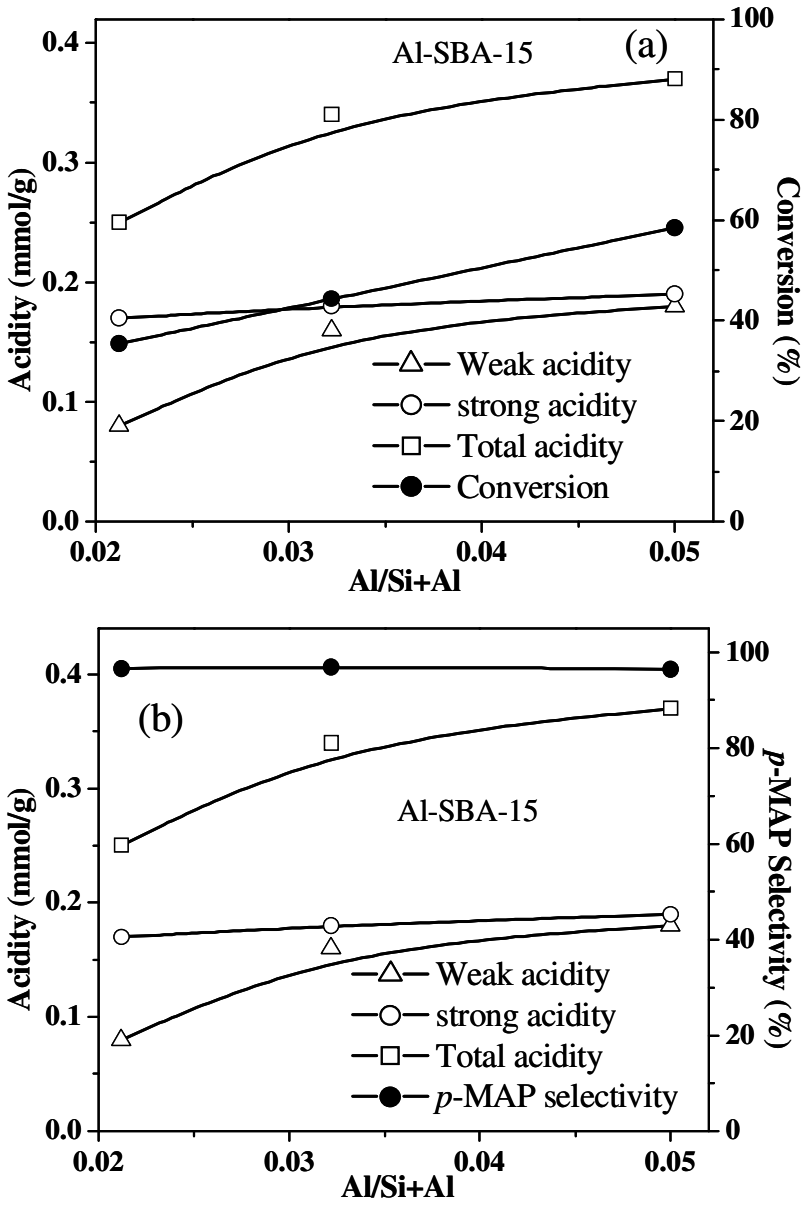

Figure 5.9 Influence of Al content and catalyst acidity on (a) conversion and (b) selectivity of *p*-MAP. Reaction conditions: T = 373 K, AN: AA=10:1 mole ratio, catalyst amount: 0.1 g, Time =3 h.

Table 5.2 Comparison of activity of SBA-15 and MCM-41 catalysts for acylation of anisole with acetic anhydride

Catalyst	Conversion (%)	*p*-MAP Selectivity (%)	*p*-MAP Yield (%)
10 wt.% PW/SBA-15	93.4	95.4	89.1
20 wt.% PW/SBA-15	99.0	94.6	93.7
30 wt.% PW/SBA-15	100	94.6	94.6
40 wt.% PW/SBA-15	100	95.1	95.1
Al-MCM-41 (21)	55.7	96.7	53.9
Al-MCM-41 (31)	36.9	96.6	35.6
Al-MCM-41 (53)	19.5	95.7	18.7
Al-SBA-15 (19)	48.2	96.8	46.7
Al-SBA-15 (30)	35.5	97.2	34.5
Al-SBA-15 (46)	27.8	96.9	26.9

Reaction Conditions: AN: AA=10:1 mole ratio, T=373 K, Catalyst amount = 0.1 g, Time = 2 h, (AN- anisole, AA-acetic anhydride, *p*-MAP- para-methoxyacetophenone).

(C) Comparison of activity of modified MCM-41 and SBA-15 catalysts

Table 5.2 presents the comparison data for the activity of MCM-41 and SBA-15 catalysts at 2 h at 373 K. The activity of the catalysts for conversion and selectivity are: in the order Al-SBA-15 < Al-MCM-41 < PW/SBA-15. Al-MCM-41 catalysts possess less acidity than Al-SBA-15, but are more active for acylation. The reason may be that the Al-ions are better dispersed inside the pores of Al-MCM-41 and much of the Al-ions contribute to more active Brönsted acidity. In the case of Al-SBA-15 catalysts, the Al-ions are deposited on the surface (pore walls) and some of it may remain as bulk Al_2O_3 possessing less active Lewis acid sites.

5.1.4 CONCLUSIONS

The Friedel-Crafts acylation of anisole with acetic anhydride catalyzed by heteropolyacids shows that both catalyst acidity and substrate conversion increase with the PW content over SBA-15. There is a close relationship between acidity and conversion, which suggests that the reaction occurs inside the pores of SBA-15. Both conversion and p-MAP formation increase with run duration while the *o*-MAP decreases. The temperature effects on conversion and selectivity show that conversion is 100 % and *p*-MAP yields are more than 95 % at 373 K for high PW contents

A comparison of the activity of MCM-41 and SBA-15 catalysts at 373 K shows that the activity of the catalysts for conversion and selectivity are in the order: Al-SBA-15 < Al-MCM-41 < PW/SBA-15. Al-MCM-41 catalysts possess less acidity than Al-SBA-15 but exhibit higher activity for acylation.

5.2 PART 2 ALKYLATION OF M-CRESOL

5.2.1 INTRODUCTION

Alkylation of phenol is an industrially important reaction as many alkyl phenols are used in the manufacture of surfactants, pharmaceuticals, dye stuffs, pesticides, paints and plastics [18]. Among the several isopropylation products of methyl phenols, the m-cresol derived 2-isopropyl-5-methylphenol (thymol) is the most important because it is a precursor of menthol [19]. Natural thymol is extracted from the oil of thyme and mint. It has antiseptic properties and antimicrobial activity [20]. It is also an important intermediate used in perfumery. Hydrogenation of thymol leads to menthol, a component of fragrances with a peppermint odour.

There are several methods available for the preparation of thymol. Liquid phase alkylation of m-cresol with propylene over an acidic catalyst [21] and the gas phase alkylation with propylene in the presence of supported metal sulphates [22], wide pore and medium pore zeolites [23] and γ-alumina [24-25] have been reported. In an industrial process employed by Bayer AG, thymol is obtained by liquid phase isopropylation of m-cresol in the presence of activated alumina at 633 K and 50 bar pressure [26]. m-Cresol isopropylation has been reported over Mg-Al hydrotalcite [27] with nearly 80 % selectivity towards thymol at 40 % m-cresol conversion. The gas phase isopropylation of m-cresol has been reported over an oxide catalyst containing Fe, Si, Cr and K, at atmospheric pressure [28]. Gas phase reaction using zinc aluminate spinel ($ZnAl_2O_4$) has been reported with m-cresol conversion of 78.2 % and thymol selectivity of 88.4 % [29]. Maheshwari et al. have reported that in vapor phase alkylation of m-cresol with isopropanol over Al-MCM-41 catalysts with different n_{Si}/n_{Al} ratios, the activity of the Al-MCM-41 [30] depends on its acidity which increases with decreasing n_{Si}/n_{Al} ratio and a high temperature (573 K) was required to get a high m-cresol conversion. The authors also reported that consecutive alkylations and deactivation of the catalyst by coke deposition did not occur due to the scattered Brönsted acid sites and large pore diameters with less diffusional constraints in Al-MCM-41 catalysts. The reaction of m-cresol with isopropyl acetate over Al-MCM-41 and Al, Zn-MCM-41 has revealed that the reaction depends on the acid sites (moderate, strong and weak) of the catalysts and their hydrophilic and hydrophobic properties. It was found that Al, Zn-MCM-41 was less active than Al-MCM-41due to its greater hydrophilicity [31]. Vinu et al. have reported that isopropylation occurs

over Al-SBA-15 catalysts at 73.5 % m-cresol conversion and 45.7 % thymol selectivity [32].

In the present work, the vapor phase alkylation of m-cresol with isopropanol over Al-MCM-41, Al-SBA-15 and PW/SBA-15 catalysts is being investigated. The influence of reaction parameters such as temperature (498-623 K), WHSV, mole ratio of the reactants and time on stream was studied over MCM-41 and SBA-15 based catalysts.

5.2.2 EXPERIMENTAL

(a) Reaction procedure

The catalytic experiments were carried out in a vertical down flow glass reactor (i.d. = 15 mm and 35 cm length) at atmospheric pressure using 1.5 g of the catalyst. The catalyst was pelletized and then sieved to 16-20 mesh size prior to use. The reactor was placed inside a temperature controlled vertical furnace. The thermocouple tip was centered at the middle of the catalyst bed. A mixture of m-cresol (Aldrich) and isopropanol (AR grade, E-Merck, India) was fed using a syringe pump (SAGE instrument). The WHSV values were calculated based on the total feed injected. The catalyst was calcined at 823 K for 6 h before start of run. The reaction products were analyzed using a GC (Chrompack CP 9001, column OV-101, 50 m, id = 0.2 mm). Identification of the products was done by GC-MS and GC-IR.

5.2.3 RESULTS AND DISCUSSION

Isopropylation of m-cresol was investigated over Al-MCM-41, Al-SBA-15 and PW/SBA-15 catalysts. Both O- and C-alkylations occurred to give a mixture of products as shown in the reaction scheme (Figure 5.10). Among the products, thymol (A), isothymol (B), 2-isopropyl-3-methylphenol (C) and the dialkylated products, 2, 4-di-isopropyl-3-methylphenol (E) were the major products. Other products, such as 2, 6-di-isopropyl-3-methylphenol (D), isopropyl-2-isopropyl-5-methylphenylether (F) and isopropyl-3-methylphenylether (G) were also formed in minor amounts.

(A) Vapor phase isopropylation of m-cresol over Al-MCM-41

Isopropylation of m-cresol was studied over Al-MCM-41 with a Si/Al ratio of 21. The influence of different reaction parameters such as temperature, time on stream and space velocity (WHSV) was investigated over the catalyst

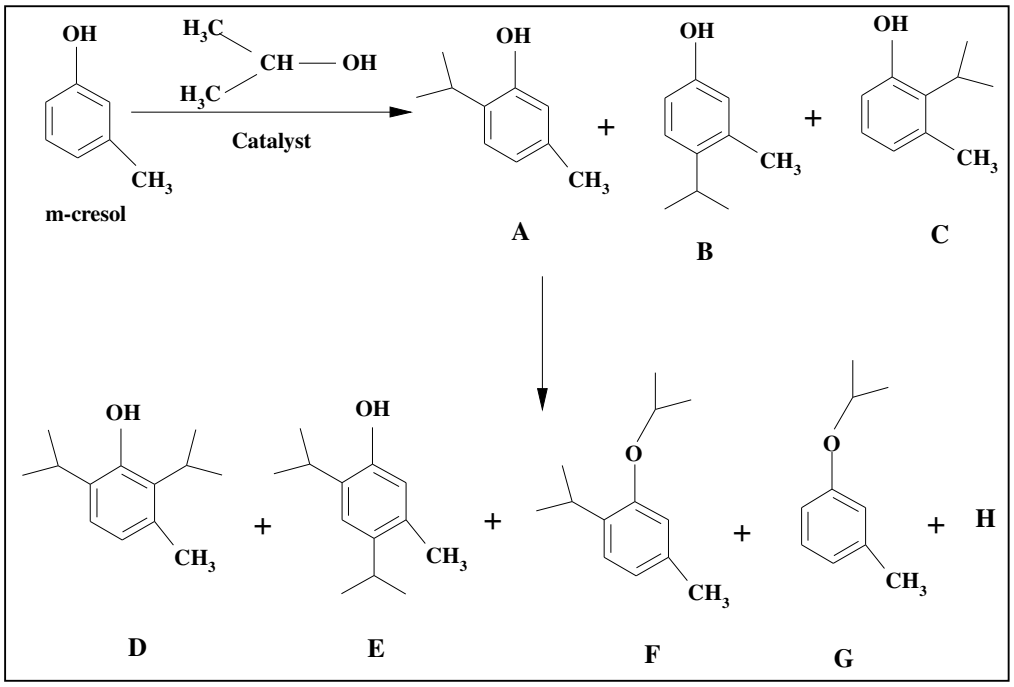

Figure 5.10 Reaction Scheme: Alkylation of m-cresol with isopropanol.

A- 2-isopropyl-5-methylphenol (Thymol)

B- 4-isopropyl- 3-methylphenol (Isothymol)

C- 2-isopropyl-3-methylphenol (2-I-3MP)

D- 2,6-di-isopropyl-5-methylphenol (2,6- DI-5MP)

E- 2,4-di-isopropyl-5-methylphenol (2,4-DI-5MP)

F- Isopropyl-2-isopropyl-5-methylphenylether (I-2I-5MPE)

G- Isopropyl-3-methylphenylether (I-3MPE)

H- Others (Low boilers and High boilers) not shown.

(i) Effect of temperature

The influence of reaction temperature on conversion and selectivity was studied at 498, 523, 548, 573 and 598 K using a constant molar feed ratio of m-cresol: isopropanol of 1:4 and WHSV of 1.76 h^{-1}.

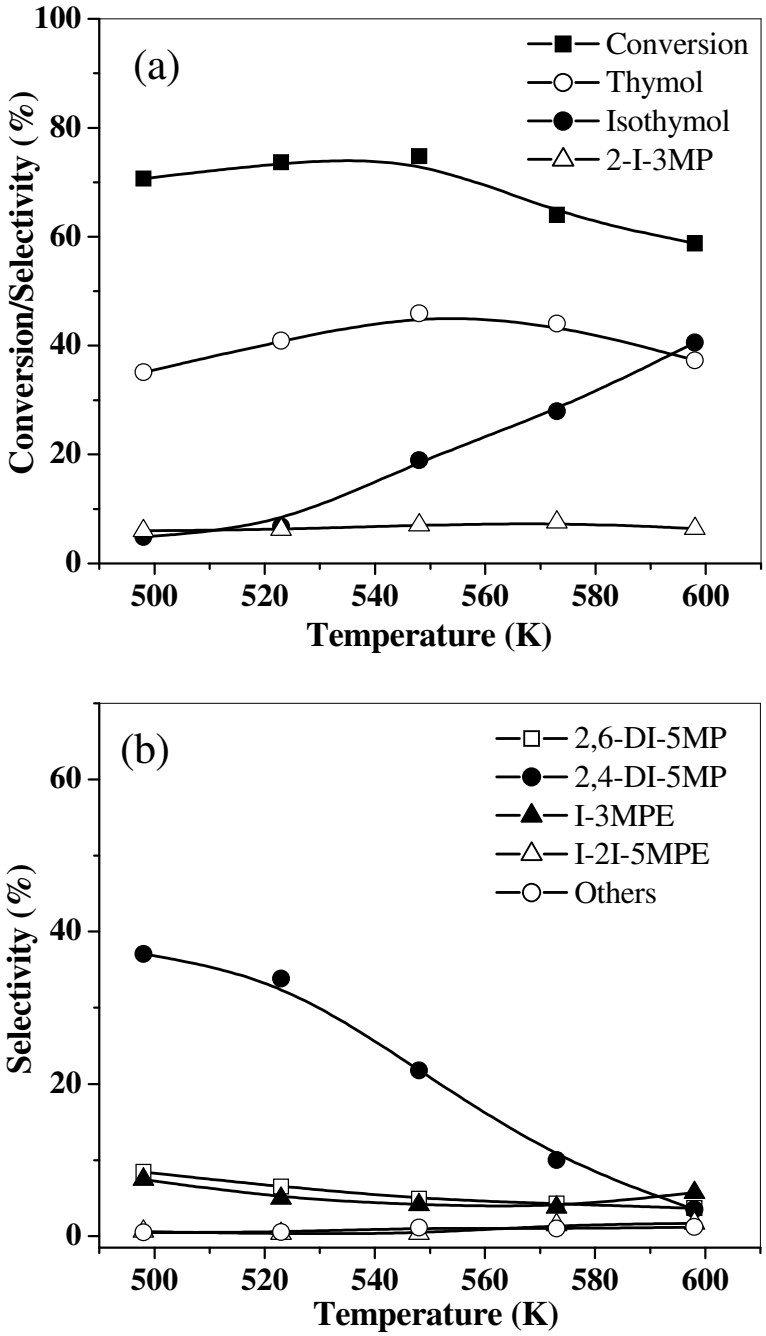

Figure 5.11 Influence of temperature on (a) m-cresol conversion and selectivity for thymol, isothymol and 2-isopropyl 3-methlylphenol, (b) selectivity for dialkylated products (see Figure 5.10 for product identification). Reaction conditions: Al-MCM-41 (21)-1.5 g, TOS = 4 h, m-cresol: IPA=1:4 molar ratio, WHSV=1.76 h^{-1}.

A slight increase in conversion is observed as the temperature is increased from 498 to 548 K (70.7 % to 74.7 %) [Figure 5.11 (a)]. Conversion however decreases significantly above 548 K. At 598 K, the conversion is found to be 58.8 % [Figure 5.11 (a)]. The decrease in m-cresol conversion at higher temperatures could be due to increased dealkylation (thermodynamic equilibrium being reached) at higher temperatures and due to deactivation of the acid sites by undesired products formed by the side reactions of isopropyl alcohol. In the present study the highest conversion was observed at 548 K. Thymol is formed more selectively than other products at all the temperatures studied. The high selectivity for thymol is probably due to chemisorption of m-cresol on the Brönsted acid sites through its OH group, favoring o-alkylation with isopropyl cation [31]. Besides the o-position is also the more reactive one (kinetically favoured) as the second and fourth carbons are sterically hindered by the methyl group, the isopropyl cation selectively attacks the sixth carbon to yield thymol.

It is also observed that at higher reaction temperatures, while the selectivity to thymol increases up to 548 K (from 35 to 46 %), the selectivity to 2, 4-DI-5MP decreases [Figure 5.11 (b)]. The high selectivity of thymol could be due to its lower kinetic diameter of this (para product) compared to other products. Song et al. [33] reported such a preferential formation of para isomers due to their difference in diffusion kinetics by computational modeling. Furthermore, the high selectivity of 2, 4-DI-5MP at lower reaction temperatures could be attributed to the greater thermodynamic stability of the di-isopropyl compound at lower reaction temperatures.

In the present study, isothymol, 2-I-3MP and 2, 4-DI-5MP is found to be the major byproducts. The selectivity for isothymol is low at low temperatures and increases at higher temperatures. Isothymol formation may be the result of a different configuration of the aromatic ring on the catalyst surface according to the mechanism proposed by Taylor and Ludlum [34]. Isothymol could also be formed via isomerization of thymol over strong acid sites. Thus, there are two routes by which isothymol could be formed in this reaction. Isomerization of thymol to isothymol is greater at lower temperature (~ 473 K) than at 673 K as reported by earlier workers [28]. But, in the present study, although isomerization of thymol can occur on the same acid sites that catalyze the formation of thymol, the selectivity to isothymol is low at low temperatures. This suggests that the sites are not acidic enough for

isomerization at low temperatures. The formation of the products such as I-3MPE and I-2I-5MPE occurs to a small extent.

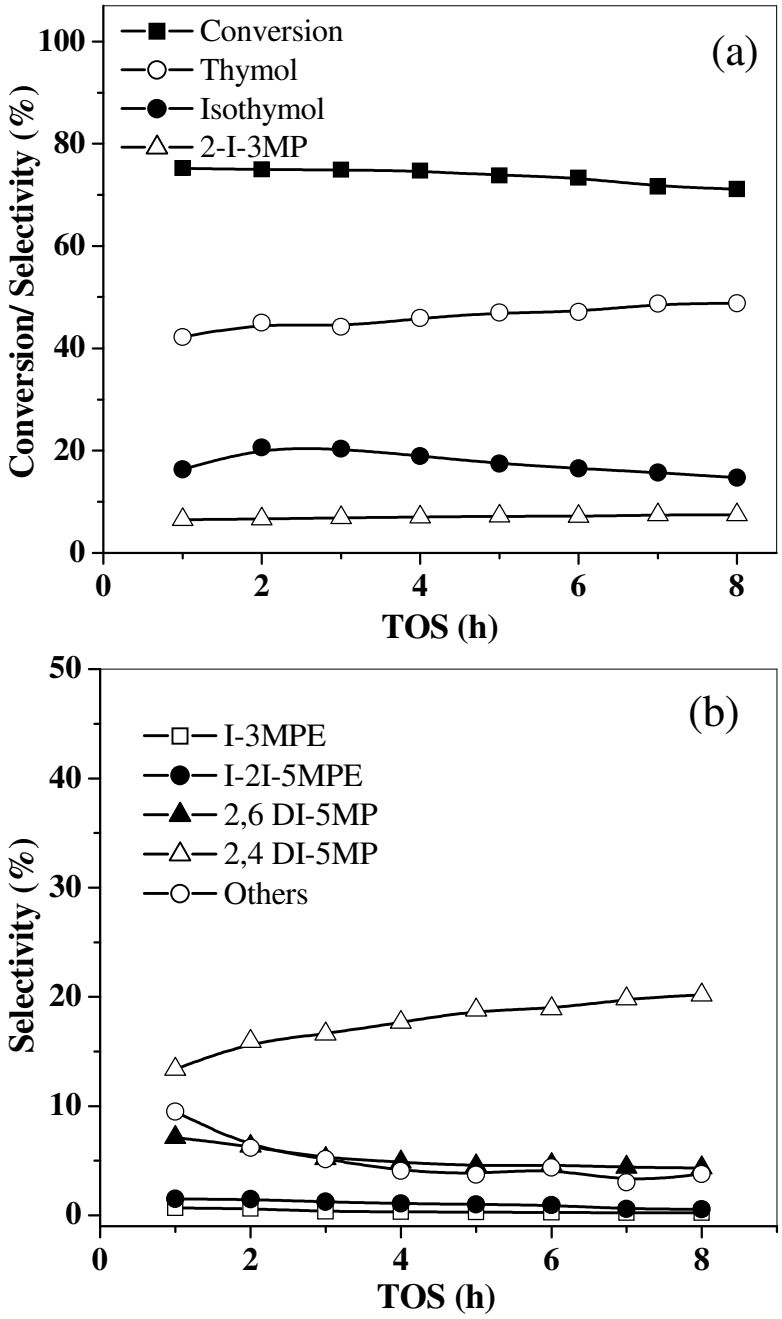

Figure 5.12 Effect of TOS on (a) m-cresol conversion and selectivity for thymol, isothymol and 2-isopropyl 3-methlylphenol, (b) selectivity for dialkylated products. Reaction conditions: Al-MCM-41 (21)-1.5 g, m-cresol: IPA=1:4 molar ratio, WHSV=1.76h^{-1}, T= 548 K.

(ii) Effect of TOS

The effect of TOS was studied over a period of 8 h (Figure 5.12) over Al-MCM-41 (21) at 548 K with a feed ratio 1:4 and at a WHSV of 1.76 h^{-1}. There is a slow decrease in m-cresol conversion as the TOS increases to 8 h (75.2 % to 71.1 %). The decrease in conversion is probably due to coke formation. The selectivity for thymol increases with increase in TOS while a reverse trend in the selectivity to isothymol is observed.

The selectivity for 2-I-3MP slightly increases with TOS (from 6.49 % to 7.42 %). Figure 5.12 (b) presents the selectivity for the dialkylated products. Selectivity for 2, 4 DI-5MP increases from 13.4 to 20.2 % with increase in TOS while selectivity for 2, 6 DI-5MP decreases from 7.1 to 4.3 %. The products, I-3MPE and I-2I-5MPE are formed in small amounts.

(iii) Effect of WHSV

The effect of WHSV on m-cresol conversion and products selectivity over Al-MCM-41 (21) at 548 K at a TOS of 4 h is shown in Figure 5.13. Conversion increases from 59.2 % to 74.7 % as WHSV increases from 1.45 to 1.76 h^{-1} but decreases on further WHSV increase to 2.0 (66.3 %).

There are two aspects that are interesting: 1) the increase in percentage conversion on increasing WHSV from 1.45 to 1.76 h^{-1} and 2) the decrease in conversion at 2.0 h^{-1}. The surprising observation is that the changes in conversion take place within a small change of 0.55 h^{-1}. Similar observations have been made by earlier workers also [31-32] who have given different explanations for the observations. Shanmugapriya et al. [31] believe that the decrease of conversion at higher WHSV is due slower diffusion of m-cresol and Vinu et al. suggest that it may be due to diffusional restrictions leading to dealkylation and rapid coke formation [32(b)] and lower m-cresol adsorption at higher flow rates [32(a)]. The absolute amounts of m-cresol converted at the three space velocities are 2.56, 3.91 and 3.94 mmol per hour over the catalyst. The fact that the amount of cresol converted at 1.76 and 2.0 h^{-1} are the same, the reaction is limited by either, i) desorption and diffusion of the products inside the pores or by, ii) the reaction at the surface, though it is not possible to identify the actual reason for the observed behavior with WHSV changes without further studies. The selectivity for thymol goes through a minimum at 1.76 h^{-1} (WHSV), while for isothymol it is maximum at this space velocity. The selectivities

for the di-isopropyl isomers increase with WHSV. This suggests that strong adsorption or slow diffusion of the product may be responsible for consecutive alkylations of the monoalkylated (primary) products.

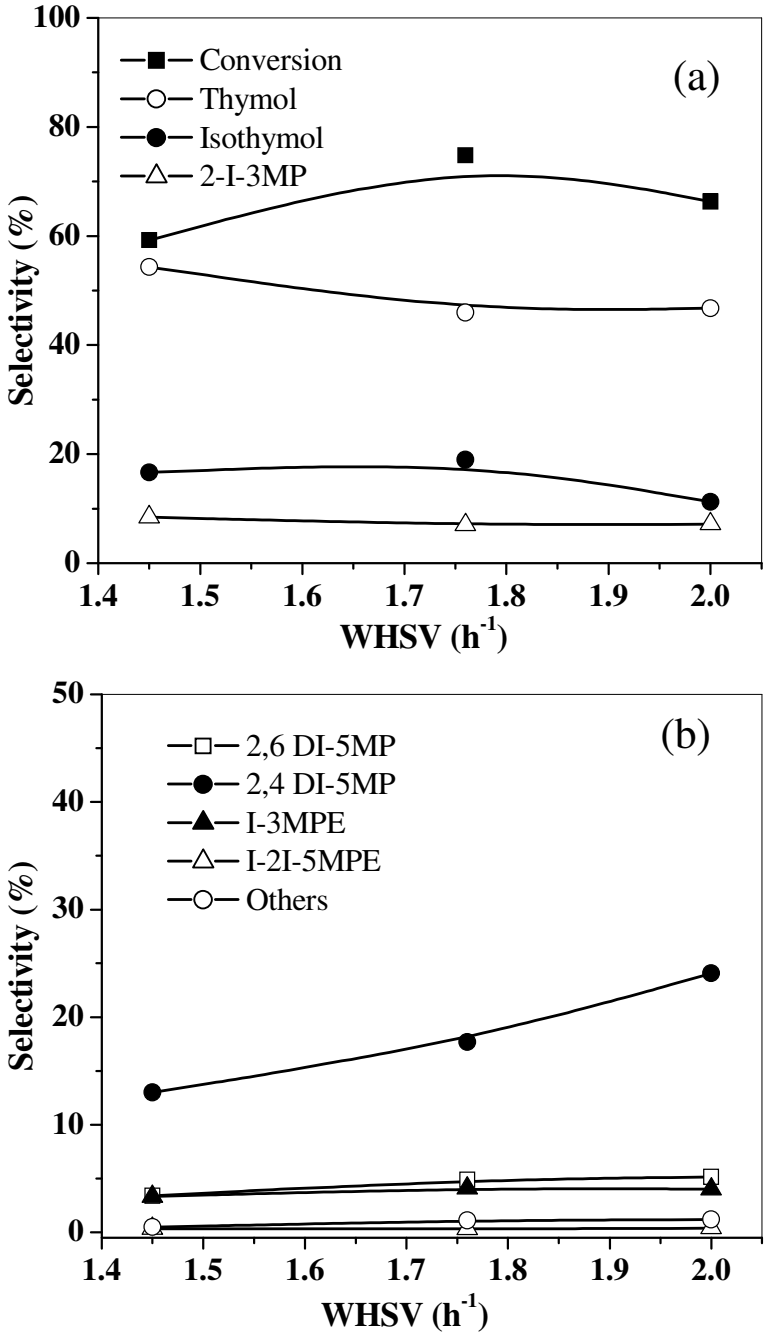

Figure 5.13 Effect of WHSV on (a) m-cresol conversion and selectivity for thymol, isothymol and 2-isopropyl 3-methlylphenol, (b) selectivity for dialkylated products. Reaction conditions: Al-MCM-41 (21)-1.5 g., TOS = 4 h, m-cresol: IPA=1:4 molar ratio, T= 548 K.

(B) Vapor phase isopropylation of m-cresol over Al-SBA-15

(i) Effect of temperature

The influence of reaction temperature on conversion and selectivity was studied at 498, 523, 548, 573 and 598 K using a feed molar ratio of m-cresol: isopropanol (1:4) and WHSV of 1.76 h^{-1} over Al-SBA-15 (19) and Al-SBA-15 (46) catalysts. A similar temperature effect was observed for both the Al-SBA-15 catalysts (Si/Al ratio 19 and 46) (Figure 5.14) as for Al-MCM-41 (21) (Figure 5.11). An increase in conversion was observed as the temperature was increased from 498 to 548 K.

However the conversion decreased significantly when the temperature was increased from 548 K to 598 K. As already explained in the case of Al-MCM-41, the decrease in m-cresol conversion at higher temperatures could be due to predominant dealkylation at higher temperatures and the blocking of acid sites by undesired products formed in larger amounts at higher temperatures. The selectivity for isothymol is low at lower temperatures and it increases at higher temperatures. Interestingly, the selectivity increase is less over Al-SBA-15 (46) than over Al-SBA-15 (19) suggesting the role of acidic sites (Al sites) in the reaction. The changes in the selectivity of all the other products over both the SBA-15 catalysts are similar to those observed over Al-MCM-41 (21).

(ii) Effect of TOS

The effect of TOS was studied for 8 h over Al-SBA-15 catalysts with Si/Al ratios of 20, 30 and 50 at 548 K using a feed ratio of 1:4 and at WHSV= 1.76 h^{-1}. The results of the studies are presented in Figure 5.15. In the case of Al-SBA-15 (19) and Al-SBA-15 (30) there is a small initial increase in conversion which peaks at about 6 h and decreases slightly at larger TOS. However, no such trend is seen in the case of Al-SBA-15 (46). The reason for the behaviour of the catalysts with larger Al contents is not yet clear though this could be an experimental artifact arising from preferential adsorption (and retention) of the heavier products (alkylates) by the catalyst bed during the early hours of the run due to greater acidity of the samples. The decrease in conversion beyond 6 h is probably due to slow deactivation due to coking or poisoning of the acid sites. The greater yield of 2, 4-DI-5MP and the decrease in yield of 2, 6-DI-5MP with duration of run suggests that the former isomer is more strongly adsorbed over the catalyst. The decrease in isothymol and 2, 6-DI-5MP yields with

time points to the slow deactivation of the catalysts. The selectivity for 2-I-3MP is constant with TOS (from 7 to 8 % for Si/Al -19, 5 to 7 % for Si/Al- 30 and 6 to 7 % for Si/Al -46). Much of the data reported in the rest of the sections have been collected at TOS beyond 4 h to avoid the above experimental effects.

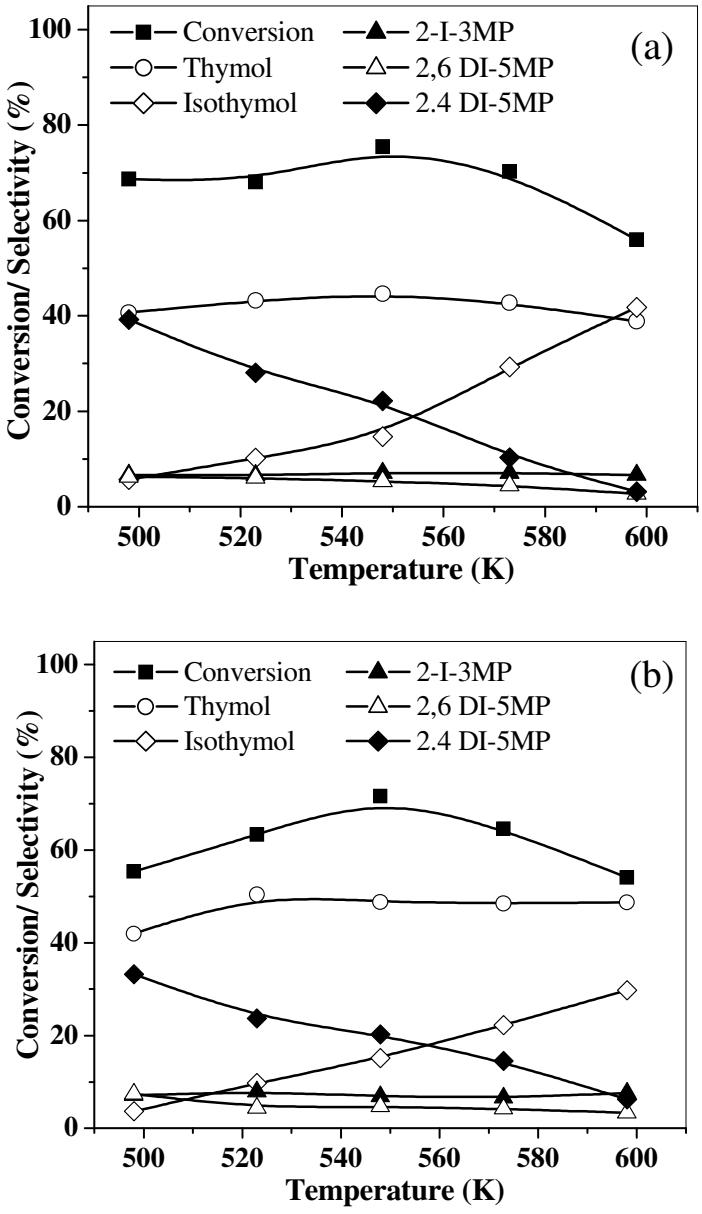

Figure 5.14 Influence of temperature on m-cresol conversion, selectivity for thymol, isothymol and dialkylated products over (a) Al-SBA-15 (19) and (b) Al-SBA-15 (46) Reaction conditions: Catalyst=1.5 g, TOS = 4 h, m-cresol: IPA=1:4 molar ratio, WHSV=1.76h^{-1}.

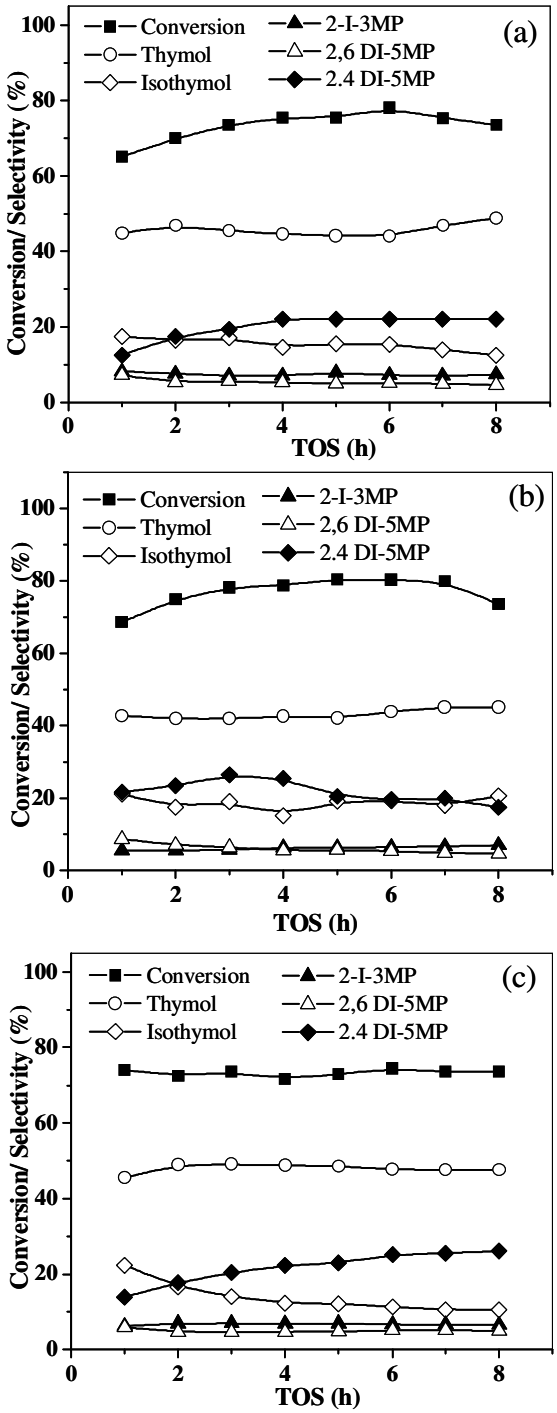

Figure 5.15 Effect of time on stream on m-cresol conversion, selectivity for thymol, isothymol and dialkylated products over (a) Al-SBA-15 (19), (b) Al-SBA-15 (30) and Al-SBA-15 (46). Reaction conditions: catalyst=1.5 g, TOS = 4 h, m-cresol: IPA=1:4 molar ratio, WHSV=1.76h^{-1}.

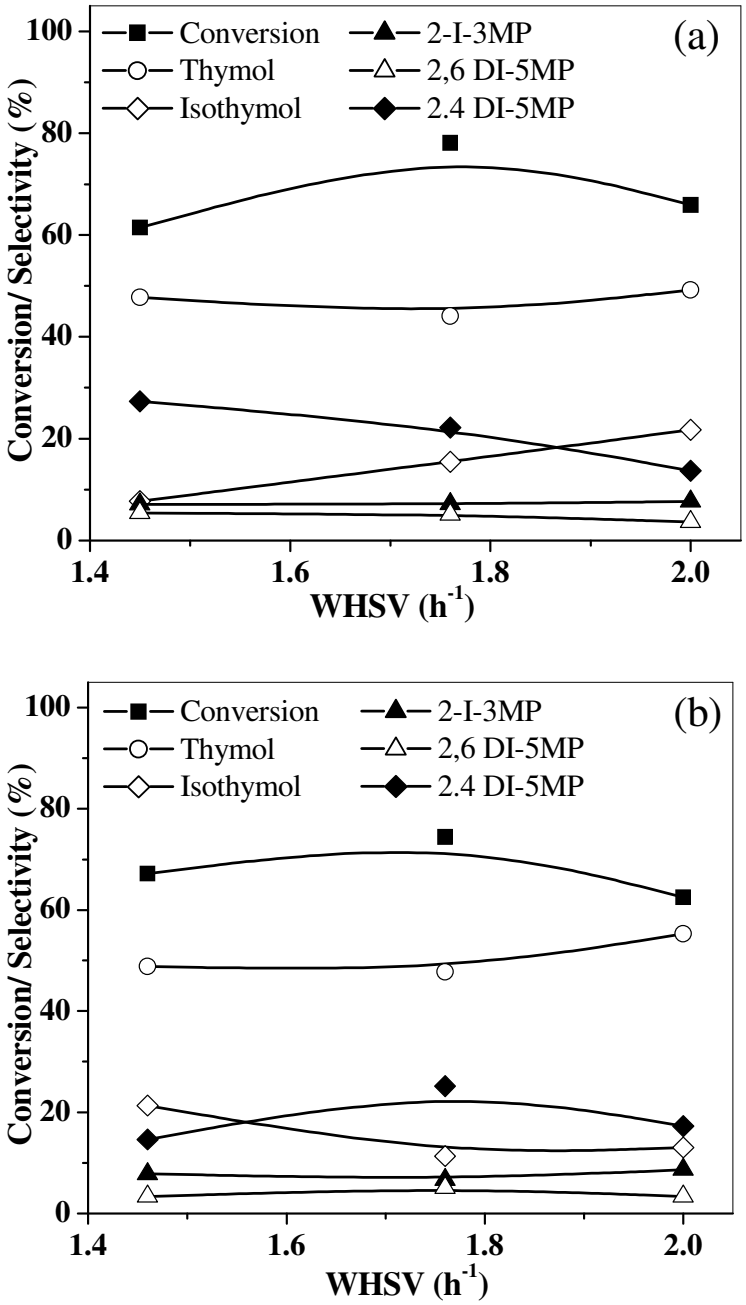

Figure 5.16 Effect of WHSV on m-cresol conversion, selectivity for thymol, isothymol and dialkylated products over (a) Al-SBA-15 (19) and (b) Al-SBA-15 (46). Reaction conditions: catalyst=1.5 g, TOS = 6 h, m-cresol: IPA=1:4 molar ratio, WHSV=1.76 h^{-1}.

(iii) Effect of WHSV

The effect of WHSV on m-cresol conversion and products selectivity over Al-SBA-15 (19) and Al-SBA-15 (46) at 548 K at TOS 4 h is shown in Figure 5.16. Conversion for Al-SBA-15 (19) increases from 61.5 % to 78.1 % as WHSV increases from 1.45 to 1.76 h^{-1}. But when the WHSV is increased to 2.0 then there is a decrease in m-cresol conversion (65.9 %). Similar results were observed for Al-SBA-15 (46) catalysts.

The absolute amounts of m-cresol converts over Al-SBA-15 (19) at the three WHSV are 2.66, 4.09 and 3.92 mmol/h (the values are similar to the ones observed in the case of Al-MCM-41). For Al-SBA-15 (46) the values are 2.85, 3.88 and 3.70 mmol/h**,** being nearly similar to the values for Al-MCM-41 (21) (2.56, 3.91 and 3.94 mmol/h) and Al-SBA-15 (19). Apparently, the amount of acidity (no. of active sites, Al ions) is not critical. It is likely that the diffusion effects are predominantly responsible for similar m-cresol conversion over both catalysts (Si/Al = 19 and 46). However if diffusion effects were the predominant reason, the activity should be more for SBA-15 catalysts as their pore diameters are larger (~100 Å) than those of MCM-41 catalysts (~30 Å). Probably, the intrinsic activities of the catalysts (active centers in the catalysts) also play a role, the MCM-41 catalysts being more active than the SBA-15 catalysts, being prepared by direct synthesis compared to the SBA-15 catalysts prepared by impregnation.

Table 5.3 Effect of feed ratio on isopropylation of m-cresol over Al-SBA-15 (19)

Catalyst	Mole ratio (m-cresol: IPA)	Conv. (%)	Product Selectivity (%)					
			A	B	C	D	E	Others
Al-SBA-15 (19)	1:2	29.3	63.5	17.9	7.8	1.5	6.1	3.2
	1:3	66.9	46.7	14.0	7.4	5.0	22.4	4.4
	1:4	75.4	44.7	14.7	7.1	5.3	22.2	6.1
	1:5	79.0	41.6	16.7	6.4	6.7	22.1	6.5

Reaction conditions: T = 548 K, TOS = 4 h, WHSV = 1.76 h^{-1}, catalyst amount = 1.5 g. others- (F + G + High Boilers). A, B, C, D, E, F and G (products as shown in Figure 5.10).

(iv)Effect of feed ratio

The effect of feed ratio on the reaction was studied over Al-SBA-15 (19) at 548 K at WHSV=1.76 h^{-1} with m-cresol to isopropanol mole ratio of 1:1, 1:2, 1:3 and 1:4. The results are presented in Table 5.3. As the isopropanol amount increases, m-cresol conversion increases while selectivity for thymol decreases. This is presumably due to the presence of larger amounts of adsorbed isopropanol on the surface of the catalyst. m-Cresol reacts with isopropyl cation by remaining in the vapor phase or in the chemisorbed state on the catalysts surface. Chemisorbed m-cresol can give mono- and di-ring alkylation but not O-alkylation it could be due to the reaction between thymol and isopropyl cation on the catalyst surface. The selectivity for isothymol increases as the feed ratio increase while the selectivity for 2-I-3MP decreases. There is not much change in the selectivity of the dialkylated product 2, 4 DI-5MP. It shows almost the same selectivity at all the feed ratios studied. A marginal increase in the selectivity is noticed for 2, 6 Di-5MP. The results show that the selectivity for higher alkylated products is independent of the dilution effect.

(C) Vapor phase isopropylation of m-cresol over PW/SBA-15

(i) Effect of TOS and PW content

Isopropylation of m-cresol was studied over PW/SBA-15 catalysts with different PW loadings of 10, 20 and 40 wt. % at 548 K with WHSV=1.76 $h^{-1}$and a TOS of 4 h. The m-cresol: isopropanol mole ratio was 1:4. The results of the TOS studies carried out on PW/SBA-15 catalysts are presented in Figure 5.17. It is observed that the conversion of m-cresol is initially high at the start of reaction and then decreases with TOS. For 10 wt. % catalyst, conversion is in the range of 76 to 59 %, for 20 wt. % it is 77 to 55 % and for 40 wt. % the initial conversion is 80 % and at TOS 8 h it decreases to 67 %. But the trend of thymol selectivity for all the catalysts is almost similar. For all the catalysts, the selectivity increases from about 36 to 48 % with increase in TOS. Isothymol selectivity decreases with increase of TOS from 1 to 8 h. The selectivity for 2-I-3MP is almost the same for all the catalysts and it increases with TOS. The selectivities for the dialkylated products (2, 4 DI-5MP and 2, 6 DI-5MP) decrease with TOS. m-Cresol conversion increases slightly as the PW content increases due to an increase (Figure 5.18) in acidity.

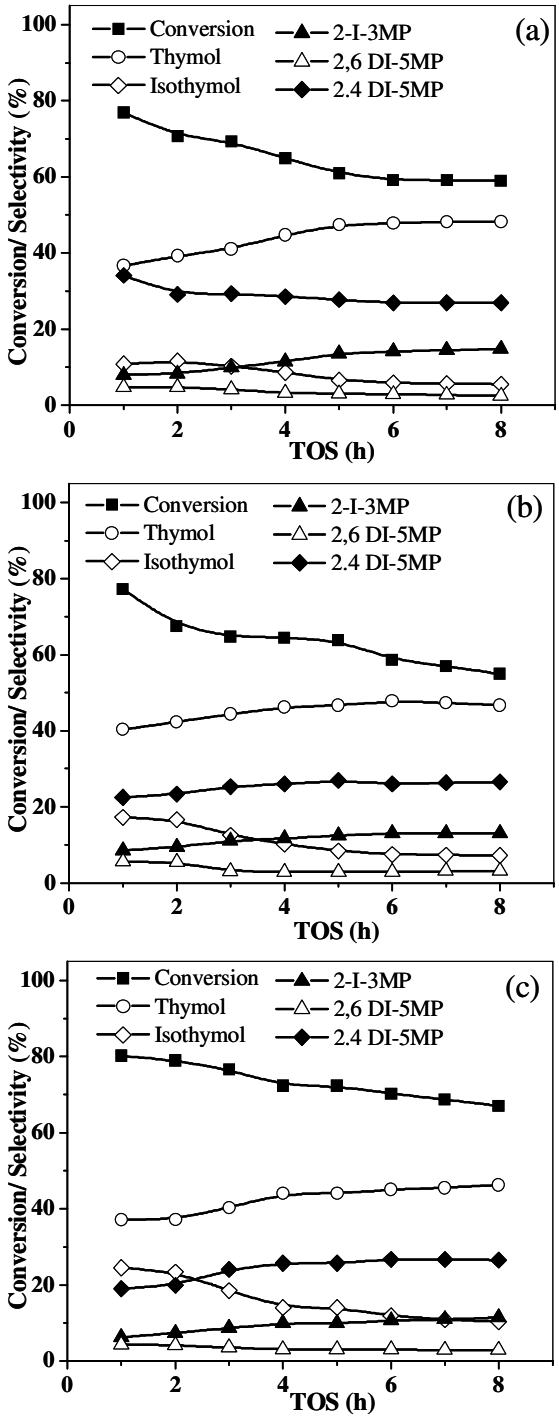

Figure 5.17 Effect of time on stream on m-cresol conversion, selectivity for thymol, isothymol and dialkylated products over (a) 10 wt. % PW/SBA-15, (b) 20 wt. % PW/SBA-15 and (c) 40 wt. % PW/SBA-15. Reaction conditions: Catalyst = 1.5 g., TOS = 4 h, m-cresol: IPA = 1:4 molar ratio, WHSV = 1.76h^{-1}

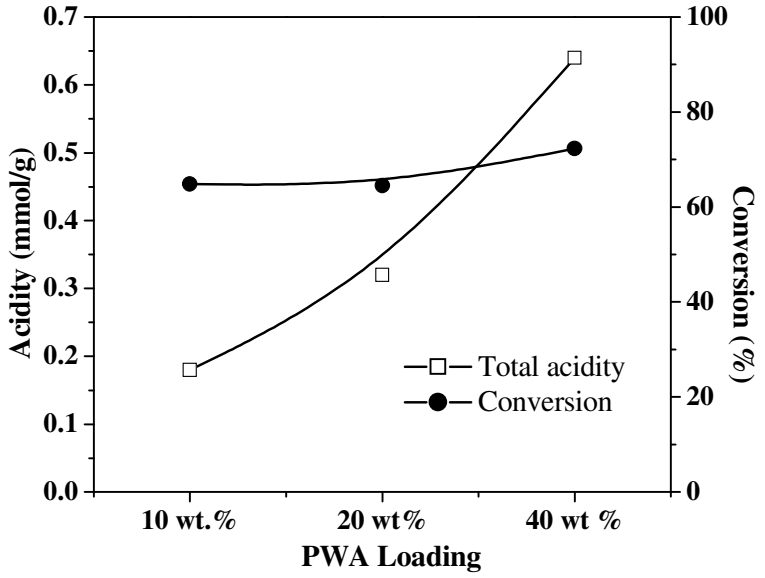

Figure 5.18 Influence of PW content and catalyst acidity on (a) m-cresol conversion over PW/SBA-15 catalysts. Reaction conditions: catalyst = 1.5 g, TOS = 4 h, m-cresol: IPA =1:4 molar ratio, WHSV = 1.76h^{-1}

Table 5.4 Comparison of the activity of different catalysts for m-cresol isopropylation

Catalyst	Conv.	Product Selectivity (%)					
	(%)	A	B	C	D	E	Others
Al-MCM-41(21)	74.7	45.9	18.9	7.02	4.9	17.7	5.5
Al-MCM-41 (31)	73.6	44.3	16.5	6.9	4.6	21.2	6.5
Al-MCM-41 (53)	68.2	43.5	16.3	5.8	4.3	24.1	6.0
Al-SBA-15 (19)	75.5	44.7	14.7	7.07	5.3	22.2	6.1
Al-SBA-15 (30)	78.8	42.6	15.1	6.3	5.5	25.5	4.8
Al-SBA-15 (46)	71.6	48.8	12.3	6.91	4.7	22.3	5.0
10 wt% PW/SBA-15	64.8	44.7	8.6	11.5	3.2	28.6	3.4
20 wt% PW/SBA-15	64.5	46.2	10.2	11.8	2.9	26.0	2.9
40 wt% PW/SBA-15	72.3	44.1	14.0	9.9	3.0	25.7	3.4

Reaction conditions: T = 548 K, TOS = 4 h, catalyst wt. = 1.5 g, m-cresol: isopropanol- 1:4, others- (F + G + High Boilers). A, B, C, D, E, F and G are the products as shown in Figure 5.10.

(D) Comparison of activities of the catalysts

A comparison of the activities of different catalysts for m-cresol isopropylation is presented in Table 5.4. Al-MCM-41 and Al-SBA-15 possess similar m-cresol conversion activities [for similar Al contents]. PW/SBA-15 catalysts are less active than the Al catalysts. The thymol selectivities of all the catalysts are in general similar.

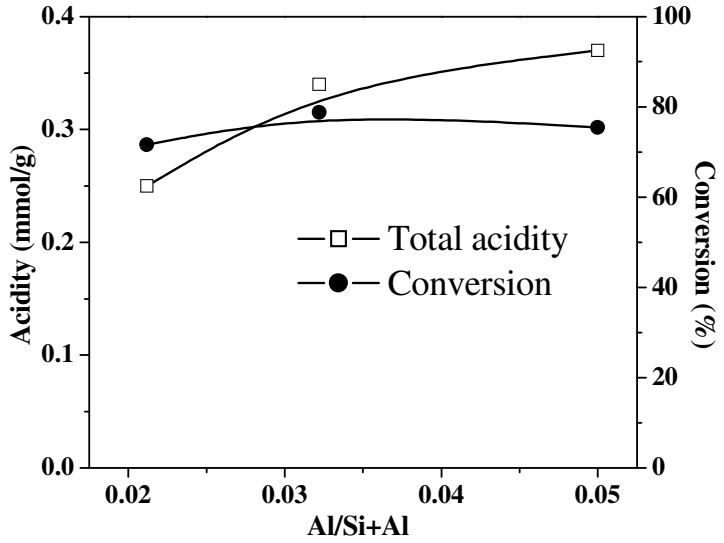

Figure 5.19 Influence of Al content and catalyst acidity on (a) m-cresol conversion over Al-SBA-15 catalysts. Reaction conditions: catalyst=1.5 g., TOS = 4 h, m-cresol: IPA=1:4 molar ratio, WHSV=1.76h^{-1}, T= 548 K.

Figure 5.19 presents the influence of aluminium content and catalyst acidity on m-cresol conversion in the case of Al-SBA-15 catalysts. Though acidity increases continuously with Al content, conversion increase is not significant. In fact, it appears to pass through a maximum at an intermediate Al content and acidity. It appears therefore, that besides the number of acid sites, other factors may also influence catalyst activity. One such factor is the possibility that some acid sites might be inaccessible when the Al loading is high due to pore blocking by the bulk Al_2O_3 species formed at the surface.

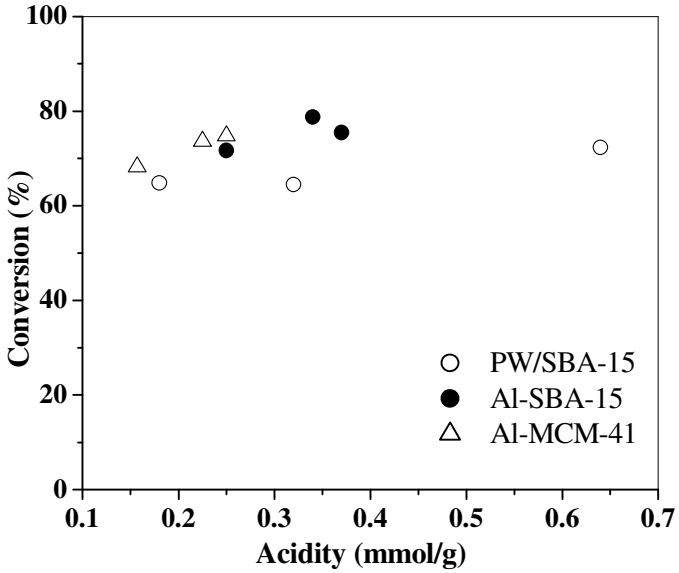

Figure 5.20 Conversion and acidity comparison for PW/SBA-15, Al-SBA-15 and Al-MCM-41 catalysts. Reaction conditions: catalyst=1.5 g., TOS = 4 h, m-cresol: IPA =1:4 molar ratio, WHSV =1.76h^{-1}, T = 548 K.

Figure 5.20 shows the effect of acidity on conversion of m-cresol for PW/SBA-15, Al-SBA-15 and Al-MCM-41 at TOS 4 h. The plot shows that conversion increases with acidity for all series of catalysts. However, the data points for all the catalysts do not fall on the same line suggesting probably the differences in the nature of acidity and mechanistic differences over the three series of catalysts. For a given acidity, the activity is similar for Al-SBA-15 and Al-MCM-41 and more than that for PW/SBA-15.

5.2.4 CONCLUSIONS

Vapor phase m-cresol isopropylation was studied over Al-MCM-41, Al-SBA-15 and PW/SBA-15 catalysts. Both O- and C-alkylations occur to give a mixture of products as shown in the reaction scheme (Figure 5.10). Among the products, thymol (A), isothymol (B), 2-isopropyl-3-methylphenol (C) and the dialkylated product 2, 4-di-isopropyl-3-methylphenol (E) are the major ones. Other products such as 2, 6-di-isopropyl-3-methylphenol (D), isopropyl-2-isopropyl-5-methylphenylether (F) and isopropyl-3-methylphenylether (G) are also formed in minor amounts.

The influence of reaction parameters such as temperature (498-623 K), WHSV, mole ratio of the reactants and time on stream was studied over MCM-41 and SBA-15 modified catalysts. The optimum reaction temperature and WHSV was found to be 548 K and 1.76 h^{-1} with m-cresol to isopropanol molar ratio of 1:4. The activity of all the catalysts was compared at the above reaction conditions and it was found to be in the order: PW/SBA-15 < Al-MCM-41 < Al-SBA-15. It is also observed that the reaction depends not only on the acid sites of the catalysts; their hydrophilic and hydrophobic properties also play an important role.

5.3 REFERENCES

1. G.A. Olah, "Friedel-Crafts and related Reactions", vol.1-4 (Wiley-Interscience, New York, (1963-1964).
2. G.A. Olah, "Friedel-Crafts and related Reactions", vol.1-4 (Wiley-Interscience, New York, (1973).
3. P. Metivier, R. A. Sheldon, H. Van Bekkum (Eds), "Fine Chemicals Through Heterogeneous Catalysis", Wiley-VCH. Weinheim (2001) 161.
4. E.G. Derouane, G. Crehan, C.J. Dillon, D. Bethell, H. He, S.B. Abd Hamid, J. Catal. 194 (2000) 410.
5. (a) F. Jayat, M. J. Sabater Picot, M. Guisnet, Catal. Lett. 41 (1996)181; (b) A. Vogt, H.W. Kouwenhoven, R. Prins, Appl. Catal. A: Gen. 123 (1995) 37.
6. M. Guisnet, G. Perot, R. A. Sheldon, H. Van Bekkum (Eds.), "Fine Chemicals Through Heterogeneous Catalysis", Wiley-VCH, Weinheim (2001) 211.
7. Y. Izumi, K. Urabe, M. Onaka, "Zeolite, Clay and Heteropolyacid in Organic Reactions", Kodansha/VCH, Tokyo, (1992).
8. (a) T. Okuhara, N. Mizuno, M. Misono, Adv. Catal. 41 (1996); (b) M. Misono, Chem. Commun. (2001) 1141.
9. I. V. Kozhevnikov, Chem. Rev. 98 (1998) 171.
10. J. Kaur, K. Griffith, B. Harrison, I.V. Kozhevnikov, J. Catal. 208 (2002) 448.
11. K. Gaare, D. Akporiaye, J. Mol. Catal. A: Chem. 109 (1996) 177.
12. I. Nerves, F. Jayat, P. Magnoux, G. Perot, F.R. Riberio, M. Gubelmann, M. Guisnet, J. Mol. Catal. A: Chem. 93 (1994) 169.
13. C. T. Kregse, D.O. Marler, G. S. Rav, B.H. Rose, US Patent 5,366 (1994) 945.
14. I.V. Kozhevnikov, A. Sinnema, R. J. J. Janse, K. Pamin, H. Van Bekkum, Catal Lett. 30 (1995) 241.
15. T. Blasco, A. Corma, A. Martinez, P. Martinez-Escolano, J. Catal. A 177 (1998) 306.
16. J. Wang, H. Zhu, Catal. Lett. 93 (2004) 209.
17. E.G. Deruane, G. Crehan, C.J. Dillon, D. Bethell, H. He and S.B. Derouane-Abd-Hamid, J. Catal. 194 (2000) 410.
18. (a) H. Fiege, in "Ullmanns Encyclopedia of Industrial Chemistry", B. Elvers, S. Hawkins, G. Schultz (Eds.) Vol. A1 9, 5th Ed., V.C.H., Weinheim, (1991) 313;

(b) R. Dowbenko, "Kirk-Othmer Encyclopedia of Chemical Technology", J. I. Kroschwit and Mary Houl-Grant (Eds.) 4th Ed., Vol. 2 (1992) 106.

19. J. C. Leffingwell, R. E. Shackelford, "Cosmetics Perfumery", 89 (6) (1974) 69.
20. N. Dirdy, L. Dubreuil, M. Pinkas, Pharmazie. 48 (1993) 301.
21. T. Yamanka, Bull. Chem. Soc. Jpn. 49 (1976) 2669.
22. M. Nitta, K. Yamaguchi, K. Aomura, Bull. Chem. Soc. Jpn. 47 (1974) 2897.
23. P. Wimmer, H. J. Buysch, L. Puppe, US Patent 5030770, (1991).
24. M. Nitta, K. Aomura, K. Yamaguchi, Bull. Chem. Soc. Jpn. 47 (1974) 2360.
25. W. Biedermann, H. Koller, K. Wedemeyer, US Patent 4086383 (1978).
26. H. G. Franc, J. W. Stadelhofer, "Industrial Aromatic Chemistry", Springer, Berlin, Heidelberg, (1988) 168.
27. S. Velu and S. Sivasanker, Res. Chem. Intermed. Vol. 24, No. 6, (1998) 657.
28. H. Grabowska, J. Wrzyszcz, Res. Chem. Intermed. 27 (2001) 281.
29. H. Grabowska, W. Mista, J. Trawxzynski, J. Wrzyszcz, M. Zawadzki, Appl. Catal. A: Gen. 220 (2001) 207.
30. Umamaheshwari, M. Palanichamy, V. Murugesan, J. Catal. 210 (2002) 367.
31. K. Shanmugapriya, M. Palanichamy, B. Arabindoo, V. Murugesan, J. Catal. 224 (2004) 347.
32. (a) A. Vinu, G. Satish Kumar, K. Ariga, V. Murugesan, J. Mol. Catal. A: Chem. 235 (2005) 57; (b) A. Vinu, K. Ariga, S. Saravanamurugan, M. Hartmann, V. Murugesan, Micropor. Mesopor. Mater. 76 (2004) 91.
33. C. Song, X. Ma, A. D. Schmitz, H. H. Schobert, Appl. Catal. A: Gen. 182 (1999)175.
34. D. R. Taylor, K. H. Ludlum, J. Phys. Chem. 76 (1972) 2882.

Chapter 6

OTHER ORGANIC TRANSFORMATIONS

The present chapter contains 3 parts. Part 1 discusses the study of the esterification of p-cresol with phenyl acetic acid over PW/SBA-15 catalysts, while part 2 presents the Prins condensation reaction of β- pinene with para formaldehyde over modified MCM-41 and SBA-15 mesoporous molecular sieves and part 3 contains the results of the oxidation of ethylbenzene over V, Fe and Sn-MCM-41 with TBHP and H_2O_2 oxidants.

6.1 PART 1 ESTERIFICATION OF P-CRESOL WITH PHENYL ACETIC ACID

6.1.1 INTRODUCTION

Organic esters are an important class of chemicals having applications in various preparations, such as cosmetics, perfumes, flavors and pharmaceuticals as intermediates in fine chemical synthesis and drugs and as food preservatives and plasticizers. Several synthetic routes have been reported to make esters [1]. Conc. H_2SO_4, dry HCl gas, HF, phosphoric acid and p-toluene sulphonic acids, are commonly used as catalysts to catalyze esterification reactions [2]. Zeolites in different forms have been studied in esterification reactions such as reactions between simple alcohols and carboxylic acids [3], amyl alcohol and acetic acid [4], and oleic acid and oleyl alcohol in the formation of jojoba oil analog [5]. Amberlyst-15, a cation exchange resin, catalyzes esterification of acrylic acid with butanol [6]. Sulphated-ZrO_2 [7], aluminophosphates and silicoaluminophosphate molecular sieves [8] have been reported for the esterification of phthalic anhydride with 2-ethylhexanol. Filtrol-24, Amberlyst-15, sulphated-ZrO_2 and heteropolyacids have been used in the synthesis of phenethyl acetate and cyclohexyl acetate [9]. Also the enzyme Lipase has been used for the esterification of different carboxylic acids with p-cresol and m-cresol [10]. Esterification of salicylic acid with phenol has been reported on hydrated oxides (alumina, silica and zirconia) in their sulphated forms and zeolites (Y, ZSM-5 and β) in their protonated forms to yield salol [11]. Fe^{3+}- K-10 montmorillonite is reported to be useful for the esterification of carboxylic acids with alcohols [12] and also in the synthesis of amides from carboxylic acids [13]. Cation exchanged montmorillonite clay has been used in the esterifiaction of succinic anhydride with p-cresol [14]. Recently Nafion functionalized MCM-41

(perfluoroalkylsulfonic acid chains anchored to MCM-41) catalysts have been reported for the esterification of long-chain fatty acid with alcohols [15].

There are a few reports on the synthesis of esters of phenyl acetic acid with phenol, cresols, nitro phenols and resorcinol over Al exchanged montmorillonite clay [16]. An eco-friendly and benign catalytic process for the preparation of perfumery grade p-cresylphenyl acetate (an important perfumery chemical) from p-cresol and phenyl acetic acid was recently reported by Yadav et al. [17] over dodecatungstophosphoric acid (DTP) supported on K-10 clay, ion exchange resins and sulphated-ZrO_2.

In the present section, the esterifaction of p-cresol with phenyl acetic acid over PW loaded SBA-15 catalysts is reported. The influence of various reaction parameters such as temperature, mole ratio, catalyst amount and different PW loading is presented.

6.1.2 EXPERIMENTAL

(a) Reaction Procedure

The reactions were carried out in a batch mode in a two-necked round-bottomed flask (capacity 25 ml) in nitrogen atmosphere using p-cresol (s.d. Fine Chemicals, India) and phenyl acetic acid (Merck) in a 10:1 mole ratio with 0.1 g of freshly prepared catalyst in the temperature range of 363-393 K. Aliquots of the reaction mixture were collected at different time intervals and analyzed by GC (Chrompack CP 9001, column OV-101, 50 m, id= 0.2 mm). Identification of the products was done by GC- MS and GC- IR.

6.1.3 RESULTS AND DISCUSSION

The catalysts used in the study were PW/SBA-15. The synthesis procedure of PW/SBA-15 catalysts has been described in chapter 2. The samples were characterized by different physicochemical techniques such as XRD, TPDA (NH_3), and N_2 adsorption. The general observation is that the acidity of the PW/SBA-15 catalysts increases with increasing phosphotungstic acid content. The impregnation with PW did not affect the pore system or overall arrangement of the pores of SBA-15 to any significant amount (upto 30 wt. % PW loading).

(A) Esterification of p-cresol by phenyl acetic acid

The reaction scheme of the esterification of p-cresol with phenyl acetic acid to yield p-cresylphenyl acetate is shown in Figure 6.1.

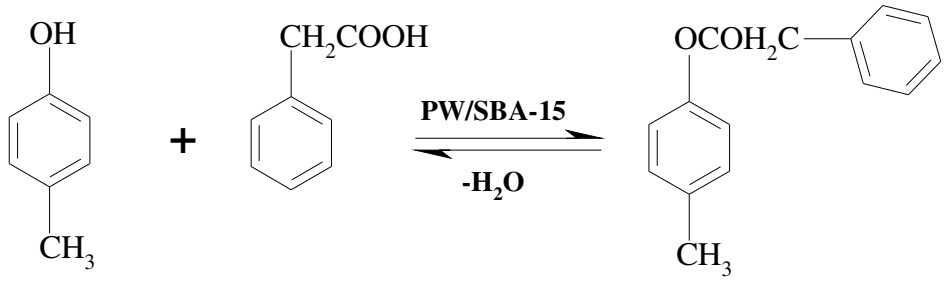

p-Cresol Phenyl acetic acid p-Cresylphenyl acetate

Figure 6.1 Reaction scheme for the esterification of p-cresol with phenyl acetic acid.

(i) Influence of duration of run

The effect of run duration on conversion and yield of p-cresylphenyl acetate over the catalysts (different PW/SBA-15) is presented in Figure 6.2. Both conversion and yield increase steadily up to 9 h, beyond which the increase is less rapid. As the PW content increases the conversion and yield also increase due to an increase in the number of active centers (acidity). The selectivity for p-cresylphenyl acetate remains 100 % over all catalysts.

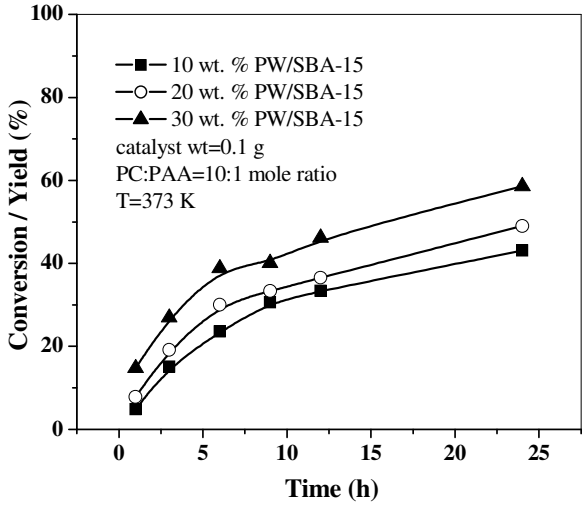

Figure 6.2 Influence of PW loading and run duration on p-cresol conversion and yield of p-cresylphenyl acetate.

(ii) Effect of amount of catalyst

Figure 6.3 shows the effect of catalyst charge and run duration on p-cresol conversion and yield of p-cresylphenyl acetate. 20 wt. % PW/SBA-15 catalyst was used in the studies. The conversion of phenyl acetic acid increases with increasing catalyst charge due to the proportional increase in the number of active sites. Comparing 12 h data, the conversion and yield increase from 2.7 to 67.5 % when the catalyst amount is increased from 0.025 g to 0.150 g.

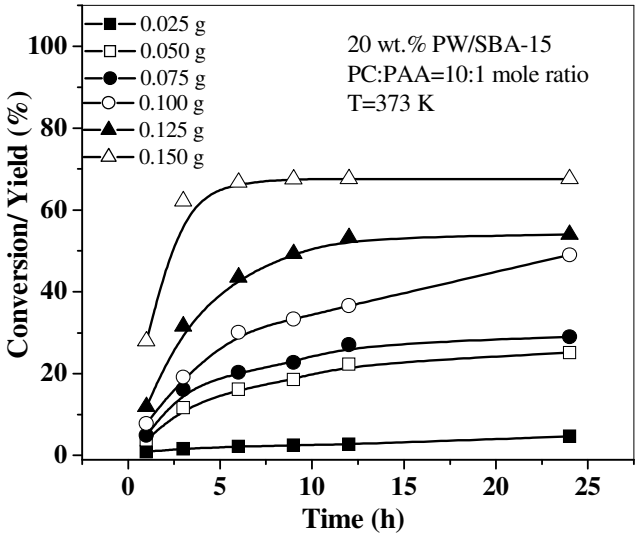

Figure 6.3 Effect of amount of catalyst and run duration on p-cresol conversion and yield of p-cresylphenyl acetate.

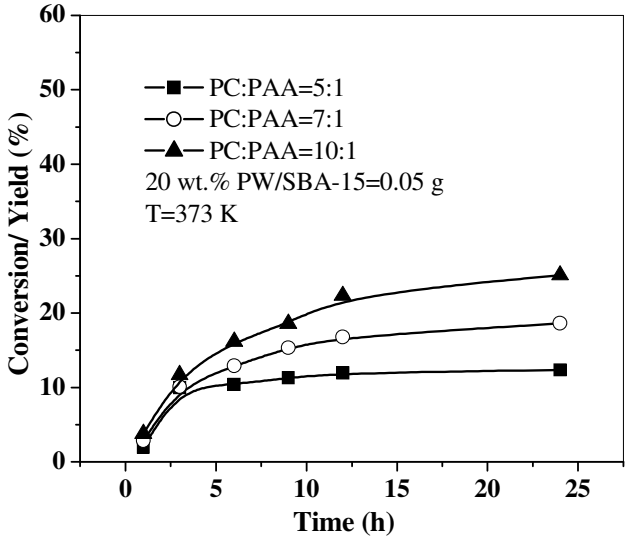

Figure 6.4 Effect of mole ratio of reactants and run duration on the p-cresol conversion and yield of p-cresylphenyl acetate.

(iii) Effect of mole ratio

Figure 6.4 shows the effect of mole ratio of p-cresol to phenyl acetic acid on conversion of p-cresol. The ratio of p-cresol to phenyl acetic acid was varied between 5:1, 7:1 and 10:1. The yield of the ester increased with increase in the concentration of p-cresol and reached a maximum of 25.1 % when p-cresol to phenyl acetic acid ratio was 10:1.

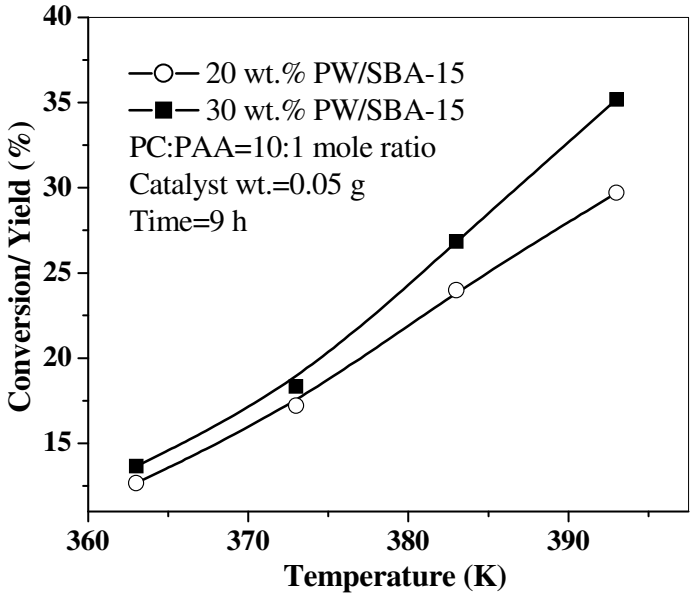

Figure 6.5 Influence of temperature on conversion and selectivity over PW/SBA-15 catalysts with different PW loadings.

(iv) Influences of temperature

The influence of temperature in the range of 363 to 393 K on p-cresol conversion and yield of p-cresylphenyl acetate over 20 and 30 wt. % PW/SBA-15 is presented in Figure 6.5. Conversion and yield increase with temperature for both catalysts. The selectivity for p-cresylphenyl acetate is 100 % for both the catalysts at all the temperatures investigated. As expected conversion over 30 wt. % catalyst is more than over the 20 wt. % catalyst.

In the esterification of p-cresol with phenyl acetic acid, the p-cresol was used in excess and therefore these reactions were considered as pseudo first order with respect to the phenyl acetic acid. The standard first order reaction rate expression,

$- \ln (1- X_a) = kt$ (1)

was used for the kinetic analysis of the reaction and the activation energy of the reaction was estimated using the Arrhenius expression:

$k = A\, e^{(-Ea/RT)}$ (2)

In equation (1) and (2), k is the rate constant, X_a is the conversion of reactant (phenyl acetic acid), A is frequency factor, E_a is the activation energy, R is the universal gas constant and T is the reaction temperature.

The experimental data on the influence of temperature on conversion in the temperature range 363 to 393 K as a function of run duration fitted into a first order model and the rate constants (k) are calculated. Arrhenius plots of the rate constants are presented in Figure 6.6. The plot for the 30 wt. % catalyst is better than at for the 20 wt. % catalyst.

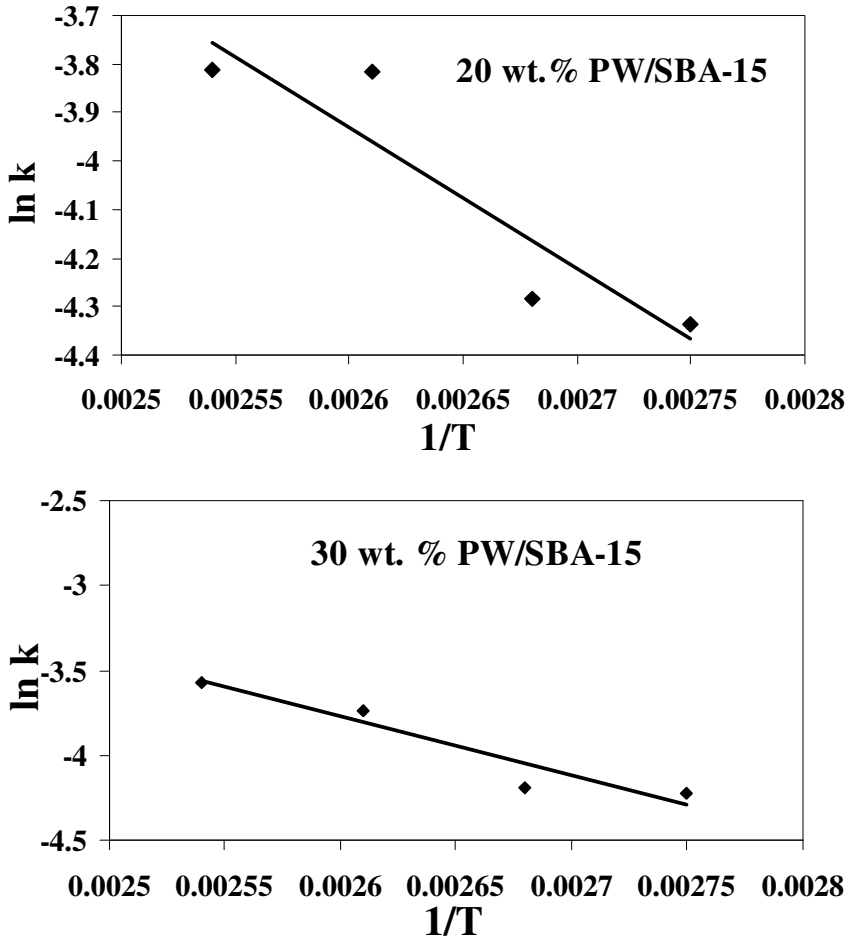

Figure 6.6 Arrhenius plots for 20 wt. % and 30 wt. % PW/SBA-15.

The values of the activation energies (E_a) for 20 wt. % and 30 wt. % PW/SBA-15 catalysts are 5.81 kcal/mole and 6.93 kcal/mole, respectively, for the reaction. The low E_a values obtained over the catalysts suggest that the overall rate of reaction is not significantly influenced by intrinsic kinetics.

(v) Influence of PW loading

A plot of p-cresol conversion with acidity (strong and weak) and PW content is shown in Figure 6.7. It is found that both acidity and conversion increase with PW content. The relationship between acidity and conversion suggests that the reaction occurs inside the pores of SBA-15 where the HPA units are located. It was earlier shown (chapter 3) that the PW molecules are well distributed inside the pores of SBA-15 upto 30 wt. % PW loading.

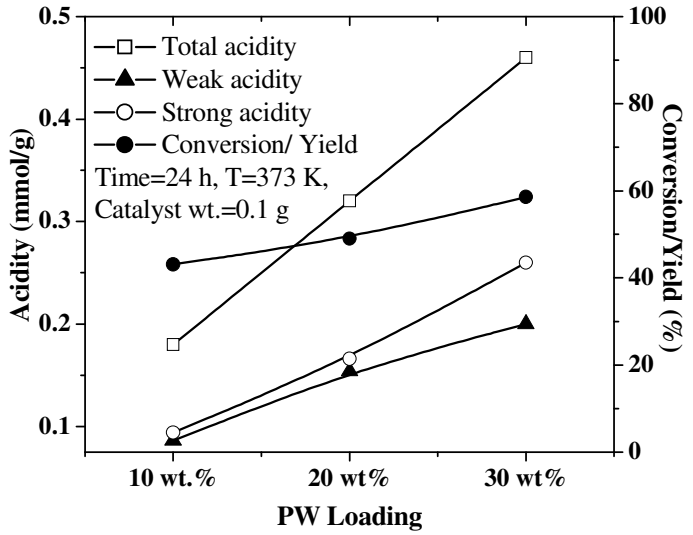

Figure 6.7 Influence of PW content and acidity on p-cresol conversion and yield of p-cresylphenyl acetate with catalyst acidity.

(vi) Mechanism of the reaction

A plausible mechanism of esterification is shown in Figure 6.8. The reaction between phenyl acetic acid and p-cresol is catalysed by Brönsted acids through the formation of a conjugated acid ion i.e., oxonium ion [16] as shown in figure. Addition

of an alcohol (cresol) to the oxonium ion forms an intermediate adduct which on loss of a proton and water leads to the formation of the ester.

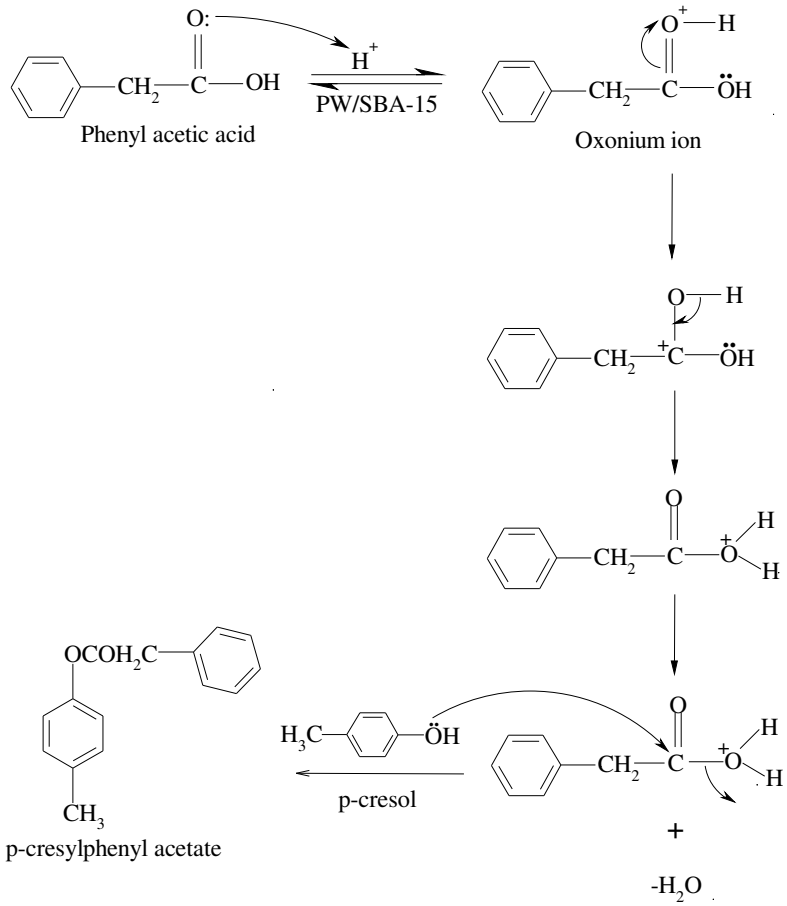

Figure 6.8 Plausible mechanism for the esterification of p-cresol with phenyl acetic acid over PW/SBA-15.

6.1.4 CONCLUSIONS

An eco-friendly and benign catalytic process, employing solid acid catalysts for the esterification of p-cresol with phenyl acetic acid to give p-cresylphenyl acetate is presented. The catalytic activity increases with PW loading and acidity. The apparent activation energies for 20 and 30 wt. % PW/SBA-15 catalyst based on a pseudo first order model are 5.81 and 6.93 kcal/mole, respectively, which suggest that the reaction is not significantly influence by intrinsic kinetics.

6.2 PART 2 PRINS CONDENSATION OF β-PINENE AND PARA FORMALDEHYDE OVER MODIFIED MCM-41 AND SBA-15 CATALYSTS

6.2.1 INTRODUCTION

Nopol is an optically active bicyclic primary alcohol, useful in the agrochemical industry for the synthesis of pesticides, soap fragrances and household products [18, 19]. It is prepared by autoclaving para formaldehyde and β-pinene at 423 to 503 K for several hours. β-pinene is an important component of wood turpentine, it occurs to the extent of about 30 % in American gum turpentine. Kriewitz [20] reported that pinene (boiling point 429-432 K) reacts with an alcoholic solution of paraformaldehye at 443-448 K to give an alcohol $C_{11}H_{18}O$ in 15 % yield. Bain [21] reported that β-pinene and formaldehyde readily condense in an equimolar mixture to form a new optically active bicyclic primary alcohol, 6,6-dimethylbicyclo-(1,1,3)-hept-2-ene-2-ethanol, which has been named nopol.

Recently, Montes de Correa et al. [22] have reported the synthesis of nopol over Sn-MCM-41 molecular sieves in the presence of toluene as a solvent at 363 K. Nopol yields higher than 90 % were obtained using a catalyst in which Sn was grafted by chemical vapor deposition (CVD) of $SnCl_4$ on MCM-41. More recently, a mesoporous iron phosphate catalyst has been reported for the selective synthesis of nopol at 353 K in acetonitrile solvent [23]. Jyothi et al. reported that the anchoring of tin chloride on a quaternary ammonium chloride functionalized MCM-41 yielded a catalyst with higher activity compared to the corresponding silica analogue in terms of turnover rates and product yield in the Prins condensation of isobutene and formaldehyde to isoprenol [24, 25]. Sn-kenyaite catalysts prepared by CVD method show high nopol selectivities but β-pinene conversion is around 50 % [26].

In this section, the Prins condensation of β-pinene to yield nopol over mesoporous catalysts is reported. The influence of various reaction parameters such as temperature, mole ratio, catalyst amount, solvent polarity and metal loading is reported over Sn-MCM-41 catalysts prepared by direct hydrothermal synthesis. The activity of the Sn catalysts is compared with those of Si-MCM-41, Fe-MCM-41, V-MCM-41, Ga-MCM-41, Al-MCM-41, Si-SBA-15 and Al-SBA-15 for this reaction.

6.2.2 EXPERIMENTAL

The synthesis procedure for the preparation of modified MCM-41 and SBA-15 catalysts was described in chapter 2. The characterization data for all the catalysts was discussed in chapter 3.

(a) Reaction procedure

The reactions were carried out in the temperature range of 343-373 K in a batch mode in a two-necked round-bottomed flask (capacity 25 ml) in nitrogen atmosphere, using β-pinene (Aldrich) (5 mmol) and para formaldehyde (Merck) (10 mmol) with 0.05 g of freshly prepared catalyst. Aliquots of the reaction mixture were collected at different time intervals and analyzed by GC (Chrompack CP 9001, column OV-101, 50 m, id = 0.2 mm). Identification of the products was done by GC-MS and GC- IR.

6.2.3 RESULTS AND DISCUSSION

(A) Prins condensation of β-pinene

The reaction scheme for Prins condensation of β-pinene with para formaldehyde is shown in Figure 6.9.

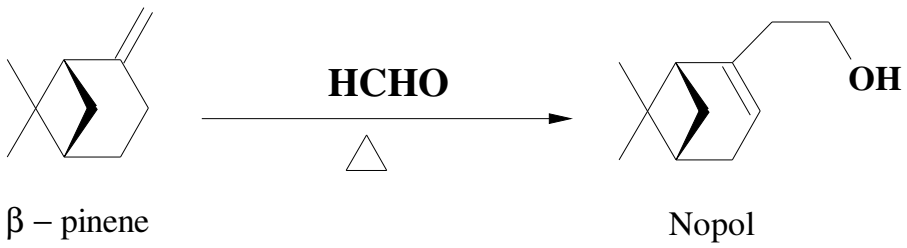

Figure 6.9 Reaction scheme for Prins condensation of β-pinene with para formaldehyde.

(i) Influence of run duration

The effect of run duration on conversion of β-pinene and yield of nopol over Sn-MCM-41 catalysts (with different Si/Sn ratios) is presented in Figure 6.10. For Sn-MCM-41 (49), conversion increases from 48.2 % to 90 % within 2 h. For Sn-MCM-41 (37) and Sn-MCM-41 (22) the reaction is faster and almost 100 % conversion is

achieved within 2 h. The selectivity for nopol is 100 % over all catalysts. It is also noticed that conversion increases with Sn content in the catalyst. The increase in conversion with Sn content is attributed to increasing catalyst acidity. Earlier workers have suggested that the reaction is catalyzed by Lewis acidity, typically Sn^{4+} [23-25].

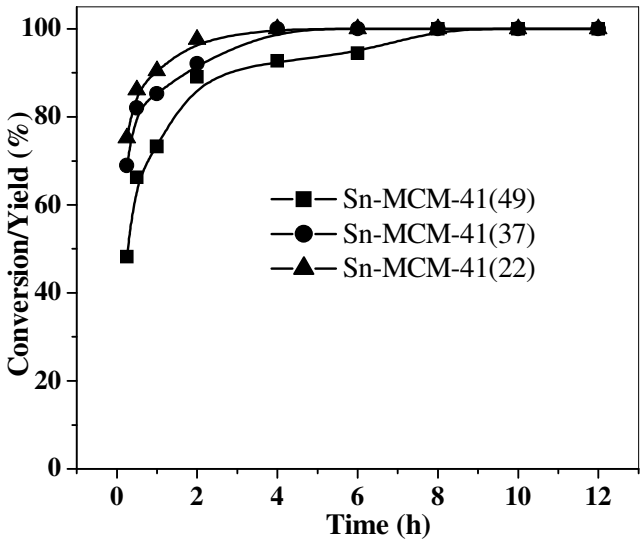

Figure 6.10 Influence of Sn content with run duration on β-pinene conversion and yield of nopol. Reaction conditions: β-pinene: para formaldehyde = 1:2 (mole), catalyst amount = 0.05 g, solvent- toluene = 4 g, T= 353 K.

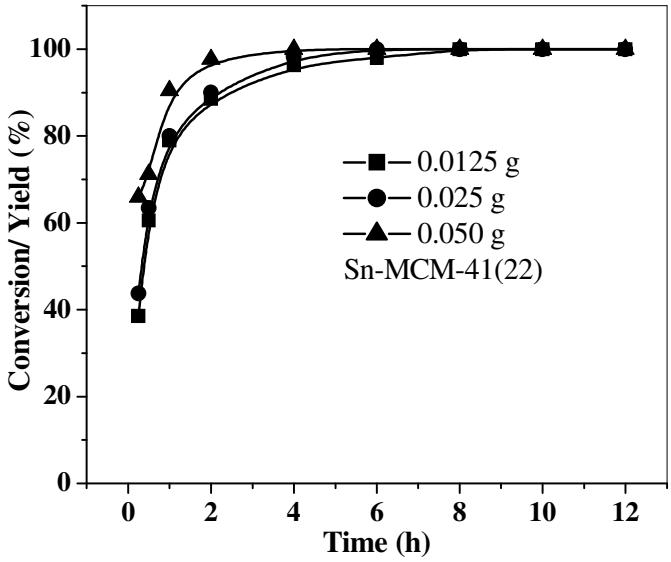

Figure 6.11 Effect of amount of catalyst (Sn-MCM-41 (22)) on β-pinene conversion and yield of nopol. Reaction conditions: β-pinene: para formaldehyde = 1:2 (mole), solvent-toluene = 4 g, T= 353 K.

(ii) Effect of amount of catalyst

Figure 6.11 shows the effect of catalyst loading in the case of Sn-MCM-41 (22) on β-pinene conversion and yield of nopol. On increasing the catalyst amount, the conversion of β-pinene increases and the time required for total conversion is shortened. The conversion reaches 100 % in 6 h when 0.0125 g catalyst is used. When 0.025 and 0.050 g of the catalyst are used, very fast and complete conversion is observed within 4 and 2 h, respectively. Selectivity for nopol is 100 % at all catalyst loadings.

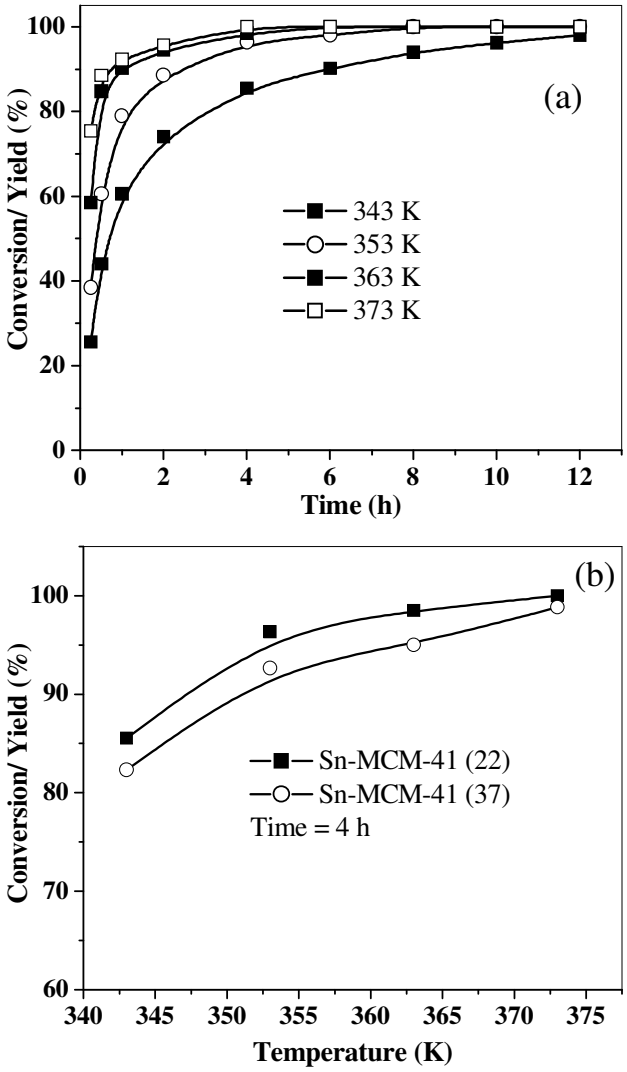

Figure 6.12 (a) Influence of temperature and run duration on conversion over Sn-MCM-41 (22). (b) Influence of temperature on conversion and yield over Sn-MCM-41 with two different Sn contents. Reaction conditions:β-pinene: para formaldehyde = 1: 2 (mole), solvent-toluene = 4 g, catalyst amount = 0.0125 g, TOS = 4 h.

(iii) Influence of temperature

The influence of temperature (343 to 373 K) on conversion (at different run duration) over Sn-MCM-41 (22) is presented in Figure 6.12 (a). Conversion and yield increase with temperature and run duration. Figure 6.12 (b) presents a comparison data at a TOS of 4 h for Sn-MCM-41 catalysts with Si/Sn ratios of 22 and 37. Conversion and yield over Sn-MCM-41 (22) are more than that over Sn-MCM-41 (37). Arrhenius plots based on initial conversion at 1 h at the different temperatures give apparent E_a values of 13.3 and 12.7 kcal/mole for Sn-MCM-41 (22) and Sn-MCM-41 (37), respectively.

(iv) Influence of solvents

The influence of different solvents on β-pinene conversion and yield of nopol with run duration over Sn-MCM-41 (22) is presented in Figure 6.13. Different solvents such as acetonitrile (ACN), toluene, ethylenedichloride (EDC), tetrachloroethane, heptane and chlorobenzene (ChBZ) were used for the reaction. The order of activity in the different solvents based on 1 h data is: EDC > tetrachloroethane > ChBz > toluene > heptane > ACN.

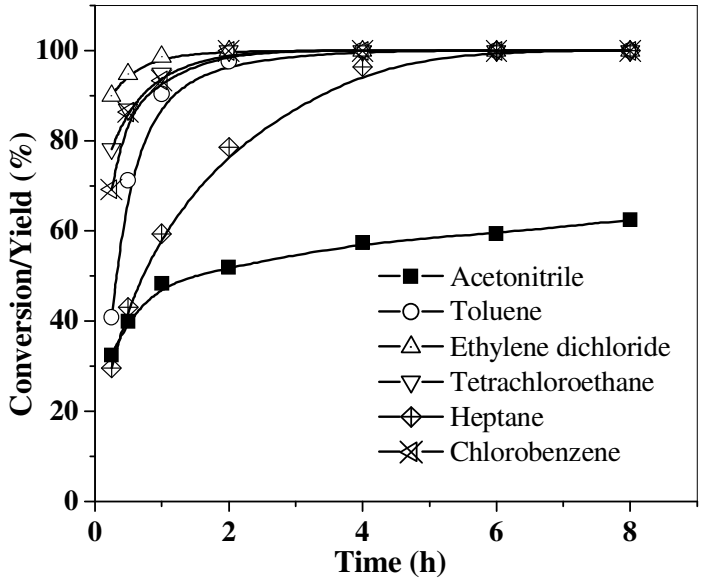

Figure 6.13 Influence of solvents on conversion and yield with run duration over Sn-MCM-41 (22). Reaction conditions: β-pinene: para formaldehyde = 1:2 (mole), solvent-toluene = 4 g, Sn-MCM-41 (22) = 0.05 g, T = 353 K.

(v) Effect of β-pinene to para formaldehyde molar ratio

Figure 6.14 presents the results of studies carried out using different mole ratios of β-pinene and para formaldehyde (1:1, 1:2, 1:4) over Sn-MCM-41 (22). A general trend of increase in conversion with mole ratio is observed. For β-pinene to para formaldehyde molar ratio of 1:1, the conversion increases from 36.5 % to 84.2 % in 4 h. In the same period, conversion increases from 48.3 % to 100 % for a ratio of 1:2 and from 55.4 % to 100 % for a ratio of 1:4. The selectivity for nopol was 100 % at all molar ratios. When aqueous formaldehyde was used instead of para formaldehyde, catalytic activity decreased suggesting (Table 6.1) that the absence of water is necessary to obtain high nopol yields.

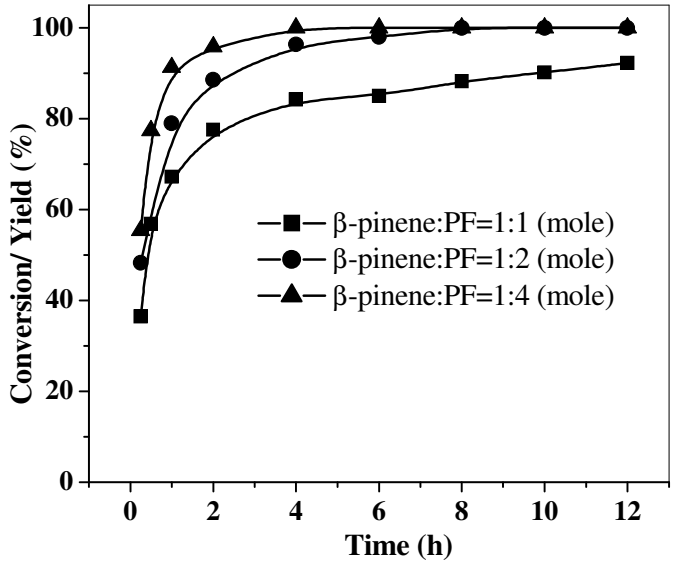

Figure 6.14 Effect of β-pinene to para formaldehyde molar ratio on conversion and yield with run duration over Sn-MCM-41 (22). Reaction conditions: solvent-toluene = 4 g, catalyst amount = 0.05 g, T = 353 K.

Table 6.1 Activity of MCM-41 catalysts with aqueous formaldehyde and 98 % para formaldehyde[a]

Expt. No.	Catalyst	Catalyst amount (g)	Conversion / Yield (%)		
			2 h	4 h	6 h
1.	Sn-MCM-41 (37)	0.10	28.8	32.8	35.7
2.	Sn-MCM-41 (49)	0.05	10.5	19.9	29.8
3.	Ga-MCM-41 (54)	0.10	4.5	6.2	10.6
4.	Fe-MCM-41 (20)	0.05	11.8	20.8	38.5
5.	Fe-MCM-41 (20)	0.10	46.1	78.7	80.7
6.	Sn-MCM-41 (22)	0.05	51.9	57.5	59.4

Reaction conditions: β-pinene: para formaldehyde = 1:2 (mole), solvent - ACN = 4 g, T = 353 K. (a- In Expt. No. 1 to 5, aqueous formaldehyde (35 %) was used and 98 % para formaldehyde was used in Expt. No. 6).

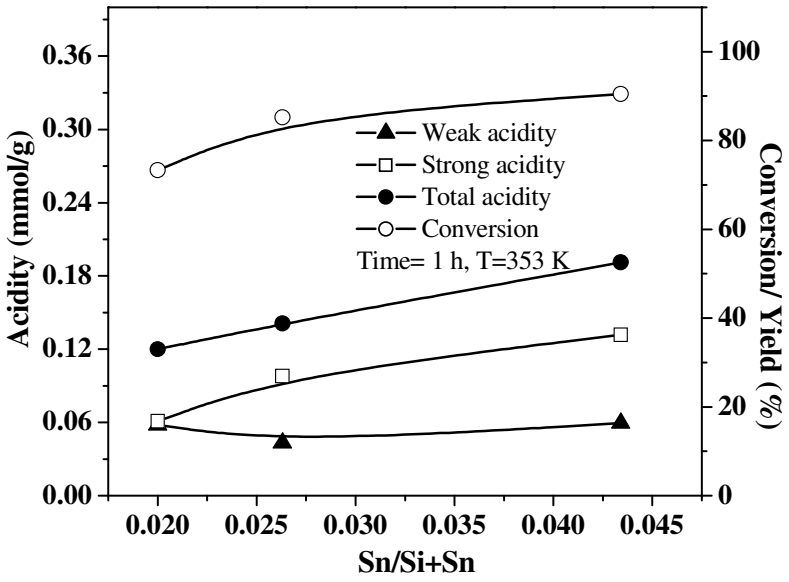

Figure 6.15 Influence of Sn content and catalyst acidity on β-pinene conversion and yield of nopol. Reaction conditions: β-pinene: para formaldehyde = 1:2 (mole), solvent-toluene = 4 g, catalyst amount = 0.05 g, T = 353 K.

(vi) Influence of Sn content and acidity

The influence of Sn content and catalyst acidity on β-pinene conversion (and yield) is shown in Figure 6.15. The result shows that conversion increases with acidity and Sn content. The formation of nopol from β-pinene and formaldehyde is known to occur through an addition reaction between the two reactants in the presence of an acid catalyst. It has been reported that weak and medium acid sites (Lewis acidity of Sn (IV) cations) are responsible for Prins condensation reactions [27]. In the catalysts investigated in this study (Sn-MCM-41), the acidity is presumably of the Lewis type and arises from Sn (IV) cations. As Sn is present in the catalyst as Sn^{4+}, it is unlikely that Brönsted acidity is created, as when trivalent ions are introduced.

Table 6.2 Comparison of activity of catalysts

No.	Catalyst	0.25 h	4 h	No.	Catalyst	0.25 h	4 h
1.	Ga-MCM-41(54)	16.6	38.2	9.	Al-SBA-15(19)	14.1	48.3
2.	Ga-MCM-41(33)	23.1	44.1	10.	Al-SBA-15 (19)[a]	29.0	88.2
3.	Ga-MCM-41(20)	38.2	82.0	11.	Al-SBA-15(30)	11.8	40.1
4.	Ga-MCM-41(20)[a]	66.1	95.3	12.	Al-MCM-41(31)	15.2	51.9
5.	Fe-MCM-41(20)	20.8	61.4	13.	Al-MCM-41(31)[a]	39.8	93.6
6.	Fe-MCM-41(20)[a]	69.0	100	14.	Al-MCM-41(21)[a]	40.2	100
7.	Sn-MCM-41(22)	38.5	96.3	15.	V-MCM-41(99)	2.4	11.9
8.	Sn-MCM-41(22)[a]	75.2	100	16.	V-MCM-41(46)[a]	5.4	38.2

Reaction conditions: β-pinene: para formaldehyde = 1:2 (mole), solvent-toluene = 4 g, catalyst amount = 0.0125 g, T = 353 K, (**a-** catalyst amount = 0.05 g and for others 0.0125 g)

(vii) Comparison data for all catalysts

A comparison of activities of different MCM-41 and SBA-15 catalysts for liquid phase Prins condensation of β-pinene with para formaldehyde is presented in Figure 6.16 (a) and Table 6.2. It is observed that the activity of the catalysts for β-pinene conversion is in the order: Sn-MCM-41 > Fe-MCM-41 > Ga-MCM-41 > Al-MCM-41 > Al-SBA-15 > Si-SBA-15 > Si-MCM-41. Sn-MCM-41 is the most active catalyst and PW/SBA-15 does not exhibit any activity. Apparently, the Lewis acid centers (Sn^{4+}) are active while the Brönsted acid sites in PW/SBA-15 are not.

The Lewis acidic character of the metal increases as: Sn > Fe > Ga > Al > V. Si-SBA-15 exhibits a higher conversion and yield than Si-MCM-41 which is probably due to the larger pore size of SBA-15 and greater accessibility of the reactants to the active sites due to faster diffusion of the bulky reactants and products. For Ga-MCM-41, activity increase with increase in Ga content (decrease in Si/Ga ratio). Similar results are observed for Al-SBA-15, Al-MCM-41, Fe-MCM-41 and V-MCM-41 samples.

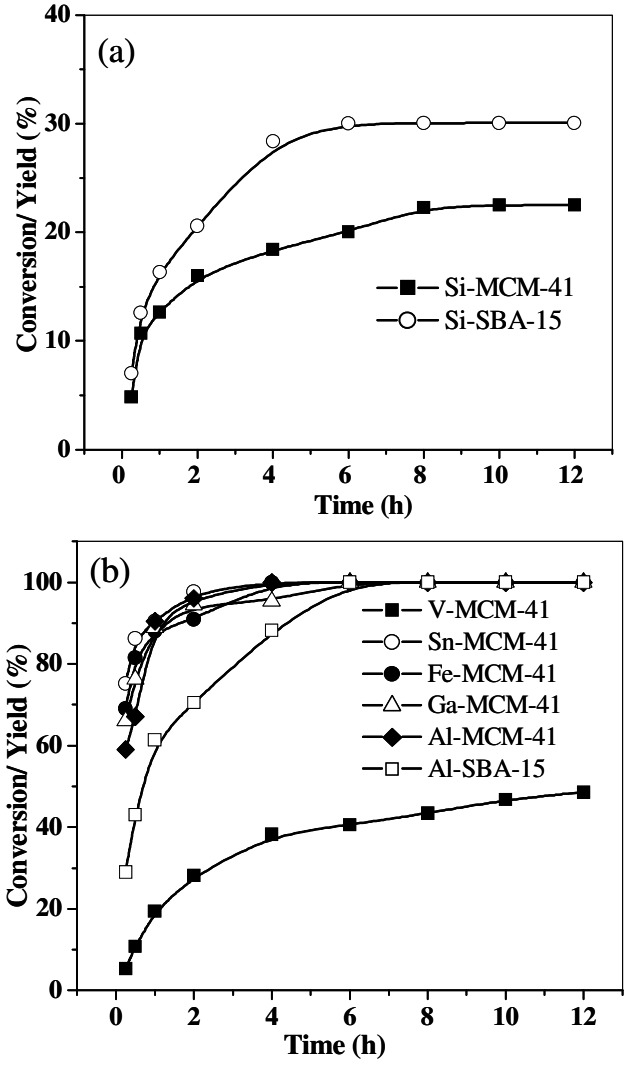

Figure 6.16 (a) Comparison of activity of Si-MCM-41 and Si-SBA-15; (b) Modified MCM-41 and SBA-15 catalysts. Reaction conditions: β-pinene: para formaldehyde = 1: 2 (mole), solvent-toluene = 4 g, catalyst amount = 0.05 g, T = 353 K.

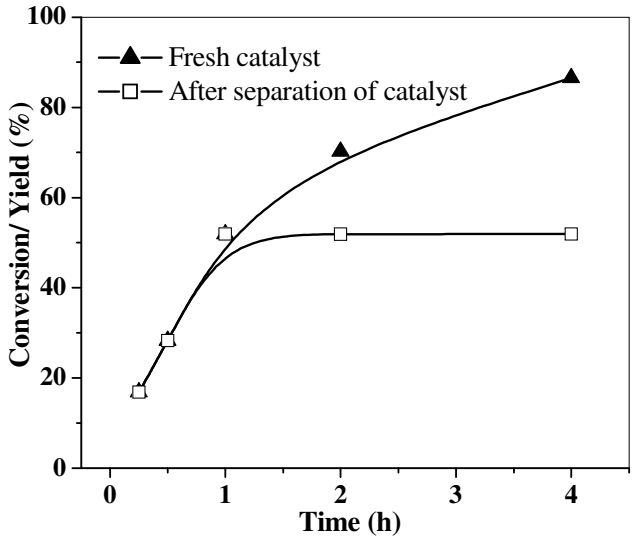

Figure 6.17 Test for heterogeneity of reaction over Sn-MCM-41 (49). Reaction conditions: β-pinene: para formaldehyde = 1:1 (mole), toluene = 4 g, T = 353 K, Sn-MCM-41 = 0.025 g.

(viii) Heterogeneity of Sn-MCM-41 for Prins condensation of β-pinene

The Prins condensation of β-pinene studied over Sn-MCM-41(49) catalyst appears to be a truly heterogeneously catalyzed reaction as the reaction stops when the catalyst is filtered off under hot conditions at the reaction temperature (353 K) after 1 h of reaction (Figure 6.17). Apparently, dissolved Sn^{4+} ions, if any, in solution do not catalyze the reaction homogeneously.

(ix) Recyclability of Sn-MCM-41 for Prins condensation of β-pinene

When the catalyst was reused after washing the used catalyst with acetone at room temperature, a small decrease in conversion is noticed (68.6 % compared to 88.3 % for the fresh catalyst after 8 h run duration) as shown in Table 6.3. The decrease may be due to the adhering of some organic materials and blocking of the pores of the catalyst. However, when the used catalyst is regenerated at 673 K (6 h), the catalyst activity is restored (88.2 % conversion for both first and second recycles)

Table 6.3 Recyclability of Catalyst

Run Number	Conversion of β-pinene (%)				
	1 h	2 h	4 h	6 h	8 h
Fresh catalyst	45.4	77.6	84.2	85.0	88.3
First recycle [a]	41.1	53.0	59.6	64.0	68.6
First recycle (calcined) [b]	51.8	71.7	82.4	85.3	88.2
Second recycle (calcined) [c]	50.8	72.0	82.5	85.6	88.2

Reaction Conditions: β-pinene: para formaldehyde = 1:1 (mole), toluene = 4 g, T = 353 K, Sn-MCM-41 (15) = 0.0125 g. (**a**- The used (once) catalyst was filtered and washed with acetone and dried at 273 K and used for further run, **b**- The used (once) catalyst was filtered, dried and activated at 673 K and used for further run, **c**- The catalyst used (twice) was filtered, dried and activated at 673 K and used for further run).

6.2.4 CONCLUSIONS

In the present work, Prins condensation reaction was studied over Sn-MCM-41 which was prepared by direct synthesis. The influence of various reaction parameters such as temperature, mole ratio, catalyst amount, solvent and different metal loading was studied in detail over Sn-MCM-41 catalysts. PW loaded SBA-15 catalysts are inactive for Prins condensation reaction. The activity of the catalysts for Prins condensation reaction decrease as: Sn-MCM-41 > Fe-MCM-41 > Ga-MCM-41 > Al-MCM-41 > Al-SBA-15 > Si-SBA-15 > Si-MCM-41. Sn-MCM-41 is the most active catalyst amongst all, which is attributed to the Lewis acidity of Sn^{4+} ions in the catalyst.

6.3 PART 3 OXIDATION OF ETHYLBENZENE

6.3.1 INTRODUCTION

Molecular oxygen (or air) is the primary oxidant used in the industry for economic and environmental reasons [28]. However, O_2 has a tendency to oxidize the substrate by mechanisms that are not readily or rationally controlled and hence it is difficult to control product selectivity. H_2O_2 is environmentally friendly as the only waste product resulting from using it is water [28, 29]. The "active oxygen" content of hydrogen peroxide, 47 % of its weight, is much higher than that of other oxidants. Other oxidants generally used for oxidation reactions include NaOCl, organic hydroperoxides, PhIO and percarboxylic acids. For both aqueous and non-aqueous reaction conditions, *tert*-butylhydroperoxide (TBHP) is often found to be the more selective oxidant [30, 31]. Also, the byproduct *t*-butanol is a valuable chemical. TBHP has been found to be by far the most preferred oxidant for epoxidation reactions [32, 33].

Metallosilicate molecular sieves, particularly titano-silicates with MFI or MEL topologies (e.g. TS-1 or TS-2) have been extensively investigated for selective oxidation reactions [34, 35] (e.g. epoxidation, hydroxylation, oxyfunctionalization of alkanes, ammoxidation and sulfoxidation). Due to the remarkable properties of TS-1 in oxidation reactions at low temperatures with dilute H_2O_2 as the oxidant [36, 38] the synthesis of Ti-containing large pore zeolites and mesoporous materials has received considerable attention [38-39]. Simultaneously, other cations like V^{4+}, Cr^{3+}, Mo^{6+}, Mn^{3+} etc. [40-42] have also been incorporated in the mesoporous molecular sieves and used in oxidation reactions. Mesoporous Ti-MCM-41 [43] and Ti-HMS [44] have been used for the epoxidation of norbornene with *tert*-butylhydroperoxide (TBHP) and oxidation of 2, 6-di-tert-butylphenol (2, 6-DTBP) with aqueous H_2O_2, respectively. The Ti and V containing MCM-41 molecular sieves have been used in a variety of oxidation reactions of bulky molecules using either H_2O_2 or TBHP as oxidant [45-47]. Although the intrinsic activity of Ti-MCM-41 was found to be lower than that of TS-1 and Ti-beta, particularly for the epoxidation of small molecules with aqueous H_2O_2, it showed higher catalytic activity in the epoxidation of bulkier norbornene with TBHP.

Studies on the liquid phase oxidation of ethylbenzene (EB) over V_2O_5/Al_2O_3 catalysts show that a loading of 15 wt. % V_2O_5 gives maximum conversion and acetophenone selectivity [48]. Mn-impregnated Si- and Al-MCM-41 catalysts are also

capable of effecting EB conversion by forming acetophenone as the major oxidized product [49]. The "neat" and zeolite-Y-encapsulated copper tri- and tetraaza macrocyclic complexes exhibit efficient catalytic activity in the regioselective oxidation of EB using TBHP [50]. C–H activation occurs at both the benzylic and aromatic ring carbon atoms. The latter is significant over the "neat" complexes in the homogeneous phase, while it is suppressed significantly in the case of the encapsulated complexes. The catalytic activity of Mn-MCM-41 has been examined for liquid phase oxidation of EB using TBHP as oxidant [51]. Both primary and secondary carbons of the side chain of EB are observed to be acted upon by activated TBHP. 1-Phenylethanol is observed as the major product. The other products obtained are acetophenone, benzaldehyde and phenylacetaldehyde. Zeolite Cu(II) complexes are quite active for the oxidation of EB with hydrogen peroxide and O_2 while Co(II) and Ni(II) are less active [52]. Vapor phase oxidation of EB with air (CO_2-free) has been studied over monometallic manganese and cobalt oxides and their bimetallic forms impregnated over Si-MCM-41 and Al-MCM-41 catalysts [53]. Cobalt (III) complexes containing 2-pyridinecarboxamide ligands have been studied for the catalytic oxidation of EB to acetophenone [54].

As part of the present thesis, the liquid phase oxidation of EB was studied over V-MCM-41, Fe-MCM-41 and Sn-MCM-41 molecular sieve catalysts prepared by a direct synthesis method (Chapter 2).

6.3.2 EXPERIMENTAL

(a) Chemicals and materials

The solvents used, acetonitrile (LOBA), ethylene dichloride (Merck), ethylbenzene (LOBA) were all ~ 99 % pure were used. The oxidant *tert*-butylhydroperoxide (TBHP) was used as 70 % solution in water, 5.5 M solution in deacane (Aldrich) and 3 M solution in EDC. The exact concentration of H_2O_2 (Qualigens-30 %) was determined by iodometric titration. Anhydrous TBHP (3 M solution in EDC) was prepared from 70 % aqueous TBHP (procured from Merck, India) according to the procedure reported in the literature [55, 56].

(b) Preparation of anhydrous tert-butyl hydroperoxide (TBHP) 3 M solution in ethylene dichloride (EDC)

A 3 M solution of TBHP in EDC was prepared by mixing 85 ml (0.61 mol) of commercial TBHP (70 % TBHP in water) with 140 ml EDC in a separating funnel. The milky mixture was allowed to stand till the phases separated. The organic layer (lower layer of about 200 ml) containing 0.6 mole TBHP was separated form the aqueous layer (about 21 ml). Then the organic layer was dried over a molecular sieve (3 A) for removal of extra water. The organic layer was transferred to a flask equipped with the Dean-Stark trap and a reflux condenser. The solution was refluxed using a heating mantle. Water accumulated in the arm of the Dean-Stark apparatus was removed from time to time. When water stopped accumulating, the solution was cooled under nitrogen and kept over activated 3 A molecular sieves. The composition of the TBHP solution was determined by standard titrimetric methods. The solution was found to be 3 M in TBHP (27 %).

(c) Reaction procedure

The oxidation of EB was carried out in a batch reactor using a 25 ml glass round bottom flask placed in a thermostatted oil bath and fitted with a water cooled condenser, at temperatures between 333 and 353 K. The molar ratio of EB to TBHP or H_2O_2 used was 1:1, 1:2 and 1:3. The amount of the catalyst used was 0.05 g. ACN and EDC were used as solvents. Aliquots of the reaction mixture were collected at different time intervals and analyzed by GC (Chrompack CP 9001, column OV-101, 50 m, id= 0.2 mm). Identification of the products was done by GC- MS and GC- IR.

6.3.3 RESULTS AND DISCUSSION

The catalysts used in the study were V-MCM-41, Sn-MCM-41 and Fe-MCM-41. The samples were characterized by different physicochemical techniques such as XRD, TPR and adsorption. The results of these studies have been presented in chapter- 3.

(A) Liquid phase oxidation of ethylbenzene

The reaction scheme for the oxidation of EB is shown in Figure 6.18. The products of the reaction are mainly acetophenone, 1-phenyl ethanol,

phenylacetaldehyde and benzaldehyde. When EB reacts with TBHP in ethylene dichloride it forms ethylbenzene tertiary butyl hydroperoxide (EBHP).

Oxidation of EB to the different products can take place in two ways. One is aromatic ring hydroxylation in which hydroxylation at the para-position occurs to a greater extent than at the ortho-position. The other is side chain (ethyl group) oxidation at primary and secondary carbon atoms. The primary and secondary carbinols formed from the side chain oxidation undergo further oxidation to the respective aldehyde and ketone. The side chain oxidation at the secondary carbon predominates over oxidation at the primary carbon atom.

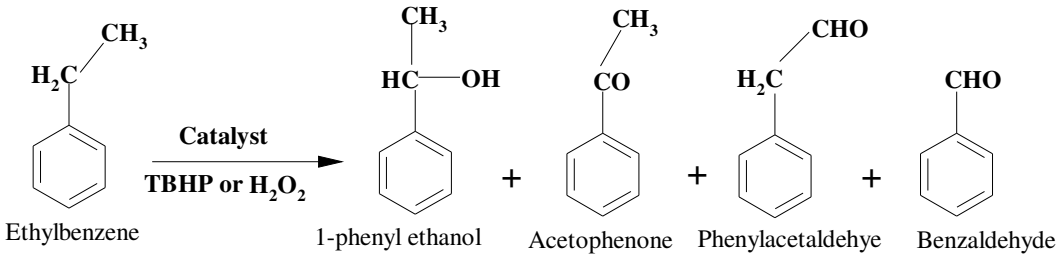

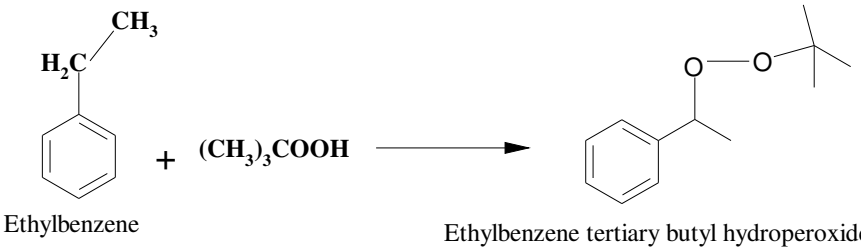

Figure 6.18 Reaction scheme for the oxidation of ethylbenzene (EB).

1-Phenylethanol from EB is produced by insertion of oxygen between the carbon hydrogen bond of the methylene group. Abstraction of an alcoholic OH hydrogen and the CH hydrogen by the activated *tert*- butylhydroperoxide oxygen yields acetophenone. Similar abstraction of OH hydrogen of 1-phenylethanol by the activated *tert*- butylhydroperoxide yields benzaldehyde by forming methane. Similar to formation of 1-phenylethanol, the methyl group of EB could also be acted upon by activated *tert*- butylhydroperoxide to yield 2-phenylethanol, which is very rapidly oxidized to phenylacetaldehyde. The rapid oxidation is evidenced through GC–MS

analysis which indicates the absence of 2-phenylethanol [51]. EB reacts with TBHP and forms the stable intermediate, ethylbenzene *tert*-butyl hydroperoxide (EBHP).

(i) Effect of different oxidants

The effect of different oxidizing agents (Table 6.4) such as H_2O_2 (26 %), TBHP in decane (5.5 M), TBHP in water (70 %) and TBHP in EDC (3 M) was studied in the oxidation of EB over V-MCM-41 (99) at 353 K with EB to oxidant mole ratio of 1:3. The solvents, decane (non-polar- dielectric constant 2.0), EDC (medium polar- dielectric constant 16.7) and water (polar- dielectric constant 80.3) were chosen for their differences in polarity. Both TBHP and EB conversion increase with time.

The order of the activity of the oxidant varied as TBHP in decane (5.5 M) < TBHP in water (70 %) < H_2O_2 (26 %) < TBHP in EDC (3 M). EB conversion was less in decane compared to TBHP in water due to the lower polarity of the former. But, it was observed that when TBHP in water was used as oxidant the reaction mixture was immiscible since EDC was used as the solvent and there was no homogeneous mixing of the reaction mixture. Hence conversion was less than when TBHP in EDC was used with EDC as the solvent. TBHP in EDC also showed higher activity than H_2O_2 which can be explained in terms of the hydrophilic surface properties caused by the surface silanol groups. Water and H_2O_2 are strongly adsorbed on the catalyst leading to a low concentration of the substrate on the catalyst surface and lowering the catalyst performance [57]. The selectivity of acetophenone increases with TOS and is highest (85.7 % at 24 h) when TBHP in EDC is used as oxidant. Other products, such as benzaldehyde, phenylacetaldehyde and 1-phenyl ethanol are formed in much smaller amounts. Benzaldehyde selectivity is high when H_2O_2 is used as oxidant compared to TBHP and decreases with time. A high selectivity (52.4 % at 24 h) for EBHP is observed when TBHP in decane is used as oxidant and it decreases with time in all the cases.

Table 6.4 Effect of different oxidant and temperature over V-MCM-41 (99) in the oxidation of EB

Oxidant	Temp (K)	EB: Oxidant Mole ratio	TOS (h)	EB Conv.	TBHP Conv.	A	B	C	D	E	F
TBHP in decane(5.5 M)	353	1:3	12	6.4	6.5	-	-	5.2	15.7	80.0	-
			24	28.1	28.2	4.5	-	5.5	38.1	52.3	-
TBHP in H_2O (70%)	353	1:3	12	29.1	37.5	8.2	-	3.3	78.5	38.6	-
			24	43.0	67.8	2.8	-	-	70.8	26.3	-
H_2O_2 (26%)	353	1:3	18	37.1	-	11.1	2.0	5.1	79.9	-	1.6
			24	48.9	-	10.1	2.9	7.0	77.7	-	2.0
		1:1	6	4.7	-	20.9	-	-	79.0	-	-
			18	18.3	-	15.5	3.2	28.6	49.4	-	3.0
TBHP in EDC (3 M)	353	1:3	12	44.7	47.4	3.2	0.7	2.0	77.0	16.9	-
			18	54.1	58.8	3.1	0.6	1.6	81.3	13.3	-
			24	64.0	73.1	2.5	0.5	-	85.6	11.2	-
TBHP in EDC (3 M)	343	1:3	12	35.2	32.6	8.2	-	2.6	85.7	3.2	-
			18	45.7	42.3	6.5	-	3.3	86.9	3.2	-
			24	52.7	51.3	1.3	-	2.9	92.6	3.0	-
TBHP in EDC (3 M)	333	1:3	12	19.2	18.0	3.2	-	6.0	84.4	6.3	-
			18	27.4	28.9	2.7	-	5.3	85.3	6.5	-
			24	34.9	35.7	2.8	-	5.5	85.6	5.9	-

Reaction conditions: T = 353 K, EDC = 5 g, V-MCM-41 (99) = 0.05 g, A- Benzaldehyde, B- Phenyl acetaldehyde, C- 1-phenyl ethanol, D- Acetophenone, E- EBHP, F-benzoic acid. When H_2O_2 was used, ACN (5g) was the solvent.

(ii) Influence of temperature

The effect of temperature on EB conversion in the temperature range of 333 to 353 K over V-MCM-41 (99) was investigated and the results are presented in Table 6.4. Both EB and TBHP conversion increase with temperature. Selectivity for acetophenone is almost similar (> 85 %) at all the temperatures studied. Selectivity for benzaldehyde and 1-phenylethanol decrease with time. The selectivity for EBHP is high at higher temperature and it decreases with decrease in temperature as well as with time.

(iii) Effect of EB to oxidant mole ratio

The influence of EB to TBHP mole ratio is presented in Table 6.5. As expected, EB conversion increases with TBHP content. The selectivity to acetophenone is also larger with mole ratio 1:3 than with 1:1.

(iv) Effect of catalyst concentration

The effect of catalyst amount on conversion of EB is presented in Table 6.5. EB conversion increases slightly when the catalyst amount increases from 0.025 to 0.05 g. But a further increase in catalyst amount to 0.1 g reveals a negligible increase in EB conversion. The selectivity to acetophenone increases when the catalyst amount is increased from 0.025 to 0.5 g with negligible further increase on going to 0.1 g catalyst loading. Also the selectivities for the other products such as benzaldehyde, phenylacetaldehyde and 1-phenyl ethanol decreases with increase in catalyst amount.

(v) Effect of metal content (Si/V)

The effect of V content of V-MCM-41 on the oxidation of EB is reported in Table 6.6 (A). These studies were carried out at EB: TBHP mole ratio of 1:1. TBHP conversion increases with increase in V content. Selectivity for acetophenone increases with increase in metal content while selectivity for benzaldehyde, phenylacetaldehyde, 1-phenylethanol and EBHP decrease with increase in metal content. Table 6.6 (B) shows the effect of V content on oxidation of EB at an EB to TBHP mole ratio of 1:3. As the V content increases, EB conversion also increases.

Table 6.5 Effect of Mole ratio of ethylbenzene to TBHP and catalyst concentration in the oxidation of EB

EB: TBHP Mole ratio	Catalyst Weight (g)	TOS (h)	EB Conv.	TBHP Conv.	A	B	C	D	E
1:1	0.050	12	18.0	71.9	2.2	3.6	4.2	41.0	48.7
		18	20.7	88.0	2.6	1.3	6.2	52.6	37.1
		24	28.0	90.0	2.7	-	0.5	68.9	27.7
1:2	0.050	12	23.3	42.4	4.4	-	10.5	67.3	17.6
		24	44.1	91.7	1.8	1.2	0.3	73.4	23.2
1:3	0.025	12	31.9	37.8	4.3	1.2	8.3	62.8	23.1
		18	38.3	47.0	4.0	1.1	5.3	65.5	24.0
		24	40.5	54.5	3.8	1.1	2.9	67.7	24.3
1:3	0.050	12	44.7	47.4	3.2	0.7	2.0	77.0	16.9
		18	54.1	58.8	3.1	0.6	1.6	81.3	13.3
		24	64.0	73.1	2.5	0.5	-	85.6	11.2
1:3	0.10	12	46.6	66.2	2.0	0.8	-	81.8	15.2
		18	57.2	90.4	1.8	0.9	0.5	81.6	15.0
		24	61.9	98.1	1.4	1.0	0.4	82.9	14.1

Reaction conditions: Catalyst- V-MCM-41 (99), T = 353 K, EDC = 5 g, oxidant- TBHP in EDC (3 M). A- Benzaldehyde, B- Phenyl acetaldehyde, C- 1-phenyl ethanol, D- Acetophenone, E- EBHP.

Table 6.6 (A) Effect of metal content in the oxidation of EB over V-MCM-41 with EB: TBHP mole ratio 1:1

Catalyst (Si/metal ratio)	TOS (h)	EB Conv.	TBHP Conv.	A	B	C	D	E
V-MCM-41(99)	12	18.0	71.9	2.2	3.6	4.2	41.0	48.7
	24	28.0	90.0	2.7	-	0.5	68.9	27.7
V-MCM-41(82)	12	8.1	38.0	3.7	-	5.0	47.9	43.1
	24	18.5	97.0	2.1	4.1	7.2	51.2	35.1
V-MCM-41(46)	12	6.2	19.7	5.6	4.8	4.6	42.5	42.0
	24	12.2	49.7	3.7	6.1	4.9	46.4	38.5

Table 6.6 (B) Effect of metal content for oxidation of EB over V-MCM-41 with EB: TBHP mole ratio 1:3

Catalyst (Si/metal ratio)	TOS (h)	EB Conv.	TBHP Conv.	A	B	C	D	E
V-MCM-41(99)	12	44.7	47.4	3.2	0.7	2.0	77.0	16.9
	18	54.1	58.8	3.1	0.6	1.6	81.3	13.3
	24	64.0	73.1	2.5	0.5	-	85.6	11.2
V-MCM-41(82)	12	30.5	29.3	3.8	2.8	3.6	36.1	53.4
	18	44.3	43.5	3.2	2.0	5.4	47.2	42.1
	24	45.0	59.2	2.8	5.0	2.2	52.0	37.2
V-MCM-41(46)	12	26.5	28.2	3.4	-	5.7	43.9	46.8
	18	38.7	46.0	3.2	5.9	3.1	48.5	39.1
	24	49.1	53.0	2.8	2.1	3.2	51.9	39.7

Reaction conditions: Oxidant: TBHP in EDC (3 M), T= 353 K, catalyst =0.05 g, A-Benzaldehyde, B- Phenyl acetaldehyde, C- 1-phenyl ethanol, D- Acetophenone, E-EBHP, EDC-5 g.

Table 6.7 Comparison for activity of MCM-41 catalysts in EB oxidation with TBHP oxidant

Catalyst (Si/metal ratio)	EB: TBHP Mole ratio	TOS (h)	EB Conv.	TBHP Conv.	A	B	C	D	E
V-MCM-41 (99)	1:3	12	44.7	47.4	3.2	0.7	2.0	77.0	16.9
		24	64.0	73.1	2.5	0.5	-	85.6	11.2
	1:2	12	23.3	42.4	4.4	-	10.5	67.3	17.6
		24	44.1	91.7	1.8	1.2	0.3	73.4	23.2
Fe-MCM-41(20)	1:3	12	11.6	11.2	-	-	8.2	3.8	87.8
		24	26.1	32.7	7.8	-	19.8	12.7	59.4
	1:2	12	4.8	8.0	-	-	24.3	7.3	68.1
		24	12.6	36.0	10.9	-	40.3	5.3	43.4
Sn-MCM-41(22)	1:3	12	2.6	3.8	-	-	37.6	40.3	21.6
		24	9.1	4.3	-	-	45.2	22.2	32.5
	1:2	12	3.2	13.1	-	-	44.3	25.6	30.0
		24	5.3	23.3	-	-	45.0	24.1	30.8

Reaction conditions: T = 353 K, EDC = 5 g, catalyst wt = 0.05 g, oxidant - TBHP in EDC (3M). A- Benzaldehyde, B- Phenyl acetaldehyde, C- 1-phenyl ethanol, D- Acetophenone, E-EBHP.

(vi) Comparison of the activity of MCM-41 catalysts

The activity of Sn-MCM-41, Fe-MCM-41 and V-MCM-41 catalysts was compared for EB oxidation using TBHP (Table 6.7) and H_2O_2 (Table 6.8) as oxidants. When TBHP is used as oxidant the order for the EB as well as TBHP conversion over MCM-41 catalysts is: V-MCM-41 > Fe-MCM-41 > Sn-MCM-41. Selectivity for acetophenone increases in the order, Fe-MCM-41 < Sn-MCM-41 < V-MCM-41. The selectivity for 1-phenyl ethanol varied as Sn-MCM-41 < Fe-MCM-41 < V-MCM-41. When H_2O_2 is used as oxidant (Table 6.8) the EB conversion is found to vary as Fe-

MCM-41 > V-MCM-41 > Sn-MCM-41. Selectivity for acetophenone increase in the order, Sn-MCM-41 < Fe-MCM-41 < V-MCM-41. Selectivity for EBHP is more over Fe-MCM-41 and follows the order: Fe-MCM-41 > Sn-MCM-41 > V-MCM-41. Selectivities for other products such as benzaldehyde and 1-phenylethanol are similar for all the catalysts.

Table 6.8 Comparison for activity of MCM-41 catalysts in EB oxidation with H_2O_2 oxidant

Catalyst (Si/Metal)	TOS (h)	EB Conv.	A	B	C	D	F
Sn-MCM-41 (20)	12	6.6	13.0	-	-	58.7	28.1
	18	30.1	10.6	-	-	58.3	24.2
	24	45.2	9.5	-	7.8	63.8	18.3
Fe-MCM-41(20)	12	36.9	5.0	-	3.0	65.2	26.6
	18	70.8	4.2	-	4.4	64.7	26.5
	24	91.9	3.9	-	5.5	63.9	26.5
V-MCM-41 (20)	12	37.1	11.1	2.0	5.1	79.9	1.6
	18	48.9	10.1	2.9	7.0	77.7	2.0
	24	62.9	8.1	2.7	7.8	80.5	0.8

Reaction conditions: Catalyst = 0.05 g, oxidant-H_2O_2 (26 %), EB: oxidant mole ratio = 1:3, T= 353 K. A- Benzaldehyde, B- Phenyl acetaldehyde, C- 1-phenyl ethanol, D-Acetophenone, F- benzoic acid.

(vii) Study of heterogeneity for V-MCM-41 (Leaching test)

Rapid leaching of metal ions is a general problem associated with the use of heterogeneous metal catalysts in liquid-phase oxidations. Leaching is a result of solvolysis of the metal-oxygen bonds, through which the catalyst is attached to the support (for example SiO_2, Al_2O_3), by polar molecules such as H_2O, ROH, or RCO_2H. Although the same situation is present on the (internal) surface of a molecular sieve, the metal-oxygen bonds appear to be more stable in this microenvironment. Nevertheless, it should be emphasized that, with the exception of TS-1, the long or even short-term stability of the various redox molecular sieves towards leaching has

not been unequivocally demonstrated. The definitive test for heterogeneity is to filter the catalyst during the course of the reaction at the reaction temperature and allow the filtrate to react further [58].

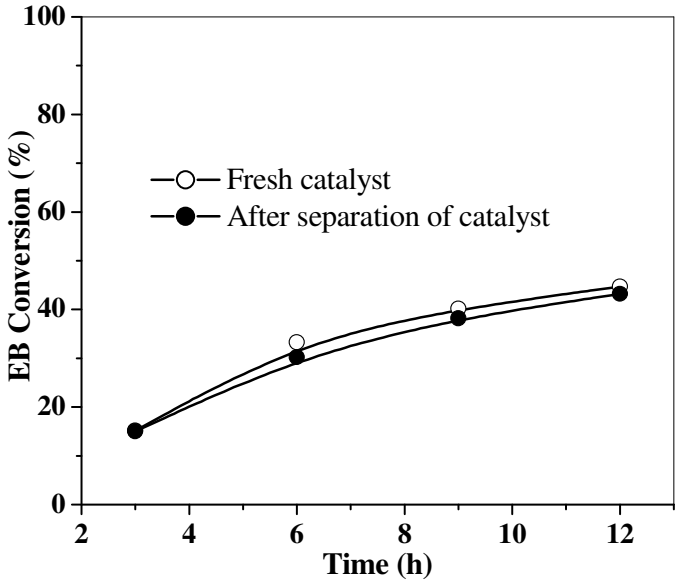

Figure 6.19 Heterogeneity test for EB oxidation over V-MCM-41 (20). Reaction conditions: oxidant- T= 353 K, EB: TBHP in EDC (3 M) mole ratio= 1:3, catalyst amount = 0.05 g.

The results of the leaching test carried out for V-MCM-41 is presented in Figure 6.19. At 3 h reaction time, the EB conversion was 15.2 %. The catalyst was filtered in hot conditions after 3 h and then the reaction was continued in the absence of the catalyst. After 3 h, the sample was analyzed and an increase in EB conversion was observed which increased further with run duration as shown in Figure 6.19. When TBHP was used as oxidant, the peroxide species attack the framework V and it goes into solution. Therefore after filtration of the catalyst, EB conversion continues to increase due to homogeneous catalysis by leached V-species. Apparently, even though solid catalysts are used in the reactions, the oxidation of EB is catalyzed mainly by the leached ions (V) in the homogeneous phase. It is believed that the situation will be similar in case of the other metallosilicates, Sn- and Fe-MCM-41.

6.3.4 CONCLUSIONS

In the present section, Sn, Fe and V-MCM-41 incorporated metal catalysts are studied for the liquid phase oxidation of EB in the presence of TBHP and H_2O_2 as oxidants. The effects of different reaction parameters such temperature, substrate to oxidant mole ratio, catalyst concentration and metal content are reported for V-MCM-41 catalysts. The activities of Sn, Fe and V-MCM-41 incorporated catalysts, were compared at similar reaction conditions. V-MCM-41 is found to be the most active catalyst for oxidation of EB. When acetonitrile is used as the solvent and TBHP as the oxidant, the oxidation of EB takes place with high selectivity for acetophenone even in the absence of catalyst. Heterogeneity tests conducted for V-MCM-41 suggests that the reaction occurs mainly in the homogeneous phase with the leached V-ions.

6.3.5 REFERENCES

15. M.A. Ogliaruso, J.F. Wolfe, "Synthesis of carboxylic acids, Esters and Their Derivatives", Wiley, New York, (1991).
16. Vogel's Textbook of Practical Organic Chemistry, 4th ed., ELBS, (1987) 501.
17. P. Laszlo, J. Lucchette, Tetra. Lett. 25 (1984) 1567.
18. J. M .Adams, T. V. Clapp, Clays Clay Miner. 34 (1986) 287.
19. M. M. Mortland, Soil Sci. Soc. Am. J. 40 (1976) 367.
20. O. Darge, F. C. Thyrion, J. Chem. Tech. Biotech. 58 (1993) 351.
21. T. S. Thorat, V. M. Yadav, G. D. Yadav, Appl. Catal. A. 90, 2, (1992) 73.
22. Z. H. Zhao, J. Mol. Catal. A: Chem. 168 (2001) 147.
23. G.D. Yadav, P.H. Mehta, Ind. Eng. Chem. Res. 33 (1994) 2198.
24. C. V. Suresh Kumar, N. G. Karanth, S. Divakar, Ind. J. Chem. 41 B (2002) 1068.
25. G. Kuriakose, N. Nagaraju, J. Mol. Catal. A: Chem. 223 (2004) 155.
26. M. L. Kantham, V. Bhaskar, B. M. Choudhary, Catal. Lett. 78, 1-4 (2002) 185.
27. K.V.N.S. Srinivas, B. Das, J. Org. Chem. 68 (2003) 1165.
28. C. Ravindra Reddy, P. Iyengar, G. Nagendrappa, B. S. Jai Prakash, J. Mol. Catal. A: Chem. 229 (2005) 31.
29. M. Alvaro, A. Corma, D. Das, V. Fornes, H. Garcia, J. Catal. 231 (2005) 48.
30. C. Ravindra Reddy, B. Vijaykumar, P. Iyengar, G. Nagendrappa, B. S. Jai Prakash, J. Mol. Catal. A: Chem. 223 (2004) 117.
31. G. D. Yadav, S. V. Lande, Org. Proc. Res. And Dev. 9 (3), (2005) 288.

K. Bauer, D. Garbe, H. Surburg (Eds.), "Common Fragrance and Flavor
18. Materials. Preparation Properties and Uses", VCH Verlagsgesellschaft, 59 (1990).
19. "Kirk-Othmer Encyclopedia of Chemical Technology", John Wiley, New York, (1997) Vol. 26.
20. Kriewitz, Ber. 32 (1899) 57.
21. J. P. Bain, JACS. 68 (1946) 638.
22. A. L. Villa de P., E. Alarcon and C. Montes de Correa, Chem. Commun. (2002) 2654.
23. U. R. Pillai, E. Sahle-Demessie, Chem. Commun. (2004) 826.

24. T. M. Jyothi, M. L. Kaliya, M. Herskowitz and M. V. Landau, Chem. Commun. 11 (2001) 992.
25. T. M. Jyothi, M. L. Kaliya, M. V. Landau, V. Miron, Ange. Chemie. 40 (15) (2001) 2881.
26. Alda Luz Villa de P, Edwin Alarcon, Consuelo Montes de C, Catal. Today. 107-108 (2005) 942.
27. (a) E. Dumitriu, D. Trong On and S. Kaliaguine, J. Catal. 170 (1997) 150; (b) E. Dumitriu, V. Hulea, I. Fechete, C. Catrinescu, A. Auroux, J-F. Lacaze and C. Guimon, Appl. Catal. A: Gen. 181 (1999) 15.
28. J.O. Edwards, R. Curci, G. Strukul, (Ed.), "Catalytic Oxidations with Hydrogen Peroxide as Oxidant", Kluwer Academic Publishers, Dordrecht, (1992).
29. I.I. Moiseev, J. Mol. Catal. A: Chem. 127 (1997) 1.
30. K. B. Sharpless, T. R. Verhoeven, Aldrich. Acta. 12 (1979) 63.
31. J. G. Hill, B.E. Rossiter, K.B. Sharpless, J. Org. Chem. 48 (1983) 3607.
32. K. B. Sharpless, C. H. Behrens, T. Katsuki, A. W. Lee, V. S. Martin, M. Takatani, S. M. Viti, F. J. Walker, S. S. Woodard, Pure Appl. Chem. 55 (1983) 589.
33. Jean-Marie Bregeault, Dalton Trans. (2003) 3289.
34. I. W. C. E. Arends, R. A. Sheldon, M. Wallau, U. Schuchardt, Angew. Chem. Int. Ed. Engl. 36 (1997) 1144.
35. P. Kumar, R. Kumar, B. Pandey, Synlett. (1995) 289.
36. B. Notari, Catal. Today. 18 (1993) 163.
37. M.G. Clerici, Appl. Catal. 68 (1991) 249.
38. M.A. Camblor, A. Corma, J. Perez-Pariente, Zeolites 13 (1993) 82.
39. A. Tuel, Zeolites 15 (1995) 228.
40. K.M. Reddy, I.L. Moudrakovski, A. Sayari, J. Chem. Soc., Chem. Comm. (1994) 1059.
41. Z. Luan, J. Xu, H. He, J. Klinowski, L. Kevan, J. Phys. Chem. 100 (1996) 19595.
42. N. Ulagappan, C.N.R. Rao, J. Chem. Soc. Chem. Comm. (1996) 665.
43. A. Corma, M. T. Navarro, J. P. Pariente, J. Chem. Soc. Chem. Comm. (1994) 147.

44. P. T. Tanev, M. Chibwe, T. J. Pinnavaia, Nature 368 (1994) 321.
45. A. Corma, M.T. Navarro, J. Perez-Pariente, J. Chem. Soc. Chem. Comm. (1994) 147.
46. P.T. Tanev, M. Chibwe, T.J. Pinnavaia, Nature 368 (1994) 317.
47. J.S. Reddy, and A. Sayari, Appl. Catal. A. Gen. 148 (1996) 7.
48. Ettireddy P. Reddy and Rajender S. Varma, J. Catal. 221 (2004) 93.
49. S. Vetrivel, A. Pandurangan, Appl. Catal. A: Gen. 264 (2004) 243.
50. T.H. Bennur, D. Srinivas, S. Sivasanker, J. Mol. Catal. A: Chem. 207 (2004) 163.
51. S. Vetrivel, A. Pandurangan, J. Mol. Catal. A: Chem. 217 (2004) 165.
52. K.O. Xavier, J. Chacko, K.K. Mohammed Yusuff, Appl. Catal. A: Gen. 258 (2004) 251.
53. S.Vetrivel, A. Pandurangan, Indust. Eng. Chem. Res. 44(4) (2005) 692.
54. Jian-Ying; Qi, Hong-Xia Ma, Xian-Jun Li, Zhong-Yuan Zhou, Choi, C. K. Chan Michael, S. C. Albert Yang, Qi-Yun Chem. Commun. 11 (2003) 1294
55. J.G. Hill, B.E. Rossiter, K.B. Sharpless, J. Org. Chem. 48 (1983) 3607.
56. K.B. Sharpless, T.R. Verhoeven, Aldrich. Acta. 12 (1979) 63.
57. Jan C. van der Waal and Herman van Bekkum, J. Mol. Catal. A: Chem. 125 (1997) 137.
58. Isabel W. C. E. Arends, Roger A. Sheldon, Martin Wallau, Ulf Schuchardt, Angew. Chem. Int. Ed. Engl. 36 (1997) 1144.

Chapter 7

SUMMARY AND CONCLUSIONS

SUMMARY AND CONCLUSIONS

The thesis reports the synthesis of mesoporous metallosilicate catalysts such as modified MCM-41 and SBA-15. In the present work Al-MCM-41, Ga-MCM-41, Sn-MCM-41, Fe-MCM-41 and V-MCM-41 with different metal loadings have been synthesized by direct hydrothermal methods while Al-SBA-15 and PW/SBA-15 catalysts were prepared by impregnation methods. Different physicochemical techniques, such as XRD, IR, UV-Vis, NMR, TPD, TPR, ESR and adsorption studies have been used for the characterization of the mesoporous catalysts. The catalytic activities of above synthesized catalysts in different organic reactions such as Claisen rearrangement, Beckmann rearrangement, acylation of anisole, alkylation of m-cresol, esterification of p-cresol, Prins condensation of β-pinene and oxidation of ethylbenzene have been investigated. The influence of reaction parameters were studied for the above reactions and the catalytic activity of different catalysts has been compared. In order to understand the reactions better and to obtain effective comparisons of the activity of the different catalysts, a kinetic analysis of the data for some reactions has been carried out.

The XRD patterns of MCM-41 and SBA-15 based catalysts were similar to those reported by earlier workers. The adsorption-desorption isotherms were of the type IV for all the catalysts. The pore diameters for MCM-41 were around 35 Å and about 60 Å for SBA-15. Incorporation of Al into MCM-41 (by direct synthesis) and SBA-15 (by post synthetic impregnation method) makes the materials acidic**,** acidity increases with increasing amount of Al. Similar results were reported for PW/SBA-15 catalysts also, acidity increasing with PW content. The acidity characterization studies were carried out by the TPD of ammonia. UV-Vis and ESR studies reveal at least two types of metal species in V and Fe-MCM-41.

The Claisen rearrangement of APE over Al-MCM-41 proceeds with ease in TCE. *o*-AP is produced initially, which then undergoes cyclization to form 2, 3-dihydro-2-methylbenzofuran. Both the catalyst acidity and substrate conversion increase with the Al content in MCM-41. There is a close relationship between acidity and conversion, which suggests that the reaction occurs inside the pores of MCM-41. The reaction kinetics was analyzed assuming it to be a first order consecutive reaction. The Claisen rearrangement has also been investigated over Ga-MCM-41, Al-

SBA-15 and PW/SBA-15. The order of activities of the catalysts for the rearrangement was: Al-SBA-15 > Al-MCM-41 > Ga-MCM-41 > PW/SBA-15.

The vapor phase Beckmann rearrangement has been studied for the transformation of cyclohexanone oxime to ε-caprolactam on SBA-15 and Al-SBA-15 samples with different Si/Al ratios. The influence of reaction conditions such as temperature, space velocity, and time on stream and also the effect of polarity of solvents have been investigated over the Al-SBA-15 catalyst. Caprolactam yield was highest for Al-SBA-15 (59 %) with Si/Al ratio 9 at 623 K and WHSV of 3.02 h^{-1}. While the acidic sites appear to catalyze the rearrangement, Si-OH groups catalyze the formation of side-products. The medium polar solvent methanol shows the best performance for caprolactam selectivity. The Beckmann rearrangement has also been studied over Fe –MCM-41, V -MCM-41, Sn-MCM-41, Ga-MCM-41, Al-MCM-41, and PW/SBA-15. The results show that both the oxime conversion and selectivity for caprolactam over the catalysts is in the order: Si-SBA-15 < NH_4-exchanged SBA-15 < Fe-MCM-41 < V-MCM-41 < Sn-MCM-41 < Ga-MCM-41 < Al-SBA-15 < Al-MCM-41 < PW/SBA-15.

The Friedel-Crafts acylation of anisole with acetic anhydride catalyzed by heteropolyacids shows that both catalyst acidity and substrate conversion increase with the PW content of SBA-15. Conversion and para-methoxyacetophneone formation increase with run duration while ortho-methoxyacetophenone decreases. The temperature effects on conversion and selectivity show that a conversion of 100 % with para-methoxyacetophenone yields greater than 95 % can be achieved at 373 K. A comparison of conversion and selectivity of MCM-41 and SBA-15 shows that the order of performance of the catalyst is: Al-SBA-15 < Al-MCM-41 < PW/SBA-15. Al-MCM-41 catalysts have lower acidity than Al-SBA-15 (for similar Si/Al ratios) but exhibit higher activity for acylation.

Vapor phase m-cresol isopropylation has been studied over Al-MCM-41, Al-SBA-15 and PW/SBA-15 catalysts. Among the products, thymol, isothymol, 2-isopropyl-3-methylphenol and dialkylated products 2, 4-di-isopropyl-3-methylphenol are the major ones. Other products, such as 2, 6-di-isopropyl-3-methylphenol, Isopropyl-3-methylphenylether and Isopropyl-2-isopropyl-5-methylphenylether are also formed in minor amounts. The effects of different reaction parameters and

catalyst acidity have been studied over a number of catalysts. The performance of the catalysts was in the order, PW/SBA-15 < Al-MCM-41 < Al-SBA-15.

An eco-friendly and benign catalytic process, employing a solid acid catalyst (PW/SBA-15) is reported for the esterification of p-cresol with phenyl acetic acid to give p-cresylphenyl acetate. The influence of various reaction parameters has been studied over PW/SBA-15 catalysts. Activity and acidity increased with PW loading, and the reaction was 100 % selective towards p-cresylphenyl acetate. A pseudo first order kinetic model was built to fit the experimental data and the apparent activation energies were calculated. The low E_a values suggest that the reaction is not intrinsically kinetically controlled.

Prins condensation of β-pinene with para formaldehyde to yield nopol was studied over a number of metallosilicates prepared by direct synthesis. A detailed investigation was done over Sn-MCM-41 catalysts. The activity of the different catalysts, for the condensation of β-pinene with paraformaldehyde was found to be in the order: Sn-MCM-41 > Fe-MCM-41 > Ga-MCM-41 > Al-MCM-41 > Al-SBA-15 > Si-SBA-15 > Si-MCM-41. The exceptional activity of Sn-MCM-41 is attributed to the Lewis acidity of Sn^{4+} ions in the catalyst.

Sn, Fe and V-MCM-41 incorporated metal catalysts were investigated in the oxidation of ethylbenzene with TBHP and H_2O_2 as oxidants. The activity of the different catalysts was compared for Sn, Fe and V-MCM-41. It is found that V-MCM-41 was the most active catalyst for oxidation of EB. However it appears that oxidation reactions over these metallosilicates may be partially (or fully) catalyzed by the metal ions leached into the solution by the peroxide.

List of Publications:

1. Rearrangement of allyl phenyl ether over Al-MCM-41 catalyst

   N. T. Mathew, **S. Khaire** , S. Mayadevi, R. Jha, S. Sivasanker; *Journal of Catalysis 229, 105-113 (2005) ,*

2. Alkylation of biphenyl with t-butylalcohol over modified Y-zeolites.

   R. Anand, **S. S. Khaire**, R. Maheshwari, K. U. Gore; *Journal of Molecular Catalysis A: Chemical 218, 241-246 (2004).*

3. Alkylation of naphthalene with t-butanol over zeolite Y: influence of reaction environment and reaction kinetics.

   R. Nagotakar, **S. S. Khaire**, S. Mayadevi, S. Sivasanker; *Indian Journal of Chemical Technology, vol.11, May 2004, 351-356.*

4. Isopropylation of naphthalene over modified faujasites: effect of steaming temperature on activity and selectivity.

   R. Anand, R. Maheshwari, K. U. Gore, **S. S. Khaire**, V. R. Chumbhale; *Applied Catalysis A: General, 249, 265-272, (2003).*

5. N-Alkylation of aniline with ethanol over HY and dealuminated HY zeolites.

   R. Anand, **S. S. Khaire**, R. Maheshwari, K. U. Gore, V. R. Chumbhale; *Applied Catalysis A: General, Vol.242, 1,171-177 (2003).*

6. Kinetics of liquid phase hydrogenation of 4-chloro-2-nitrophenol catalyzed by Pt/carbon catalyst.

   S. B. Halligudi and **Surekha S. Khaire**, *Journal of Chemical Technology and Biotechnology; 77, 25-28 (2001).*

7. Vapor phase Beckmann rearrangement of cyclohexanone oxime over Al containing SBA-15 molecular sieves.

   Surekha S. Khaire and S. Sivasanker, *Manuscript under preparation.*

8. Friedel-Crafts acylation of anisole with acetic anhydride over phosphotungstic acid supported on SBA-15.

   Surekha S. Khaire and S. Sivasanker, *Manuscript under preparation.*

9. Claisen rearrangement of allyl phenyl ether over MCM-41 and SBA-15 modified catalysts.

   Surekha S. Khaire and S. Sivasanker, *Manuscript under preparation.*

10. Vapor phase isopropylation of m-cresol over MCM-41 and SBA-15 catalysts.

    Surekha S. Khaire and S. Sivasanker, *Manuscript under preparation.*

11. Synthesis of perfumery grade p-Cresylphenyl acetate over PW/SBA-15.
    Surekha S. Khaire and S. Sivasanker, *Manuscript under preparation.*
12. Synthesis of nopol over MCM-41 and SBA-15 modified catalysts.
    Surekha S. Khaire and S. Sivasanker, *Manuscript under preparation.*

Patents:

1. An improved process for the preparation of 4, 6-diaminoresorcinol-dihydrochloride.
   S. B. Halligudi and **Surekha S. Khaire,** India, USA and Europe Patent, Filed, NF/23/2001.